



Energy Efficiency Investigations with a new Operator Training Simulator for Biorefineries

by

Stefan Kuntzsch

A thesis submitted in partial fulfillment
of the requirements for the degree of

**Doctor of Philosophy
in Bio-Chemical Engineering**

Approved, Thesis Committee:

Name and title of chair:

Prof. Dr.-Ing. Volker C. Hass, JUB

Name and title of committee member:

Prof. Dr. M. Winterhalter, JUB

Name and title of committee member:

Dr. Frank Baganz, UCL

Date of Defense: 24.02.2014

School of Engineering and Science

For
M and M

Acknowledgment

I would like to thank Prof. Dr.-Ing. Volker C. Hass for giving me the chance to work on this project and for believing in my abilities. I would also like to thank him for his intensive support in hard times, lots of helpful ideas and encouraging words. Thank you very much!

I also would like to thank Prof. Dr. Mathias Winterhalter for his effort in convincing me to look more deeply at the scientific side on life.

I further would like to express my gratitude to Dr. Frank Baganz, who agreed to become a member of the thesis committee.

Special thanks I would like to address to Dr. Florian Kuhnen, Dr. Andree Blesgen, Inga Gerlach, Simone Schwarz, Anna Schneider and all former and part-time members of the working group Chemical Engineering and System Dynamics at Hochschule Bremen. Every little conversation, either with coffee or not, has helped approaching the big aim.

I am deeply grateful to my parents, Annegret and Heiner, who made it possible for me to study this long and that they never had any doubts in what I do.

My last acknowledgment is directed to my wonderful wife and best friend Julie, who has always bolstered me, in good times and in bad times. Thank you for accepting my sometimes strange mood that came up now and then, especially when things went unexpectedly wrong. Thank you for blessing me with the two most beautiful little girls that I have ever gotten to know!

This thesis would not have been possible without the financial assistance of Hochschule Bremen and the state Bremen, financing the projects “Anaerobdetective” (17021X10) and “Eco:In” (VE0076B).

Statutory declaration

I, Stefan Kuntzsch, hereby declare that I have written this PhD thesis independently, unless where clearly stated otherwise. I have used only the sources, the data and the support that I have clearly mentioned. This PhD thesis has not been submitted for conferral of degree elsewhere.

Bremen, in February 2014

Contents

Symbols	xi
1. Introduction	1
1.1. Motivation	1
1.2. Aims	2
1.3. Outline of the work	3
2. State of the art	5
2.1. Biorefineries	5
2.2. Bioethanol	8
2.2.1. Introduction	9
2.2.2. Raw materials for ethanol production	9
2.2.3. Bioethanol processes	10
2.3. Modeling and simulation software	12
2.4. Training simulators	15
2.4.1. Training simulator classification	15
2.4.2. Fields of application	20
2.5. Scientific demand	22
3. Materials and methods	25
3.1. OTS development framework	25
3.2. Functional description of the bioethanol process	26
3.2.1. Yeast cultivation	30
3.2.2. Cross-flow filtration	31
3.2.3. Rectification	34
3.3. Process model structure and implementation	39
3.4. Software tools used for OTS development	41
3.4.1. eStIM	41
3.4.2. WinErs	42
3.4.3. GRAFCET	43
3.4.4. AutoHotkey	45
4. Mathematical description of the bioethanol process	47
4.1. Auxiliary components	47
4.1.1. Valves	47

4.1.2.	Pumps	50
4.1.3.	Tanks	51
4.1.4.	Heat exchangers	53
4.1.5.	Sensors	58
4.1.6.	Controllers	59
4.2.	Yeast cultivation	61
4.2.1.	Kinetics sub-model	61
4.2.2.	Unit sub-model	66
4.2.3.	Plant sub-model	69
4.2.4.	Automation sub-model	71
4.2.5.	Model validation	76
4.3.	Cross-flow filtration	77
4.3.1.	Unit sub-model	79
4.3.2.	Plant sub-model	85
4.3.3.	Automation sub-model	87
4.3.4.	Model validation	89
4.4.	Rectification	92
4.4.1.	Kinetics sub-model	92
4.4.2.	Unit sub-model	95
4.4.3.	Plant sub-model	103
4.4.4.	Automation sub-model	104
4.4.5.	Model validation	107
5.	Operator Training Simulators	111
5.1.	Bioreactor 1 and 2	111
5.1.1.	Graphical user interfaces	111
5.1.2.	Energy demand and consumption materials . . .	114
5.2.	Cross-flow filtration	114
5.2.1.	Graphical user interfaces	114
5.2.2.	Energy demand	116
5.3.	Rectification	117
5.3.1.	Graphical user interfaces	117
5.3.2.	Energy demand	120
5.4.	Virtual Biorefinery	120
5.4.1.	Interface connection	120
5.4.2.	Specific production costs	121
6.	Simulation studies	123
6.1.	Cultivation	123
6.2.	Cross-flow filtration	126
6.3.	Rectification	130

6.4. Virtual biorefinery	136
6.4.1. Semi-continuous process	136
6.4.2. Continuous process	143
7. Discussion, conclusions and outlook	149
7.1. Discussion and conclusions	149
7.1.1. Method	149
7.1.2. Simulation results	150
7.2. Outlook	151
8. Abstract	153
Appendix	156
A. Appendix	157
A.1. Model parameters	157
A.1.1. Cross-flow filtration	157
A.1.2. Rectification	157
A.2. Cross-flow filtration block structures	158
A.3. Rectification source code	162
A.4. Technical description of the BioProcess Trainer	172
A.5. GRAFCET-plans	177
A.6. Virtual Biorefinery - connected in a continuous process .	181
A.7. Comparing efficiencies	185
A.8. P&ID flow chart of the biorefinery	185
A.9. Biorefinery process - tank volumes	187
Bibliography	189

Symbols

Latin Letters

A	area	m^2
AU	arbitrary unit	AU
C	costs	$AU \cdot unit^{-1}$
c	concentration	$g \cdot L^{-1}$
c_M	molar heat capacity	$J \cdot mol^{-1} \cdot K^{-1}$
c_P	specific heat capacity	$J \cdot kg^{-1} \cdot K^{-1}$
d	diameter	m
e	control error	<i>variable</i>
g	gravity acceleration	$m \cdot s^{-2}$
ΔH_V	heat of evaporation	$J \cdot mol^{-1}$
h	height	m
I	inhibition factor	-
k	heat transfer coefficient	$W \cdot m^{-2} \cdot K^{-1}$
k_{La}	oxygen transport coefficient	s^{-1}
G	control system gain	-
K_S	monod constant	$g \cdot s^{-1}$
\dot{L}	molar flow rate	$mol \cdot s^{-1}$
l	characteristic length	m
\dot{m}	mass flow rate	$kg \cdot s^{-1}$
M	molar weight	$g \cdot mol^{-1}$
m	mass	kg
\dot{n}	substance amount flow rate	$mol \cdot s^{-1}$
N	number	-
n	rotations per minute	min^{-1}
n	substance amount	mol
NC	number of components	-
P	power input	W
p	pressure	Pa
pO_2	dissolved oxygen	%
Δp_{TMP}	trans membrane pressure	Pa
q	specific rate	s^{-1}
Q	energy, heat	J
\dot{Q}	energy flow, heat flow	W

Q_R	heat of reaction	W
R	revenues	$AU \cdot unit^{-1}$
r	radius	m
r	revolution speed	min^{-1}
r	specific cake resistance	m^{-2}
RC	filter cake resistance	m^{-1}
RM	membrane resistance	m^{-1}
S	substrate	-
T	temperature	$^{\circ}C$
t	time	s
T_B	boiling temperature	$^{\circ}C$
t_D	effective dead time	s
t_I	reset time	s
u	reflux interval	s
\dot{V}	volumetric flow rate	$m^3 \cdot s^{-1}$
\dot{V}	vapour flow rate	$mol \cdot s^{-1}$
v	reflux ratio	-
V_{RV}	reflux valve	-
w	velocity	$m \cdot s^{-1}$
w_p	mass fraction	-
X	biomass	-
X	molar fraction in liquid	$mol \cdot mol^{-1}$
Y	molar fraction in vapour phase	$mol \cdot mol^{-1}$
Y	yield	-
Y'	non-ideal molar fraction in vapour phase	$mol \cdot mol^{-1}$

Greek Letters

α	heat transmission coefficient	$W \cdot m^{-2} \cdot K^{-1}$
η	dynamic viscosity	$N \cdot m \cdot s^{-1}$
η'	tray efficiency	-
λ	friction factor	-
ω	opening degree	%
ρ	density	$kg \cdot m^{-3}$
τ	time constant	s
ζ	standard normal distributed factor	-

Superscripts

0	in, inlet
---	-----------

1	out, outlet
<i>BM</i>	biomass
<i>EtOH</i>	ethanol
<i>G</i>	glucose
<i>N</i>	nitrogen source

Subscripts

0	reference
1	counter variable
2	counter variable
<i>a</i>	active
<i>C</i>	(filter) cake, cooling
<i>c</i>	channel
<i>D</i>	distillate
<i>deg</i>	degradation
<i>E</i>	ethanol
<i>F</i>	feed
<i>f</i>	filter
<i>H</i>	heater, heating jacket
<i>i</i>	inactive, inner
<i>j</i>	counter variable
<i>Lo</i>	losses
<i>M</i>	mantle, wall
<i>perm</i>	permeate
<i>pr.</i>	practical
<i>R</i>	reactor medium
<i>ret</i>	retentate
<i>S</i>	solution, substrate
<i>t</i>	transfer
<i>th.</i>	theoretical
<i>U</i>	surroundings
<i>v</i>	viable
<i>W</i>	water

1. Introduction

1.1. Motivation

In the last decades the scarcity of fossil fuels has led to an increasing demand of alternative synthesis pathways for energy resources. New technologies converting biogenic raw materials into energy carriers (biofuels) have evolved. Biodiesel and bioethanol as liquid, and biomethane as gaseous fuels are the most familiar representatives.

Bioethanol is produced by fermentation of sugars. The *first generation biofuels* were exclusively based on plant parts that could simultaneously be used as a nutrition source (sugar cane, corn, sugar beat, wheat). Due to the upcoming competition with the food processing industry, society insisted on more sustainable methods for producing energy fuels. The *second generation biofuels*, as a result of this rivalry, facilitated producing energy fuels from organic residues and less accessible substrates [Walker, 2011].

Worldwide governments promote the development of biofuels as a substitution for fossil fuels [Delucchi, 2010]. Bioethanol can substitute a certain amount of petrol used in cars (in Germany 5% : *E5*, 10% : *E10*, cp. Brazil 25% [Socol et al., 2010]), and by that contribute to the CO₂ reduction aims of the European Union (EU). Additionally, the EU Directive 2009/28/EG (renewable energy directive) [European Parliament and the EU, 2009] dictates to establish 10% of renewable energies in the automotive sector until the year 2020. Further (sustainability-) criteria in this directive specify that greenhouse gas emissions must be proven by the producers of biofuels, and that, compared to fossil fuels, savings of greenhouse gas emissions during the complete life cycle must reach 35% for new production sites from 2011, and existing facilities from 2013.

In order to be able reaching the given requisites from that directive, the question for a more economic, sustainable and efficient production of bioethanol has evolved. To a large extent the amount of CO₂-emissions in bioethanol production are connected with the efficiency of the overall process [Amigun et al., 2011]. As a biorefinery consists of several unit

operations, all individual members of the supply chain must undergo an efficiency analysis. However, it is also necessary to consider the effects of changes in single unit operations (up-stream, down-stream, utilities) on the overall system. While static analysis methods (short-cut) can be carried out for a first rough estimation of optimal process conditions [Bieker and Erdmann, 1990], more complex and comprehensive analysis methods are needed for automation and process control strategy optimisation. Such optimisation approaches cannot be tested in real plants, since the risk of maloperation and damages is too high. Also the danger of economical losses is too high when disturbing a running process.

A further aspect that has to be considered when thinking of process optimisation is that demands on operators' skills have greatly changed [Bergmann, 1999]. Operating complex processes today requires a very abstract way of thinking, due to the fact that process control systems (PCS) carry out the majority of those operations. In order to train operators in handling complex processes, Operator Training Simulators (OTS) are used. OTS represent an accurate copy of the real plant, including the process control system [Reinig et al., 2004]. Operation, not only of standard procedures, but also of emergency cases and abnormal situations, can be trained completely riskless [Yang et al., 2001]. Besides the training aspect, OTS also support engineering issues. For example, the automation system may be tested and optimized with the simulator before it comes to implementation in the real plant [Klatt, 2009]. This poses a major contribution to increasing efficiency: failures in the real plant are avoided and thus, damages to plant equipment or facility staff are excepted.

1.2. Aims

It seems obvious that the development of such complex operator training simulators involve high expenses, and thus high costs associated. This might be a reason why OTS are predominantly used in the petrochemical industry [Madhavan, 1984] or at power plants [Díaz et al., 2006], next to other fields like training for pilots (airplanes [Lee and Liu, 2003], ships [Murai et al., 2011]) and surgeons [Kneebone, 2003]. Operator training simulators for bio-technological processes are still rather rarely seen [Hass, 2005; Gerlach et al., 2013] and for biorefineries, however, not published yet, although several publications for process models exist. A facilitation in the approach of developing training simulators could open

the door for this discipline in biotechnological processes. Hence, the aims of this research work are as follows:

- provide a suitable framework for the development of Operator Training Simulators, that is applicable to different processes,
- application of this framework for establishing a realistic, interactive, full-scope training simulator for an ethanol biorefinery,
- the simulator shall comprise of the unit operations yeast cultivation, biomass separation with cross-flow filtration and ethanol purification in a rectification unit,
- the simulator shall be able to transparently demonstrate the influence of automation and process control strategies on the energy demand, and by this
- show, if plant operators have an influence on the efficiency of a bioethanol production process, and if so, to quantify this influence.

1.3. Outline of the work

There are functional and technical requirements resulting from the aims. The simulator must be able to allow for developing, applying, testing and evaluating different process control strategies. This requires process models that are valid throughout the complete operation from start-up until shut-down and that consist of a complete control and automation system. Furthermore, the models need to be fully dynamic, in order to be usable in a training simulator. Lastly, the OTS must show a behaviour that is qualitatively and quantitatively close to reality.

In order to reduce computation time, the biorefinery simulator shall be allocatable to different process tasks that can also be carried out on different personal computers, e. g. in a network. For this reason the simulator shall be distributed to three single OTS. A side effect would be that the simulators could also be used as stand-alone versions for answering questions in the respective processes.

New process models for the cross-flow filtration and rectification have to be developed. A part of this development process includes the development of plant components, as valves, tanks, heat exchangers and pumps. All these model parts have to be combined, together with the yeast cultivation, in order to build a virtual biorefinery. The cultivation simulator is

already available and used for educational purposes at Linköping University [Gerlach et al., 2013]. This simulator needs to be modified, so that it may be used in a combined process simulator like the biorefinery. The process models will be implemented into a suitable modeling environment, and finally into a process control system that consists of a simulator functionality.

With the realised virtual biorefinery different process control strategies shall be tested and evaluated with regard to energy efficiency. In the presented work the operator will be replaced by an automation system. Process sequences will be implemented in GRAFCET plans. By using the automated sequence control for process control strategy design, it can be ensured that the results received in tests are reproducible and do not include uncertainties produced by human error.

The present work is divided into eight sections. After this introducing chapter an overview of the current state of the art is given (chapter 2). Here the different biorefinery types are described and the bioethanol production, as modeled in this work, is shown. Furthermore, software tools for process modeling and simulation are introduced. Operator Training Simulators are then described in more detail, giving examples for the fields of application and the scope of functionality. At the end of this chapter a final recapitulation of the state of the art and a deduction of the scientific demand is outlined.

In chapter 3 the materials and methods that were applied are represented. In this context the general framework for OTS development is portrayed. The respective steps from the idea of a training simulator to its final application are described in the sections of this chapter. Also the software packages used for simulator development and the laboratory rectification column used for model validation are described here.

After the description of materials and methods, the process models will be exposed, including auxiliary components that are used in the processes, like pumps, valves and tanks. The unit operation process models are illustrated in a detailed way (yeast cultivation, cross-flow filtration and rectification; chapter 4). Chapter 5 introduces the training simulators and their functions. In the 6th chapter simulation studies are presented. These are discussed in chapter 7, where also an outlook for future work is given. The abstract of this thesis is provided in the 8th chapter.

2. State of the art

2.1. Biorefineries

A biorefinery is a plant, in which biomass is processed into different products [Kamm and Kamm, 2004]. On the one hand, these are for instance material products like food, dye, insulating materials or basic and fine chemicals for the chemical industry. These products are isolated from the raw material or produced by various chemical processes. On the other hand, the product can be energy in the form of fuels, electricity or heat [Brookman, 2010]. The concept of biorefineries with a holistic use of biomass is currently an object of research and development. In several fields of application this concept is already established, like in bioethanol and biodiesel production.

Generally, biorefineries may be divided into three different categories [Kamm and Kamm, 2004]. These are the *Whole Crop Biorefinery*, the *Green Biorefinery* and the *Ligno-cellulose Feedstock Biorefinery* (LCF). The *Whole Crop Biorefinery* uses raw materials such as cereals or maize as substrates. The *Green Biorefinery* converts naturally wet biomass like grass, lucerne or immature cereals. The *Lignocellulose Feedstock Biorefinery* (LCF) uses naturally dry raw materials, like cellulose-containing biomass or municipal solid waste.

While at the beginning of the last two decades the idea of converting whole crops like corn or wheat into energy carriers was absolutely fine, the upcoming competition to the food industry, and the aspect that actually food is used for energy purposes, led to a rethinking in society. The technology of converting difficultly accessible plant parts became prominent and the term of *Second Generation Biofuels* was born [Evans, 2008].

Nonetheless, by further processing and conversion of the whole crop many intermediate products can theoretically be generated in such a biorefinery (see figure 2.1). Kamm [2010] states that for various conversion steps the appropriate catalysts still have to be found.

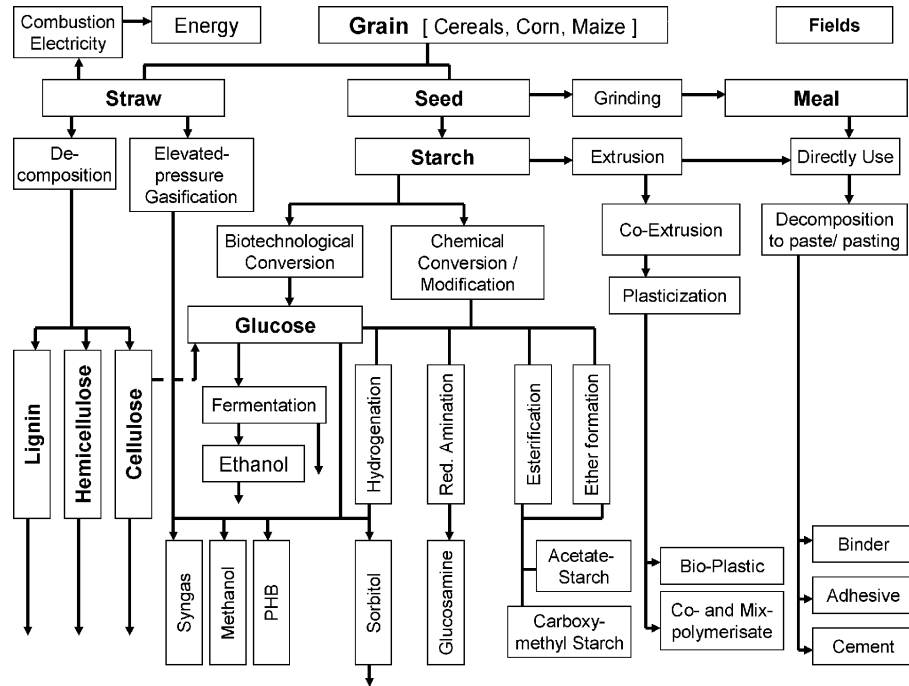


Figure 2.1.: Schematic of a *Whole Crop Biorefinery* [Kamm and Kamm, 2004].

The main focus nowadays lies on the LCF Biorefinery and the Green Biorefinery. The substrates used in these technologies are mainly residues or such, that are not used in any other way. The LCF Biorefinery (figure 2.2) uses the ingredients (lignin, cellulose, hemicellulose) of e.g. cereals, reed, wood, paper, as well as municipal solid waste. Next to a variety of basic chemicals (furfural, levulinic acids), which can substitute the respective petrochemical raw materials, glucoses can be produced. From these sugars several fermentation products like fuels (ethanol), organic acids (lactic acid) and solvents (acetone) can be extracted.

There are many papers dealing with the analysis of the optimal strategy for making all ingredients a valuable product [Liu, 2010; Toledano et al., 2010; Alriols et al., 2010; Cherubini, 2010]. Especially the pre-treatment (hydrolysis) of the feedstock plays an important role. The disadvantages of the technology are still the ineffective separation of cellulose, hemicellulose and lignin. A suitable method called organosolv (decomposition with ethanol/ water mixture) seems to be a very promising approach [Park et al., 2010; Quesada-Medina et al., 2010; Unkelbach et al., 2009].

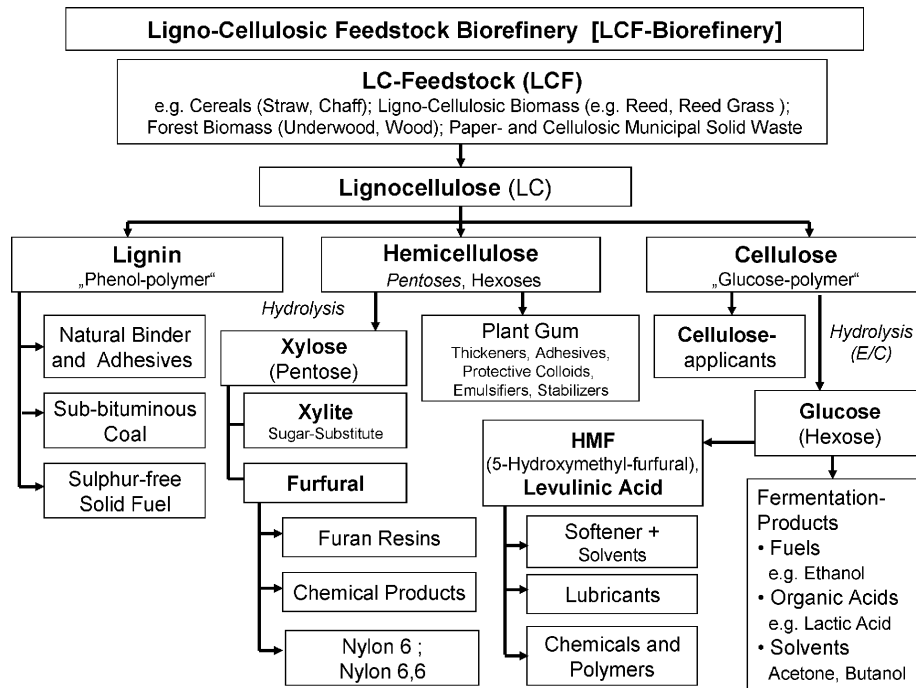


Figure 2.2.: Schematic of a *Lignocellulose Feedstock Biorefinery* (LCF) [Kamm and Kamm, 2004].

The second type of *sustainable* biorefineries - next to the LCF Biorefinery - is the Green Biorefinery, which uses green wet raw materials as substrates. Both the wet and dry fraction of the substrate contain valuable ingredients that can be used for a large spectrum of products. Grass for example contains many biologically usable ingredients and is available on approximately 600.000 ha of grassland in Germany. Grass is known as a provider of lactic acid, which is used for the production of bio-based plastics, like polylactide. One liter of pressed juice contains 80 grams of lactic acid, so that the extraction can be cost-effectively [Ulber, 2010].

A generalized and condensed schematic of conversion methods for biomass to different fuel types is given by Kaltschmitt [2007]. Here the different conversion paths are described in detail:

- thermo-chemical conversion
 - carbonisation
 - gasification
 - pyrolysis

- physico-chemical conversion
 - pressing/ extraction
 - trans esterification
- bio-chemical conversion
 - fermentation
 - anaerobic degradation
 - aerobic degradation

The results from these conversion paths are solid fuels (e.g. coal), gaseous fuels (product gas, pyrolysis gas) and liquid fuels (methyl ester, ethanol and biogas). In order to raise the efficiency of biorefinery processes, synergies are searched for so that several biorefineries are linked and intermediate or main products from one biorefinery are used in downstream processes, like Sieker [2010] demonstrates (integrated biorefinery). Today's focus definitely is to be laid on the optimisation through integration of biorefinery units, which are mainly operated by smaller or medium-sized enterprises (SME) [Hausberg, 2010].

Especially in integrated biorefineries, where recirculation of heat and mass flows occur, the energy demand is supposed to be highly dependent on the chosen process control strategy. Until now there are no published investigations, proving this assumption. This might be due to the fact that real processes may not be interrupted for scientific investigations. The risks for financial losses and damages to machines in the plant are simply too high.

2.2. Bioethanol

As it could be seen there are many ways of processing the different raw materials into valuable products. In this work the focus was laid on ethanol production. Ethanol production covers three different process types that are interesting for investigations concerning the operator's influence on energy demand.

In the cultivation process, e. g. the feeding strategy has a strong effect on the ethanol yield. The cross-flow filtration is very sensitive to process parameters, i. e. feed flow rate and trans membrane pressure, while the rectification is a very energy-intensive process. In all three sub-processes

there could be a high potential for raising the energy efficiency by optimisation of process control strategies.

2.2.1. Introduction

Ethanol became a very important component of the world's energy strategy after the oil crisis in the 70s, since it can act as a substitution for petrol in the automotive sector [Delucchi, 2010].

In context of the Kyoto Protocol, which forced the reduction of carbon-dioxide emissions, the utilisation of bio-based energy carriers became politically meaningful and many governments substituted several aspects dealing with biofuels, their usage and their production (e. g. EU Directive 2009/28/EG: renewable energy directive) [European Parliament and the EU, 2009].

This political commitment towards renewable energies, and in particular the production of biofuels based on nutrition feed stock (maize, wheat), gave reason to criticism (e. g. [Thompson and Meyer, 2013; Mohr and Raman, 2013]). In many parts of the world people do not have enough food to survive, while in other, wealthier parts of the world, food is used for taming energy needs.

In order to improve the standing of biofuels, different processing methods and different feedstock options became subject to research and development. The utilisation of lignocellulosic material, different plants and plant parts or even municipal waste, got into the focus of interest [Wang et al., 2013b; Bayrakci and Kocar, 2014; Pilavtepe et al., 2013; Alriols et al., 2010; Cherubini, 2010; Liu, 2010]. On the other hand there are no research efforts carried out dealing with the influence of process control strategies on the energy demand of such biorefinery processes.

2.2.2. Raw materials for ethanol production

Generally, bioethanol is produced by microbial fermentation of sugars. The type of sugar providing raw material depends on the region, where it is used. In South- and Latin-America e. g., mainly sugar cane is utilised [de Souza Ferreira Filho and Horridge, 2014], while in North-America corn is the predominant feedstock [Blanco and Isenhouer, 2010]. In Europe, on the other hand, wheat [Wang et al., 2013a] and sugar beet [Weinberg and Kaltschmitt, 2013] are the main plants used in ethanol

producing processes. Further plants are sweet sorghum [Molaverdi et al., 2013], triticale [Beauchet et al., 2013], algae [Yoon et al., 2012] and (soft and hard) wood [Gonzalez-Garcia et al., 2012].

All those mentioned substrates either provide already easy-accessible sugars directly (sugar beet, sugar cane) or in the form of starchy materials (corn stover, wood), which have to be processed prior to fermentation. At the same time the different plants consist of different components in different compositions. This again leads to varying ethanol yields, as shown by Walker [2011] for selected first generation crops (table 2.1). In Semencenko et al. [2013] different hybrids of corn were tested with respect to the ethanol yield which is dependent on the starch content in the plant.

Table 2.1.: Ethanol yield of some first-generation crops [Walker, 2011].

Crop	Ethanol yield ($t \cdot ha^{-1}$)
Sweet sorghum	4.0 - 6.5
Wheat	4.8
Sugar beet	3.3 - 3.8
Potato	2.0 - 2.9
Chicory	2.0 - 3.9
Jerusalem artichoke	4.0 - 4.7

There is a large variety of different raw materials that may be used for bioethanol production. These even differ within a given group (from one product line to the next), regarding the composition of sugars (or starches). This fact shows that there could be a demand to adapt the plant operation in order to achieve optimum operational conditions at varying substrate compositions.

2.2.3. Bioethanol processes

There are several bioethanol processes. On the one hand bioethanol may be converted from different sources (lignocellulosic biomass and sugar/starch). On the other hand the conversion process itself can vary. In the thermo-chemical conversion path biomass is converted to syngas, which is liquefied and synthesised to ethanol in a further processing step.

A further conversion path is the biochemical conversion with the help of microorganisms. These microorganisms (i. e. yeasts) metabolise glucose to biomass, energy and - under the absence of oxygen - ethanol.

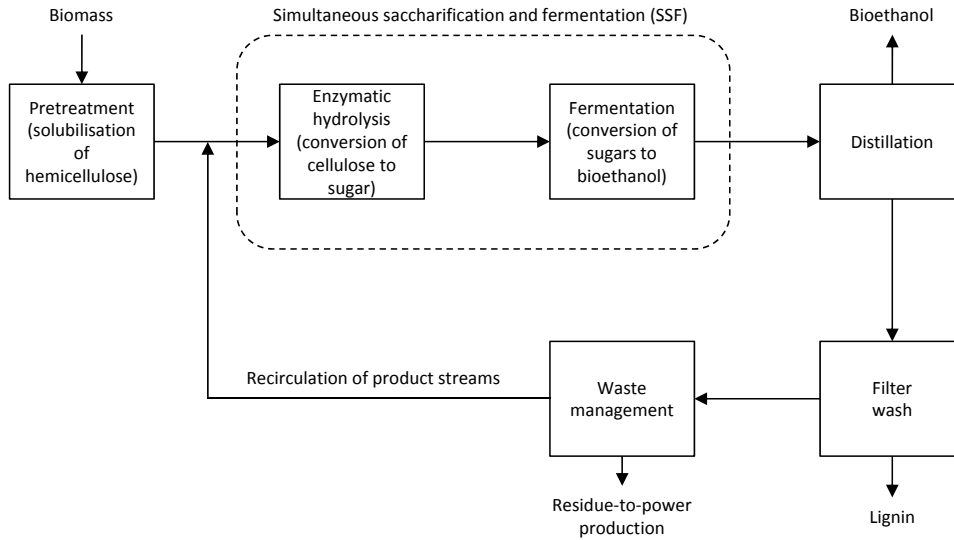


Figure 2.3.: Schematic flow sheet for the conversion of biomass to bioethanol [Balat et al., 2008].

A general scheme for the conversion of biomass to ethanol is given by Balat et al. [2008] (figure 2.3). Biomass is firstly pretreated with different techniques so that the hemicellulose gets solubilised. After this step the hemicellulose is converted into sugars (enzymatic hydrolysis), before the sugars are converted into ethanol and biomass in the cultivation process. The two latter steps can either be carried out simultaneously (Simultaneous saccharification and fermentation \rightarrow SSF) or these two steps are carried out consecutively.

In both process variants the mixture received by fermentation is passed on to a distillation or rectification unit, in which the ethanol is separated from the watery phase. Not shown in this figure is a further dehydration step in which the enriched bioethanol is dried, e. g. in molecular sieves, in order to receive a purity of $> 99\%$.

The residues in the rectification reboiler are then washed in a filter, in order to separate the lignin. A fraction of the product stream is continuously recirculated and fed back into the SSF step. In continuously

els. The user does not necessarily need to have skills in a programming language.

Flow sheet and balancing modeler are very often used in order to optimise existing processes, or to design planned processes. With the help of mass and energy balances that are implemented in unit operations (provided as pre-assembled blocks), the regarded process is modeled within a flow sheet. ASPEN Plus (ASPENTECH, <http://www.aspentech.com/products/aspentech.aspx>) is a simulation system that may be used for design, optimisation and performance monitoring. Its main fields of application are the chemical, polymer, specialty chemical, metals and minerals, and coal power industries.

In Götz et al. [2012] the simulation tool ASPEN Plus is used to analyse process parameter changes in a diethanolamine washing procedure of a biogas plant. The same tool was used for the investigation of optimal parameters in a syngas chemical looping process [Li et al., 2010].

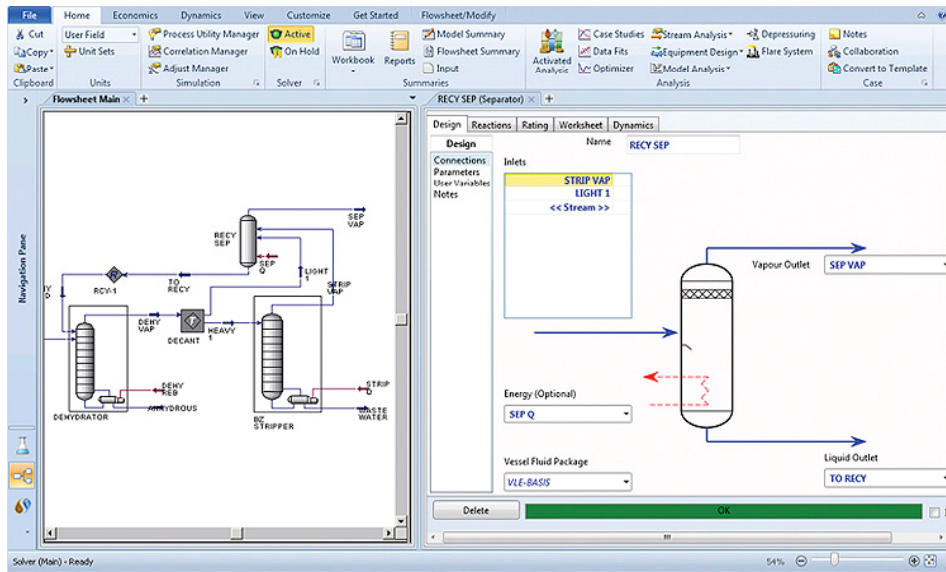


Figure 2.5.: Aspen HYSIS flow sheet modeling environment [ASPENTECH, <http://www.aspentech.com/products/aspentech.aspx>].

Another well-known and widely-spread software is HYSIS (also ASPENTECH, <http://www.aspentech.com/products/aspentech.aspx>). HYSIS (figure 2.5) is designed for steady-state, as well as for dynamic sim-

ulation of chemical processes. With the help of this software the productivity and reliability, as well as the profitability of a plant life cycle of a liquefied natural gas (LNG) process was improved [Ebenezer, 2005]. HYSIS was also used for design purposes in distillation [Bumbac et al., 2008; Ghaee et al., 2008] and biodiesel processes [Martinez et al., 2010].

gPROMS (PROCESS SYSTEMS ENTERPRISE LIMITED, <http://www.ps-enterprise.com/gproms.html>) is a further tool based on flow sheet modeling. It may be used for process modeling, optimisation and simulation purposes. Some examples for application are described for a polymerisation process [Jovic et al., 2013] and a crystallisation unit [Shaikh et al., 2013]. Generally this tool is used for modeling processes in the chemical and pharmaceutical industry.

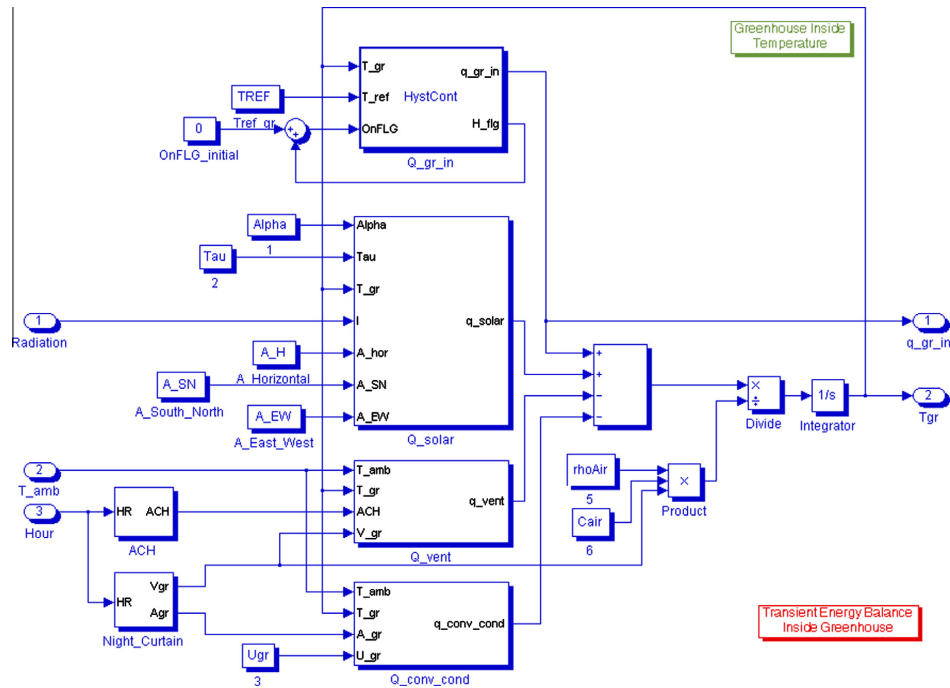


Figure 2.6.: Block structure for the calculation of heat flows and temperatures in a greenhouse, having a solar heating system [Kiyan et al., 2013], realised in MATLAB/ SIMULINK.

Next to the described modeling environments CHEMCAD is definitely to mention, since it is also a very famous representative of the flow sheet modelers. CHEMCAD (CHEMSTATIONS, INC., <http://www.chemstations.com/>) includes libraries for chemical components, and offers pos-

sibilities for controller tuning and process control. It was used for investigations regarding the dehydration of alcohols from dilute solutions [Vane and Alvarez, 2013], and also in batch-distillations in the food industry [Claus and Berglund, 2009].

A slightly different approach is followed with MATLAB. MATLAB is a programming language and an interactive environment for numerical calculations, visualisation and programming [Mathworks, 2013]. It can also be used for data analysis, development of algorithms and own models. These models may be integrated into SIMULINK, a graphical block diagram environment with which comprehensive systems may be realised. SIMULINK is an add-on for MATLAB. The block structure for an investigation regarding the temperature development in a greenhouse with MATLAB/ SIMULINK is shown in figure 2.6 [Kiyan et al., 2013].

A very comprehensive compilation of modeling and simulation tools, complementing the already mentioned ones here, and for different problems in process and chemical engineering issues is given in Lam et al. [2011].

2.4. Training simulators

While the previously described tools are predominantly used for process design and optimisation, a special group of simulation tools is represented by simulators that are primarily used for training and educational purposes. The following parts describe the different training simulator types and give an overview of the fields of application.

2.4.1. Training simulator classification

The scope of training simulators is distinguished in the way the process dynamics and the control system are realised. The degree of realism and the linked costs for the development of simulators have a certain dependency, as figure 2.7 shows. The more realistically the process dynamics are modeled, and the higher the degree of realism is, concerning the automation system and the graphical user interfaces, the higher the expenses for such a training simulator get.

According to Klatt [2009], simulators may be divided into

- Dynamic Simulation,

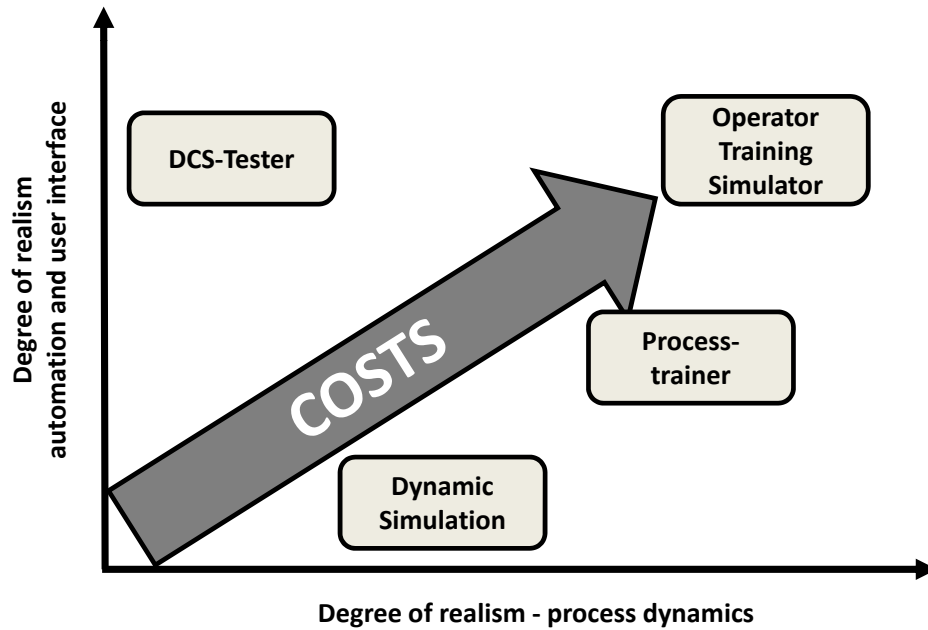


Figure 2.7.: Classification of training simulator types depending on the degree of realism of the process dynamics and the automation, respectively the graphical user interface (GUI) (according to [Klatt, 2009]).

- DCS-Tester (Distributed Control System),
- Process-trainers and
- Operator Training Simulators (OTS).

The dynamic simulation lacks operational and automation functions. Hence, this type cannot be seen as an actual training simulator. The dynamic simulation is often used in the design- and dimensioning-phase of processes.

DCS-Tester are used to test the automation system. Process behaviour is not rigorously modeled, but depicted by simple functional blocks. Regarding the automation, original software and user interfaces are employed. The DCS-Tester is the easiest and cheapest simulator type. Nevertheless, this type is very far away from simulating real process behaviour.

Process trainers consist of detailed dynamic models which represent the process mechanisms quite very well. Next to a rigorous description of

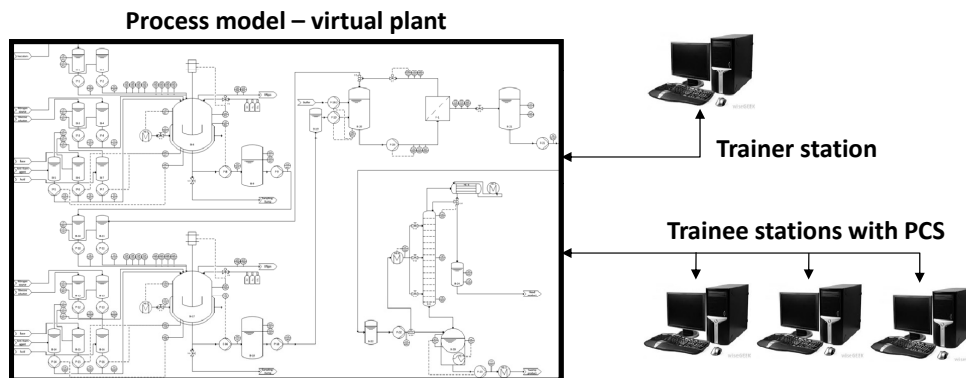


Figure 2.8.: Structure of Operator Training Simulators, according to [Klatt, 2009]. The virtual process (virtual plant) can be manipulated by the trainer. The trainees have to correct the introduced disturbances from the trainee station that looks and feels like the real PCS.

thermodynamics and kinetics of reactions, the geometric and isometric aspects of a machine (or a plant), basic pump data (or other components), information about pressure drop coefficients of valves and pipes, and velocities of actuators are taken into account [Klatt, 2009]. The functionality of the automation system is replicated with appropriate simplifications. Also, the user interface is reduced to the basic needs.

By implementing - next to the criteria of a process trainer - a one by one copy of the graphical user interface and of the automation system, as used in the real process, a full scope Operator Training Simulator is completed (figure 2.8). Only the OTS consists of all important components that are needed to investigate the operator's influence on the energy demand within a given process.

OTS are very often custom-made and represent a single given (or planned) process. Due to the complexity of such simulators, including the connection of a process control system (PCS), PCS-manufacturers are mainly producing OTS (ABB, Bilfinger Mauell GmbH, SIEMENS), next to special simulator developers (Bayer Technology Services, Honeywell, Rheinmetall Defence Electronics).

With their general appearance (graphical user interface) the OTS operation is carried out very intuitively, while for other simulation tools (as described in chapter 2.3) a certain program know-how is needed, before

a simulation can be run.

Table 2.2 lists the different simulator types and their specific scope of services. While the other simulator types are predominantly suited for specific tasks, the Operator Training Simulator covers the complete field of potential training and engineering functions. The OTS is the only simulator type, with which start-up/ shut-down procedures may be tested, and that thoroughly allows for developing and testing new process control strategies.

Table 2.2.: Scope of services of different simulator variants [Klatt, 2009].

Functions	OTS	Process trainer	DCS- Tester
Testing automation software	X	-	X
Development/ test of control strategies	X	O	O
Tuning of controller parameters	X	O	-
Training for experienced operators	X	X	O
Training for novice operators	X	X	O
Teaching PCS-handling	X	-	X
What if-scenarios	X	X	O
Start-up support/ troubleshooting	X	O	-

Despite their manifold fields of application, OTS basically consist of the following components:

- the process model,
- the field control station (FCS), and
- the control and observation stations.

When looking at the structure of modern process control systems, a further training simulator classification can be made. In figure 2.9 the different levels within a process control system (PCS) are shown. At the lowest level the process or the unit operations of a plant are located (plant-/process level). Via sensors and actuators (e. g. temperature measurements, valves), the process is connected to the control level of

single sub-units and aggregate (individual control level).

The next higher level is the group control level, in which aggregated sub-processes are controlled and coordinated. In the example shown in figure 2.9 each unit operation has an individual group control station. These group control stations are often located close to the real process, directly in field (\rightarrow field control stations: FCS). The uppermost level of the structure is the process control level. Here the complete process may be controlled and manipulated. For this purpose observation and control stations are installed (panels, personal computers).

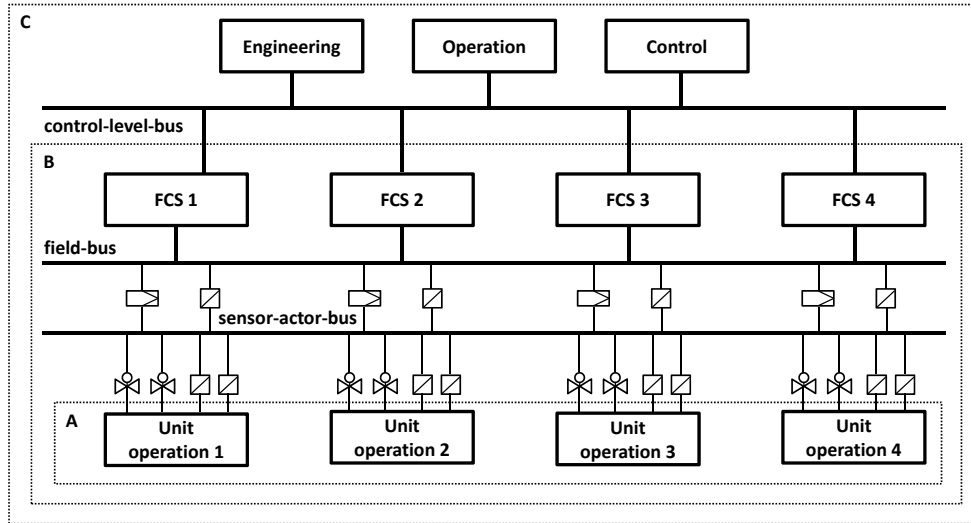


Figure 2.9.: Structure of process control systems according to Bergmann [1999] (slightly modified) and the classification of different simulator types to this structure with A: exclusive process simulation; B: process simulation together with simulation of field control stations (sensors and actuators); C: full-scope training simulator including the control and observation stations.

Regarding the utilisation options and the development complexity, Holl et al. [1995] suggest following classification, according to figure 2.9:

- A: the simulator stimulates the field control stations and the control and observation stations, i. e. only the very process is mapped by the simulator. In this case the simulator operation is carried out by the available process control system.

- B: the simulator only stimulates the control and observation stations of an already existing PCS, while the FCS are emulated by the simulator. The operation is carried out via the control system.
- C: the training simulator consists of all components, including an emulation of the control and observation stations (full scope training simulator).

In order to fully map the effects of different process control strategies on the energy demand, a full scope training simulator is needed. This type is the only simulator that can show the operator's influence, since it offers the same components as in the real plant.

2.4.2. Fields of application

Starting in the early 1990s, the application of training simulators rose due to different reasons, which are summarized by Reinig et al. [2004]. On the one hand the upcoming sensitivity for ecological and economical losses has increased drastically, and thus, the need for a more sustainable industrial responsibility has formed.

On the other hand the operation of industrial processes has changed as well. Due to integration of processes, plant-(facility-) operation has become more and more complex. The higher complexity entailed a higher degree of automation which caused new requirements to the operators' skills (see figure 2.10). At the beginning of the 20th century up to the early 40ies the plant operators had to perform all necessary functions of the process on their own and directly on-site.

With beginning of the middle of the century the processes were controlled with control panels in analogue technique. Still some functions had to be carried out by the operators on-site, but many of the functions were adopted by the automation system.

In modern control rooms today the operators are sitting in front of personal computers, controlling the process by clicking on symbols on their monitors, just like in a video game. In this context one has to consider that the process efficiency is - to a great extent - dependent on the decisions the operators make [Bergmann, 1999].

Modeling and simulation technology have a special meaning for Operator Training Simulators, since modeling itself is responsible for up to 50% of

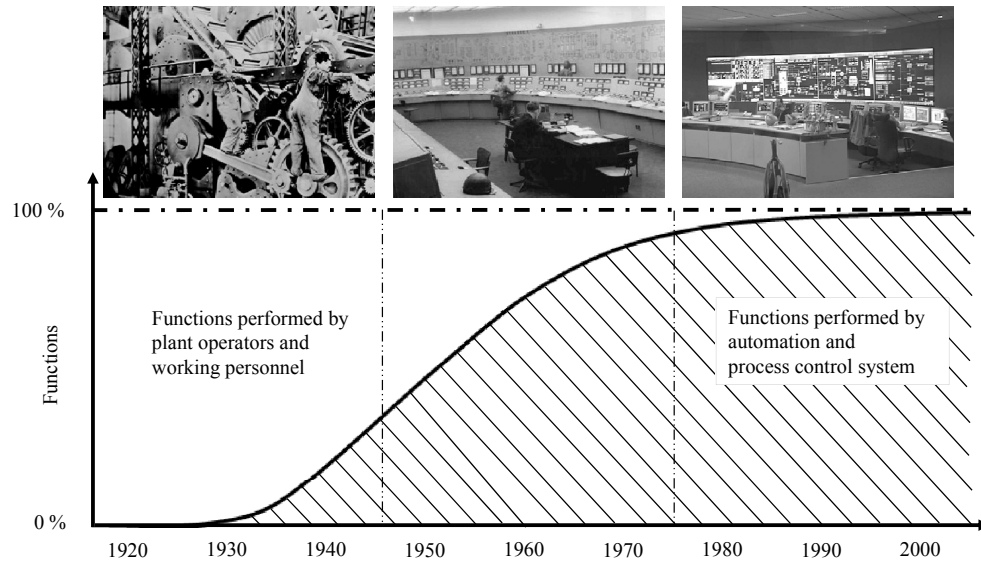


Figure 2.10.: Change of function distributing between plant operators and machine [Bergmann, 1999].

the total development costs [Kroll, 2003]. Hence, the goal should be to reduce these costs significantly. Nonetheless, the high expenses for developing process models and implementing them into a simulator software might be a reason, why OTS are currently predominantly deployed in the energy sector [Díaz et al., 2006], the petro-chemical industry [Madhavan, 1984] and for the training of pilots ([Lee and Liu, 2003], ships [Murai et al., 2011]) and surgeons [Kneebone, 2003].

Further, process industry-relevant examples have been subject to research in the last two decades ([Zhiyun et al., 2003]: fine chemical production, [Jayanthi et al., 2011; Park et al., 2004]: nuclear power plant, [Balaton et al., 2013]: batch-process, [Velez et al., 2013]: civil engineering). This shows the upcoming significance of Operator Training Simulators.

OTS are used to support the training of operators by demonstrating operational strategies of a process. Next to start-up and shut-down procedures and the correct operation mode in normal situations, the OTS can be used to train abnormal situations and cases of emergency. By this sort of issues approximately 10 to 20 billion US-\$ are lost annually in the process industry [Ogden-Swift, 2013]. Here, 40% are addressed to human error, as e. g. incorrectly adjusted controller parameters.

By ensuring real-time capability, the simulator may be used for testing and evaluating new controller parameters. This is a reason why OTS are also often applied in the training departments of companies and in universities [Birk, 1995; Feyo de Azevedo et al., 1994; Hoffmann, 2002; Liefeldt et al., 2002; Young et al., 2001].

A further important attribute of OTS is the consistency in the sequences of real and virtual process. This offers the opportunity for operators/trainees to interactively manipulate the running process and see the consequences of these measures directly. With this visual and direct demonstration the effects and phenomena can more easily be taught as compared to an abstract mathematical model.

2.5. Scientific demand

Process modeling and simulation is a very ambitious and constantly emerging sector in engineering today. The tasks that can be treated with these technologies are numerous and comprise for instance the design of new processes, as well as the optimisation of existing processes. At the same time simulators may be used for training and for educational purposes.

Operator Training Simulators have become more and more important for chemical and process engineering within the last decades, e. g. [Reinig et al., 2004; Schaich and Friedrich, 2003; Kroll, 2003]. The beneficial aspects of using Operator Training Simulators are numerous, as Blesgen [2009] summarizes:

- **Optimized operation at steady state:**

Prevention of negative or even harmful maloperation. This implies misuse of pumps, valves, motors and other aggregate which could lead to bursting pipes or the breakdown of complete technical sub-systems.

- **New process control strategies:**

The efficiency of a facility or a single production process is highly dependent on the chosen process control strategy. With an OTS a new strategy can first be tested on the computer without touching the real process and - by that - prevent the process from being run in an unproductive way.

- **Optimized control and controller set-up:**

Using the simulator for analysing the existing control strategy can detect weaknesses in the controller set-up. To find the optimal setting the OTS can be used in a first step. These measures can bring out an improvement of the control performance and thus, help reducing the energy demand of a process and furthermore protect the technical systems involved in the process.

- **Coping with disturbances:**

Disturbances or dangerous situations can occur in most of the regarded processes, especially in chemical engineering. These can lead to damages at technical devices, persons and the environment. While temporary failures primarily cause economical losings, disturbances of the machinery or the peripheral system often cause serious accidents. With OTS the personnel can be trained in coping with such disturbances and prevent from accidents.

- **Simulation of start-up and shut-down procedures:**

Start-up and shut-down of a plant always is a special situation for plant operators. In order to exactly know the sequence of these procedures, start-up and shut-down can be trained with the simulator. This, on the other hand, results in shorter starting times of operation which has positive effects on economic aspects.

- **To deepen the general understanding of the regarded processes:**

OTS offer a deep insight into participating sub-processes of the overall process for operating or planning personnel so that their awareness on the whole process and terms like energy saving or sustainability can be raised.

Today there are several providers for simulation software which are mainly focusing on the fields of chemical and process engineering, but there are only few that offer custom-made OTS for the environmental or biological technology [Hass, 2005; Gerlach et al., 2013].

A thorough literature research has revealed that especially those simulators are missing, which do not only cover the conversion processes (e.g. cultivation), but also include the up- and down-stream processing of the feedstock, respectively the products, and take account for the dynamic behaviour and the physical phenomena in such combined processes.

Today's optimising effort in bioethanol production is predominantly focused on the feedstock (choice of feedstock, different pretreatment methods, genetic manipulation through metabolic engineering), and the integration of processes, in order to reuse waste heat and water. The question of the influence exerted by the process operator is currently not subject of research.

Compared to chemical engineering processes, biological or environmental engineering processes are more unsteady due to varying and often changing qualities of substrates or microbial systems. The fact that these biological systems - like in a bioreactor - are very sensitive to the general environmental conditions, demands optimized process control strategies.

An inappropriate feeding rate of substrates e.g. leads to lower bioethanol yields. Moreover, the process control strategy and the process operation is strongly connected to the energy demand and thus, to process efficiency. With the help of an Operator Training Simulator following interesting scientific question shall be answered: does the chosen process control strategy have an influence on the energy demand of biorefinery processes?

3. Materials and methods

A systematical structure facilitates the development process. Hence, a general framework is introduced at first. This framework portrays all necessary steps to take from the idea and purpose of a training simulator up to its final application. The single elements of this framework are then discussed in the succeeding sections.

3.1. OTS development framework

For the present work a framework shown in figure 3.1 was used. At the very beginning the aims of the application have to be cleared. All following steps are carried out with respect to the formulation of the simulation aims. After the aims have been defined, the process that is to be modeled has to underlie an intensive process analysis which includes a functional description. Both, the defined objectives and the process analysis, influence all further steps in the development procedure [Blesgen and Hass, 2010].

The overall process then has to be split into appropriate sub-models. These sub-models may originate from different sources. Either own process models can be developed, or existing models from a model library, or already published mathematical process descriptions can be taken into consideration.

All these steps lead to one or more sub-models that have to be parameterised and verified, which demands suitable process data that can have different sources. Either real process data or experimental data from pilot- or lab-scale experiments can be used. If it should not be possible to perform adequate experiments, one might have to divert to published process data and literature values.

The sub-models are equipped with graphical user interfaces (GUI), control loops/ automation and a system for data monitoring and storage which finally results in an OTS.

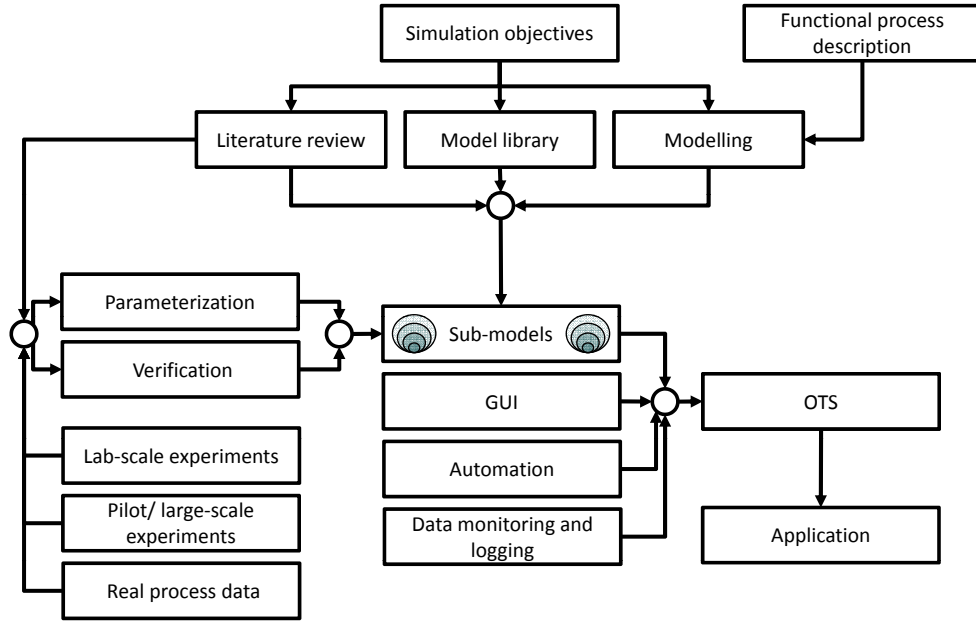


Figure 3.1.: Operator Training Simulator development framework, modified according to [Blesgen and Hass, 2010] (explanation see text).

3.2. Functional description of the bioethanol process

The reference process (figure 3.2, larger version in the Appendix) which is used for the investigation in this work is composed of two bioreactors, a cross-flow filtration unit and a rectification column. Cultivation is subdivided into an aerobic (biomass cultivation) and an anaerobic part (bioethanol production). Both operational modes can be carried out in both bioreactors (B-8 and B-17), this is why the two cultivation processes are identical.

The process starts with filling B-8 with the desired volume of water and substrates (glucose, nitrogen source, e. g. yeast extract), that is provided by tanks B-3 and B-4 and pumped via P-3 and P-4, respectively. When the desired volume is reached (indicated by level sensor LIRC-806), a sterilisation has to be carried out. For sterilisation the reactor media has to be heated to 121 °C for a predefined time (approx. 20 min). The temperature in the reactor is measured with temperature sensor TIRC-801 and controlled with valve V-2 that determines the incoming temperature of the heating oil from heat exchanger HE-1.

3.2. FUNCTIONAL DESCRIPTION OF THE BIOETHANOL PROCESS

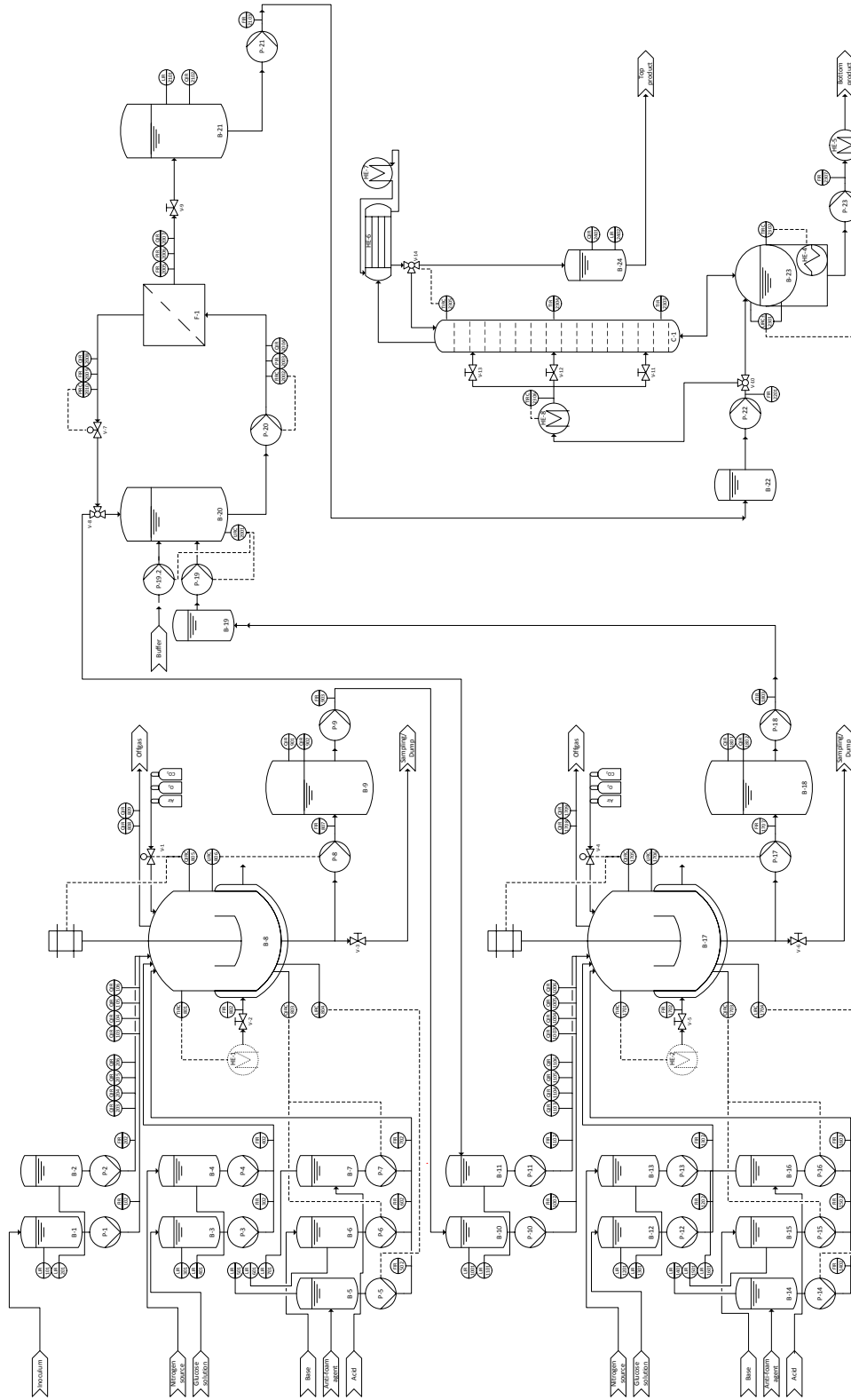


Figure 3.2.: P&ID diagram of the bioethanol process.

After sterilisation the reactor needs to be cooled down to process temperature (approx. 32-35 °C). After reaching process temperature, inoculum is added via B-1 and P-1. The inoculum contains yeast cells in a given concentration. Inoculum flow rate and concentration are indicated and registered by sensors FIR-102 and QIR-103. Tank B-2, pump P-2 and the sensors FIR-202, QIR-104 to QIR-106, and QIR-203 to QIR-206 are not in use in aerobic operation mode.

During cultivation pH is measured by a pH electrode (QIRC-803) that activates the pumps P-6 and P-7 which transport acid or base into the reactor. Both flow rates are indicated and registered with flow sensors (FIR-602, FIR-702). The foam level is measured with a level sensor LIRC-804, while pump P-5 conveys antifoam agent from B-5 to the bioreactor. The tank volume is measured via level sensor LIRC-806. Pump P-8 is used for controlling the level in tank. This pump brings the bioreactor broth to the product tank B-9. The control of dissolved oxygen takes place via electrode QIRC-805 and two actuators. The first, fast acting actuator is the stirrer, while the second actuator is the controllable aeration valve V-1.

Via valve V-3 samples can be taken. Offgas concentrations are indicated and registered with gas sensors QIR-808 (oxygen) and QIR-809 (carbon dioxide). When the desired concentration of biomass is produced, the bioreactor volume is pumped via P-8 to the product tank B-9. Concentrations of biomass (QIR-901) and ethanol (QIR-902) are measured in the tank. The product from B-9 is pumped (via P-9, indicated with FIR-903) further to tank B-10 in the second cultivation process, where it acts as inoculum. The second cultivation process generally mirrors the first cultivation process. Nonetheless, some differences have to be pointed out.

Since the bioethanol process is a continuous process, biomass - which is washed out together with the cultivation broth - has to be re-added. This is done via perfusion [Hass and Pörtner, 2011] in the cross-flow filtration unit that separates the cells from the liquid and feeds them to storage tank B-11. The flow rate of P-11 is indicated and registered with flow sensor FIR-1102. Feed concentrations of biomass (QIR-1103), ethanol (QIR-1104), glucose (QIR-1105) and nitrogen source (QIR-1106) are also indicated and registered.

Here the product from tank B-18 is pumped via P-18 (flow rate indicated by FIR-1803) to a buffer tank B-19 in the cross-flow filtration unit. From

this buffer tank pump P-19 conveys the broth into production tank B-20. Depending on the operational mode, level control in B-20 is carried out via level sensor LIRC-2001 and P-21 (diafiltration) or P-19 (continuous process). P-20 pumps the product into the filter unit F-1, in which the separation of the cultivation broth takes place. In continuous flow operation, FIRC-2002 and P-19 control the flow to the filter.

The concentrated retentate passes via a controllable valve V-7 and a further three-way-valve V-8 either back to the production tank, or to storage tank B-11. The retentate pressure behind the filter element (PIRC-2010) is controlled via V-7. The permeate (flow, pressure and concentration measured with FIR-2005, PIR-2006 and QIR-2007) passes via valve V-9 to the product tank B-21 in which the level (LIR-2101) and the ethanol concentration (QIR-2102) are indicated and registered.

The biomass-free water/ethanol-mixture is pumped via P-21 (indicated by flow sensor FIR-2103) to buffer tank B-22. From here the mixture is pumped via P-22 either to the reboiler B-23 (start-up phase), or via heat exchanger HE-8 and one of the valves V-11 (stage 4), V-12 (stage 8) or V-13 (stage 12) directly into the column C-1 (continuous operation). In HE-8 the mixture is heated up close to boiling temperature of the stage in which the feed shall be inserted.

The reboiler is heated by HE-4, which is also integrated into the heat control, for which temperature sensor TIRC-2302 is used. Level control in the reboiler is realised via level sensors LIRC \pm -2301 and pump P-23 (flow rate indicated with FIR-2307), that conveys the bottom product via HE-5 out of the process. When the mixture in the reboiler reaches boiling temperature, evaporation starts and vapour enters column C-1 at the bottom. Here, a temperature sensor is installed (TIR-2303). The vapour rises upwards the column, passing a temperature sensor in the center (TIR-2304) and top (TIRC-2305), before it leaves the column and enters the condenser (HE-6, fed with coolant from HE-7). Via TIRC-2305 and reflux valve V-14 the head temperature in the column is controlled.

The condensed distillate either flows back into the column or into product tank B-24, from which the head product can be taken. The level and the ethanol concentration of the product are indicated and registered with sensors QIR-2401 and LIR-2402.

The complex structure of the bioethanol process as shown in the P&ID diagram (figure 3.2) consists of single unit operations. The unit operations' functional descriptions were developed with different approaches. While the cultivation process was already available as a verified training simulator (BioProcess Trainer, [Hass, 2005; Gerlach et al., 2013]), the other processes still had to be developed. The cross-flow filtration and its operation had to be derived from screen shots and descriptions in an operating manual, while for the rectification process a laboratory plant could be used. All three principles are explained in the following sections.

3.2.1. Yeast cultivation

The cultivation process has already been modeled and implemented into an operator training simulator (OTS) that is currently used at HOCHSCHULE BREMEN for educational purposes (figure A.6). The BioProcess Trainer deals with training issues regarding ethanol production with *Saccharomyces cerevisiae*, and offers options to train process management, process automation and process regulation. The biological model implemented in the simulator (see section 4.2) was originally developed by Witte [1996], later extended to a process model, as described in Hass [2005], and finally enhanced by Gerlach et al. [2013] with additional model characteristics.

The cultivation process model used in the simulator was calibrated and verified (cp. chapter 4.2.5) with a laboratory bioreactor (BIOSTAT® C, manufactured and distributed by B.BRAUN BIOTECH GMBH, Melsungen). The comprehensive functional description of that laboratory plant is given in the operator manual [B. Braun Biotech International, 2000].

In order to get an overview of the functionality of this OTS, a functional description of an exemplary simulation is provided in the appendix A.4, published by S&H INGENIEURGESELLSCHAFT MBH, BREMEN [Kühn, 2012].

In figure 3.3 a typical example for a fed-batch cultivation with *Saccharomyces cerevisiae* is given [Gerlach et al., 2013]. After sterilisation (not shown here), the bioreactor is filled with an initialising substrate concentration (in this case $3 \text{ g} \cdot \text{L}^{-1}$) and the inoculum ($1 \text{ g} \cdot \text{L}^{-1}$). In the aerobic phase which persists for approximately 8.5 hours, the glucose is consumed. At the same time biomass is produced and also some ethanol

(crabtree-effect). After switching to anaerobic conditions (8.5 hours), a certain feeding strategy was chosen (indicated by the increasing glucose concentration). In the consequence less biomass and more ethanol is produced. In this example, the cultivation was terminated after 18 hours. The result of this experiment was an ethanol concentration of $60 \text{ g} \cdot \text{L}^{-1}$.

In this experiment two important process parameters are shown, influencing the result of the cultivation experiment. The switching time from aerobic to anaerobic conditions and the feeding rate of substrate, i. e. mainly glucose. The variation of these two parameters leads to different ethanol yields at the end of a batch-cultivation. Hence, an optimisation of process control strategies should be applicable.

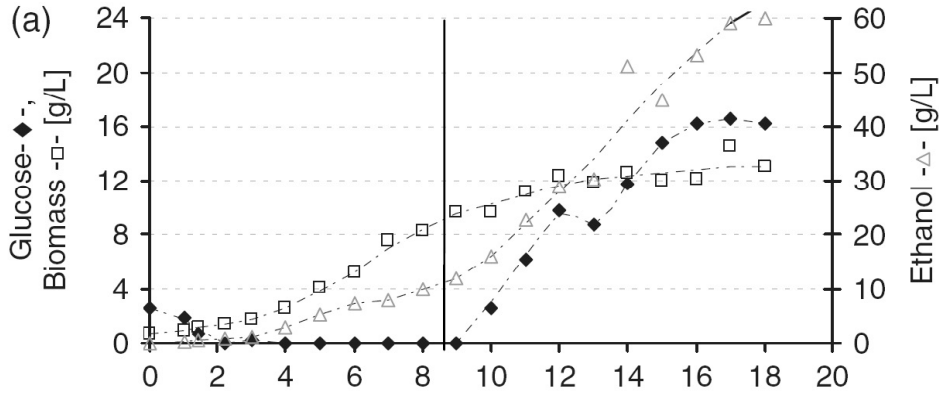


Figure 3.3.: Yeast cultivation experiment with *Saccharomyces cerevisiae*. The vertical line represents the switching time from aerobic to anaerobic conditions [Gerlach et al., 2013].

3.2.2. Cross-flow filtration

For the cross-flow filtration process a new model had to be developed. Its functionality was identified with an operating manual for an existing crossflow filtration system (SARTOFLOW® Study, SARTORIUS STEDIM BIOTECH GMBH, Göttingen, whom I would like to thank for the kind support) [Sartorius Stedim Biotech GmbH, 2012].

The screen shot of that particular laboratory plant shows all relevant sensors and actuators, like pumps, valves and measurements for flow, quality and pressure at the respective places within the process. Furthermore,

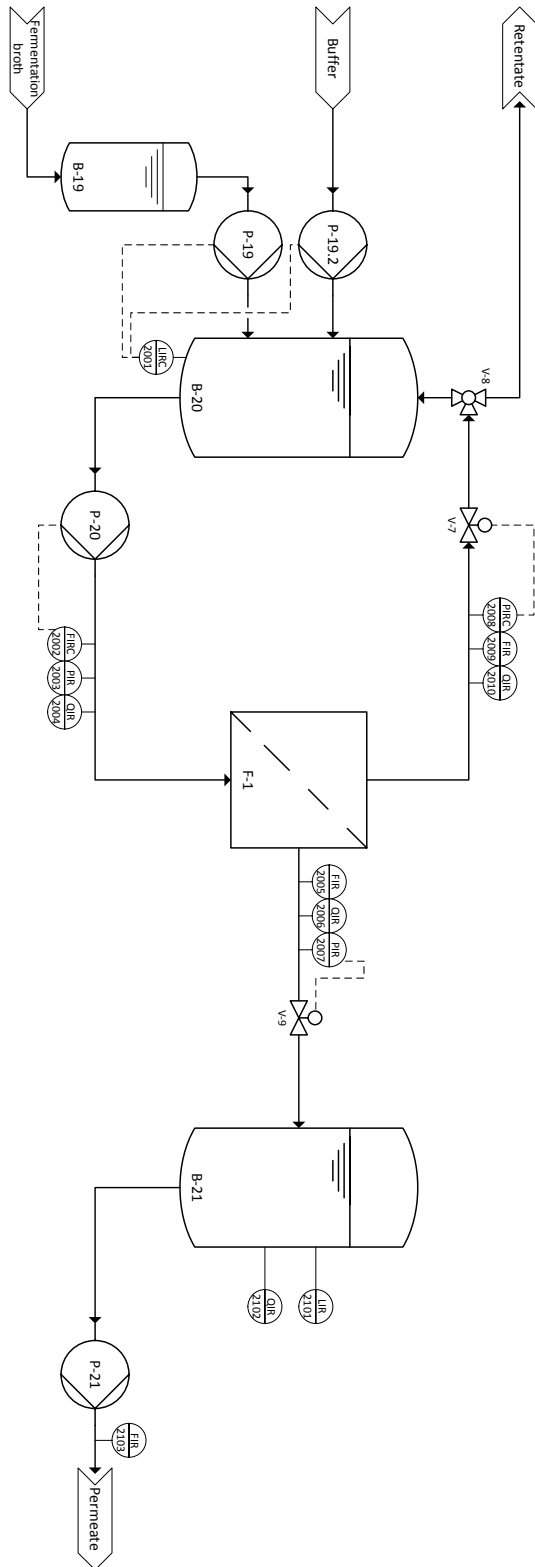


Figure 3.4.: P&ID flow chart of the cross-flow filtration process, according to the electronic panel of the laboratory cross-flow filtration unit SARTOFLOW® Study [Sartorius Stedim Biotech GmbH, 2012].

controller values are given. According to that screen shot a P&ID-flow chart of the cross-flow process was developed (figure 3.4).

The process starts with filling the tank B-20 with the solution to be separated via a pump P-19. The actual content in the tank is measured with a scale (LIRC-2001). Via pump P-20 the solution is pumped into the filter module F-1 which may consist of several packed filter units. Located in front of the filter, a pressure measurement shows the actual pressure at that place (PIR-2003). The retentate flows back to the tank, where it passes a controllable valve (V-7). This valve is used for pressure control. The permeate (filtrate) flows through another valve V-8 out of the system, or back into tank B-20. For the retentate, as well as for the permeate line, measurements for pressure (PIR-2007, PIRC2008), quality (QIR2006, QIR2010) and flow (FIRC2005, FIR2009) are installed.

In this system two pressure controls are indicated. One pressure control refers to the trans membrane pressure (Δp_{TMP}), while the second control refers to the pressure drop in the system (Δp). In both cases the controllable valve V-7 is used to keep the respective control parameters at a constant level. Due to process dynamics (blocking of filters, rising viscosity), the opening degree of that valve has to be adjusted, in order to receive constant control parameters.

An exemplary cross-flow process is shown in figure 3.5. The trans membrane pressure and the permeate flow rate are plotted as a function of process time. In the experiment the feed flow rate was controlled at a constant rate of $1560 \text{ mL} \cdot \text{min}^{-1}$. In the very beginning of the process the permeate flow rate is quite high, due to no filter cake existing on the membrane. After a while the permeate flow rate decreases (as a result of cake building). When the TMP was stepwise increased from 0.5 to 1.0 bar after 20 minutes, the permeate flow rate increased again. Finally it remained at approximately $65 \text{ mL} \cdot \text{min}^{-1}$. Towards the end the permeate flow rate decreased again which can be explained with the increasing viscosity from the concentration in the tank.

This experiment shows the dependency of the permeate flow rate, i. e. the velocity of the process, on process parameters like the trans membrane pressure (and also on the feed flow rate), or the viscosity. This leads to the conclusion that optimisation by process control strategy adjustment should be possible.

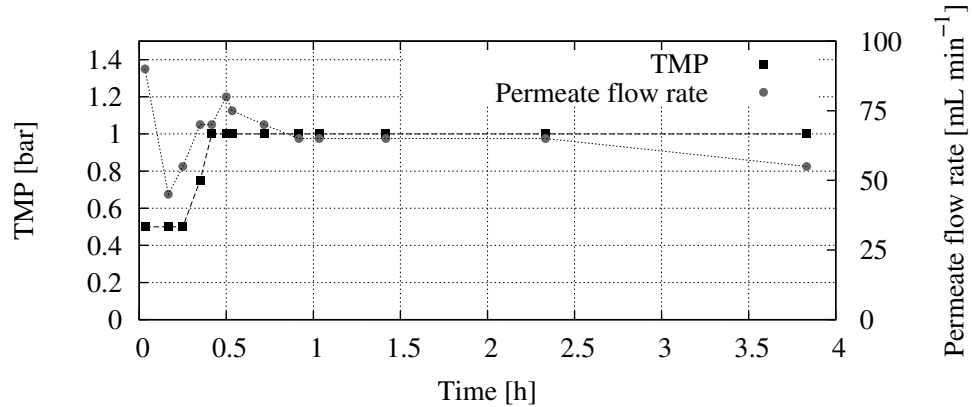


Figure 3.5.: Experimental data for a cross-flow process with yeasts (Sartoclon Slice 0.2 μm Hydrosart, $1560 \text{ mL} \cdot \text{min}^{-1}$). The TMP (black squares) and the permeate flow rate (gray circles) are plotted as a function of process time (further explanation see text).

3.2.3. Rectification

For the development, calibration and validation of the rectification process model a custom-made version of the *Multi-purpose rectification and extraction plant 6 L* manufactured by ILUDEST was used. The apparatus is a laboratory rectification and extraction plant which can be used both for batch and continuous rectification processes. The plant is suitable for thermal separation of liquid mixtures, whose compositions in the liquid, as well as in the gaseous phase, differ from each other in the temperature range from 0 °C to 180 °C.

The rectification plant includes a heated reboiler (6 L, 1.5 kW), a two-shot packed column (each 0.7 m, DN 50), a reflux condenser (0.3 m^2), a product cooler, and a product collector (6 L). From the still, between the two shots of the column and from the distillate samples can be taken. Samples were analysed with an ABBE refractometer (2WAJ, PCE DEUTSCHLAND GMBH). Temperatures are measured with Pt 100 temperature sensors in the reboiler, bottom of the column, between the column sections and in the head of the column. The temperatures are recorded with the process automation and control system WinErs (Version WinErs Professional 4.5.A). WinErs also enables the operator to adjust all actuating variables of the plant, as e. g. heating power and reflux ratio.

The functional description of the rectification plant refers to the P&ID flow chart illustrated in figure 3.7. The 6 L reboiler B-1 is filled via a filler plug with the mixture to be separated. During operation samples can be taken via the valve V-3, in order to determine the composition in the reboiler. The temperature measurement in the reboiler is carried out by the Pt 100 temperature sensor TIRC-1. The controllable valve V-1 is used for emptying the reboiler or for continuous extraction of bottom product.

A heating mantle is used for heating up the mixture. The mantle has a built-in temperature sensor for overtemperature protection and a switch for setting up the heating zones. The vapour rises from B-1 via the controllable three-way valve V-4 into the non-mirrored packed column C-1 (DN50) with two shots and vacuum jacket and condenses in the cooler HE-1. In C-1 there are 3 temperature measurements (column bottom TIR-2, between the two shots TIR-3, column head TIR-4). The manual valve V-5 between the column sections can be used for sampling during discontinuous mode, and as a feed inlet in continuous operation.

The differential pressure measurement between bottom and top of the column takes place via two pressure sensors, whose difference is aggregated in PDIR-1. The condensate flows via a reflux divider V-6 back to the column or into the distillate cooler HE-2, where the product is cooled, and further into the graduated pre-receiving tank B-3. Here again samples can be taken in order to determine the product composition. Finally, the product is released via the controllable valve V-7 to the 6L collecting container B-2. The collection container is emptied via the manual valve V-8 which can also be used for sampling. The cooler HE-1 is fed by the thermostat HE-3. For emptying the packed column the manual valve V-9 underneath the column is used. All technical characteristics are summarised in table 3.1.

A complete batch-rectification was carried out and the temperatures were measured continuously. The results are given in figure 3.6. After filling the reboiler and switching on the heater, the temperature in the reboiler starts rising. When the boiling temperature of the given mixture is reached, evaporation begins and the vapour enters the column. This effect may be seen at the increasing temperatures of the respective column positions.

The head temperature remains at a boiling temperature of approximately 78°C. This represents the boiling point of pure ethanol at atmospheric

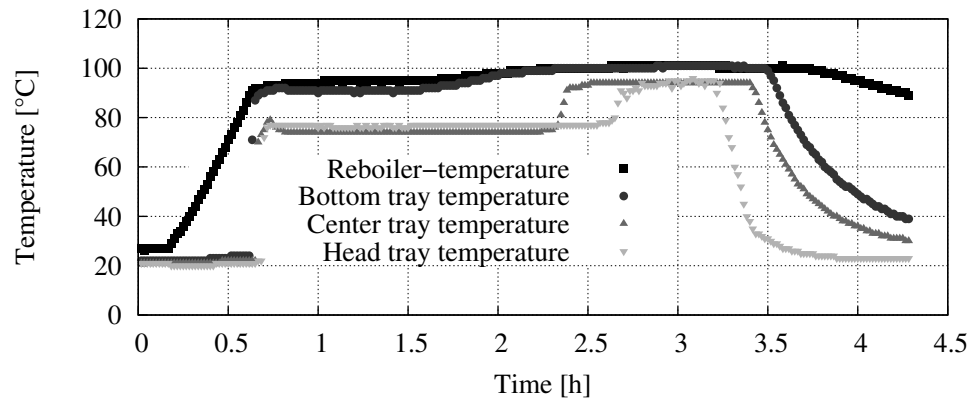


Figure 3.6.: Temperatures recorded during an experiment with the laboratory rectification column (own experimental results). Complete batch-rectification, explanation see text.

pressure. After 2.25 h the head temperature increases quite rapidly. At this point all of the ethanol has passed the column and the process may be stopped. All temperatures are slowly decreasing, due to cooling effects. The results of such an experiment are strongly connected to the heating input in the reboiler (evaporation rate, turbulence in the column), and to the chosen reflux ratio. An optimisation of these two parameters should lead to a reduction of the energy demand.

Table 3.1.: Components of the rectification plant and their specifications.

Components	Specifications
Basic materials	Borosilicate glass 3,3 / PTFE / PFA / stainless steel
Column K1	Packed column, borosilicate, DN 80/DN50 with vacuum jacket, ca. 0.7 m, 1 connection for temperature sensors per segment
Heater	Metal covered heating jacket 230 V / 50 Hz, 1,5 kW with two heating zones, integrated temperature sensor Pt100 for overtemperature protection
Reboiler	6 L vessel with connections for column DN80, a temperature sensor, switches for level
Continuation on next page	

Table 3.1 – continuation

Components	Specifications
	indication, sampling and filling via a notch with PTFE-covered silicone gasket, bottom valve
Connector	Steel-armored PTFE connector between the two column shots, with 3 connections for feed, a temperature sensor and sampling via a screw cap with PTFE-covered silicone gasket
Reflux separator	Reflux separator, borosilicate, DN50, consisting of two parts, both with vacuum jacket, upper part 80° arch with closed glass tube for uptake of the glass push rod with iron core, flanges DN80, lower part with connectors for temperature sensors and sampling via a screw cap with PTFE-covered silicone gasket and electronic ring magnet 24 V DC for lifting the push rod
Condenser	Spiral heat exchanger DN15, borosilicate, heat exchanger area 0.3 m^2 , horizontal layout, max. cooling fluid pressure 2 bar overpressure
Distillate cooler	Distillate bridge DN15, borosilicate, with Liebig cooler, exchanger surface 0.045 m^2 , connection for pressure equalisation
Pre-receiving tank	Anschütz-Thiele drum, borosilicate glass, ca. 0.25 L, calibrated, for determining distillate flow rate, with 3-way-valve
Product tank	6 L vessel with connections for product flow, aeration via a screw cap with PTFE-covered silicone gasket, with adjacent electromagnetic open/close valve

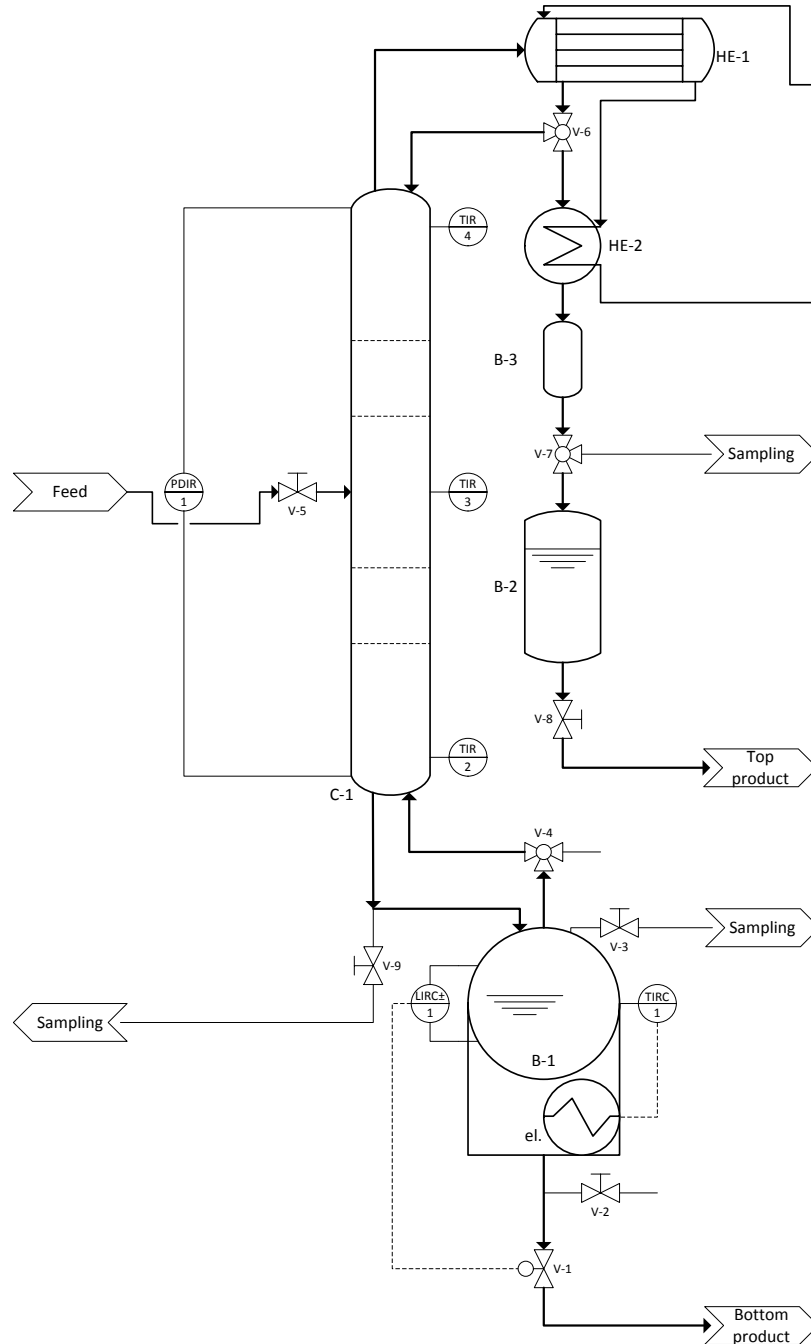


Figure 3.7.: P&ID flow chart of the laboratory rectification plant.

3.3. Process model structure and implementation

In order to organise the complex bioethanol process, an adequate modeling technique had to be found. Here, a shell structure that was applied to a biogas plant simulator earlier [Blesgen, 2009] was utilised. The biogas process was divided into a biological sub-model, a physico-chemical sub-model, a reactor sub-model and a surrounding plant- and peripherals sub-model. The sub-models were embedded in a shell structure.

For the bioethanol process used in this work, the shell structure was modified. The adaption of this method includes the changes shown in figure 3.8. The physico-chemical sub-model and biological sub-model were merged to a **kinetics sub-model**, in which (in the bioethanol process) the kinetics of a reaction, the conversion or equilibrium mechanisms are described.

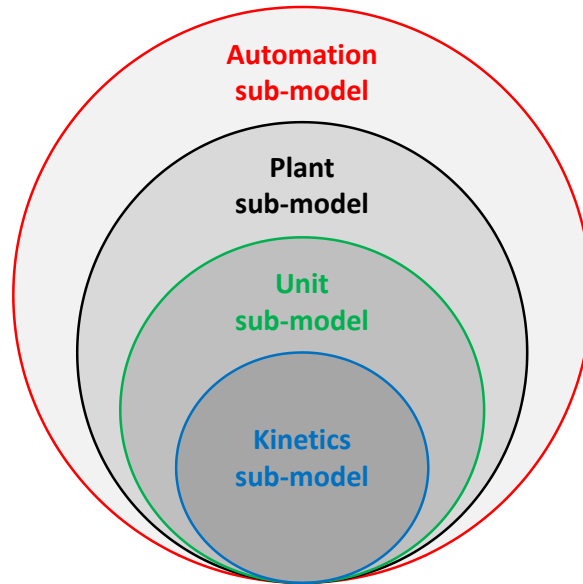


Figure 3.8.: Shell structure for a process models according to Blesgen [2009] with modifications described in the text.

The **unit sub-model** defines the space, in which the reaction, conversion or equilibrium kinetic takes place. Here these units are a reactor (fermenter), a filter in the cross-flow process and a theoretical stage or the reboiler in the rectification column. In this sub-model the material and energy balances are formulated.

The two innermost sub-models are wrapped by the **plant sub-model**. This sub-model consists of all components that complete the plant. These components contain valves, pumps, heat exchangers, tanks and sensors. In the outer shell, the **automation sub-model**, the control structures of a process are modeled. All realised control loops, as well as the automatic sequence control with GRAFCET are part of this sub-model.

The benefit of such a shell structure is that single components of the process model can easily be modified and adapted to changing boundary conditions or scientific questions. For the question that is to answer in the present work, the chosen model structure has some further advantages.

By breaking down the sub-models - from kinetics, via definition of control volumes, until the integration into a complete plant configuration with controls and automation - all necessary elements for creating an OTS are considered (see chapter 2.4.1). This model structure allows for investigating the influence of operator's intervention within a given process control strategy (predominantly carried out by the **automation sub-model**), while respecting the fundamental conversion or equilibrium correlations and the mass- and energy-balances of the system. The plant configuration stays untouched.

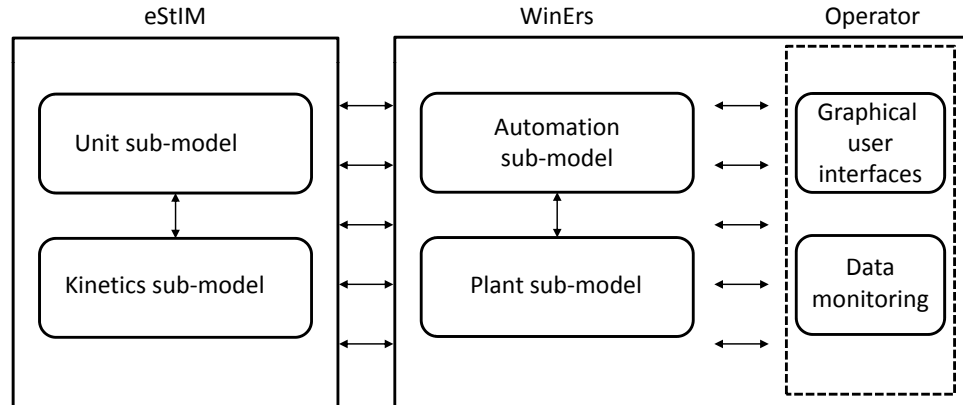


Figure 3.9.: Sub-model implementation using the software systems eStIM and WinErs. WinErs also provides the GUI and data monitoring.

Lastly, this structure is suited for implementation in the modeling and simulation tools that were used. The different sub-models were imple-

mented using two software tools as depicted in figure 3.9.

Since the formulation of kinetics and mass- and energy-balances is easy to carry out in text form, these two sub-models were implemented in eStIM, while plant configuration and automation were graphically implemented in WinErs.

3.4. Software tools used for OTS development

3.4.1. eStIM

The **kinetics sub-models** and **unit sub-models** are composed of systems of ordinary differential equations (ODE). As an instrument for the numeric solving and the identification of parameters and initial values the software eStIM is used [Witte, 1996; Kuhnén, 2008]. eStIM was first developed at the TECHNISCHE UNIVERSITÄT HAMBURG-HARBURG and afterwards enhanced at HOCHSCHULE BREMEN. The software combines several algorithms for solving systems of ODEs and the identification of parameters, which differ from each other regarding accuracy and speed (GEAR [Gear, 1971], DASSL [Petzold, 1982], Runge-Kutta [Butcher, 1987]). The genuine code was programmed in FORTRAN 77 and later on converted to FORTRAN 90 (including e.g. the permutation to double precision).

The model implementation is also text-based in the language FORTRAN. Parameters, initial values and time-dependently changing state variables (profiles) are provided in text files (control- and profile data files; Germ.: Steuer- und Profildateien: *.str, *.prf). The results of the calculation are provided in text files, too. Here, a differentiation between results of the ODEs (simulation value: *.sim) and any other output variable is made (intermediate value; Germ.: Zwischengröße: *.zwg).

The readily programmed sub-model of a process is then translated with a suitable compiler into an executable file (*.exe). At call of the executable file all initial values, parameters, profiles and the set-up of the solver are read from the parameter file. Depending on the solver algorithm (called from the INTERNATIONAL MATHEMATICAL AND STATISTICAL LIBRARY (IMSL)), the calculation takes place either with static or dynamic step size (see speed/ accuracy). The executable program can be used for test-

ing and validation of the described model.

Next to the executable file so called Dynamic Link Libraries (DLLs) can be compiled. These DLLs can be implemented into the process control and simulation program WinErs after successful validation (see following chapter 3.4.2). The combination of these two software tools facilitates the development of interactive process simulators considerably. The DLLs can be treated like a model library for unit operations.

3.4.2. WinErs

WinErs is a modular structured process automation system with integrated Soft-SPS, that can be used for process visualisation, control, simulation, monitoring, logging and as a complete process control system for personal computers (PCs), running MICROSOFT WINDOWS NT/ 2000/ XP/ VISTA/ 7/ 8. With the user-editable graphical user interfaces (GUIs), a complete observation and interaction of the running process is given. For data logging and storage individual storage options with memory cycles from 1 ms are available. Also comprehensive options for statistical and graphical analyses, variable depiction of measured data, on-line export of data and archiving are provided [Schoop, 2008].

The realisation of control mechanisms or algebraic correlations is carried out graphically in block structures and functional plans (figure 3.10). WinErs contains a large library with analogue and binary standard blocks (e.g. standard controllers P, I, PI, PID, switches, relays, etc.). These blocks can be combined with other controller algorithms, respectively among each other arbitrarily.

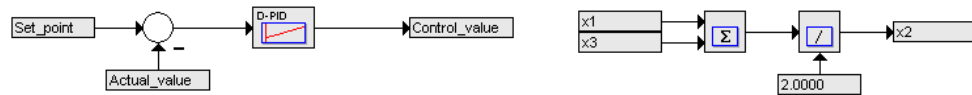


Figure 3.10.: Realisation of control mechanisms (left side) and algebraic correlations (right side) using WinErs block structures.

Further automation functions are sequence control with functional plans (GRAFCET, batch-recipes), fuzzy-controllers with graphical development environment, interface for own programmed algorithms (DLL-block) and

user-defined blocks for differential equations, a function generator and a program generator. Together with the 4th-order RUNGE-KUTTA-ALGORITHM with fixed step size, systems of coupled differential equations can be solved numerically [Schoop, 2008] and in real time, which is a prerequisite for Operator Training Simulators.

The coupling of FORTRAN-based source code and WinErs, i.e. the communication between different sub-models, takes place via the already mentioned DLL interface. The DLL can pass a specific range of state variables to WinErs, while in the opposite direction relevant state variables - calculated in WinErs - are passed backwards to the DLL (figure 3.11). In this work the **plant sub models** and the **automation sub-models** are implemented in WinErs.

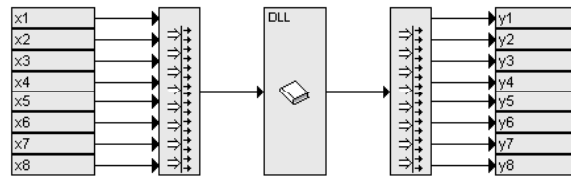


Figure 3.11.: Implementation of model source code (FORTRAN) via the DLL interface in WinErs.

3.4.3. GRAFCET

For process automation (automation sub-model) GRAFCET is used (**GRA**phe **F**onctionnel de **C**ommande **E**tapes/**T**ransitions) [Deutsches Institut für Normung DIN, 2002]. This normed functional plan is the successor of the *DIN 40719-6 functional plan* which was substituted in 2005. With GRAFCET the sequence of any process can be graphically described. The process control and simulation system WinErs allocates a GRAFCET editor that is directly connectable to any of the process model variables (sensors, actuators, parameters, time stamps), and which is compiled and translated into a control system. This offers the possibility to define process control strategies very easily and without an additional interface between simulator and automation system.

A GRAFCET-plan consists of steps, transition conditions and actions which are all connected with each other with functional lines [Gernaey

et al., 2000; Marichal and González, 2012]. The basic principle of a GRAFCET-plan may be described as follows:

- a plan is divided into steps and transitions, that alternate
- only one step may be active at a time
- any number of actions can be appended to a step
- the sequence may have branches (alternative or parallel)

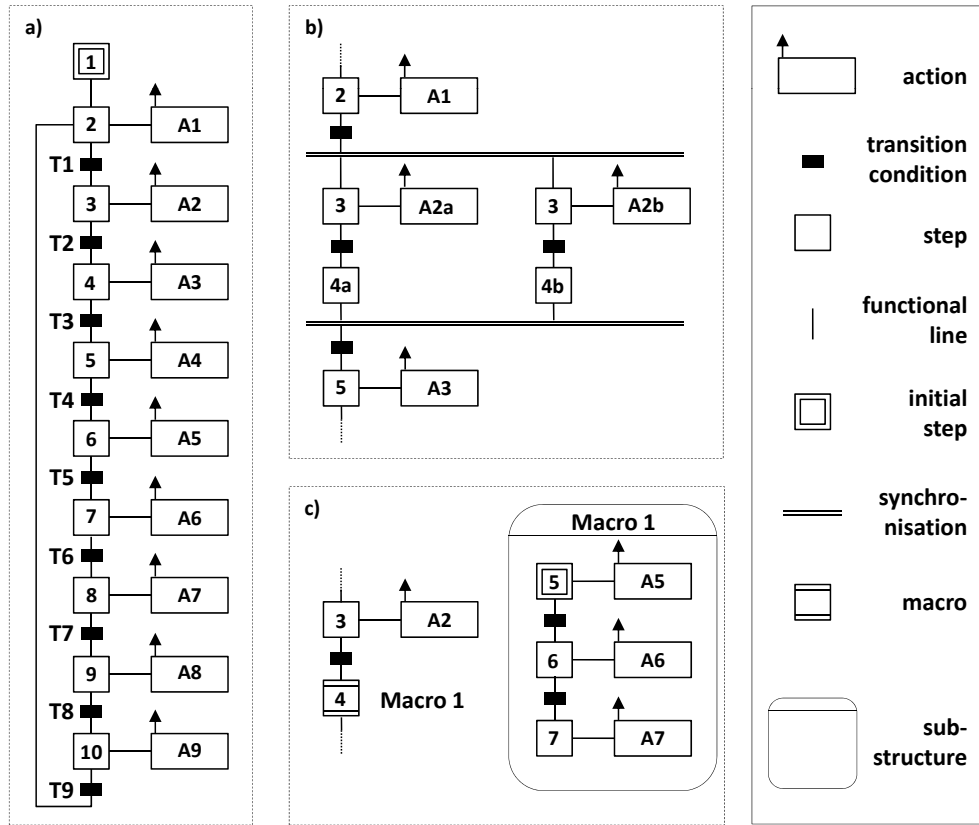


Figure 3.12.: Variants for linking the elements of a GRAFCET-plan. a) single-loop structure, b) parallel synchronisation, c) macro with sub-structure [Festo Didactic GmbH & Co. KG, Troisdorf, 2008]

In figure 3.12 the GRAFCET elements used in this work are illustrated. With the sequential execution of process-relevant actions GRAFCET is

perfectly suited for the automation of batch-processes [Gernaey et al., 2000].

3.4.4. AutoHotkey

AutoHotkey is a script-language which is freely available (<http://www.autohotkey.com/>). It is a tool with which the Windows user interface can be automated. In this work it was used to link graphical elements in the GUI of a training simulator to executable files, in order to open other training simulator executives. The tool also recognises, if a simulator is already running, and in such a case, just brings the respective simulator GUI to the front of the screen.

By this, it is achieved that operating different training simulators feels like operating just one training simulator. The script, as shown in figure 3.13, is translated into an executable file that can be called from the process control and simulation system.

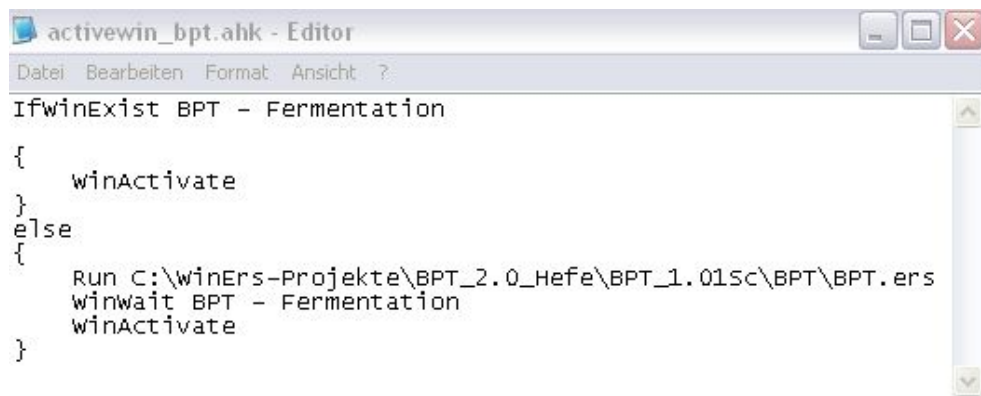


Figure 3.13.: AutoHotkey script that checks, if a simulator window is already opened. In case it is not, the respective program is started. Otherwise, the window is brought to the front of the screen. The script is translated into an executable which may be used in the simulator tool.

4. Mathematical description of the bioethanol process

The following chapter deals with the mathematical description of the bioethanol process, as introduced in chapter 3.2. At the beginning the additional models for auxiliary components in the plant are shown (tanks, valves, pumps, controller etc.). After this part the particular unit operation process models will be described individually. This section starts with the yeast cultivation, continues with the cross-flow filtration and closes with the rectification. Each process model will be described in terms of structure, mathematical buildup, and a validation of the mathematical model.

4.1. Auxiliary components

4.1.1. Valves

Standard valves

Regarding the whole process there are several valves of different types. Standard valves (figure 4.1) are modeled as binary systems without reaction time. These valves can either be opened (1) or closed (0).



Figure 4.1.: P&ID flow chart symbol for standard valves.

$$V = \begin{cases} \text{opened, if} & V = 1 \\ \text{closed, if} & V = 0 \end{cases} \quad (4.1)$$

Three-way-valves

In three-way-valves (figure 4.2) the flow direction of a certain fluid is defined. This type of valve can either lead the flow into one direction

(valve= 1), or into the other direction (valve= 0). A special version of the three-way-valve is the controlled three-way-valve which works in the rectification process as a reflux separator.

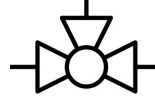


Figure 4.2.: P&ID flow chart symbol for three-way-valves.

$$V = \begin{cases} \text{left outlet opened, if} & V = 1 \\ \text{right outlet opened, if} & V = 0 \end{cases} \quad (4.2)$$

Reflux valve

The reflux valve (V_{RV}) is a hydraulic push rod that can either be opened (1) or closed (0). In order to compute a reflux ratio, time needs to be used as an auxiliary quantity.

The reflux valve is working in manual and automatic mode. In automatic mode the valve is further operable in controlled mode. The manual mode is initialized via a signal $V_{RV,set}$. In this mode the operator manually sets the valve. The automatic mode (initialized via a signal $V_{RV,auto}$) activates an algorithm which calculates the reflux ratio in the following way:

$$V_{RV} = \begin{cases} \text{opened (1), if} & \text{mod}(t, u) < \frac{u}{1+v} \\ \text{closed (0), if} & \text{mod}(t, u) \geq \frac{u}{1+v} \end{cases} \quad (4.3)$$

Parameter u describes the reflux interval that defines a period of time (e. g. 60 s). Parameter v is the reflux ratio that is realised within the reflux interval (u). A combination of $u = 60$ s and $v = 5$ opens the reflux valve for 10 seconds (production) while for the next 50 s it is closed (reflux). Decreasing the reflux interval causes the switching frequency to increase. Figure 4.3 represents switching frequencies of the reflux valve with different combinations of reflux interval and reflux ratio.

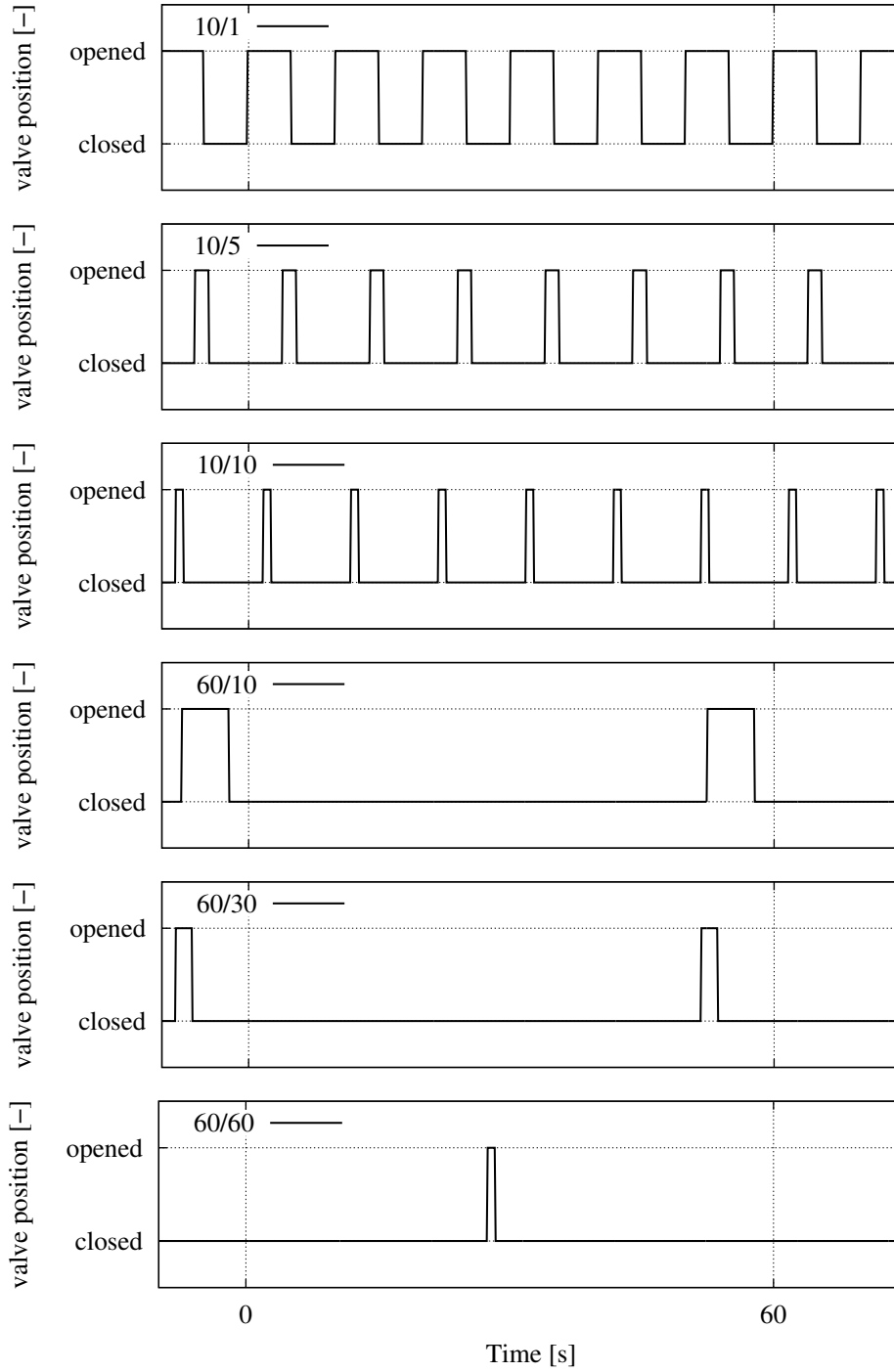


Figure 4.3.: Switching frequencies of the reflux valve at different combinations of reflux interval (u) and reflux ratio (v) given as u/v .

Control valves

Control valves (figure 4.4) are used for influencing a desired control variable by opening or closing the valve (flow rate, pressure, level). This sort of valve can be opened in the range of 0% (opened) to 99% (closed). By multiplying the opening degree (ω) with the input flow rate, the output flow rate may be received (V^*):

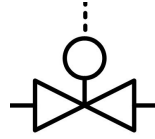


Figure 4.4.: P&ID flow chart symbol for control valves.

$$\dot{V}^* = \dot{V} \cdot \omega_{\text{valve}} \quad (4.4)$$

4.1.2. Pumps

The pumps (figure 4.5) in the cultivation process were modeled as the valves, mentioned before. The flow rates can be adjusted manually. The dynamic behaviour of pumps in the other processes, on the other hand, was modeled with a non-oscillating PT_2 -system as described in Bergmann [1999]. The time constants τ_1 , τ_2 and the system gain G may be adjusted, so that the start-up process of the pump is simulated, according to a real pump. The desired flow rate ($V^0(t)$) is given into the PT_2 -system which computes the real flow rate ($V^1(t)$) (equation 4.5). The qualitative step response of such a PT_2 -system is shown in figure 4.6.

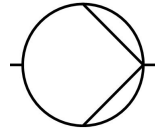


Figure 4.5.: P&ID flow chart symbol for pumps.

$$\tau_1 \cdot \tau_2 \cdot \ddot{V}^0(t) + (\tau_1 + \tau_2) \cdot \dot{V}^0(t) + V^0(t) = G \cdot V^1(t) \quad (4.5)$$

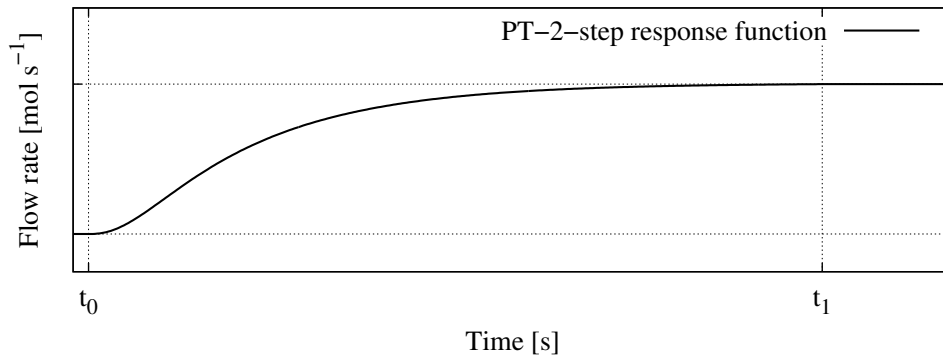


Figure 4.6.: Dynamic behaviour of a pump, modeled as a PT_2 -system, according to Bergmann [1999].

4.1.3. Tanks

The tanks (figure 4.7) used in the bioethanol process are mainly applied for storage purposes. There are receiving tanks, product tanks, buffer tanks, substrate tanks and utility tanks. In all these tanks changes of volume and concentrations are calculated. The tanks are considered to be ideally mixed control volumes which cause the effluent concentrations to be identical with those in the tank. Further, a tank may have various inlets, but it always has got only one effluent flow. All flows can have a variable number of components, whose concentrations are given together with the flows (figure 4.8).

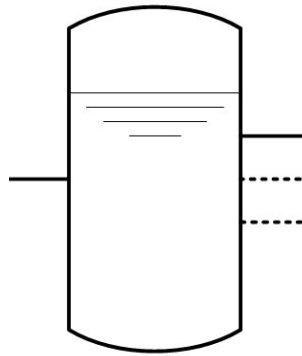


Figure 4.7.: P&ID flow chart symbol for tanks.

The volume change in such a tank is the sum of all feed flows (number of feeds: NF) minus the outlet flow:

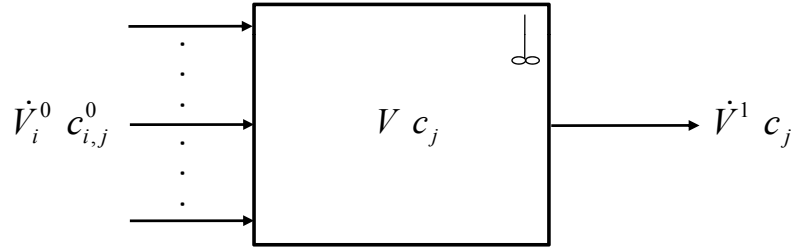


Figure 4.8.: Tank model realised as an ideally mixed tank. The tank may have a various feeds, but always one outlet.

$$\frac{dV}{dt} = \sum_{i=1}^{NF} \dot{V}_i^0 - \dot{V}^1 \quad (4.6)$$

The concentration change of one component (j) in a tank is expressed as:

$$\frac{dc_j}{dt} = \underbrace{\frac{\dot{V}_i^0 \cdot c_{i,j}^0}{V}}_{\text{input flows}} - \underbrace{\frac{\dot{V}^1 \cdot c_j}{V}}_{\text{ouput flow}} - \underbrace{\frac{c_j}{V} \cdot \frac{dV}{dt}}_{\text{dilution}} \quad \forall j = 1 \dots NC \quad (4.7)$$

The concentration is influenced by all input flows with the regarding concentrations, the output flow with the actual concentration, and a dilution term that considers the volumetric changes in the tank. Inserting equation 4.6 in equation 4.7 gives following result:

$$\frac{dc_j}{dt} = \underbrace{\frac{\dot{V}_i^0 \cdot c_{i,j}^0}{V}}_{\text{input flows}} - \underbrace{\frac{\dot{V}^1 \cdot c_j}{V}}_{\text{ouput flow}} - \underbrace{\frac{c_j \cdot \left(\sum_{i=1}^{NF} \dot{V}_i^0 - \dot{V}^1 \right)}{V}}_{\text{dilution}} \quad \forall j = 1 \dots NC \quad (4.8)$$

The ideally mixed tank causes the effluent concentration to be the same as the actual concentration in the tank, so some cancellations may be applied. After rearranging the equation gets [Witte, 1996]:

$$\frac{dc_j}{dt} = \frac{c_{i,j}^0 \cdot \dot{V}_i^0 - c_j \cdot \sum_{i=1}^{NF} \dot{V}_i^0}{V} \quad \forall j = 1 \dots NC \quad (4.9)$$

4.1.4. Heat exchangers

In the bioethanol process there are two different types of heat exchangers that were modeled. One type is a heat exchanger without phase change, while the other heat exchanger includes phase change (condensation).

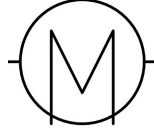


Figure 4.9.: P&ID flow chart symbol for heat exchangers.

Heat exchanger without phase change

Heat exchangers without phase change are modeled as a cascade of ideally mixed tanks (figure 4.10), according to Epple et al. [2009]. In the upper section of an ideally mixed tank the feed flows from the left side to the right side with its temperatures ($T_F(j)$), flows ($\dot{n}_F(j)$) and energies ($\dot{Q}_F(j)$). In the lower section the heating fluid ($T_F(j)$, $\dot{n}_F(j)$, $\dot{Q}_F(j)$) is handed in from the right side to the left.

By this means a counter-current heat exchanger is modeled. The heating fluid transfers heat to the feed through a separating wall ($\dot{Q}_t(j)$). Heat losses to the surroundings ($\dot{Q}_{Lo}(j)$) are considered at the outer shell of the heat exchanger.

In order to keep the model simple, changes of amounts of substances were neglected and given as a fixed value:

$$\frac{dn_F}{dt} = 0.00 \quad (4.10)$$

$$\frac{dn_H}{dt} = 0.00 \quad (4.11)$$

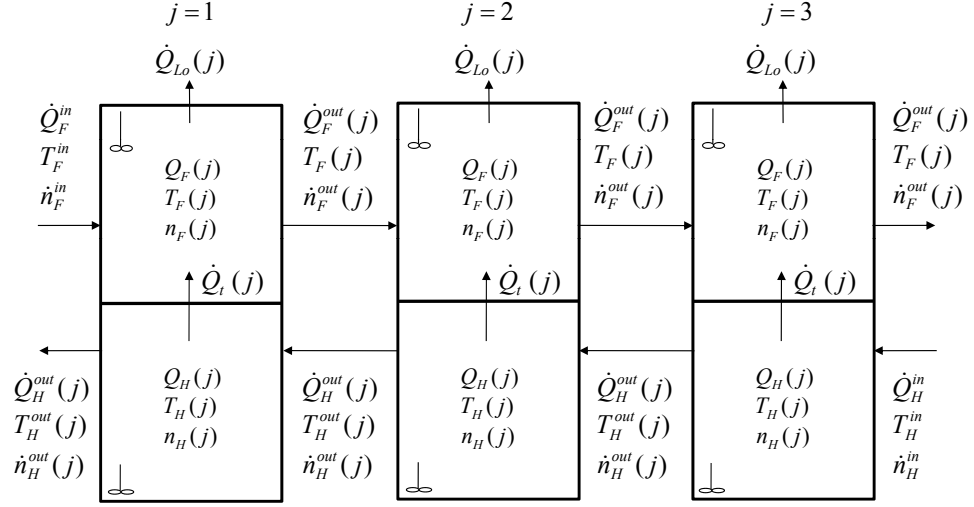


Figure 4.10.: Model of a segmented heat exchanger with 3 segments. In the upper part of each mixed tank the feed is lead, while the heating fluid is lead through the lower part and in the opposite direction.

The energy balance for both fluids in the first cascade element ($j = 1$) is written as:

$$\frac{dQ_F(1)}{dt} = \dot{Q}_F^{in} - \dot{Q}_F^{out}(1) + \dot{Q}_t(1) \quad (4.12)$$

$$\frac{dQ_H(1)}{dt} = \dot{Q}_H^{out}(2) - \dot{Q}_H^{out}(1) - \dot{Q}_t(1) - \dot{Q}_{Lo}(1) \quad (4.13)$$

The energy contents are:

$$Q_F(1) = n_F(1) \cdot c_{M,F} \cdot (T_F(1) - T_0) \quad (4.14)$$

$$Q_H(1) = n_H(1) \cdot c_{M,H} \cdot (T_H(1) - T_0) \quad (4.15)$$

So the differential equations for both compartments can be formulated:

$$\frac{dT_F(1)}{dt} = \frac{\dot{Q}_F^0 - \dot{Q}_F^1(1) + \dot{Q}_t(1)}{n_F(1) \cdot c_{p,F}} \quad (4.16)$$

$$\frac{dT_H(1)}{dt} = \frac{\dot{Q}_H^1(2) - \dot{Q}_H^1(1) - \dot{Q}_t(1) - \dot{Q}_{Lo}(1)}{n_H(1) \cdot c_{p,H}} \quad (4.17)$$

All convective energy flows ($\dot{Q}_F^*(j), \dot{Q}_H^*(j)$) are modeled in the form:

$$\dot{Q}_{F,H}^*(j) = \dot{n}_{F,H}^*(j) \cdot c_{p,F,H} \cdot (T_{F,H}(j) - T_0) \quad (4.18)$$

The heat transfer through the separating wall is:

$$\dot{Q}_t(j) = k_t \cdot A_t(j) \cdot (T_H(j) - T_F(j)) \quad (4.19)$$

And the heat losses:

$$\dot{Q}_{Lo}(j) = k_{Lo} \cdot A_{Lo}(j) \cdot (T_H(j) - T_U) \quad (4.20)$$

Figure 4.11 shows the temperatures of the two fluids across the heat exchanger surface area in stationary condition.

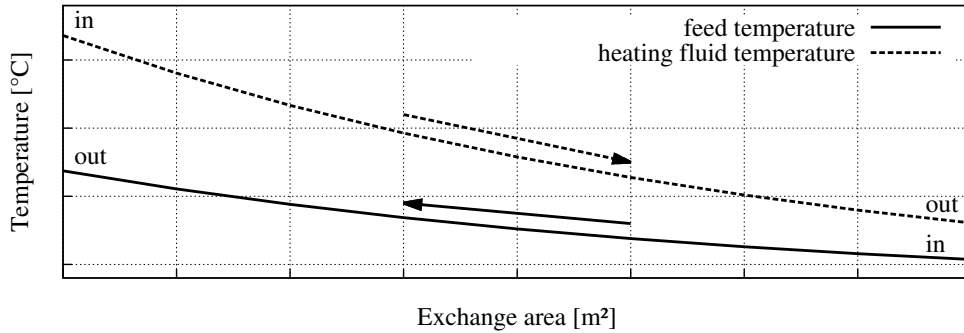


Figure 4.11.: Temperatures of two fluids in a counter-current heat exchanger, as shown e. g. in [Vauck and Müller, 2000].

Condenser

In order to save computing time the condenser for the rectification process was modeled with some simplifications (figure 4.12). The energy needed to cool down the entering vapour to a given (liquid) temperature is calculated. Furthermore, it is assumed that the condensation process takes place immediately.

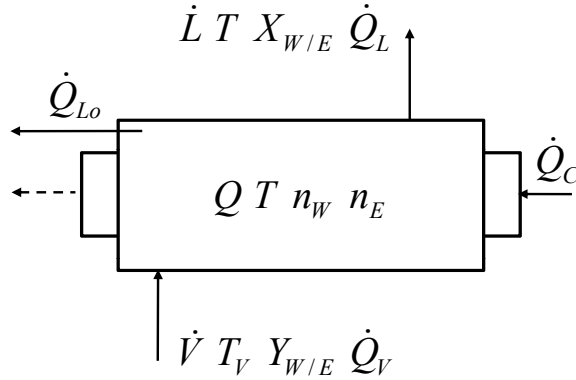


Figure 4.12.: Condenser model. Vapour entering the aggregate is totally condensed. \dot{Q}_c represents the "cooling energy flux", which is assumed to be equivalent to the condensation enthalpy, which is set free by the condensation process.

In order to receive a continuous and dynamic reflux runoff from the condenser (\dot{L}), Torricelli's law was applied [Bohl, 2002]. It is assumed that a certain hold-up is generated in the condenser. In this hold-up space the amounts of substances (n_W, n_E) are increased by the entering vapour (\dot{V}) and decreased by the condensed effluent distillate:

$$\frac{dn_{W/E}}{dt} = \dot{V}(j) \cdot Y_{W/E}(j) - \dot{D} \cdot X_{W/E} \quad (4.21)$$

From the amounts of substances the molar fractions of ethanol and water in the condensate are obtained:

$$X_E = \frac{n_E}{n_E + n_W} \quad (4.22)$$

$$X_W = 1 - X_E \quad (4.23)$$

The height (h_C) of this hold-up can be calculated and thus, by giving a dimension for the reflux void, the condensate flow rate (\dot{L}) is given as:

$$h_C = \frac{\frac{n_W \cdot M_W}{\rho_W} + \frac{n_E \cdot M_E}{\rho_E}}{\pi \cdot r_1^2} \quad (4.24)$$

$$w = \sqrt{2 \cdot g \cdot h_C} \quad (4.25)$$

$$\dot{L} = w \cdot \pi \cdot r_2^2 \cdot \left(\frac{\rho_W}{M_W \cdot X_W} + \frac{\rho_E}{M_E \cdot X_E} \right) \quad (4.26)$$

The condensate flow rate is the result of the flow velocity (w), a surface area ($\pi \cdot r_2^2$) and the respective substance fractions (reconversion from $m^3 \cdot s^{-1}$ to $mol \cdot s^{-1}$).

The energy balance for the condenser results from the energy input from the vapour ($\dot{Q}_V(j-1)$), the energy amount needed for the withdrawal of heat (\dot{Q}_C), a heat loss through the condenser wall (\dot{Q}_{Lo}), and the convective energy flow of the distillate (\dot{Q}_D):

$$\frac{dQ}{dt} = \dot{Q}_V + \dot{Q}_C - \dot{Q}_{Lo} - \dot{Q}_L \quad (4.27)$$

The heat content of the control volume is given as the product of amounts of substances (n_W, n_E), their specific molar heat capacities ($c_{m,W}, c_{m,E}$) and the temperature difference ($T - T_0$):

$$Q = (n_W \cdot c_{m,W} + n_E \cdot c_{m,E}) \cdot (T - T_0) \quad (4.28)$$

Hence, the temperature change is expressed as:

$$\frac{dT}{dt} = \frac{\dot{Q}_V + \dot{Q}_C - \dot{Q}_{Lo} - \dot{Q}_L}{n_W \cdot c_{m,W} + n_E \cdot c_{m,E}} \quad (4.29)$$

Convective heat flows are written as the product of amount of substance flow, specific molar heat capacities and temperature difference (liquid) or heat of evaporation (gaseous):

$$\dot{Q}_L = \dot{L} \cdot (T - T_0) \cdot (X_W \cdot c_{m,W} + X_E \cdot c_{m,E}) \quad (4.30)$$

$$\dot{Q}_V = \dot{V} \cdot (Y_W \cdot \Delta H_{V,W} + Y_E \cdot \Delta H_{V,E}) \quad (4.31)$$

Heat loss is defined as heat transfer through a wall (with/without insulation):

$$\dot{Q}_{Lo} = k_{Lo} \cdot A_{Lo} \cdot (T - T_U) \quad (4.32)$$

The dissipated heat needed for total condensation is calculated as the enthalpy difference between vapour ($\Delta H_{V,W}(T), \Delta H_{V,E}(T)$) and liquid flow at set point temperature ($\Delta H_{V,W}(wT), \Delta H_{V,E}(wT)$):

$$\begin{aligned} \dot{Q}_C = Y_W \cdot (\Delta H_{V,W}(T) - \Delta H_{V,W}(wT)) \\ + Y_E \cdot (\Delta H_{V,E}(T) - \Delta H_{V,E}(wT)) \end{aligned} \quad (4.33)$$

4.1.5. Sensors

Two different types of sensors (figure 4.13) are implemented in the bio-ethanol process. The temperature sensor TIRC-801, the pH sensor QIRC-803, the level sensor for foam LIRC-804, the sensor for dissolved oxygen QIRC-805, the level sensor LIRC-806, and the offgas sensors QIR-808 and QIR-809 are all modeled with a normal distribution noise on the calculated values and a delay time, realised with a first order differential equation element (PT_1 element).

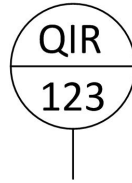


Figure 4.13.: P&ID flow chart symbol for sensors.

This is done by multiplication of the calculated value ($T^0(t)$) with a time-dependent random value ($\zeta(t)$) and a first order differential equation, describing the step response of a PT_1 system, where τ is time constant and G is the system gain.

$$T^0(t) \cdot (\tau_1 \cdot \dot{T}^0(t) + \zeta(t)) = G \cdot T^1(t) \quad (4.34)$$

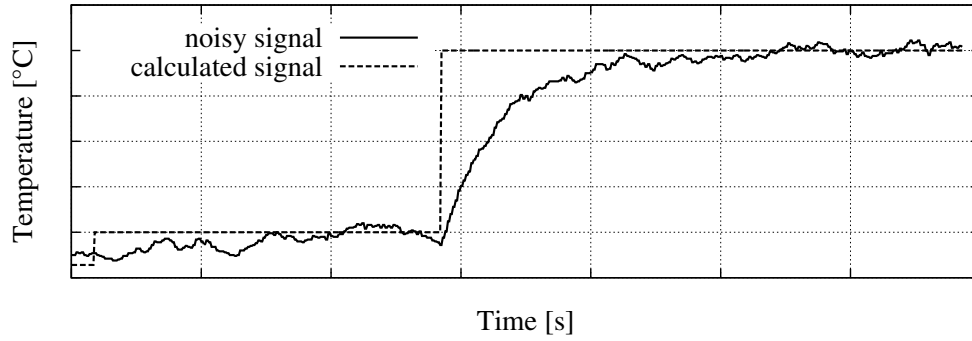


Figure 4.14.: Noise and step response behaviour (PT_1 -system) of a temperature sensor.

The measurement instrumentation for all temperature sensors in the rectification process (TIRC-2302, TIR-2303, TIR-2304, TIRC-2305, TIRC-2306) is modeled with a standard normal distribution noise on the calculated values.

$$T^1(t) = T^0(t) \cdot \zeta(t) \quad (4.35)$$

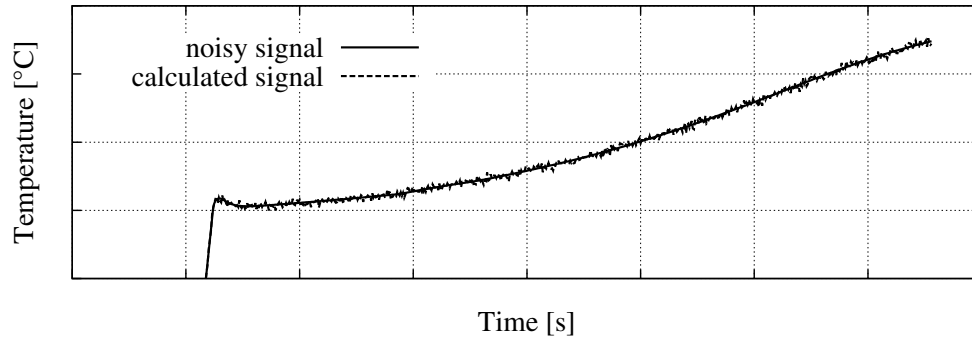


Figure 4.15.: Noise of a temperature sensor.

4.1.6. Controllers

All controllers deployed in the bioethanol process are either PID- or PI-controllers. A PID-controller is defined by following equation [Corriou, 2004]:

$$u(t) = G \left[e(t) + \frac{1}{t_I} \int_0^t e(\tau) d\tau + t_D \frac{d}{dt} e(t) \right] \quad (4.36)$$

The actuating variable of a PID-controller ($u(t)$) results from a proportional element (P) that is composed of the controller gain (G) and the control error ($e(t)$), an integral element (I), with the reset time (t_I), and the differential element (D) with the effective reaction time (t_D) as important parameters [Corriou, 2004].

By setting $t_D = 0.0$ in equation 4.36 a PI-controller is obtained. A PID-controller is included in the toolbox of the process control system and can therefore easily be used for the tasks of this work.

4.2. Yeast cultivation

The cultivation process model used here was originally developed by Witte [1996], later extended to a process model by Hass [2005] and lastly enhanced by Gerlach et al. [2013], adding specific model characteristics.

The yeast cultivation model is organised in a shell structure, as shown in figure 3.8. For the investigations carried out in this thesis, the existing process model was further enhanced. The **kinetics sub-model** stayed untouched. In order to integrate the simulator into a biorefinery process, the **unit sub-model** had to be modified. The mass and energy balances had to be expanded by the respective terms for additional feed streams (from cross-flow filtration).

The **plant sub-model** was also enhanced with the respective pumps and tanks needed between the single unit operations. The (buffer) tanks are important, since these act as the interfaces in the connected biorefinery (chapter 5.4).

The **automation sub-model** was developed completely new. In this sub-model the mechanisms for designing process control strategies are included. This is an elementary part of this work, since the energy efficiency investigations are carried out with respect to process control strategies.

The adaption of the model structure to the cultivation process is depicted in the P&ID flow chart shown in figure 4.16. The single elements of the model structure will be described in the following sections.

4.2.1. Kinetics sub-model

The innermost sub-model represents the biological part of the cultivation process. This model describes the different metabolic pathways within the yeast cells from substrate uptake to product, biomass and energy formation (figure 4.17). This includes e. g. growth on glucose and nitrogen, diauxic growth, and maintenance metabolism [Gerlach et al., 2013].

In this model the rate-limiting factor for metabolism in the cells is the uptake rate of substrate (q_S). It was assumed that all substrate uptakes follow a Monod kinetic, with $q_{S,max}$ as the maximum substrate uptake

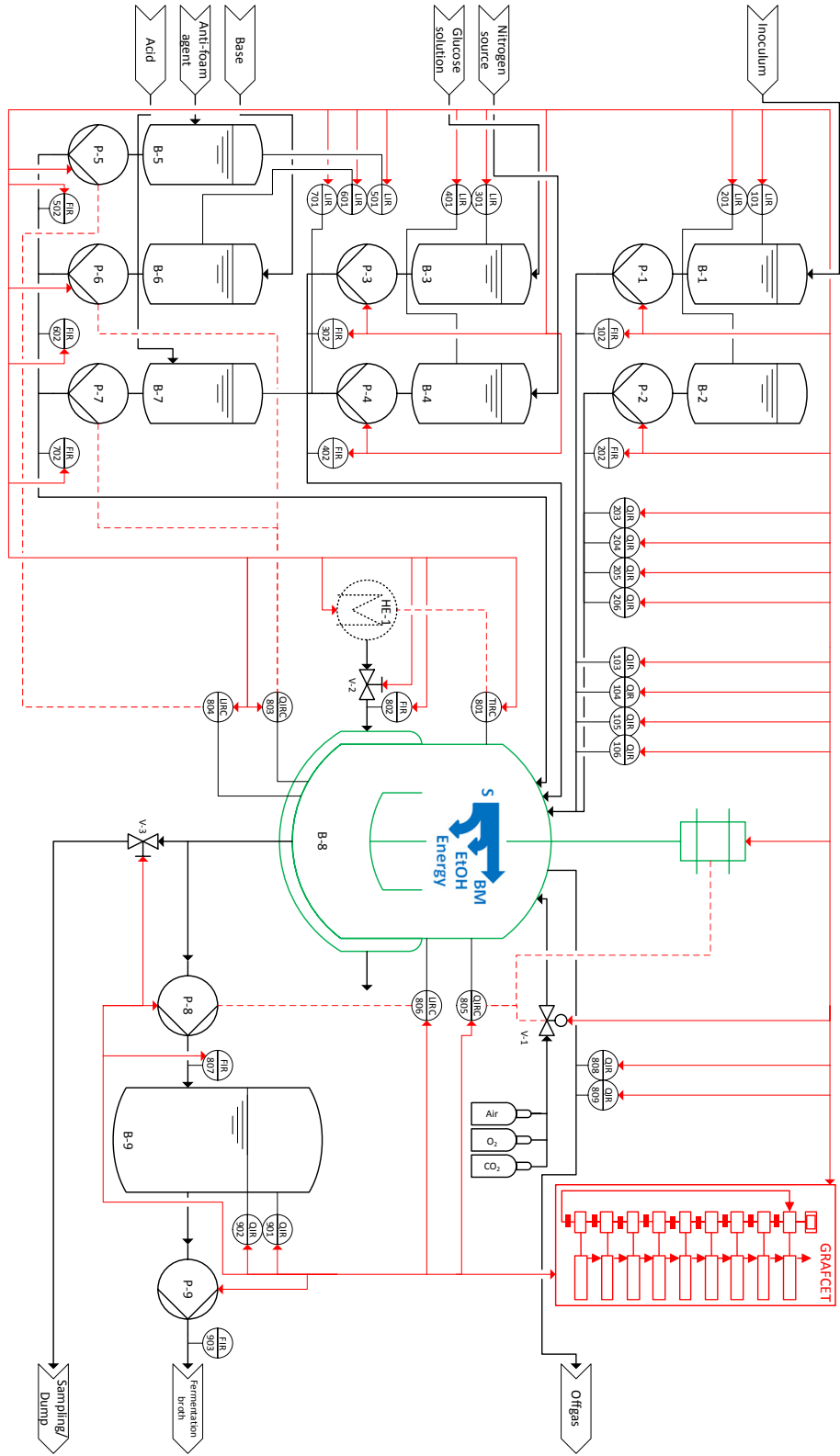


Figure 4.16.: Adaption of the sub-model structure to the cultivation process model. **Kinetics sub-model**, **unit sub-model**, **plant sub-model**, **automation sub-model**.

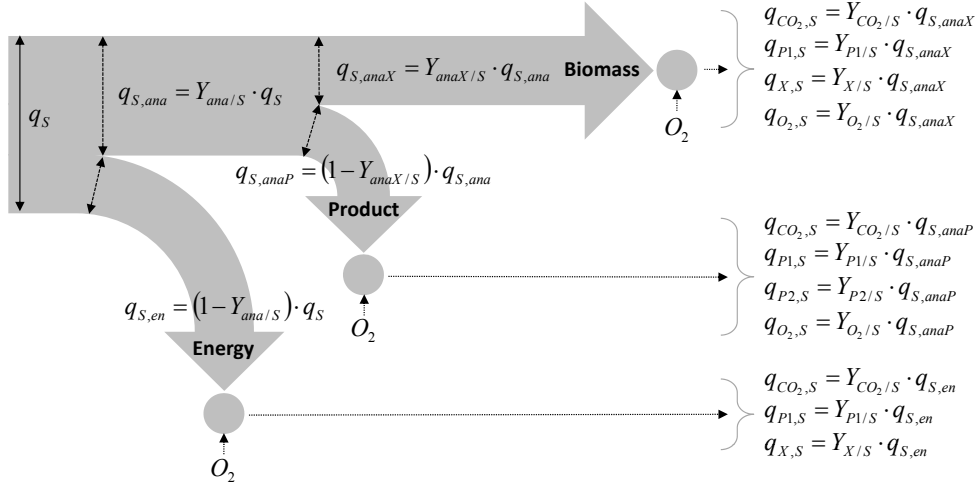


Figure 4.17.: Biological sub-model for the cultivation process, according to Gerlach et al. [2013].

rate, K_S as the Monod constant and S as the substrate being consumed.

$$q_S = q_{S,max} \cdot \frac{S}{K_S + S} \cdot I \quad (4.37)$$

In the Monod equation a state dependent factor I was inserted. This factor takes several circumstances into consideration that may cause a reduction of substrate conversion (e. g. aerobic/anaerobic conditions, non-optimal temperatures, pH, substrate and product concentrations). These inhibition factors, as well as the yield coefficients for calculation of the anabolic pathways ($Y_{ana/S}$, $Y_{anaX/S}$), are computed with a double-sigmoidal function (eq. 4.38).

The double-sigmoidal function has parameters, with which the general appearance may be adjusted. An example for this application is shown in figure 4.18. Here the influence of pH on substrate uptake is shown for two different parameter sets. Yeast representing pH-range 1 has a larger bandwidth in which growth is not disturbed, while yeasts represented by pH-range 2 have a narrow bandwidth of optimal growth.

$$y(x) = \left(Y_{LS} + \frac{Y_{mid} - Y_{LS}}{1 + e^{-K_{SL} \cdot (x - x_{50,LS})}} \right) \cdot \left(1 + \frac{\frac{Y_{RS}}{Y_{mid}} - 1}{1 + e^{-K_{SL} \cdot (x - x_{50,RS})}} \right) \quad (4.38)$$

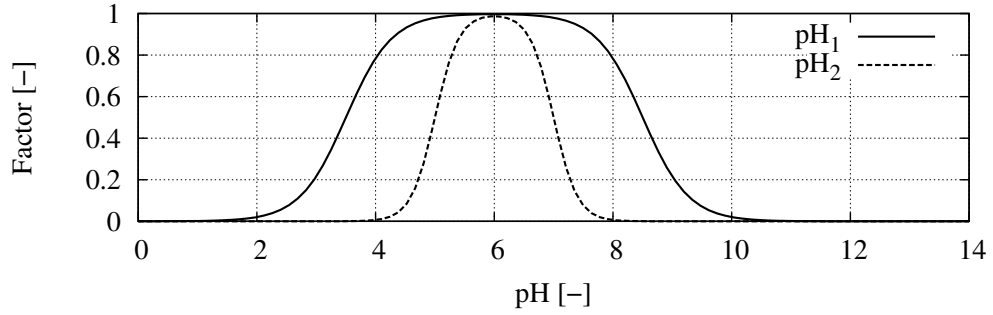


Figure 4.18.: Application of the double-sigmoidal function to define an optimal pH-range for the yeast. By varying the parameters from equation 4.38, the pH-range in which the yeast metabolism is not inhibited can exactly be determined.

In equation 4.38 the parameters are:

- $y(x) \rightarrow 0 \leq y(x) \leq 1$: factor that considers the inhibition caused by given process conditions,
- Y_{LS}, Y_{RS} : highest/ lowest value on the left/right side of the function,
- Y_{mid} : the upper/ lower limit between the left and the right inflexion points
- $x_{50,LS}, x_{50,RS}$: inflection points on the left/ right side,
- K_{SL} : the slope, and
- x as the function argument (temperature, pH, concentration).

In case of determining yield coefficients for the anabolic pathways, the function argument in the double-sigmoidal function is the oxygen availability and the glucose concentration.

The yields that are needed for assessing the final fluxes in the model (by-product (P1), product (P2), biomass (X), carbon dioxide (CO_2) and oxygen (O_2)) are calculated with the overall stoichiometric equation, according to Doran [2012]:



The stoichiometric coefficients a to e are determined with following correlation:

$$Y_{i/S} = j \cdot \frac{M_i}{M_S} \quad (4.40)$$

The yield of a component i ($Y_{i/S}$) is the product of the stoichiometric coefficient a to e , represented as j , and the ratio of the molar weight of that component (M_i) and the molar weight of the substrate (M_S).

Having the yields for each product formed by the yeast cells, the production rates can be determined. This is done by multiplication of the yield with the glucose fluxes in the respective pathways:

$$q_{i/S}^{biomass} = Y_{i/S} \cdot q_{S,anaX} \quad (4.41)$$

$$q_{i/S}^{product} = Y_{i/S} \cdot q_{S,anaP} \quad (4.42)$$

$$q_{i/S}^{energy} = Y_{i/S} \cdot q_{S,en} \quad (4.43)$$

A further mechanism taking place in the biological sub-model is the differentiation between different types of biomass (active, inactive) [Witte, 1996]. In the model theory active biomass can degrade to inactive biomass, while inactive biomass can also be reactivated. The inactivation of active biomass depends on the existence of active biomass. In such a case the rate of deactivation is proportional to the amount of active biomass (X_a) in the total, viable biomass (X_v). Another double-sigmoidal function is used for disturbing purposes (I) while the factor (K_i) was introduced to parameterise the function:

$$q_{deg} = K_i \cdot \frac{X_a}{X_v} \cdot I \quad (4.44)$$

Reactivation, on the other hand, depends on the concentrations of inactive biomass ($\frac{X_i}{X_v}$) and substrate uptake rate (as a Monod kinetic), for which in this case glucose was taken. Thus, the reactivation rate is expressed as:

$$q_{react} = K_{act} \cdot \frac{X_a}{X_v} \cdot \frac{\frac{X_i}{X_v}}{K_{act}^2 + \frac{X_i}{X_v}} \cdot \frac{S}{K_S + S} \cdot I \quad (4.45)$$

4.2.2. Unit sub-model

The unit sub-model describes the reaction space, in which the biological conversion from substrate to biomass, products and energy takes place (bioreactor B-8, B-17). Since the kinetics and the unit sub-model consist of more than 2000 lines programming code, only the most relevant model parts will be explained in the following section. At first, figure 4.19 gives an overview of the unit sub-model.

Into the reactor there are the feed flows of acid and base ($\dot{V}_{acid}, \dot{V}_{base}$) for controlling the pH, an antifoam agent (\dot{V}_{af}), and a feed (\dot{V}_F) containing all possible components of the reactor itself (biomass, ethanol, glucose and nitrogen source). This poses the earlier described extension of the original model, in order to prepare it for continuous operation. Originally it was used only for inoculum. The bioreactor medium is heated by a thermal oil which is passed through a heating jacket around the bioreactor (\dot{V}_H, T_H). Lastly, an air flow may be injected to the reactor (\dot{V}_{air}) with a certain concentration of oxygen (c_{O_2}).

Knowing the in- and effluents from the reactor, a mass and energy balance can be formulated. The change of volume in the reactor is as described with eq. 4.6. The concentration changes are given by the inflow and outflow streams, by an additional term that includes dilution effects, and by a conversion rate, as described in the biological sub-model:

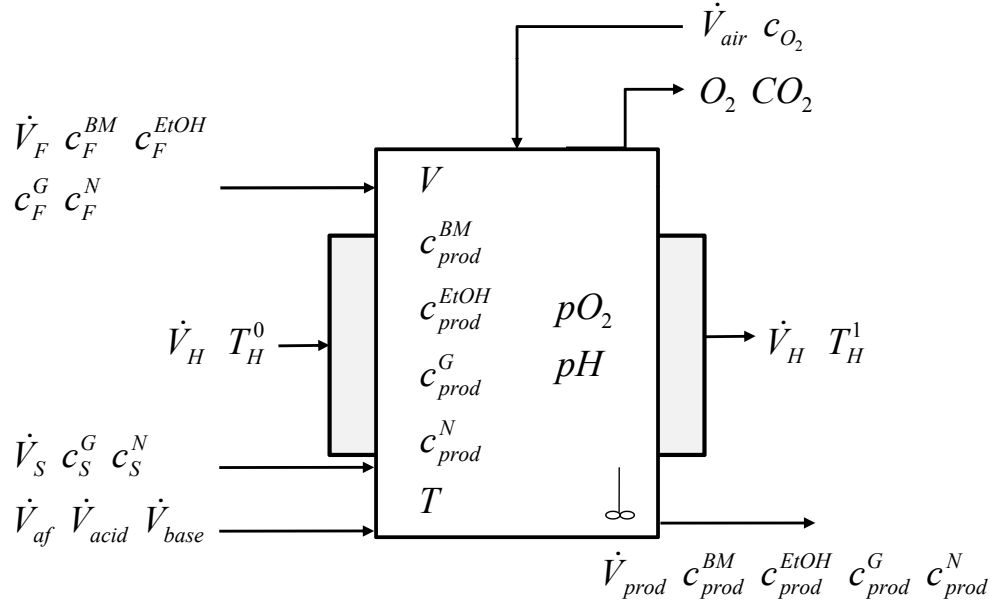


Figure 4.19.: Reactor sub-model (bioreactor) with all input and output flows.

$$\frac{dc_{prod}^i}{dt} = \frac{\dot{V}_S \cdot c_S^i + \dot{V}_F \cdot c_F^i - c_{prod}^i \cdot \sum \dot{V}_j^{in}}{V} - \underbrace{q_S^i \cdot X_V}_{conversion} \quad j \rightarrow S, F, acid, base, af \quad (4.46)$$

For the change of dissolved oxygen in the bioreactor (pO_2) another differential equation was formulated, taking the oxygen transfer and the oxygen uptake by the yeast into consideration:

$$\frac{dpO_2}{dt} = \underbrace{\left(k_{La} \cdot \frac{O_2}{0.21} - pO_2 \right)}_{transfer} - \underbrace{\left(100.0 \cdot q_{O_2} \cdot \frac{X_V}{pO_2^{max}} \right)}_{uptake} \quad (4.47)$$

In this equation k_{La} is the oxygen transport coefficient, O_2 is the oxygen concentration in the exhaust gas, q_{O_2} is the oxygen uptake rate, and pO_2^{max} is the maximum solubility of oxygen. The oxygen transport coefficient is dependent on the power input of the stirrer and was modeled according to empiric correlations [Hass, 2005].

The calculation of pH depends on the amount of protons available in the cultivation broth. The protons are correlated to the amount of nitrogen source in the bioreactor, and by formation during the cultivation process. Further, the amount of acid and base added influence the number of protons, and thus, the pH in the system. The pH model used in the reactor sub-model was developed by Kuhnen and Meiwes [2008].

The oxygen uptake and carbon dioxide evolution rates are described by:

$$R_{O_2} = q_{O_2} \cdot X_V \quad (4.48)$$

$$R_{CO_2} = q_{CO_2} \cdot X_V \quad (4.49)$$

q_{O_2} and q_{CO_2} are functions that are modeled using the double-sigmoidal function described earlier.

Lastly, the temperature changes in the bioreactor (T) and in the heating jacket (T_H) are modeled. The temperature is affected by the power input of the stirrer (P_{stirr}), the heat transfer from the heating jacket to the bioreactor ($k_H \cdot A_H \cdot (T_H - T)$), heat losses to the surroundings ($k_L \cdot A_L \cdot (T - T_U)$), the heat of reaction (Q_R), the energy bound to the feed ($\dot{V}_F \cdot c_{p,F} \cdot T_F$) and to the outflow ($\dot{V}_{prod} \cdot c_{p,R} \cdot T$) and a dilution term that considers the changing volume in the bioreactor ($\frac{T}{V} \cdot \frac{dV}{dt}$).

$$\begin{aligned} \frac{dT}{dt} = & \underbrace{\frac{P_{stirr}}{m_R \cdot c_{p,R}}}_{\text{stirrer input}} + \underbrace{\frac{Q_R}{m_R \cdot c_{p,R}}}_{\text{heat of reaction}} + \underbrace{\frac{k_H \cdot A_H \cdot (T_H - T)}{m_R \cdot c_{p,R}}}_{\text{heat transfer}} \\ & - \underbrace{\frac{k_L \cdot A_L \cdot (T - T_U)}{m_R \cdot c_{p,R}}}_{\text{heat losses}} + \underbrace{\frac{\dot{V}_F \cdot c_{p,F} \cdot T_F}{V \cdot c_{p,R}}}_{\text{input}} \\ & - \underbrace{\frac{\dot{V}_{prod} \cdot c_{p,R} \cdot T}{V \cdot c_{p,R}}}_{\text{output}} - \underbrace{\frac{T}{V} \cdot \frac{dV}{dt}}_{\text{dilution}} \quad (4.50) \end{aligned}$$

After inserting the mass balance into the temperature equation and canceling $c_{p,R}$ in the output term, the formula becomes:

$$\begin{aligned}
\frac{dT}{dt} = & \underbrace{\frac{P_{stirr}}{m_R \cdot c_{p,R}}}_{\text{stirrer input}} + \underbrace{\frac{Q_R}{m_R \cdot c_{p,R}}}_{\text{heat of reaction}} + \underbrace{\frac{k_H \cdot A_H \cdot (T_H - T)}{m_R \cdot c_{p,R}}}_{\text{heat transfer}} \\
& - \underbrace{\frac{k_L \cdot A_L \cdot (T - T_U)}{m_R \cdot c_{p,R}}}_{\text{heat losses}} + \underbrace{\frac{\dot{V}_F \cdot c_{p,F} \cdot T_F}{V \cdot c_{p,R}}}_{\text{input}} \\
& - \underbrace{\frac{\dot{V}_{prod} \cdot T}{V}}_{\text{output}} - \underbrace{\frac{T}{V} \cdot (\dot{V}_S + \dot{V}_F + \dot{V}_{acid} + \dot{V}_{base} + \dot{V}_{af} - \dot{V}_{prod})}_{\text{dilution}} \quad (4.51)
\end{aligned}$$

Further rearrangement finally leads to:

$$\begin{aligned}
\frac{dT}{dt} = & \frac{P_{stirr} + Q_R + k_H \cdot A_H \cdot (T_H - T) - k_L \cdot A_L \cdot (T - T_U)}{m_R \cdot c_{p,R}} \\
& + \frac{\dot{V}_F \cdot c_{p,F} \cdot T_F}{V \cdot c_{p,R}} - \frac{T \cdot \sum \dot{V}_j^{in}}{V} \\
& j \rightarrow S, F, acid, base, af \quad (4.52)
\end{aligned}$$

The temperature in the heating jacket is calculated with a balance over incoming and leaving heating fluid ($\dot{V}_H \cdot T_H^0$, $\dot{V}_H \cdot T_H^1$), the heat transfer and heat losses to the surroundings:

$$\begin{aligned}
\frac{dT_H}{dt} = & \frac{\dot{V}_H \cdot (T_H^0 - T_H^1)}{V_H} \\
& - \frac{k_H \cdot A_H \cdot (T_H - T) - k_{L,H} \cdot A_{L,H} \cdot (T_H - T_U)}{V_H \cdot \rho_H \cdot c_{p,H}} \quad (4.53)
\end{aligned}$$

4.2.3. Plant sub-model

The plant sub-model comprises all additional components that are involved in the cultivation process (pumps, valves, various tanks for different media and the sensors which indicate e.g. temperatures). The overall cultivation plant sub-model is shown in figure 4.16 (black elements). The components, their description, specification and applied model are summarized in table 4.1.

Table 4.1.: Tanks and components used in the plant model of the cultivation process

Name	Description	Specification	Model
B-1	Inoculum tank	10 L	4.6 and
B-2	Retentate tank	20 L	
B-3	Substrate tank (G)	10 L	
B-4	Substrate tank (N)	10 L	
B-5	Antifoam tank	2 L	4.9
B-6	Base tank	2 L	
B-7	Acid tank	2 L	
B-9	Product tank	20 L	
P-1	Inoculum pump	0 ... 2000 $mL \cdot min^{-1}$	none
P-2	Retentate pump	0 ... 2000 $mL \cdot min^{-1}$	
P-3	Substrate pump (G)	0 ... 400 $mL \cdot min^{-1}$	
P-4	Substrate pump (N)	0 ... 400 $mL \cdot min^{-1}$	
P-5	Antifoam pump	0 ... 600 $mL \cdot min^{-1}$	none
P-6	Base pump	0 ... 600 $mL \cdot min^{-1}$	
P-7	Acid pump	0 ... 600 $mL \cdot min^{-1}$	
P-8	Product pump	0 ... 2000 $mL \cdot min^{-1}$	
P-9	Product pump	0 ... 2000 $mL \cdot min^{-1}$	none
V-1	Aeration valve	0 ... 100%	4.4
V-2	Heating fluid valve	0 or 1	4.1
V-3	Sampling valve	0 or 1	4.1
HE-1	Heating fluid HE	0 ... 200 °C	none
Sensors			
LIR-101	Level	0 ... 10 L	none
FIR-102	Flow	0 ... 2000 $mL \cdot min^{-1}$	
QIR-103	Quality (EtOH)	750 $g \cdot L^{-1}$	
QIR-104	Quality (BM)	750 $g \cdot L^{-1}$	
QIR-105	Quality (G)	750 $g \cdot L^{-1}$	
QIR-106	Quality (N)	750 $g \cdot L^{-1}$	
LIR-201	Level	0 ... 10 L	none
FIR-202	Flow	0 ... 2000 $mL \cdot min^{-1}$	
QIR-203	Quality (EtOH)	750 $g \cdot L^{-1}$	
QIR-204	Quality (BM)	750 $g \cdot L^{-1}$	

Continued on next page

Table 4.1 – continued from previous page

Name	Description	Specification	Model
QIR-205	Quality (G)	$750 \text{ g} \cdot \text{L}^{-1}$	
QIR-206	Quality (N)	$750 \text{ g} \cdot \text{L}^{-1}$	
LIR-301	Level	$0 \dots 10 \text{ L}$	none
FIR-302	Flow	$0 \dots 400 \text{ mL} \cdot \text{min}^{-1}$	
LIR-401	Level	$0 \dots 10 \text{ L}$	none
FIR-402	Flow	$0 \dots 400 \text{ mL} \cdot \text{min}^{-1}$	
LIR-501	Level	$0 \dots 2 \text{ L}$	none
FIR-502	Flow	$0 \dots 600 \text{ mL} \cdot \text{min}^{-1}$	
LIR-601	Level	$0 \dots 2 \text{ L}$	none
FIR-602	Flow	$0 \dots 600 \text{ mL} \cdot \text{min}^{-1}$	
LIR-701	Level	$0 \dots 2 \text{ L}$	none
FIR-702	Flow	$0 \dots 600 \text{ mL} \cdot \text{min}^{-1}$	
FIR-802	Flow	$0 \dots 20 \text{ L} \cdot \text{min}^{-1}$	none
TIRC-801	Temperature	$0 \dots 200 \text{ }^{\circ}\text{C}$	
QIRC-803	Quality (pH)	$0 \dots 14$	4.34
LIR-804	Level (Antifoam)	$0 \dots 30 \text{ L}$	
QIRC-805	Quality (pO_2)	$0 \dots 100\%$	4.34
LIRC-806	Level	$0 \dots 30 \text{ L}$	
FIR-807	Flow	$0 \dots 2000 \text{ mL} \cdot \text{min}^{-1}$	4.34
QIR-808	Quality (CO_2)	$0 \dots 100\%$	
QIR-809	Quality (O_2)	$0 \dots 100\%$	
QIR-901	Quality (EtOH)	$750 \text{ g} \cdot \text{L}^{-1}$	none
QIR-902	Quality (BM)	$750 \text{ g} \cdot \text{L}^{-1}$	
QIR-903	Quality (G)	$750 \text{ g} \cdot \text{L}^{-1}$	
QIR-904	Quality (N)	$750 \text{ g} \cdot \text{L}^{-1}$	
FIR-905	Flow	$0 \dots 2000 \text{ mL} \cdot \text{min}^{-1}$	

4.2.4. Automation sub-model

The automation sub-model comprises all controls taking place in the process, as well as the automatic sequence control.

Controls

Following controls were implemented into the model:

- antifoam control
- pH control
- temperature control
- level control
- dissolved oxygen control

The control of foam-level in the bioreactor (LIRC-804) is realised with a dosing pump that continuously switches on and off. The frequency of the switch may be parameterised. At first an upper limit of foam level needs to be defined. When this set point is reached, a pumping switch is activated in a given frequency (e. g. 10 s). I. e., every 10 seconds the pump is switched on. When the pump is switched on, it will stay on for a given percentage of this period (e.g. 50% \rightarrow 5 s). Lastly, another parameter defines the volumetric flow of the antifoam agent (in $\text{mL} \cdot \text{min}^{-1}$) that is pumped into the bioreactor during these 5 seconds. The example described here is depicted in figure 4.20.

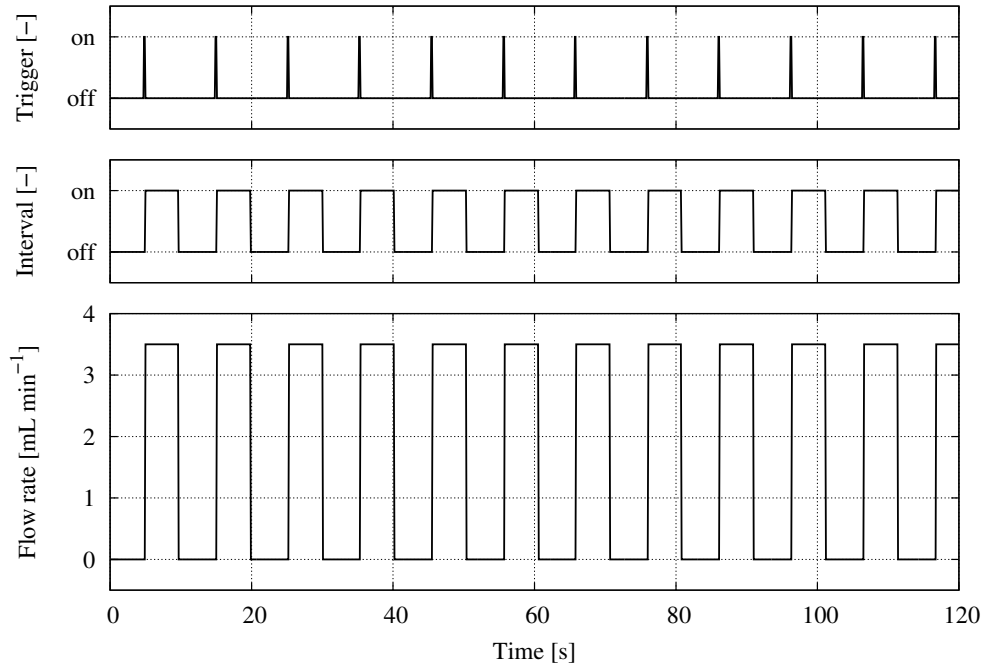


Figure 4.20.: Switching frequency of the antifoam pump (top), pumping interval (center) and flow rate of antifoam agent (bottom).

The pH control (QIRC-803) is realised with a PID-controller that controls the flows of acid and base into the bioreactor (figure 4.21). The set point pH is compared with the actual pH. When the control error ($e = wpH - pH$) is negative, the acid pump (P-7) is activated, in order to reduce the pH. With a positive control error ($wpH > pH$) the pump of the base tank (P-6) is activated. Since there is no explicit model for the pumps, the volumetric flow rates (\dot{V}_{acid} , \dot{V}_{base}) are the control variables.

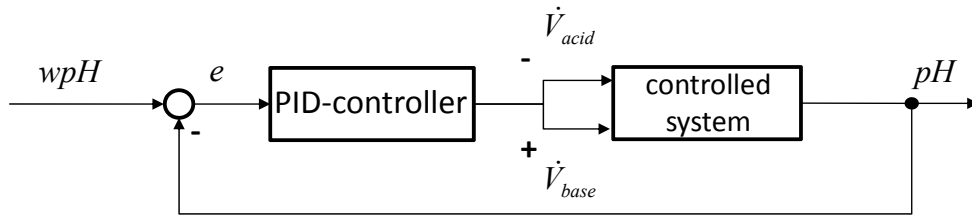


Figure 4.21.: Control loop of the pH control. A negative control error activates the acid pump (\dot{V}_{acid}), while a positive control error starts the base pump (\dot{V}_{base}).

Temperature control (TIRC-801) in this model is also realised with a PID-controller (figure 4.22), that influences the temperature of the heating jacket fluid at the inlet of the jacket (T_H^0). The set point temperature (wT) is compared to the actual temperature in the reactor (T). When the control error gets negative ($T < wT$), the temperature of the heating fluid is increased.

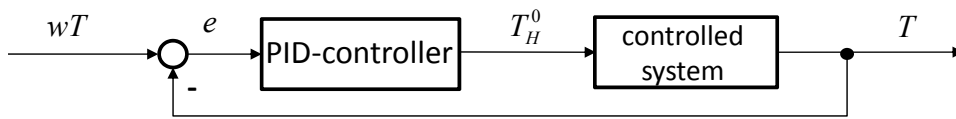


Figure 4.22.: Temperature control loop. If the reactor temperature is lower than the set point temperature ($T < wT$), the temperature of the heating fluid (T_H^0) is raised.

During the process several fluids are added to the bioreactor (substrates, antifoam, acid, base, feed, inoculum). This causes the volume to grow. In order to prevent the reactor from flooding, a level control was implemented (LIRC-806). Level control works with the volume in the reactor. When the set point volume (wV) is higher than the actual volume in

the bioreactor (V), then nothing happens. In case the control error gets positive ($V > wV$), the product pump P-8 is activated which pumps the respective volume into the receiving tank B-9 (inverse control logic). The control loop for level control is given in figure 4.23.

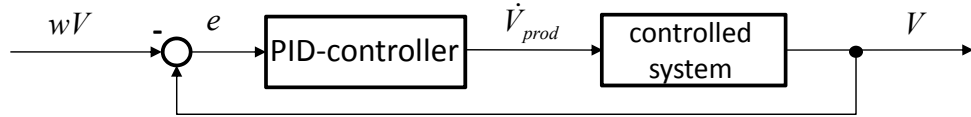


Figure 4.23.: Level control loop with inverse control logic. If the volume in the reactor exceeds the set point volume ($V > wV$), the product pump is activated (\dot{V}_{prod}).

In order to control the dissolved oxygen (pO_2) in the bioreactor (QIRC-805), two actuating variables are accessed. For both variables a control loop must be established (4.24). The first control loop has the stirrer speed (N_{stirr}) as a fast acting control variable, while the air flow (\dot{V}_{air}) acts as the slow control variable of the second control loop. Both controls are realised with a PID-controller. The structure of the control loops is given in figure (4.24). The set point value of dissolved oxygen (wpO_2) is compared with the actual value (pO_2). When there is a positive control error ($wpO_2 > pO_2$), the stirrer speed is increased. In the same way the aeration flow rate is increased, but more slowly, due to the parameters of the PID-controller.

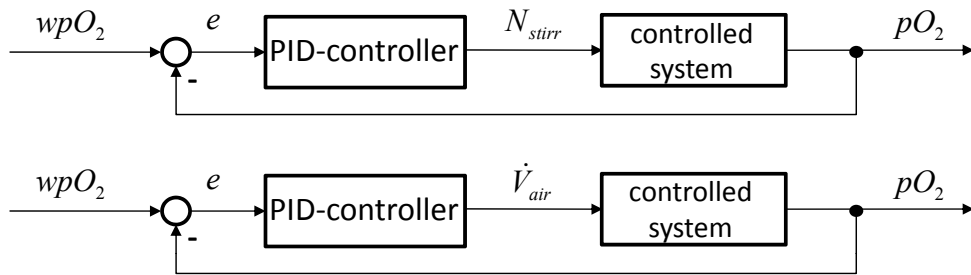


Figure 4.24.: Control loops for dissolved oxygen. The upper control loop uses the stirrer speed as control variable, while in the lower control loop the aeration rate serves as the control variable.

Automatic sequence control

The automatic sequence control was newly developed, in order to have a tool with which process control strategies can be designed and tested quickly, and to investigate the influence of those strategies on the energy demand of the process.

A batch cultivation process has got several process stages that need to be carried out in a predetermined order (sterilisation, aerobic phase, anaerobic phase). These phases are coupled to further actions that must be performed at the right time and in the right way. For this task a general automatic sequence control was developed and applied to the described model.

The standard operating procedure of a batch-cultivation can be organised as follows:

- activation and initialisation of the sequence control,
- definition of starting volume and -concentrations in the bioreactor (substrates, inoculum),
- fill the feed tanks (antifoam, base, acid, substrates),
- fill the bioreactor,
- after filling to the desired volume, start stirrer (set point 200 rpm),
- set flow rate of heating fluid to a desired value,
- switch on temperature control for the bioreactor (set point 122 °C),
- hold sterilization temperature for 20 min,
- after sterilization change to process temperature (set point 32 °C),
- when bioreactor has cooled down, start inoculation,
- start controls for pO_2 , antifoam, pH and level with appropriate set points,
- start aerobic operation (biomass growth),
- if enough biomass is produced, set point for pO_2 must be set to 0 (anaerobic operation/ ethanol production starts),
 during both operational phases automatically refill substrate and utility tanks,

- when the desired product concentration is reached:
 - stop stirrer,
 - stop heating (flow rate of heating fluid $\rightarrow 0$),
 - deactivate all controls,
 - activate product pump P-8,
- if bioreactor empty, deactivate product pump, and
- re-initialise the sequence control for the next batch-cultivation run.

The standard operating procedure for the batch-cultivation was implemented into a GRAFCET-plan that can be seen in figure A.7 in the appendix.

4.2.5. Model validation

Model validation was carried out with a fed-batch cultivation for ethanol production with *Saccharomyces cerevisiae* [Gerlach et al., 2013]. The cultivation took place in a 10 L BIOSTAT[®] C laboratory bioreactor (cp. p. 30) . The process shows a large bandwidth of potential process control strategies having different results, as Herbst [2012] could show experimentally.

The validation results are given in figure 4.25. During the experiment concentrations of biomass, ethanol and glucose have been determined once per hour. After two hours process time feeding started. The amount of substrates was continuously increased manually. After the biomass concentration has reached $10 \text{ g} \cdot \text{L}^{-1}$, the process was switched to anaerobic conditions (ethanol production). This took place after approximately 9 hours. The experiment was terminated after the ethanol-concentration increased to $60 \text{ g} \cdot \text{L}^{-1}$.

The same experiment was carried out with the model described earlier. Again biomass-, ethanol- and glucose-concentrations have been recorded during the whole process. Also the operation mode was switched after $10 \text{ g} \cdot \text{L}^{-1}$ biomass was reached in the bioreactor. The concentration courses of the real experiment and the simulation are depicted in figure 4.25.

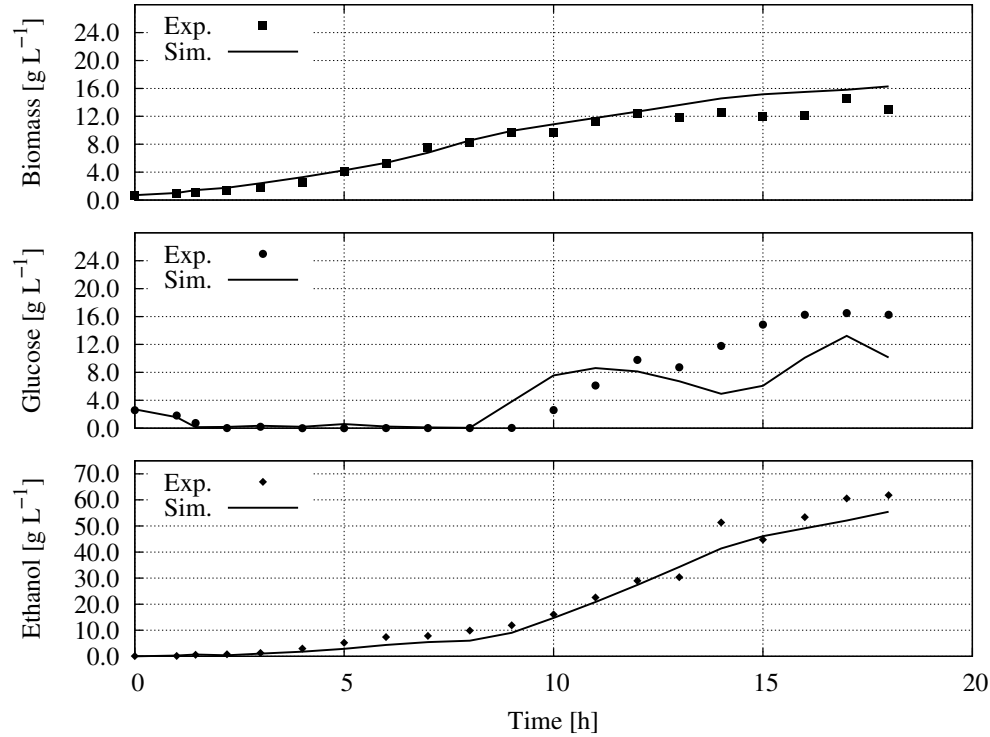


Figure 4.25.: Experimental (symbols) and simulated (lines) concentrations of biomass (top), glucose (center), and ethanol (bottom) [Gerlach et al., 2013].

4.3. Cross-flow filtration

The cross-flow filtration process model shall be used to show the influence of the main process control parameters (TMP and feed flow rate) on the energy demand of this unit operation. Therefore, the filtration mechanisms need to be described appropriately in the **unit sub-model**.

Further, the feed pump has to be modeled in a way that different boundary conditions (pressure, flow rate) lead to varying power demands (**plant sub-model**).

In the **automation sub-model** the different process control strategies shall be defined. The adaption of the shell structure to the cross-flow filtration process is expressed in figure 4.26. The elements of the sub-model structure are described in the following sections.

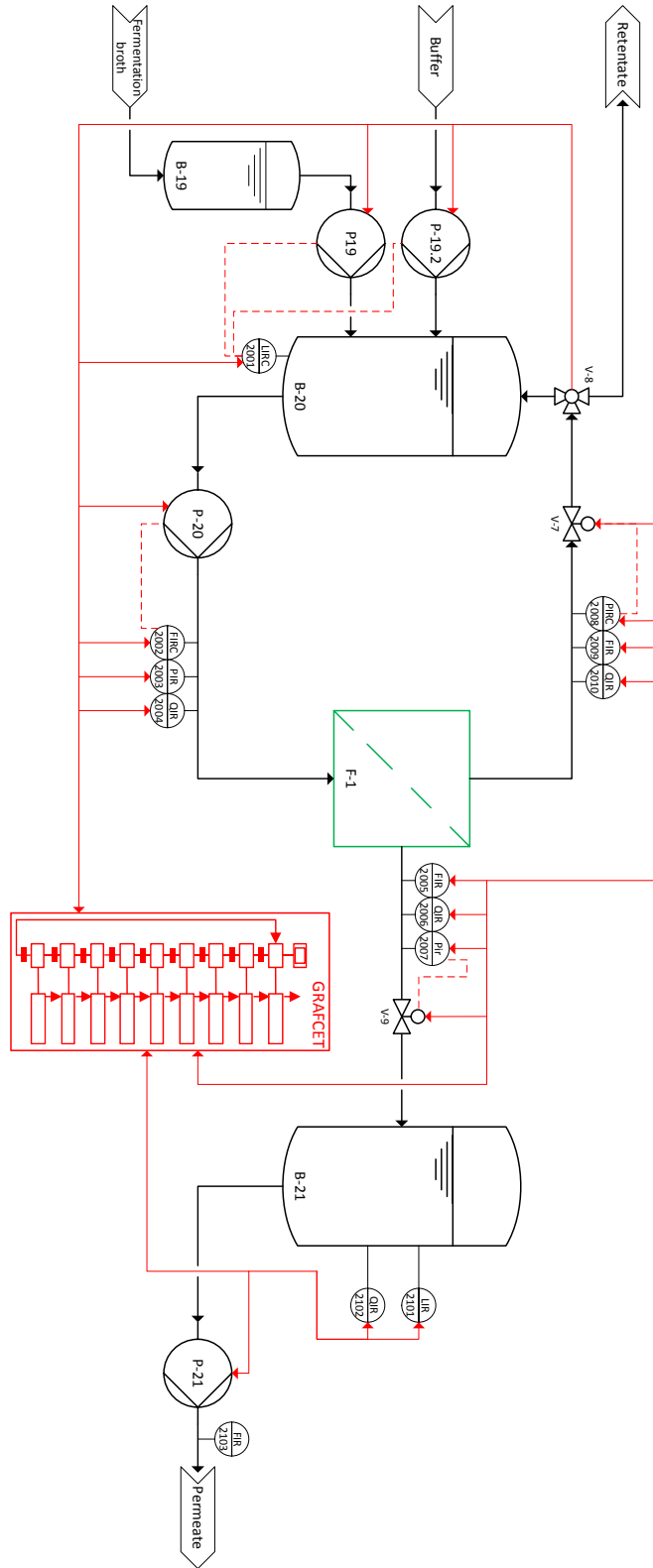


Figure 4.26.: Adaption of the sub-model structure to the cross-flow filtration process model. **Kinetics sub-model, unit sub-model, plant sub-model, automation sub-model.**

4.3.1. Unit sub-model

In the unit sub-model all flows in and out of the filter are balanced and the characteristic dimensions, like diameters or filter area, are given here. Figure 4.27 shows the model for a segment of a filter module.

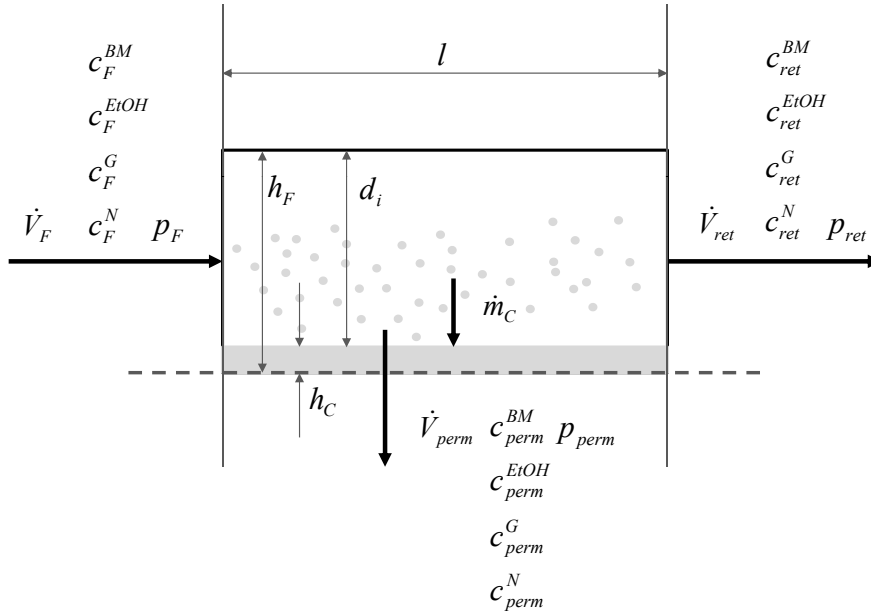


Figure 4.27.: Filter model with all relevant input and output variables and the respective parameter, describing the geometry of the filter. From the left-hand side a suspension (\dot{V}_F) flows tangentially across the filter membrane. The particle-free permeate flow (\dot{V}_{perm}) leaves downwards, while the particle-containing retentate flow (\dot{V}_{ret}) leaves on the right-hand side.

The feed, given as a volumetric flow (\dot{V}_F) is inserted into the filter element (F-1), carrying the biomass (c_F^{BM}), ethanol (c_F^{EtOH}), glucose (c_F^G), and nitrogen source (c_F^N). Further, the pressure at the feed side is given (p_F). The corresponding variables at the permeate and at the retentate side of the filter are indexed \dot{V}_{perm}^* , c_{perm}^* , p_{perm} and \dot{V}_{ret}^* , c_{ret}^* , p_{ret} respectively. A particle mass flow from the feed to the filter (\dot{m}_C) cake is also given.

The driving force in filtration is the trans membrane pressure (TMP) that determines how a particle-containing fluid passes a membrane with

a given pore size. The TMP is defined as the mean difference between the pressure before and behind a filter element minus the pressure predominating on the permeate side [Pahl et al., 2006]:

$$\Delta p_{TMP} = \frac{p_F - p_{ret}}{2} - p_{perm} \quad (4.54)$$

From the yeast cultivation process a broth containing water, biomass, ethanol, glucose and a nitrogen source, is passed to the cross-flow filtration. It is assumed that only ethanol and water can pass the membrane and all other components (i. e. biomass, glucose, nitrogen source) are detained with the filter. The flow through the membrane filter is computed as [Rautenbach, 1997]:

$$\dot{V}_{perm} = \frac{\Delta p_{TMP}}{\eta_{perm} \cdot (RM + RC)} \quad (4.55)$$

The permeate flow (\dot{V}_{perm}) is strongly connected to the TMP. Further parameters influencing the flux are the resistances of the membrane (RM) and of the filter cake (RC) and the dynamic viscosity of the filtrate (η_{perm}). Since water and ethanol are the only passing components, the viscosity remains constant.

Membrane resistance is a material bound characteristic of the membrane used in the filter and must be taken from data sheets. For this work it was assumed to be constant (no fouling effects). The cake resistance on the other hand is linked to the height of the filter cake. The height of the filter cake is influenced by two forces. Force A ($f_{1,flux}$) is produced by the flux. The higher the flux gets, the stronger the particles are pressed towards the filter cake (figure 4.28).

Force A is reduced by a force B ($f_{2,w}$), triggered by the cross-flow velocity along the filter element. The higher the flow velocity gets, the stronger the particles will be released from the cake surface again and transported back into the retentate flow. These two values need to get into an equilibrium (reversible cake build-up, [Rautenbach, 1997]). For both cases linear correlations were used (figures 4.29 and 4.30).

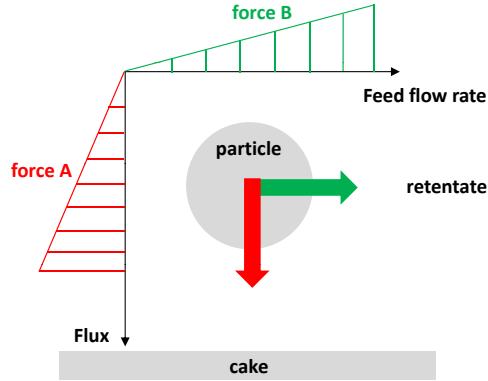


Figure 4.28.: Forces on a particle in the filter channel. Feed flow rate (and with this the cross-flow velocity), as well as flux are influencing the path of a particle (either to the cake, or back into the retentate flow).

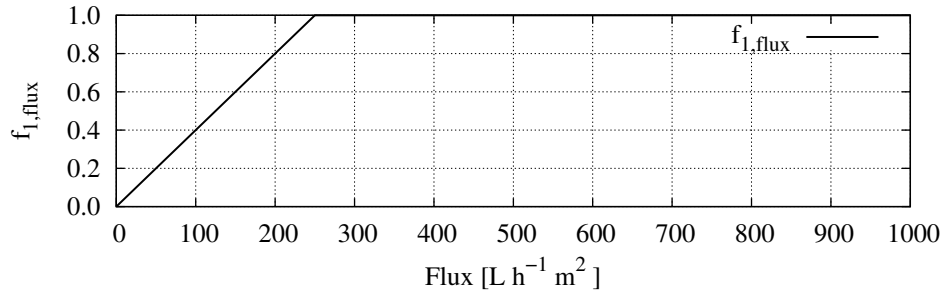


Figure 4.29.: Factor describing the correlation between flux and the degree of particle movement **to** the cake. Fluxes higher than $250 L \cdot h^{-1} \cdot m^2$ bear the maximum force towards the filter cake.

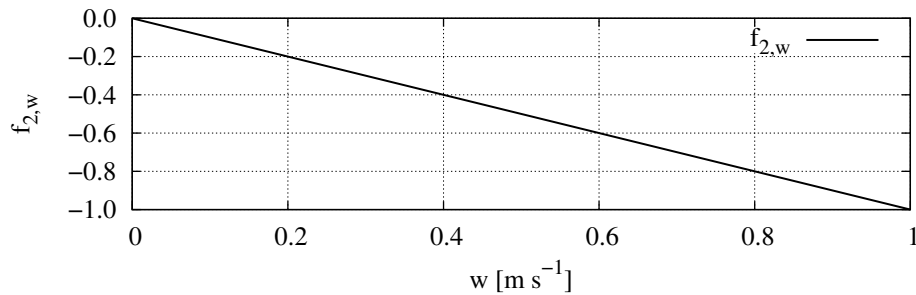


Figure 4.30.: Factor describing the correlation between cross-flow velocity (w) and the degree of particle movement **from** the cake (with negative values).

The force equilibrium is computed with a PI-controller (figure 4.31) that calculates the respective cake resistance related to the force equilibrium. With fluxes higher than $250 \text{ L} \cdot \text{h}^{-1} \cdot \text{m}^2$ and high cross-flow velocities the equilibrium cannot be achieved any longer. This causes a continuously decreasing cake height, until no cake is left (see chapter 6.2), due to a higher abrasive force as compared to the compressing force.

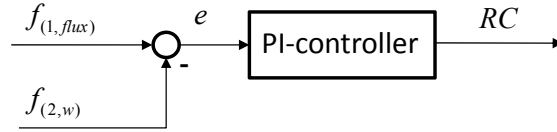


Figure 4.31.: Control loop for calculation of the equilibrium cake resistance that is related to the flux and the cross-flow velocity.

With the cake resistance the cake height may be computed (giving a cake specific resistance factor (r_C), [Nguyen, 2004]):

$$h_C = \frac{RC}{r_C} \quad (4.56)$$

The change of filter cake height ($\frac{dh_C}{dt}$) gives the mass flow of particles:

$$\dot{m}_C = \frac{dh_C}{dt} \cdot A_f \cdot 1000.0 \frac{\text{kg}}{\text{m}^3} \quad (4.57)$$

The height of the cake, together with the height of a feed channel (h_F) gives the inner diameter (d_i) of the filter channel, available for feed flow:

$$d_i = h_F - h_C \quad (4.58)$$

A further value to be calculated is the average flow velocity which is needed for the computation of pressure losses. The average flow velocity is the quotient of the mean volumetric flow rates (filter entry and filter exit) of the feed and the cross-sectional area (A_c) of the channel where the fluid passes through. The cross-sectional area can be calculated with the inner diameter:

$$A_c = \pi \cdot \frac{d_i^2}{4} \quad (4.59)$$

Hence, the average flow velocity gets:

$$w_F = \frac{\frac{\dot{V}_F + \dot{V}_{ret}}{2}}{A_c} \quad (4.60)$$

The pressure drop (Δp) in the filter was modeled as follows, assuming turbulent flow [Schmidt, 1967]:

$$\Delta p = \lambda \cdot \frac{l}{d_i} \cdot \frac{\rho_F}{2} \cdot w_F^2 \quad (4.61)$$

The friction factor (λ) describes the characteristic roughness of the tube walls, through which the feed flows. For the friction factor, as well as for the density of the feed (ρ_F), static values were chosen.

The pressure drop is used to determine the pressure in front of the filter elements (p_F). The pressure behind the filter (p_{ret}) is an adjustable value (valve-controlled). Here a linear correlation between opening degree (ω) of the valve V-7 and the pressure was chosen:

$$p_{ret} = \omega_{V-7} \cdot 0.05 \quad (4.62)$$

With this retentate-side pressure the feed-side pressure gets:

$$p_F = p_{ret} + \Delta p \quad (4.63)$$

The last pressure that may be influenced is the permeate side pressure. Here again a valve is used to influence the pressure (eq. 4.62). The correlation between opening degree and pressure is shown in figure 4.32.

Finally, a material balance, based on concentrations and volumetric flow rates, is formulated. The volumetric flow rate of the retentate (\dot{V}_{ret}) is the difference between the volumetric flow rates of the feed and of the permeate (\dot{V}_{perm}):

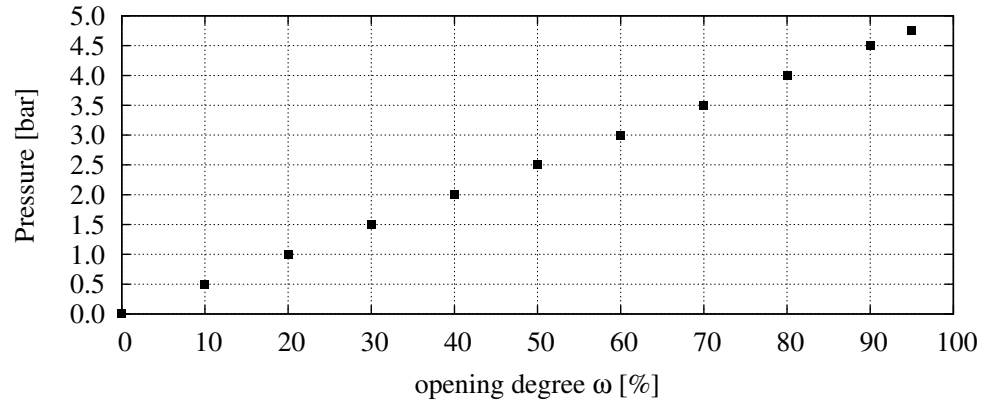


Figure 4.32.: Pressure as a function of opening degree (ω) of a controlled valve.

$$\dot{V}_{ret} = \dot{V}_F - \dot{V}_{perm} \quad (4.64)$$

When there is no permeate (i. e. no production), the concentration of biomass in the retentate equals the concentration in the feed:

$$c_{ret}^{BM} = c_F^{BM} \quad (4.65)$$

In the production phase the amount of biomass, settling on the filter cake, has to be subtracted:

$$c_{ret}^{BM} = c_F^{BM} - \frac{\dot{m}_C}{\dot{V}_{perm}} \quad (4.66)$$

Simplifying, the concentrations of all components, except ethanol, were assumed to persist in the retentate:

$$c_{ret}^G = c_F^G \quad (4.67)$$

$$c_{ret}^N = c_F^N \quad (4.68)$$

and thus:

$$c_{perm}^i = 0.0 \quad i \rightarrow BM, G, N \quad (4.69)$$

Since ethanol is the only component that can pass the membrane (next to water), the concentrations in the permeate as well as in the retentate must be calculated. At first the percentage of ethanol in the liquid phase of the feed has to be determined. For a first estimate densities of all components were set to $1000.0 \text{ g} \cdot \text{L}^{-1}$:

$$w_F^{EtOH} = \frac{c_F^{EtOH}}{1000.0 \frac{\text{g}}{\text{L}} - c_F^{BM} - c_F^G - c_F^N} \quad (4.70)$$

Having the percentile fraction of ethanol contained in the liquid phase, this value is used to calculate the concentrations of ethanol in the permeate and in the retentate:

$$c_{perm}^{EtOH} = w_F^{EtOH} \quad (4.71)$$

$$c_{ret}^{EtOH} = w_F^{EtOH} \cdot (1000.0 - c_{ret}^{BM} - c_{ret}^G - c_{ret}^N) \quad (4.72)$$

4.3.2. Plant sub-model

In the plant sub-model (depicted in figure 4.26 in black colour) the pumps, different valves, and tanks are integrated. The measuring instrumentation (sensors) in this process model were assumed to be noise-free. The components used in this plant model are listed in table 4.2.

Table 4.2.: Tanks and components in the cross-flow filtration process

Name	Description	Specification	Model
B-19	Buffer tank	20 L	4.6
B-20	Production tank	20 L	and
B-21	Product tank	20 L	4.9
Continued on next page			

Table 4.2 – continued from previous page

Name	Description	Specification	Model
P-19	Broth pump	$0 \dots 2000 \text{ mL} \cdot \text{min}^{-1}$	4.5
P-19.2	Buffer pump	$0 \dots 2000 \text{ mL} \cdot \text{min}^{-1}$	
P-20	Feed pump	$0 \dots 2000 \text{ mL} \cdot \text{min}^{-1}$	
P-21	Product pump	$0 \dots 2000 \text{ mL} \cdot \text{min}^{-1}$	
V-7	Control valve (p)	$0 \dots 100\%$	4.4
V-8	Three-way-valve	0 or 1	4.2
V-9	Control valve (p)	$0 \dots 100\%$	4.4
Sensors			
LIRC-2001	Level	$0 \dots 10 \text{ L}$	none
FIRC-2002	Flow	$0 \dots 2000 \text{ mL} \cdot \text{min}^{-1}$	
PIR-2003	Pressure	$0 \dots 5 \text{ bar}$	
QIR-2004	Quality (BM)	$750 \text{ g} \cdot \text{L}^{-1}$	
QIR-2005	Quality (EtOH)	$750 \text{ g} \cdot \text{L}^{-1}$	
QIR-2006	Quality (G)	$750 \text{ g} \cdot \text{L}^{-1}$	
QIR-2007	Quality (N)	$750 \text{ g} \cdot \text{L}^{-1}$	
FIR-2008	Flow	$0 \dots 2000 \text{ mL} \cdot \text{min}^{-1}$	
PIR-2009	Pressure	$0 \dots 5 \text{ bar}$	
QIR-2010	Quality (BM)	$750 \text{ g} \cdot \text{L}^{-1}$	
QIR-2011	Quality (EtOH)	$750 \text{ g} \cdot \text{L}^{-1}$	
QIR-2012	Quality (G)	$750 \text{ g} \cdot \text{L}^{-1}$	
QIR-2013	Quality (N)	$750 \text{ g} \cdot \text{L}^{-1}$	
PIRC-2014	Pressure	$0 \dots 5 \text{ bar}$	
FIR-2015	Flow	$0 \dots 2000 \text{ mL} \cdot \text{min}^{-1}$	
QIR-2016	Quality (BM)	$750 \text{ g} \cdot \text{L}^{-1}$	
QIR-2017	Quality (EtOH)	$750 \text{ g} \cdot \text{L}^{-1}$	
QIR-2018	Quality (G)	$750 \text{ g} \cdot \text{L}^{-1}$	
QIR-2018	Quality (N)	$750 \text{ g} \cdot \text{L}^{-1}$	
LIR-201	Level	$0 \dots 10 \text{ L}$	none
QIR-202	Flow	$0 \dots 2000 \text{ mL} \cdot \text{min}^{-1}$	
FIR-203	Quality (EtOH)	$750 \text{ g} \cdot \text{L}^{-1}$	

4.3.3. Automation sub-model

The automation sub-model of the cross-flow filtration process is composed of control loops and the automatic sequence control, with which process control strategies are defined.

Controls

Following controls were implemented into the automation sub-model:

- flow control (constant flow)
- TMP control (constant trans membrane pressure)
- pressure drop control (constant pressure drop)

All three controls are used for operational strategies that may be applied on the cross-flow filtration process. Flow control is used to apply a constant feed flow rate during the process. Due to increasing viscosity of the fluid (caused by concentration of biomass), the flow rate decreases when the revolution of the pump (rpm) remains constant. In order to keep the flow rate constant, the revolution of the pump must be increased, respectively. This is carried out with a PI-controller (figure 4.33) that controls the revolution speed (r), corresponding to a certain input volumetric flow (here simplified $rpm = \dot{V}$). This flow is then used in the pump model (V_0 , described with eq. 4.5), where a second order dynamic is applied.

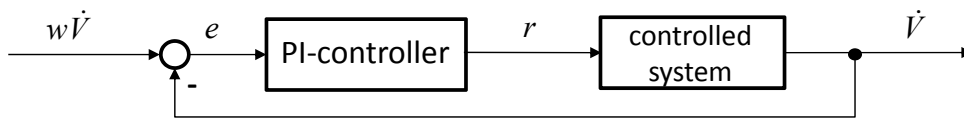


Figure 4.33.: Control loop for constant flow operation mode.

The TMP control keeps the trans membrane pressure constant at the set point value during the process. The influences on changing TMP are manifold (viscosity, flow rate, resistance of cake). By adjusting the opening degree of the pressure control valve (ω_{V-7}), the TMP may be kept constant. The control loop for this task is given in figure 4.34. When the set point TMP is higher than the measured one, the opening degree of the valve is reduced. This is caused by the negative algebraic sign at

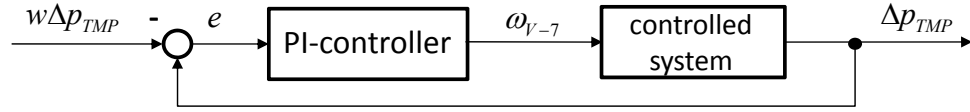


Figure 4.34.: Control loop for constant trans membrane pressure operation mode.

the respective place in the control loop.

A pressure drop control is the third variant for process control implemented in this process model. Pressure drop may change during processing due to fluid viscosity and to higher cake resistance. The latter is a result from a growing filter cake (or fouling). According to equation 4.61 the pressure drop also depends on the inner diameter of a tube. This diameter reduces by building a layer of particles on the membrane. Decreasing inner diameter lets the term increase, so the pressure drop increases as well. Here again, the pressure control valve (V-7) is used for control (figure 4.35).

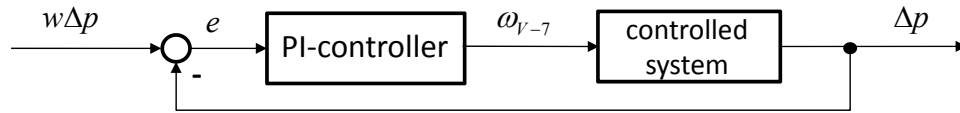


Figure 4.35.: Control loop for constant pressure drop operation mode.

In the last control loop the sense of control is contrary to that one for TMP control. Here a positive control deviance ($w\Delta p > \Delta p$) lets the opening degree of the control valve increase.

Automatic sequence control

A generalised standard operating procedure for the cross-flow filtration process was developed. In this sequence, several parameters may be changed (starting volume and concentration, flow rates, TMP, etc.). The effects of the modification of the process control strategy may then be evaluated with the simulator. The standard operating procedure is:

- activation and initialisation of the sequence control,
- filling buffer tank with the desired volume and concentrations,

- filling the production tank with the desired volume,
- activation of feed pump with the desired volumetric flow rate and wait for equilibrium,
- select process control strategy (e. g. constant TMP) and the set point for this strategy,
- open control valve V-9 (0%) and start production,
- stop process when product tank is empty,
- deactivate all pumps,
- re-initialising the sequence control for the next batch-cross-flow filtration run.

The described sequence was translated into a GRAFCET-plan as shown in figure A.8 in the appendix.

4.3.4. Model validation

The cross-flow filtration model was qualitatively checked for typical phenomena occurring in that process. The first phenomenon is due to cake formation which was modeled as described earlier (particle movement to and from the cake).

A dynamic cake formation causes the correlation between TMP and flux to be non-linear. This means that at a certain trans membrane pressure a further increase of TMP does not result in a higher flux. In Rautenbach [1997] this phenomenon is explained with an increasing cake resistance that is a result of a higher pressure, compressing the filter cake.

For the evaluation of this correlation the filter was fed with a continuous flow with a constant concentration of biomass. The control valve V-7 was constantly closed in 10%-steps and the resulting TMP, as well as the flux were noted. When a TMP of approximately 2 bar was reached, the flux stopped further increasing (figure 4.36).

When such an equilibrium state is reached, further changes in the pressure regime only lead to short deviations from the original state. This is valid for higher, as well as for lower pressure applied. This correlation is also given by Rautenbach [1997]. This phenomenon was again simulated,

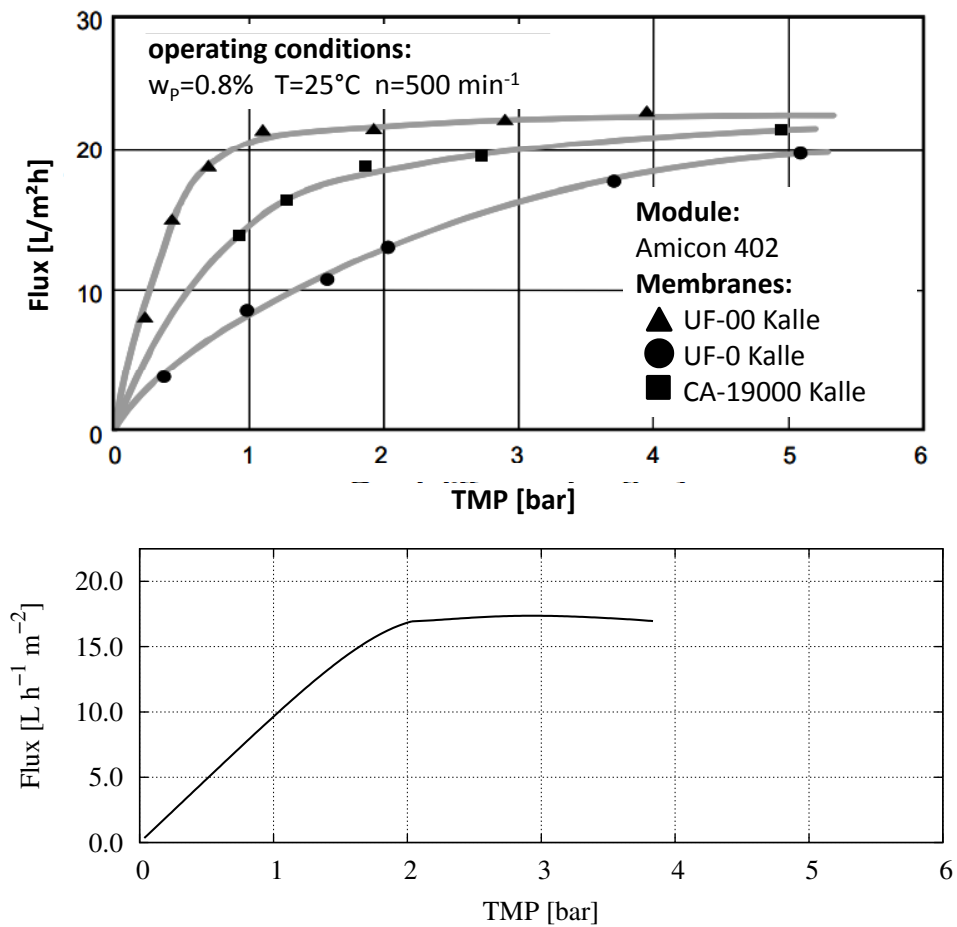


Figure 4.36.: Flux as a function of trans membrane pressure (TMP) for different membrane types and given conditions (top, [Rautenbach, 1997]), and simulated values (bottom).

in order to show the qualitatively reasonable quality of that model (figure 4.37).

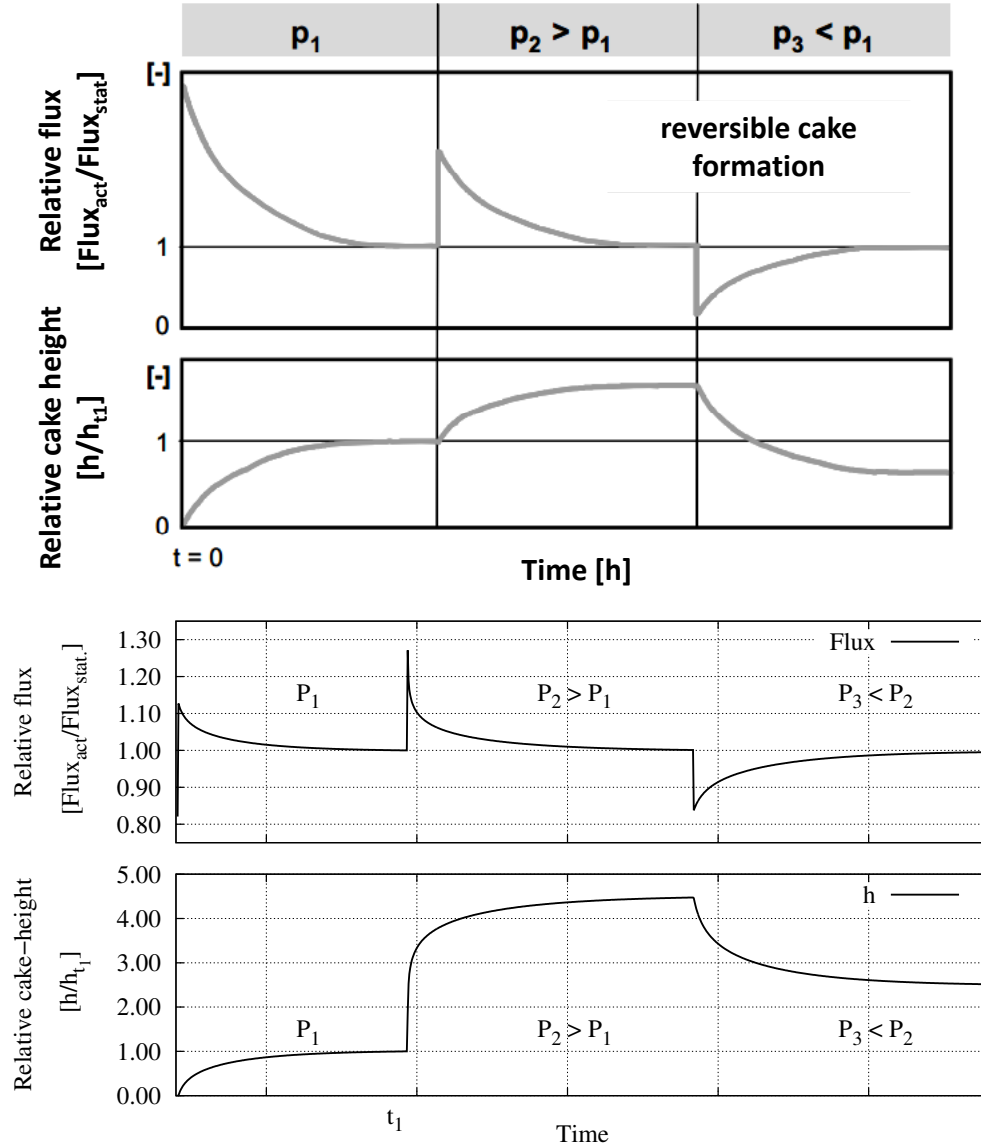


Figure 4.37.: Relative flux and relative cake height caused by TMP changes from Rautenbach [1997] (top) and simulated results (bottom).

4.4. Rectification

The rectification process was modeled according to the P&ID diagram of the laboratory rectification plant (figure 3.7) with some extensions. The major difference is the enhancement to continuous operation, due to the nature of the bioethanol process. Further, some additional valves, as well as intermediate receiving tanks were added or put into a different place.

The rectification process model was structured in a way as described in chapter 3. Again an **automation sub-model** was developed, with which different process control strategies may be tested and evaluated in reference to the energy demand of the process. The single sub-models were adopted to the process as shown in figure 4.38. The description of the sub-models follows in the next sections.

4.4.1. Kinetics sub-model

The inner core of the rectification process model is represented by the thermodynamic equilibrium of the binary mixture ethanol and water. Within this sub-model the distribution of both components into the liquid and the gaseous phase are described. The substance mol-fraction of ethanol in the liquid phase is computed from the amount of ethanol in the total substances amount:

$$X_E = \frac{n_E}{n_W + n_E} \quad (4.73)$$

The substance mol-fraction of ethanol in the gaseous phase being at equilibrium state is derived from an equilibrium curve (polynomial on the basis of equilibrium data [DDBST GmbH, 2013]). In order to fit the data optimally, the curve was subdivided into two sections (1. section ≤ 0.2608 > 2. section). The first section is described by a polynomial:

$$\begin{aligned} Y_{E1} = & -8919.6 \cdot X_E^6 + 9405.1 \cdot X_E^5 - 4055.1 \cdot X_E^4 + 935.68 \cdot X_E^3 \\ & - 127.96 \cdot X_E^2 + 11.053 \cdot X_E + 0.00007 \\ & \forall X_E \leq 0.2608 \end{aligned} \quad (4.74)$$

The second section is expressed by another polynomial:

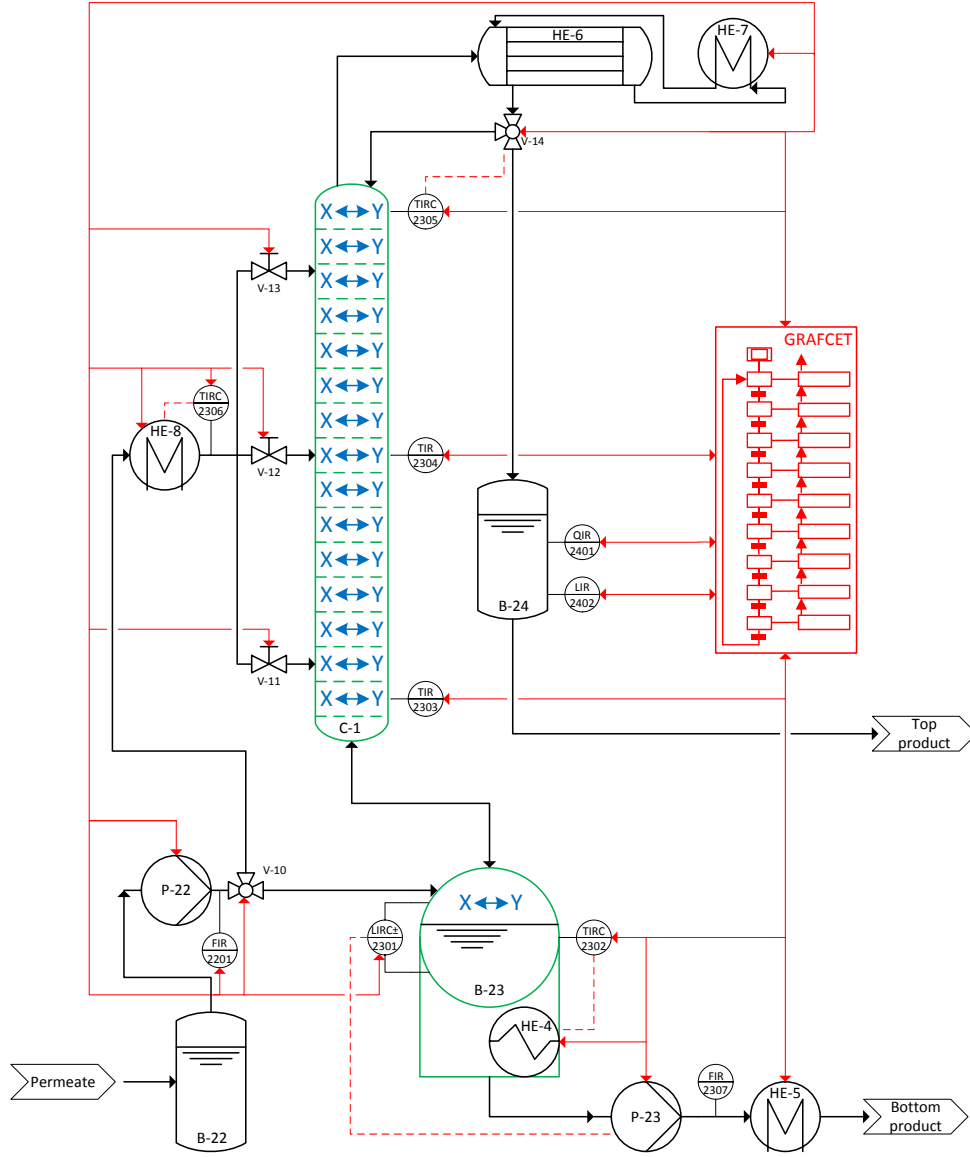


Figure 4.38.: Adaption of the sub-model structure to the rectification process model. **Kinetics sub-model**, **unit sub-model**, plant sub-model, **automation sub-model**.

$$Y_{E2} = 0.6395 \cdot X_E^3 - 0.7129 \cdot X_E^2 + 0.6513 \cdot X_E + 0.4249$$

$$\forall X_E > 0.2608 \quad (4.75)$$

As both components - in liquid and gaseous phase - always need to sum up as 1 (in order to comply with the mass balance), following boundary conditions needs to be fulfilled:

$$\sum_{i=1}^{NC} X_i = 1; \sum_{i=1}^{NC} Y_i = 1 \quad (4.76)$$

The polynomials (eqs. 4.74, 4.75) describe an ideal system with ideal equilibrium states (theoretical stage). However, in real rectification processes the effectiveness of mass and energy transfer are dependent on the gas and liquid flows in the column [Klemola and Ilme, 1997]. In order to simulate such an effectiveness, a tray efficiency factor (η') was introduced.

The tray efficiency factor depends on the vapour flow rate (\dot{V}_0) at the column entrance (bottom) [Duessel et al., 2008]. Reaching gas-liquid-equilibrium is supposed to be a very fast process compared to other transport phenomena, so it is modeled in a stationary manner:

$$\eta' = A \cdot \dot{V}_0^2 + B \cdot \dot{V}_0 \quad (4.77)$$

By implementing a tray efficiency factor, the original equilibrium curve is shifted towards the 45°-line. The lower the tray efficiency factor, the closer the equilibrium curve gets to the 45°-line (fig. 4.39). The new equilibrium curve according to the corresponding tray efficiency is given by:

$$Y'_E = Y_E - \left[(1 - \eta') \cdot (Y_E - X_E) \right] \quad (4.78)$$

The efficiency of heat and mass transfer is coupled to the flow regime inside the column. With the function written in equation 4.77 it is achieved that low as well as high vapour flow rates lead to decreased tray efficiencies (figure 4.40). By adjusting the dimensionless parameters A and B an optimal operating point for the rectification column can be set.

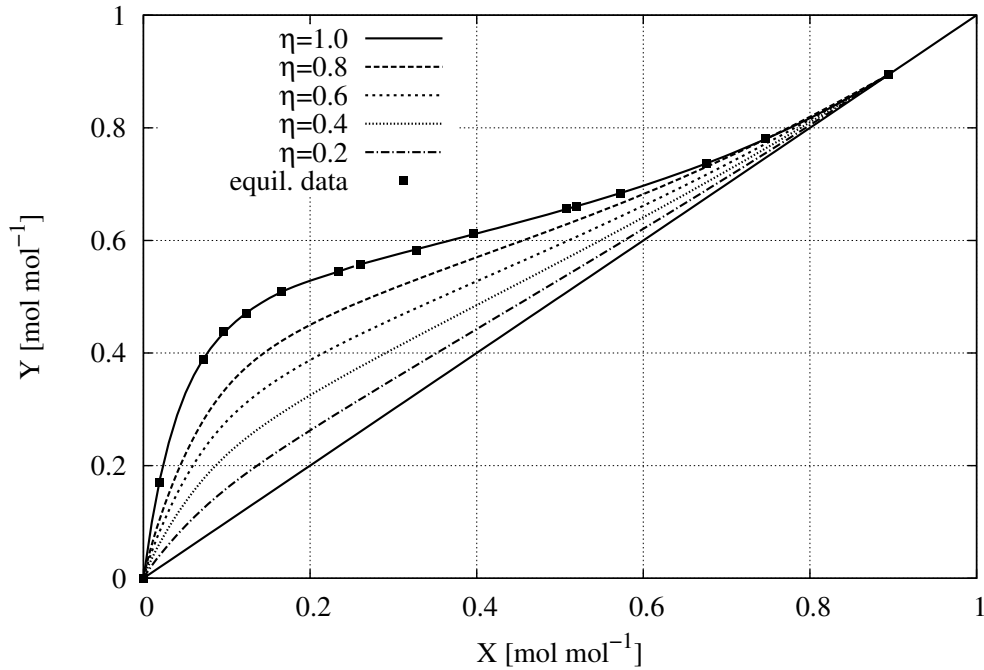


Figure 4.39.: Equilibrium curves for ethanol/water at different tray efficiencies and equilibrium data taken from the Dortmund Datenbank [DDBST GmbH, 2013] (black squares) [Kuntzsch et al., 2014].

4.4.2. Unit sub-model

The unit sub-model consists of the kinetics sub-model and is extended with dynamic mass and energy transport mechanisms in the column (figure 4.41).

In order to use the model within a training simulator, these dynamic elements are a prerequisite. Otherwise, an investigation of process control strategies on the energy demand would not be possible, since both the energy demand and process control strategies are time-dependent.

The reboiler forms a unit sub-model, as well as a single stage of the rectification column. In each stage the dynamic changes of temperatures and amount of substances are calculated. Furthermore, the stage model contains design parameters of the respective unit (diameters, heights, etc.) and specific values (heat capacities, heat transfer coefficients, exchange areas) of the involved components (table A.2, appendix).

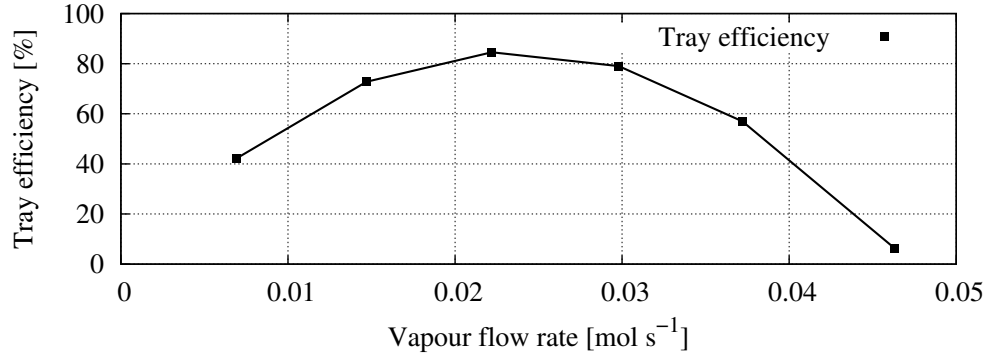


Figure 4.40.: Tray efficiency as a function of vapour flow rate. For this representation parameters were chosen ($A = -1520.4$; $B = 71.834$) to create an optimum at a flow rate of approximately $0.022 \text{ mol} \cdot \text{s}^{-1}$ [Kuntzsch et al., 2014].

The amount of substances within a stage or the reboiler changes by added feed (\dot{n}_F), liquid run-off ($\dot{L}(j)$) and vapour leaving the stage ($\dot{V}(j)$). The balances for the components ethanol and water can be expressed as follows:

$$\begin{aligned} \frac{dn_W(j)}{dt} = & \underbrace{\dot{n}_F \cdot X_{W,F}}_{\text{feed}} - \underbrace{\dot{L}(j) \cdot X_W(j)}_{\text{local run-off}} \\ & + \underbrace{\dot{V}(j-1) \cdot Y_W(j-1)}_{\text{downstream evaporation}} - \underbrace{\dot{V}(j) \cdot Y_W(j)}_{\text{local evaporation}} \\ & + \underbrace{\dot{L}(j+1) \cdot X_W(j+1)}_{\text{upstream run-off}} \quad (4.79) \end{aligned}$$

$$\begin{aligned} \frac{dn_E(j)}{dt} = & \underbrace{\dot{n}_F \cdot X_{E,F}}_{\text{feed}} - \underbrace{\dot{L}(j) \cdot X_E(j)}_{\text{local run-off}} \\ & + \underbrace{\dot{V}(j-1) \cdot Y_E(j-1)}_{\text{downstream evaporation}} - \underbrace{\dot{V}(j) \cdot Y_E(j)}_{\text{local evaporation}} \\ & + \underbrace{\dot{L}(j+1) \cdot X_E(j+1)}_{\text{upstream run-off}} \quad (4.80) \end{aligned}$$

It is important that the model also covers the heating up phase and the start of evaporation (relevant for evaluating the influence of process

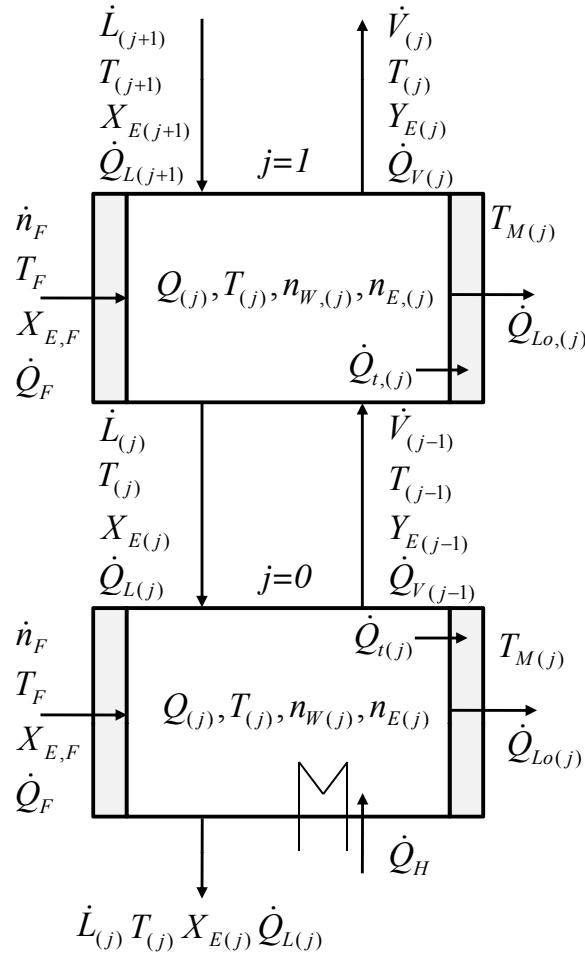


Figure 4.41.: Stage model applied to the reboiler and the first stage of the column. All entering and leaving substance and energy flows are covered. These are: feed (\dot{n}_F), liquid run-off (\dot{L}), vapour flow (\dot{V}), temperatures (T), compositions (X, Y), heat flows (\dot{Q}). Additionally, an insulating column wall temperature model was implemented (T_M) [Kuntzsch et al., 2014].

control strategies on the energy demand). After reaching boiling temperature, evaporation starts. The model realises evaporation with a control loop (figure 4.42). The control algorithm dynamically calculates evaporation and thus, is suited for the implementation in a dynamic simulator.

In this control loop the control variable is given by the currently calculated temperature of the mixture ($T(j)$) in the reboiler or a stage. The

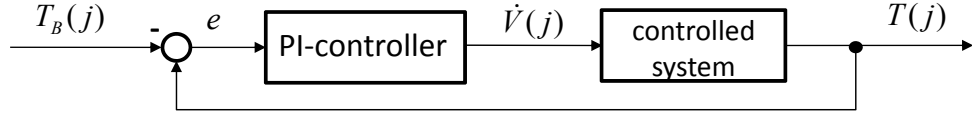


Figure 4.42.: Control loop for evaporation.

actuating variable is the vapour flow rate ($\dot{V}(j)$). The set point variable is described by the boiling temperature ($T_B(j)$) according to the boiling-curve of an ethanol/water mixture at atmospheric pressure. Here again, two polynomials were used to fit the data taken from [DDBST GmbH, 2013]. The boiling curve was separated in the same way as described in equations 4.74 and 4.75. The polynomials are:

$$\begin{aligned} T_{B1}(j) = & -38606.0 \cdot X_E(j)^5 + 31125.0 \cdot X_E(j)^4 - 10545.0 \cdot X_E(j)^3 \\ & + 2054.1 \cdot X_E(j)^2 - 259.68 \cdot X_E(j) + 99.925 \\ & \forall X_E(j) \leq 0.2608 \quad (4.81) \end{aligned}$$

and

$$\begin{aligned} T_{B2}(j) = & -1.213 \cdot X_E(j)^3 + 11.412 \cdot X_E(j)^2 - 18.377 \cdot X_E(j) + 86.314 \\ & \forall X_E(j) > 0.2608 \quad (4.82) \end{aligned}$$

Figure 4.43 illustrates the data points from Dortmund Data Bank and the polynomial fit.

From the control loop it can be seen that the control error in any stage of the column and in the reboiler ($e(t)(j)$) is:

$$e(t)(j) = T(j) - T_B(j) \quad (4.83)$$

A positive control error ($T(j) > T_B(j)$) starts evaporation. In conjunction with this evaporated flow a certain amount of energy is carried out of the mixture ($\dot{Q}_V(j)$ and \dot{Q}_{vap}). This causes a reduction of the temperature in the mixture (equations 4.88, 4.94 and 4.95) which, again, decreases the control error. The calculation of the corresponding vapour flow rate is carried out by a PI-controller:

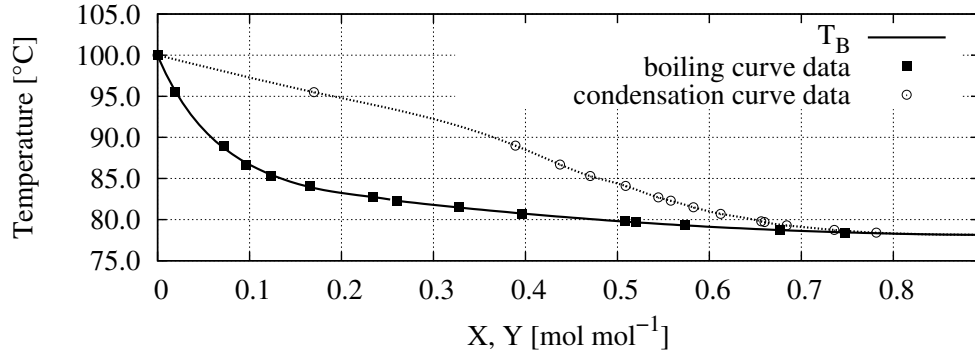


Figure 4.43.: Boiling curve (black) with data points (solid squares, [DDBST GmbH, 2013]) and the polynomial fit using two polynomials (eqs. 4.81 and 4.82).

$$\dot{V}(j) = G \cdot \left[e(t)(j) + \frac{1}{t_I} \cdot \int_0^t e(\tau) dt \right] \quad (4.84)$$

It is desirable to have the controller running into a smooth control regime without heavy fluctuations. This is done by adjusting the parameters of the PI-controller (G and t_I). In figure 4.44 the evaporation rate for a given simulation is shown together with the boiling and mixture temperature. An almost constant control error is achieved and thus, a constant, non-fluctuating evaporation rate is generated by the controller.

Liquid run-off from a stage was modeled according to Torricelli [Bohl, 2002]. At first the height of liquid holdup on a stage is calculated. Using design parameters of the column (esp. radii, table A.2), the resulting velocity of the liquid, and finally the amount of liquid run-off can be determined:

$$h(j) = \frac{\frac{n_W(j) \cdot M_W}{\rho_W} + \frac{n_E(j) \cdot M_E}{\rho_E}}{\pi \cdot r_1^2} \quad (4.85)$$

$$w(j) = \sqrt{2 \cdot g \cdot h(j)} \quad (4.86)$$

$$\dot{L}(j) = w(j) \cdot \pi \cdot r_2^2 \cdot \left(\frac{\rho_W}{M_W \cdot X_W} + \frac{\rho_E}{M_E \cdot X_E} \right) \quad (4.87)$$

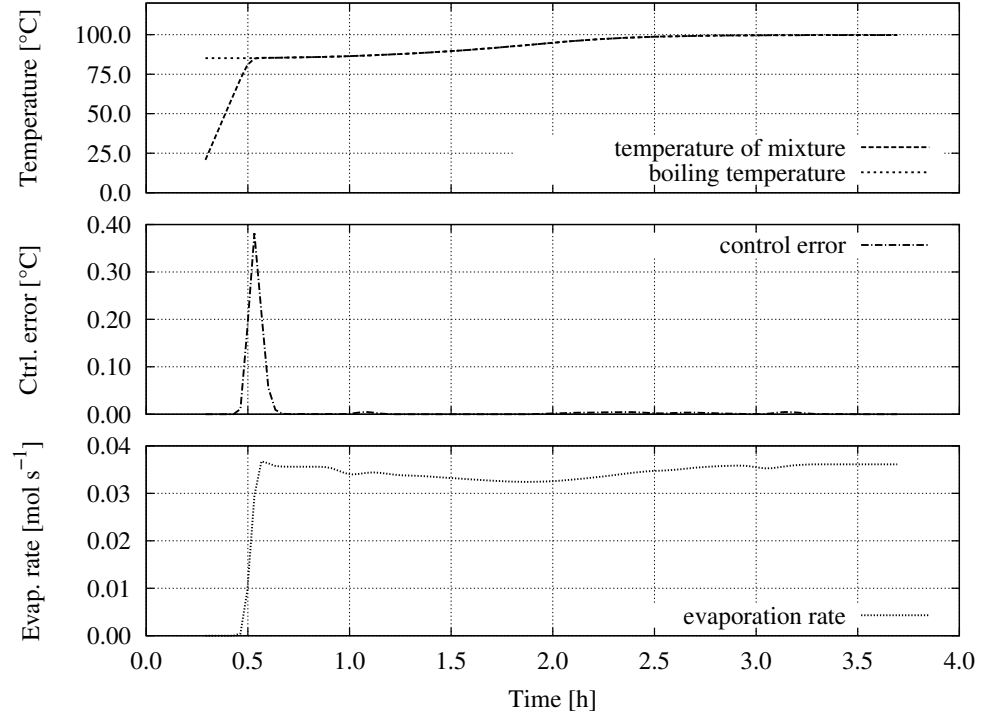


Figure 4.44.: Long-term evolution of measured temperature and boiling temperature (top) and the correlating control error (middle) and evaporation rate (bottom) for a batch-rectification. The control error is minimised after its activation (after approximately 0.5 h). This results in a relatively constant evaporation rate.

After the components' balances the energy balance can be formulated. The energy content of one control volume is increased by the heat inserted with the feed (\dot{Q}_F), the heating energy put in the reboiler (\dot{Q}_H , only in the reboiler), the run-off from upstream stages ($\dot{Q}_L(j+1)$) and the vapour flows from downstream stages ($\dot{Q}_V(j-1)$). At the same time energy is released by liquid run-off ($\dot{Q}_L(j)$) and vapour ($\dot{Q}_V(j)$) leaving the regarded stage. Moreover, heat is transferred to the column wall (\dot{Q}_t). The energy balance for a stage becomes:

$$\begin{aligned} \frac{dQ(j)}{dt} = & \dot{Q}_F + \dot{Q}_H + \dot{Q}_L(j+1) + \dot{Q}_V(j-1) \\ & - \dot{Q}_L(j) - \dot{Q}_V(j) - \dot{Q}_t \quad (4.88) \end{aligned}$$

The energy content of a control volume can be written as the product of the amount of substances (n_W, n_E), their specific molar heat capacities ($c_{M,W}$ and $c_{M,E}$) and a temperature difference ($(T(j) - T_0)$, with T_0 reference temperature: table A.2). The low mass of the steam, as compared to the liquid, and eventually occurring heat of solution were neglected, in order to keep the model simple:

$$Q(j) = (n_W(j) \cdot c_{M,W} + n_E(j) \cdot c_{M,E}) \cdot (T(j) - T_0) \quad (4.89)$$

In order to further simplify the model, mixing enthalpies as well as the volumetric contraction of the water-ethanol-mixture were neglected. By insertion of equation 4.89 in equation 4.90 and rearrangement following differential equation for the change of temperature is obtained:

$$\frac{dT(j)}{dt} = \frac{\dot{Q}_F + \dot{Q}_H + \dot{Q}_L(j+1) + \dot{Q}_V(j-1) - \dot{Q}_L(j) - \dot{Q}_V(j) - \dot{Q}_t}{n_W(j) \cdot c_{m,W} + n_E(j) \cdot c_{m,E}} \quad (4.90)$$

Material-bound heat flows are the product of substance amount flow rate and heat content. Energy flows coupled to liquids are given as follows:

$$\dot{Q}_F = \dot{n}_F \cdot (T_F - T_0) \cdot (X_{W,F} \cdot c_{m,W} + X_{E,F} \cdot c_{m,E}) \quad (4.91)$$

$$\dot{Q}_L(j) = \dot{L}(j) \cdot (T(j) - T_0) \cdot (X_W(j) \cdot c_{m,W} + X_E(j) \cdot c_{m,E}) \quad (4.92)$$

$$\begin{aligned} \dot{Q}_L(j+1) = \dot{L}(j+1) \cdot (T(j+1) - T_0) \\ \cdot (X_W(j+1) \cdot c_{m,W} + X_E(j+1) \cdot c_{m,E}) \end{aligned} \quad (4.93)$$

Gaseous heat flows include the enthalpy of evaporation of the components:

$$\dot{Q}_V(j) = \dot{V}(j) \cdot (Y_W(j) \cdot \Delta H_{V,W} + Y_E(j) \cdot \Delta H_{V,E}) \quad (4.94)$$

$$\begin{aligned} \dot{Q}_V(j-1) &= \dot{V}(j-1) \\ &\cdot (Y_W(j-1) \cdot \Delta H_{V,W} + Y_E(j-1) \cdot \Delta H_{V,E}) \end{aligned} \quad (4.95)$$

Heating input from the heater into the reboiler is represented by direct heat input. The power of the heater can be set to a desired value (e. g. 500 W), and this energy is then entirely used for heating and evaporation.

$$\dot{Q}_H = P_{input} \quad (4.96)$$

Moreover, a function that computes the temperature of the column wall ($T_M(j)$) was modeled. The differential equation for the temperature changes in the column wall is similar to the temperature equation for the mixture temperature. Important parameters here are the mass of the column wall ($m_M(j)$) and its specific heat capacity ($c_{p,M}$). The energy flow from the mixture to the column wall ($\dot{Q}_t(j)$) is given by convective heat transfer which is the product of heat transfer coefficient (α), heat transfer area ($A_t(j)$) of the regarded stage and the temperature difference ($T(j) - T_M$). The column's heat losses (\dot{Q}_{Lo}) are finally considered in the insulation/wall temperature equation as heat transfer through a wall.

$$\dot{Q}_t(j) = \alpha_t \cdot A_t(j) \cdot (T(j) - T_M(j)) \quad (4.97)$$

$$\dot{Q}_{Lo}(j) = k_{Lo} \cdot A_{Lo}(j) \cdot (T_M(j) - T_U) \quad (4.98)$$

By adjusting the heat transfer coefficient k_{Lo} in equation 4.98, an insulation layer can be added to the wall. The change of wall temperature is expressed by:

$$\frac{dT_M(j)}{dt} = \frac{\dot{Q}_t(j) - \dot{Q}_{Lo}(j)}{m_M(j) \cdot c_{p,M}} \quad (4.99)$$

4.4.3. Plant sub-model

The components of the plant sub-model are the condenser for the distillate, heat exchangers for preheating the feed and cooling down the product from the reboiler, a receiving tank, pumps, valves and diverse sensors (figure 4.38). The components used in the rectification plant model are listed in table 4.3.

Table 4.3.: Tanks and components used in the plant model of the rectification process

Name	Description	Specification	Model
B-22	Buffer tank	20 <i>L</i>	4.6-4.9
B-23	Reboiler	20 <i>L</i>	
B-24	Product tank	20 <i>L</i>	
P-22	Feed pump	0 ... 2000 <i>mL · min⁻¹</i>	4.5
P-23	Swamp pump	0 ... 2000 <i>mL · min⁻¹</i>	
V-10	Three-way-valve	0 or 1	4.2
V-11	Standard valve	0 or 1	4.1
V-12	Standard valve	0 or 1	
V-13	Standard valve	0 or 1	
V-14	Reflux valve	0 or 1	4.3
HE-4	El. heater	0 ... 1500 <i>W</i>	4.96
HE-5	Cooler	0 ... 1500 <i>W</i>	4.10-4.20
HE-6	Condenser	0 ... 1500 <i>W</i>	4.21-4.33
HE-7	Air cooler	0 ... 1500 <i>W</i>	4.10-4.20
HE-8	Feed heater	0 ... 1500 <i>W</i>	4.10-4.20
Sensors			
FIR-2201	Flow	0 ... 2000 <i>mL · min⁻¹</i>	none
LIRC-2301±	Level	0 ... 20 <i>L</i>	none
TIRC-2302	Temperature	0 ... 150 °C	4.35
TIR-2303	Temperature	0 ... 150 °C	
TIR-2304	Temperature	0 ... 150 °C	
TIRC-2305	Temperature	0 ... 150 °C	
TIRC-2306	Temperature	0 ... 150 °C	
FIR-2307	Flow sensor	0 ... 2000 <i>mL · min⁻¹</i>	none

Continued on next page

Table 4.3 – continued from previous page

Name	Description	Specification	Model
QIR-2401	Quality (EtOH)	$750 \text{ g} \cdot \text{L}^{-1}$	none
LIR-2402	Level sensor	$0 \dots 20 \text{ L}$	

4.4.4. Automation sub-model

The automation sub-model of the rectification process is composed of control loops and the automatic sequence control, with which process control strategies are defined.

Controls

Following controls were implemented into the automation sub-model:

- Temperature control in the column head
- Level control in the reboiler
- Heating rate control for heating up procedure
- Cooling energy control for the condenser

All controls were accomplished with PI-controllers (eq. 4.36 with $t_D = 0.0$). The **temperature control loop** structure is shown in figure 4.45. The temperature is used as an auxiliary quantity for the ethanol concentration at the column head. Having a high reflux ratio (v) leads to a higher ethanol concentration and thus, to a lower boiling temperature (pressure changes neglected) in the head of the column. A positive control error ($wT_{head} > T_{head}$) reduces the reflux interval (u) and raises the reflux ratio (v).

The **level control loop** (figure 4.46) is particularly needed in continuous mode. The permanent feed at a certain position of the column fills up the reboiler constantly. The reflux (\dot{L}) can be seen as a disturbance variable. Comparing the desired volume (wV_R) with the currently measured volume (V_R) a value for the flow rate of the respective pump (\dot{m}) is generated. A negative control error ($wV_R < V_R$) increases the pump flow rate.

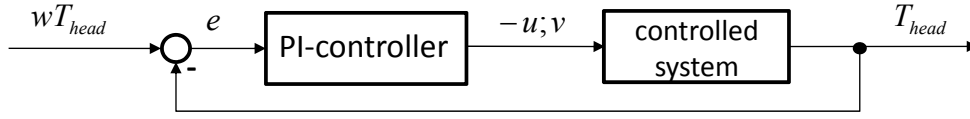


Figure 4.45.: Control loop of the temperature control in the head of the column. Positive control errors ($wT_{head} > T_{head}$) let the reflux interval decrease, while the reflux ratio is increased [Kuntzsch et al., 2014].

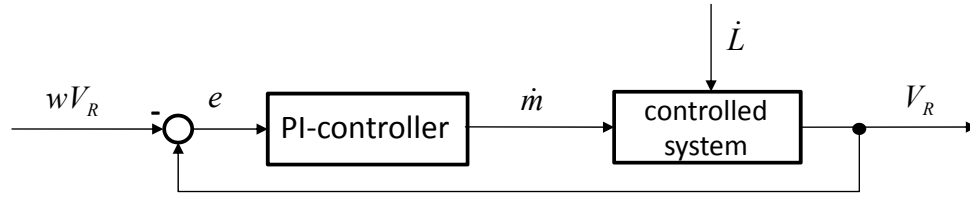


Figure 4.46.: Control loop of the reboiler's level control. Negative control errors ($wV_R < V_R$) increase the pump rate. The control scheme is inverse.

The **heating rate control loop** allows for heating up the mixture in the reboiler with a desired heating rate. The actual heating rate is determined with a derivative element ($\frac{dT}{dt}$) and compared to the desired heating rate ($\frac{wdT}{dt}$). A positive control error ($\frac{wdT}{dt} > \frac{dT}{dt}$) increases the heating input (\dot{Q}_H) (figure 4.47).

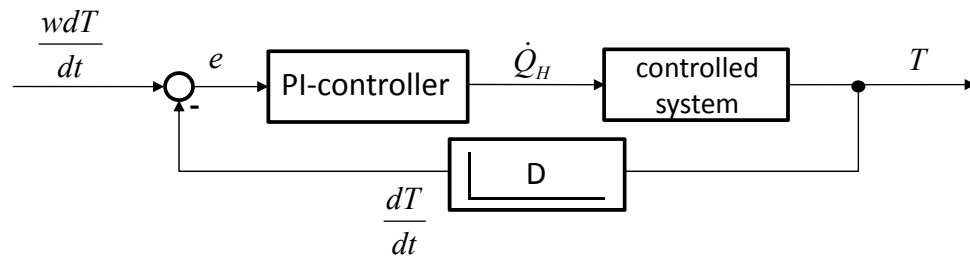


Figure 4.47.: Control loop of the heating rate for the mixture in the reboiler. A positive control error ($\frac{wdT}{dt} > \frac{dT}{dt}$) increases the heating input.

The **cooling fluid control loop** (figure 4.48) defines the energy amount required for total condensation of the distillate (cp. 4.1.4, page 55). Here the control error is built by the difference of desired distillate temper-

ature (wT_D) and actual distillate temperature (T_D). When the control error is positive, the heat that needs to be conducted is increased.

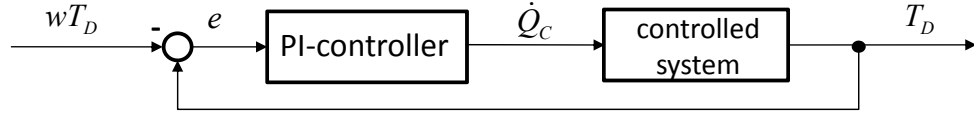


Figure 4.48.: Control loop for the amount of energy needed for conducting heat from the vapour (for condensation). Positive control errors ($dT > wdt$) increase the energy needed for conducting the heat from the vapour. The control logic is inverse.

Automatic sequence control

For the batch-rectification the operating phases warming-up, production, cooling-down, and emptying were integrated into a GRAFCET functional plan. The parameters in the transitions and actions of this GRAFCET plan are constant/ variable reflux ratio, reflux interval, reflux ratio, desired product quality and quantity in the reboiler, and heating rate and heating power input. These can be manipulated, in order to investigate process control strategies. The operational sequence for batch-operation of the column was formulated in form of a GRAFCET and comprises the subsequent major steps:

- activation and initialisation of the sequence control,
- definition of starting volume and -concentration in the reboiler,
- filling the reboiler,
- activation of the heater and of the heating rate control,
- deactivation of heating rate control after reaching of boiling conditions,
- setting the heating power to a desired value,
- activation of the condenser after temperature increase in the middle position of the column,

- reaching a thermal equilibrium along the whole plant with total reflux (all temperature sensors are constant),
- setting the reflux ratio and the type of valve control (constant/variable),
- begin production,
- stop production after reaching the desired product volume,
- setting reflux valve to total reflux; deactivate heating,
- cooling-down,
- deactivating the condenser when head temperature is below a set point,
- emptying the reboiler, and
- re-initialising the sequence control for the next batch-rectification run.

The rectification sequence was transferred into a GRAFCET functional plan (figure A.9 in the appendix).

4.4.5. Model validation

For model validation the laboratory rectification plant described in chapter 3.2.3 was used. A defined volume of 3 L was filled into the reboiler. The ethanol concentration of $260 \text{ g} \cdot \text{L}^{-1}$ was achieved by mixing 99 Vol.-% ethanol and tap water in the needed ratio, concentration was checked with an ABBE refractometer.

The experiment was carried out at room temperature (21.0 °C). The heating input was set to 700 W. Reflux valve was determined to operate in constant reflux mode with a reflux interval of 10 s and a reflux ratio of 5. In order to verify not only the standard operating points, as e. g. needed in optimising continuous rectification processes, a complete batch-rectification was proceeded.

This experiment included the warming-up and cooling-down phases (figure 4.49). With this strategy the correctness of the model in a large bandwidth should be demonstrated. With the process control system

the temperatures in the reboiler, and in the column bottom, center and head were measured and recorded with a given interval (1 min^{-1}).

At first, the mixture was warming-up. The temperature in the reboiler rose up to the boiling temperature, according to the composition of the mixture. After reaching boiling conditions, vapour got into the column which was indicated by rising temperatures, first in the bottom, then in the center and finally in the head of the column. After reaching thermal equilibrium (all temperature sensors constant), the reflux valve was opened and production started.

Triggered by this event, the temperatures began to increase continuously, in the reboiler as well as in the other positions of the column. This was induced by the continuously changing compositions at those places. Temperatures in the center and head of the column firstly remained constant. After reaching a temperature of $100 \text{ }^{\circ}\text{C}$ in the reboiler, only water flew into the column. The water vapour rose towards the column head, shown by increasing temperatures. The heating was deactivated, as no ethanol was left in the plant (all temperatures $100 \text{ }^{\circ}\text{C}$). At this time the reflux valve was set to total reflux. At the end the cooling-down phase was recorded.

The simulation experiment was carried out with the help of the automatic sequence control described earlier. Model parameters were taken from literature (material and substances specifics) or manually adapted (table A.2 in the appendix) for a best possible fit of the model to the measured data (esp. heat transfer coefficients). A comparison between measured and simulated results is given in figure 4.49.

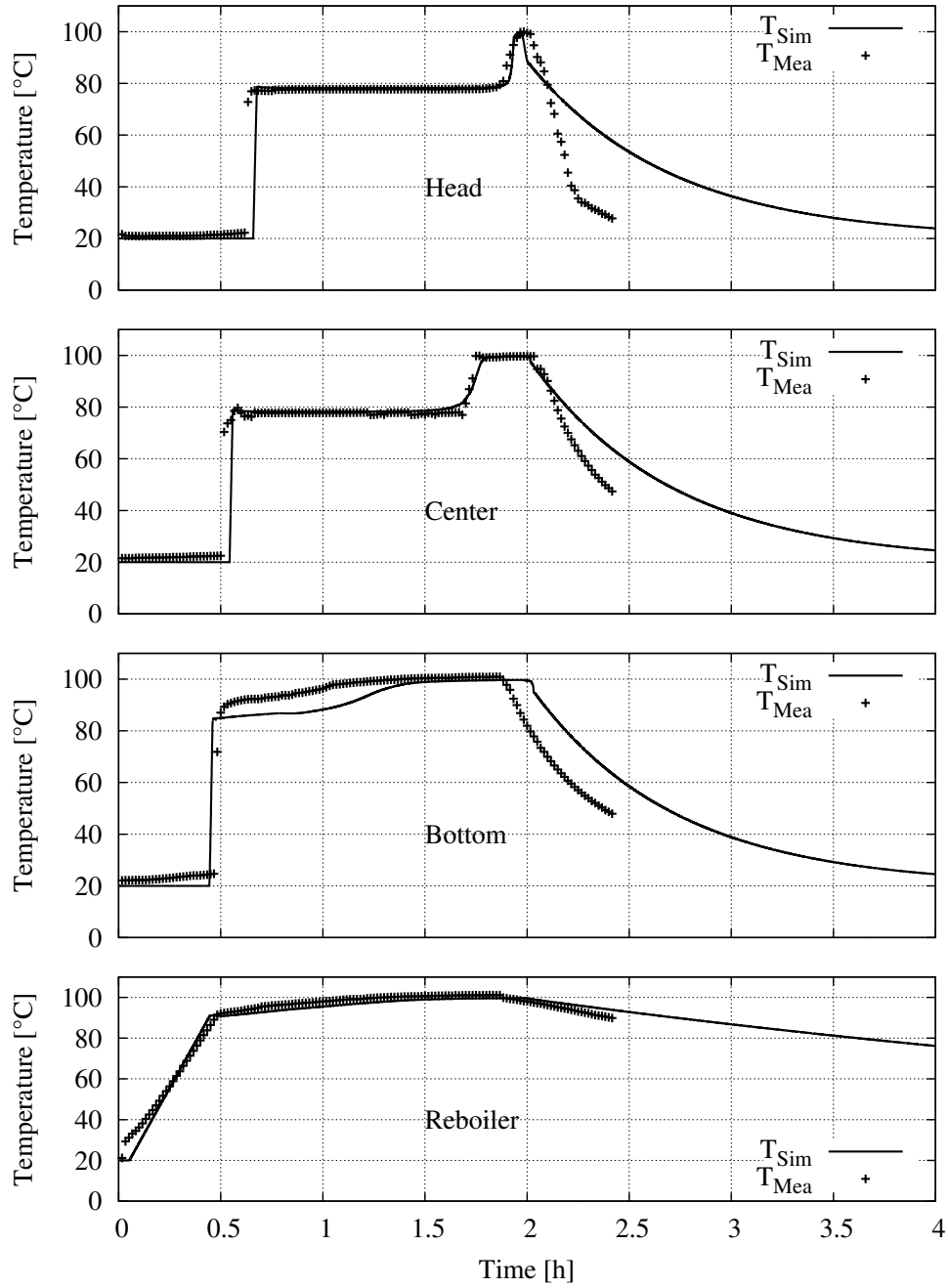


Figure 4.49.: Batch operation of a rectification column. Measured (symbols) and simulated (lines) temperatures in the reboiler, bottom, center and top of the column. The experiment includes warming-up ($\rightarrow 0.5$ h), rectification ($\rightarrow 2.0$ h) and cooling-down ($\rightarrow 4.0$ h).

5. Operator Training Simulators

The following chapter describes the unit operation training simulators and their combination to form a virtual biorefinery. The cultivation simulators (bioreactor 1 and bioreactor 2) are based on the identical mathematical model, as described in the preceding chapter. Here a duplicate was created so that one cultivation process may be used for yeast cultivation under aerobic conditions, while in the second bioreactor ethanol is produced under anaerobic conditions.

All simulators may also be used as stand-alone versions, in order to practice, optimise and test automation and process control strategies of the regarded unit operation, and to investigate the influence on energy demand. The simulators have got intuitive graphical user interfaces (GUIs) that are comparable to those in real plants [Reinig et al., 2004].

Furthermore, the simulators provide the operator with dynamic trends of important variables. The simulation may be accelerated, interrupted, initial conditions can be invoked and measurements are recorded. Finally, the simulator calculates the energy needed and the amount of substrates and auxiliary materials (e. g. antifoam agent) used in simulation experiments. In the following section the training simulators and their characteristics are introduced.

5.1. Bioreactor 1 and 2

5.1.1. Graphical user interfaces

Each training simulator has got a main graphical user interface, in which the simulated process is depicted in a centralised position of the screen (see figure 5.1). The process is illustrated as a simplified P&ID flow chart with all relevant elements. Some of these elements (pumps, valves) may be used directly here to open sub windows, as e. g. the pump station (figure 5.2 b).

In the lower space of the main GUI some further push-buttons are placed. These buttons call the process automation interface (figure 5.2 a), the

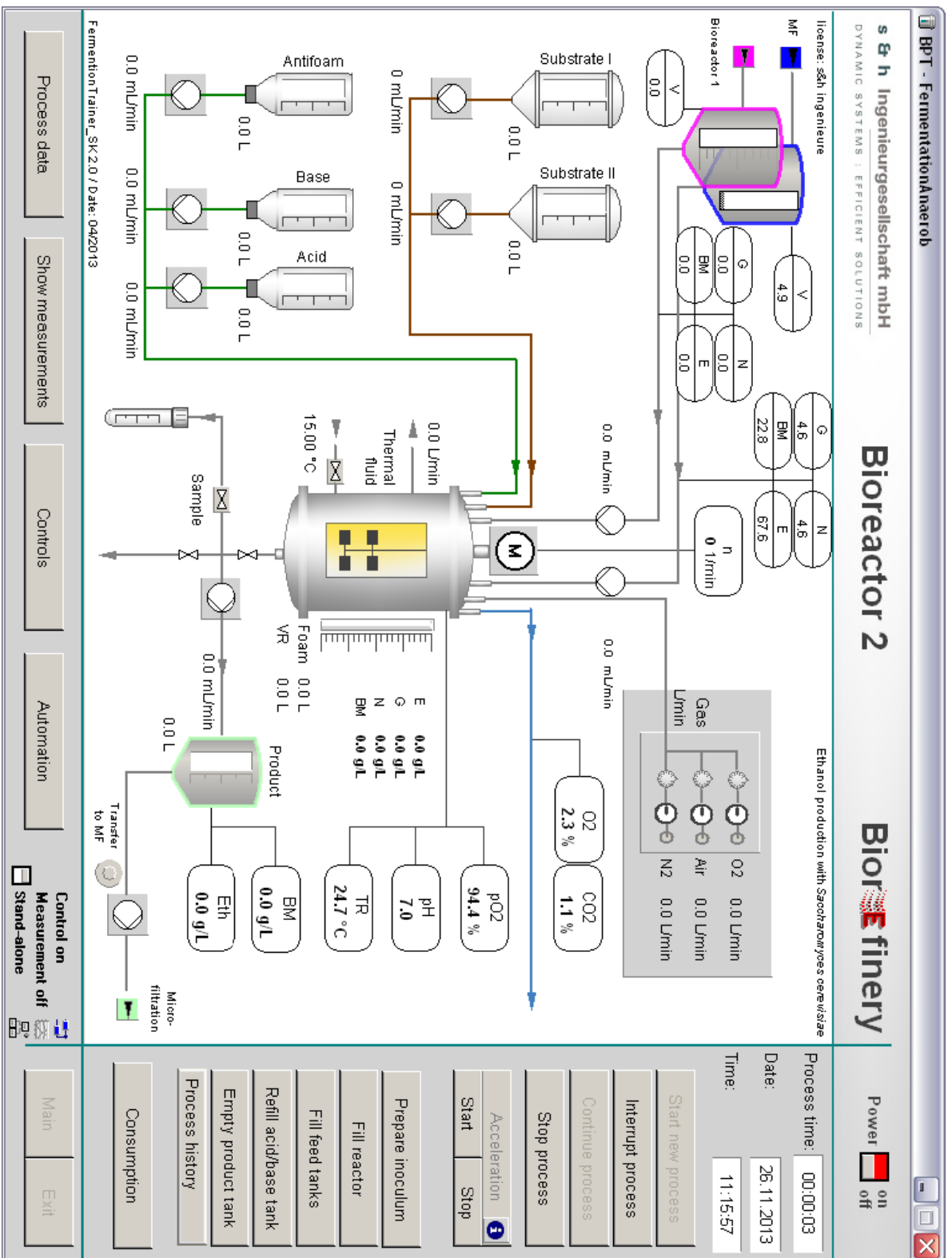


Figure 5.1.: Main graphical user interface (GUI) of the cultivation training simulator.

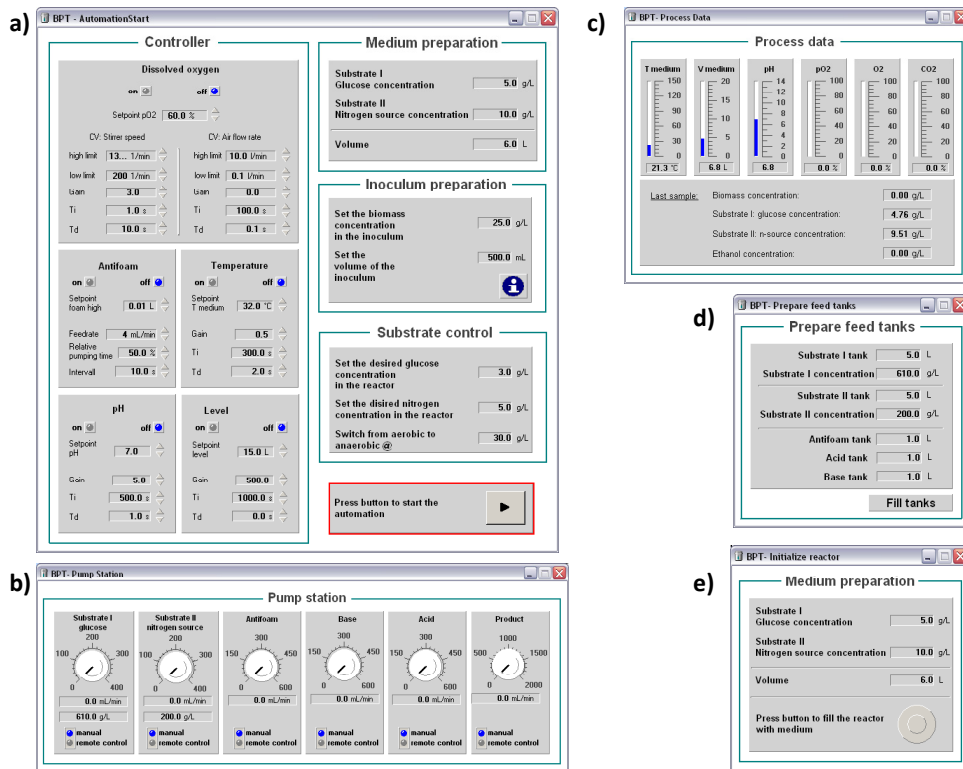


Figure 5.2.: Auxiliary graphical user interfaces within the bioreactor 1 and 2: a) Automation window - here the process control parameter for the automated process run are adjusted prior to simulation; b) Pump station - adjustment of all pumps within the cultivation process; c) Process data - overview of online states (temperature, pH, etc. and results of last sampling (biomass, glucose, ethanol, etc.)); d) Prepare feed tanks - adjustment of filling degree and starting concentrations in the feed tanks; e) Medium preparation - set-up of the starting volume and concentrations in the bioreactor

controller set-up interface (not shown, but very similar to the automation interface), or actual process states (figure 5.2 c). In the bottom right corner there is also some information about the simulator status shown (is the simulator running?, is the simulation mode active?, are measurements activated?). It is also here, where the stand-alone simulators are connected to the biorefinery via a switch. This is carried out with the help of AutoHotkey (see chapter 3.4.4).

5.1.2. Energy demand and consumption materials

Bioreactor 1 and 2 may be used for investigations regarding energy and materials consumption (glucose, nitrogen source, antifoam agent, base, acid and air). The consumption materials are integrated over the time. The mass of glucose and N-source are computed as:

$$m_i = \int_{t_0}^{t_{end}} \dot{V}_i \cdot c_i \, dt$$
$$i \rightarrow \text{glucose, N - source} \quad (5.1)$$

The other materials are given as:

$$V_i = \int_{t_0}^{t_{end}} \dot{V}_i \, dt$$
$$i \rightarrow \text{antifoam, base, acid, air} \quad (5.2)$$

The energy demand refers to the heat that is needed to keep the bioreactor temperature at a constant and desired level. Power input caused by pumps or the stirrer is neglected. Here it is assumed, that the influence of those aggregate is weighing not so heavily on the overall energy demand. The heating energy is expressed as:

$$Q_{input} = \int_{t_0}^{t_{end}} \dot{V}_H \cdot c_{p,H} \cdot (T_H^0 - T_H^1) \, dt \quad (5.3)$$

5.2. Cross-flow filtration

5.2.1. Graphical user interfaces

In order to guarantee an easy-to-adopt look and feel of the different processes, the general appearance of the OTS was built up in an identical manner. The main graphical user interface shows the process as a P&ID flow chart in a centralised position of the window (figure 5.3).

As auxiliary GUIs there are those that open online trends for characteristic variables (i. e. flux, filter cake height, flow rates, pressure; figure 5.4 a, b) and the controller setting for the control loops (figure 5.4 c) described in chapter 4.3.3. Here also some further process control options, like diafiltration or back flushing may be initialised.

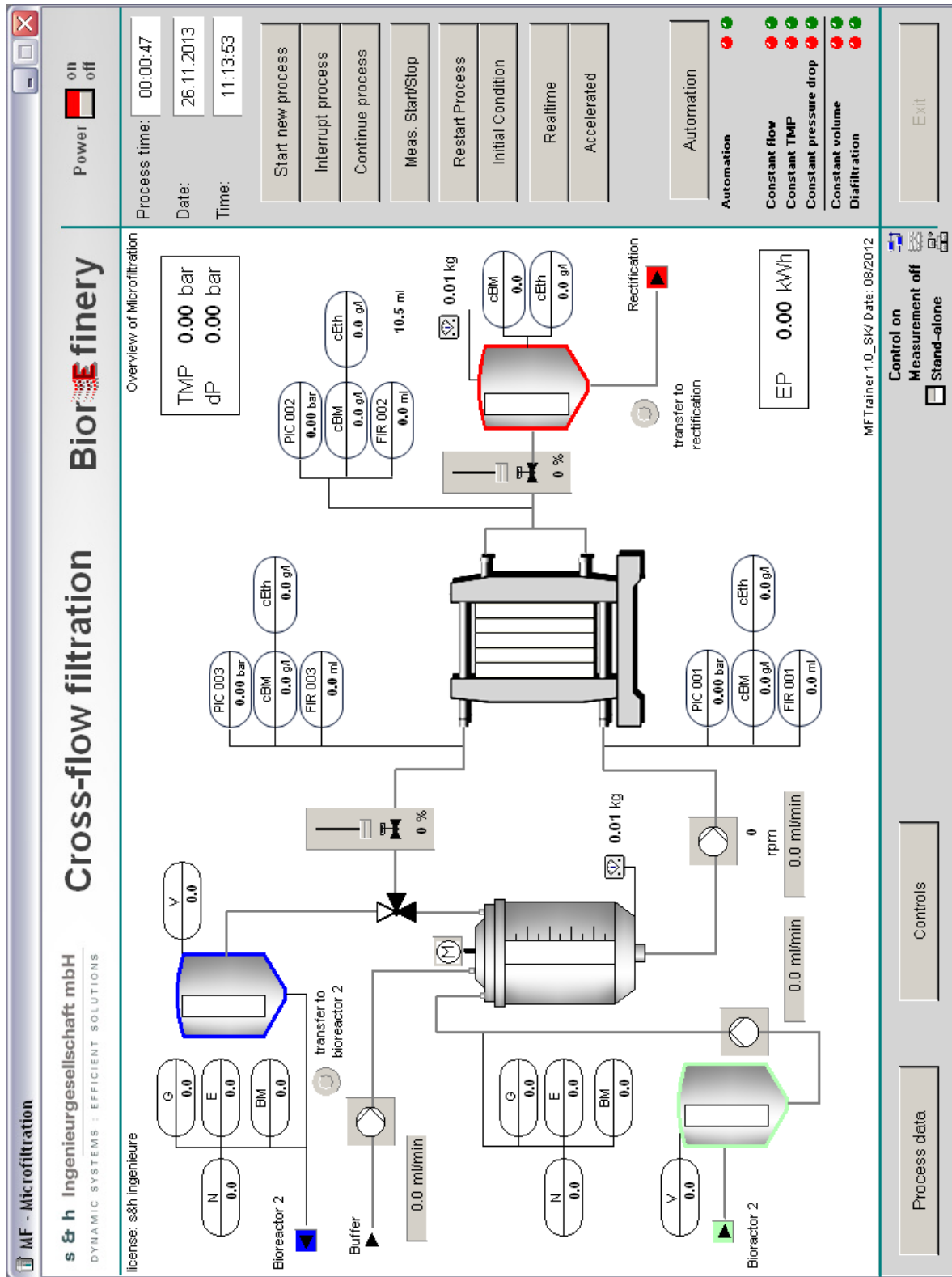


Figure 5.3.: Main graphical user interface (GUI) of the microfiltration training simulator.

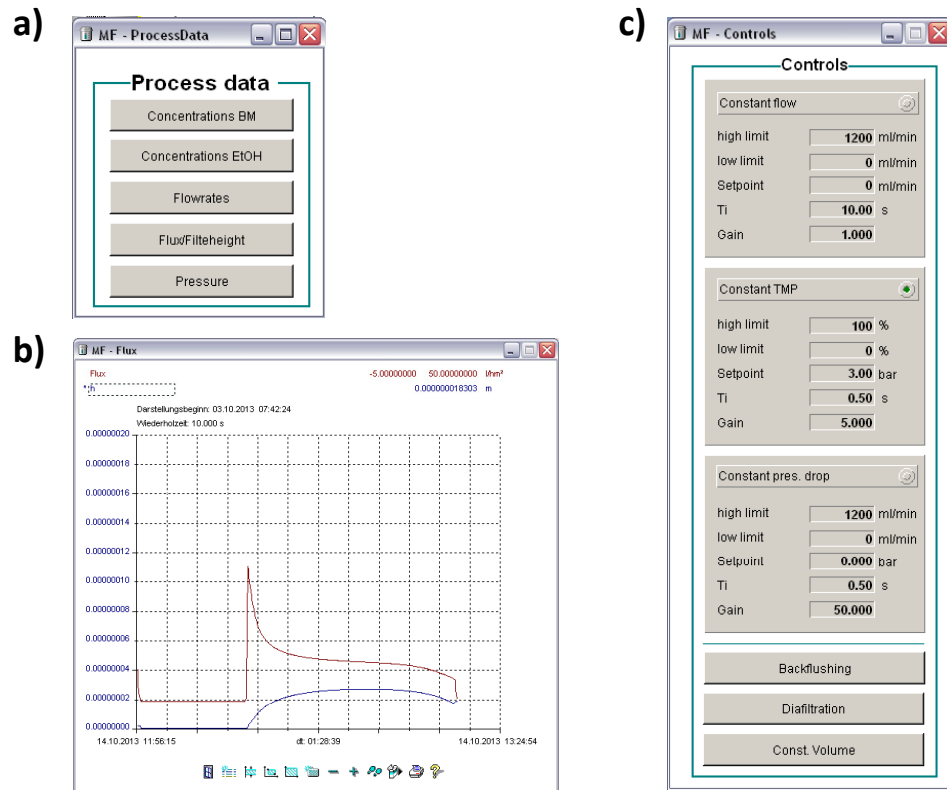


Figure 5.4.: Auxiliary graphical user interfaces within the cross-flow filtration simulator: a) Process data - here online trends for several variables can be selected; b) Online trend for flux and filter cake height; c) Controls - here the control loops can be adjusted and activated. Further process control options may be activated (back flushing, diafiltration, constant volume).

5.2.2. Energy demand

The training simulator can be used to investigate the effects of flow rate and trans membrane pressure on the duration of a batch experiment and on the energy demand caused by the main feed pump (P-20). It was assumed that the feed pump is the main influencing energy consumer in this system. For this purpose a correlation between revolution speed, pressure and power input was modeled. In VERDER Deutschland GmbH [2013] this relation is described for a peristaltic pump that fits into the range of the laboratory plant simulated here. The power input is proportional to the revolution speed of the pump. With increasing systematic

pressure the power input increases as well (figure 5.5).

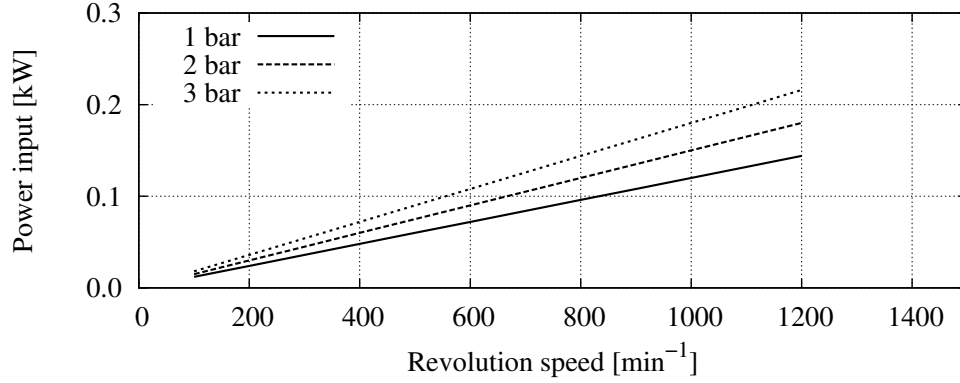


Figure 5.5.: Power input of the feed pump as a function of revolution speed and for different pressures behind the pump.

Assuming all those curves are passing the y-axis at 0.0, the slope is the only changing parameter. The slope in a given power input range is received by following equation:

$$m_{slope} = 0.3 \cdot 10^{-4} \cdot p_F + 0.9 \cdot 10^{-4} \quad (5.4)$$

The slope multiplied with the revolution of the pump (in a given range) gives the power input (P):

$$P = m_{slope} \cdot RPM \quad (5.5)$$

The integrated power input for a complete batch filtration gives the total energy consumption of the process:

$$Q_{input} = \int_{t_0}^{t_{end}} P \, dt \quad (5.6)$$

5.3. Rectification

5.3.1. Graphical user interfaces

The rectification simulator has got an equivalent layout regarding the graphical user interfaces (figure 5.6).

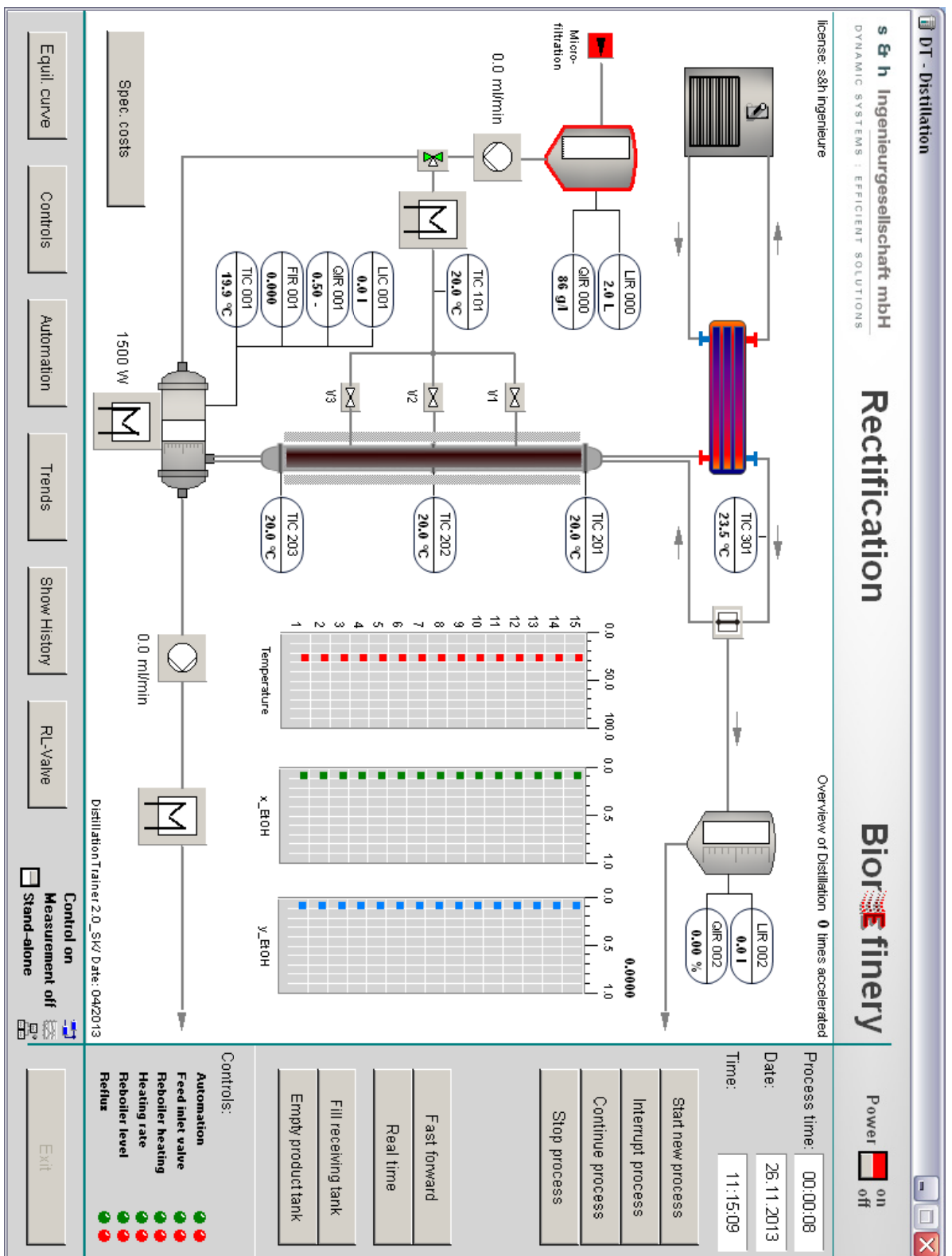


Figure 5.6.: Main graphical user interface (GUI) of the rectification training simulator.

5.3. RECTIFICATION

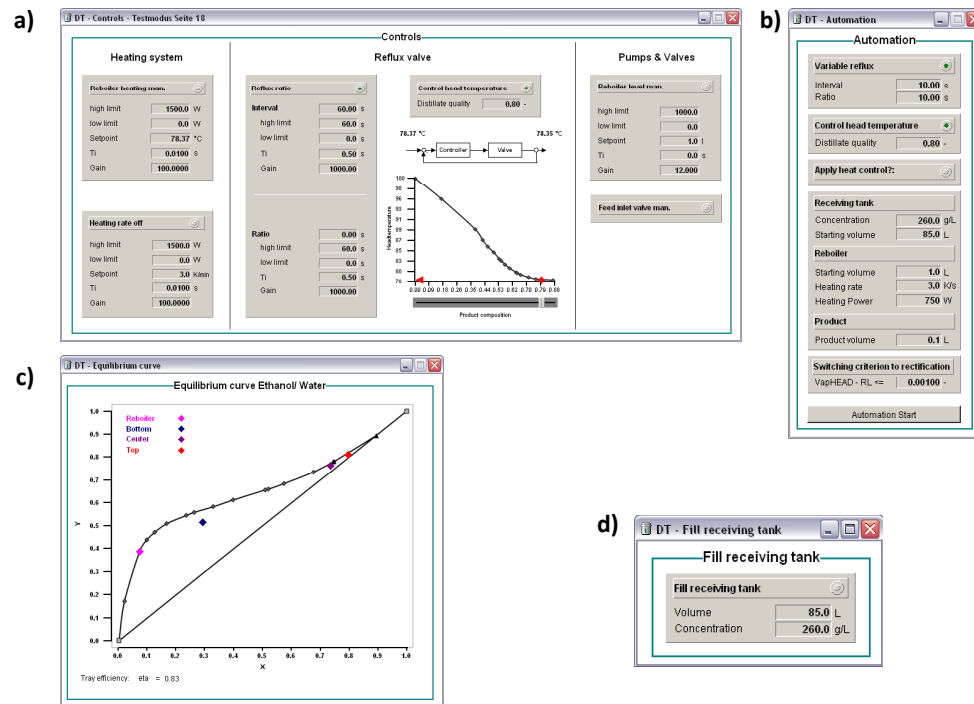


Figure 5.7.: Auxiliary graphical user interfaces within the rectification training simulator: a) Controls - here the controller parameter are set; b) Automation - in this GUI the parameter of the process control strategy are set (link to the GRAFCET plan); c) Equilibrium curve - the current status of the plant in an equilibrium curve; d) Fill receiving tank - setup of starting volume and concentration in the buffer tank B-22.

In the centralised position of the simulator window, the complete process (including heat exchangers, buffer tanks, etc.) is depicted. Next to the common push buttons some space was reserved for graphical elements that visualize the actual distribution of ethanol in the liquid and vapour phase and the temperature profile along the column.

The auxiliary GUIs here comprise of sub windows in which the controller parameters and the controllers themselves are adjusted and switched on/off (figure 5.7 a), or where the parameters of the GRAFCET plan can be varied (figure 5.7 b), for changing the process control strategy. In another auxiliary GUI the current distribution of ethanol and water is shown in a dynamic equilibrium curve (figure 5.7 c). In order to fill the buffer tank B-22 with the desired volume and starting concentration, the according

window is opened which offers input fields for these parameters (figure 5.7 d).

5.3.2. Energy demand

The total energy demand in the rectification process is the integrated power input of the reboiler and the condenser (and in continuous operation: the feed pre-heater and product cooler):

$$Q_{input} = \int_{t_0}^{t_{end}} \dot{Q}_H + \dot{Q}_C \left(+\dot{Q}_{pre-heater} + \dot{Q}_{productcooler} \right) dt \quad (5.7)$$

5.4. Virtual Biorefinery

The virtual biorefinery combines the single unit operations. With the linked simulators a continuous process control strategy may be initiated. With the virtual biorefinery influences of changes in single unit operations on the energy demand of the overall process may be demonstrated.

5.4.1. Interface connection

For the interface connection a special driver was used (WRPServ Router: [Schoop, 2008]). With the router driver project signals may be transferred to other simulator projects via a network. The TCP/IP network protocol is used, which allows for distributing the single simulators to different personal computers. This allows for creating a virtual plant in a PC-lab and, on the other hand, helps accelerating computation.

In order to structure the communication between the simulators, a master (write)/slave (read) mechanism was set up (figure 5.8). In the virtual biorefinery bioreactor 1 acts as a master for bioreactor 2, which in this case is the corresponding slave. At the same time bioreactor 2 acts as the master for the cross-flow filtration, which again is a slave in this connection, but a master to the rectification.

The rectification is a slave for all other simulators. The interface connection between the simulators is performed via the buffer tanks in all processes. The variables' values are either written (master) or read (slave),

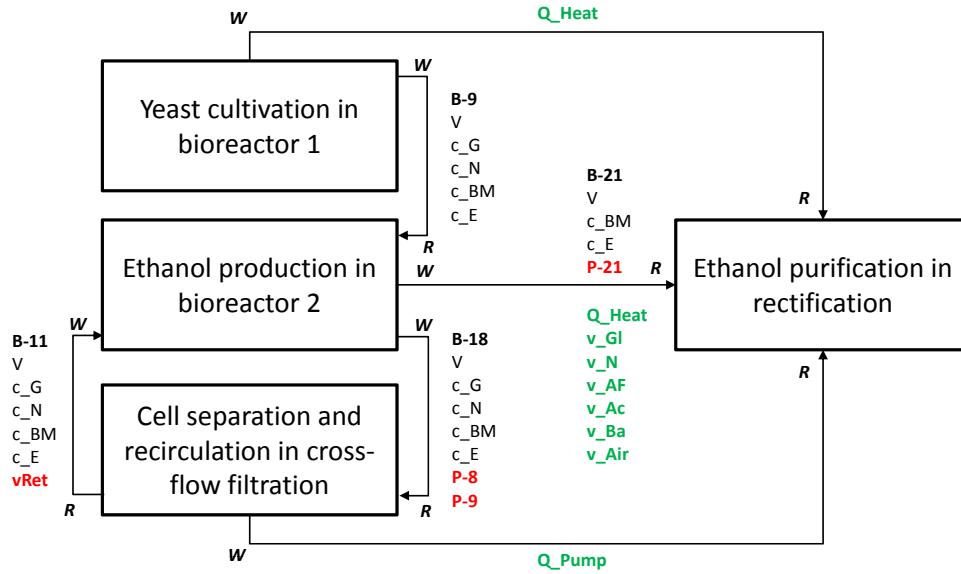


Figure 5.8.: Read- (R) and write-permissions (W) in the virtual biorefinery. Tank information (volumes and concentrations in black), consumption values (green) and flow rates for continuous operation (red).

so that the associated simulator can compute with the values transferred.

Furthermore, the actual energy consumption values in all unit operations are transferred to the rectification simulator, where a final energy balance is computed. With this energy balance the efficiency of a continuously running process can be displayed online.

5.4.2. Specific production costs

For evaluating the process efficiency, a cost function that considers all energy and consumed materials in terms of money was created. The production costs are related to the actual production revenues (amount of ethanol and quality). The cost function gives back the current status of a process in continuous operation.

The consumption materials and the energy are expressed in arbitrary units (AU) per specific unit. These are represented in table 5.1.

Table 5.1.: Costs for auxiliary materials and energy.

Cost factor	Price
Glucose	$0.3 \text{ AU} \cdot g^{-1}$
N-source	$0.3 \text{ AU} \cdot g^{-1}$
Antifoam agent	$0.025 \text{ AU} \cdot mL^{-1}$
Base	$0.025 \text{ AU} \cdot mL^{-1}$
Acid	$0.025 \text{ AU} \cdot mL^{-1}$
Air	$0.025 \text{ AU} \cdot mL^{-1}$
Energy	$0.3 \text{ AU} \cdot W^{-1}$

The momentary costs per revenues ($\frac{C}{R}$) are the ratio of current expenses for energy and consumed materials, and the revenues for the product (R_P), which is a function of product concentration [Brueggemann Alcohol Wittenberg, 2012]. The production revenues are time-averaged (in order to avoid peaks which are caused by the reflux valve that opens in intervals). A higher $\frac{C}{R}$ leads to a less efficient production, since the amount of costs per revenues gets worse.

$$\frac{C}{R} = \frac{\sum \dot{Q}_{input} \cdot C_{Energy} + \sum \dot{V}_i \cdot c_i \cdot C_i + \sum \dot{V}_j \cdot C_j}{\dot{V}_{Product} \cdot R_P(f(X_{Product}))} \quad i \rightarrow G, N; j \rightarrow acid, base, af, air \quad (5.8)$$

with

$$R_P = 0.0091 [AU/g \cdot L^{-1}] \cdot c_{Product}[g \cdot L^{-1}] + 0.0652[AU] \quad (5.9)$$

6. Simulation studies

The training simulators were used to investigate the influence of process control strategies on the energy demand. The results of these simulation studies are described and discussed in the following chapter.

6.1. Cultivation

The cultivation simulator was used to show the influence of the switching time between aerobic and anaerobic phase on several process characteristics, as e. g. substrate demand, energy demand, biomass and ethanol produced and reactor volume.

The GRAFCET plan described in chapter 4.2.4 was used for the definition of process control strategies. All process parameters were kept constant between the different runs (feed concentrations $500 \text{ g} \cdot \text{L}^{-1}$). Substrate concentration within the reactor was controlled with a PI-controller to equal quantities (constant $1 \text{ g} \cdot \text{L}^{-1}$ glucose, $5 \text{ g} \cdot \text{L}^{-1}$ N-source). The switching time was varied between 4 h and 10 h in 2 h steps. The process was terminated after 24 h.

In figure 6.1 the reactor volume, the ethanol concentration and the biomass concentration are depicted for switching times at 4 h, 6 h, 8 h and 10 h. In the middle positioned graph biomass concentrations are shown. The exponential growth phase within aerobic operation ends at the respective switching times. After 4 h, 6 h and 8 h biomass concentration slightly increases in a linear manner.

After 10 h the concentration of biomass is decreasing at the beginning of the anaerobic phase. This can be explained with a dilution effect, resulting from the high substrate demand caused by the chosen process control strategy and the high concentration of biomass at this process state. In table 6.1 the produced mass of ethanol, and the consumption amounts for energy, glucose and nitrogen source are listed. With these information some ethanol-specific consumption values shall be provided.

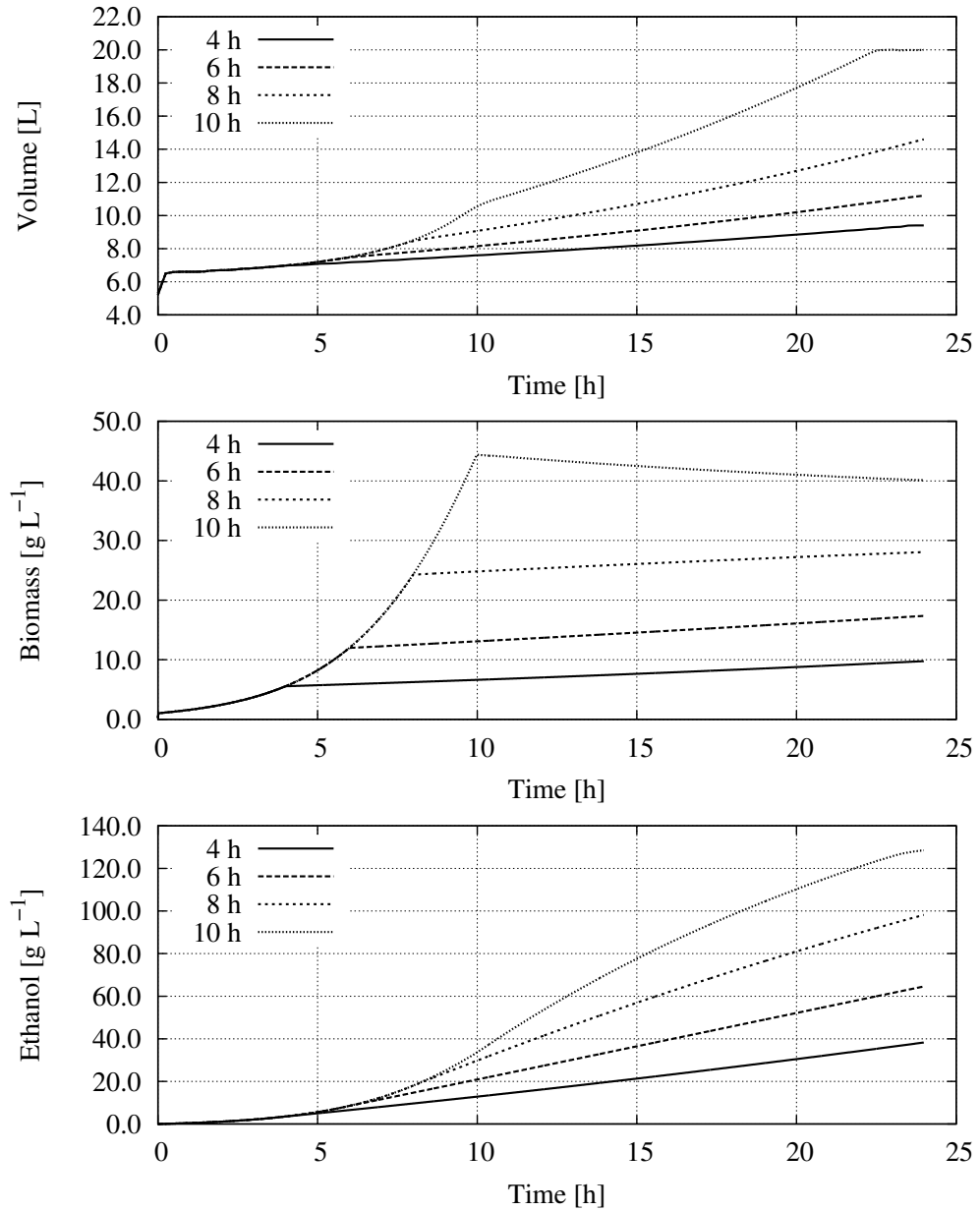


Figure 6.1.: Dynamic Volume (top), biomass (middle) and ethanol concentration (bottom) in the bioreactor during a 24 h production run with switching times from 4h to 10 h. The run with switching time at 10 h reaches the reactor volume limit after 23.7 h. The surplus fermentation broth is pumped into the product tank.

Table 6.1.: Mass of produced ethanol and total energy, glucose and nitrogen source consumption.

Switching time	Ethanol [g]	Energy [kWh]	Glucose [g]	N-source [g]
4 h	359.7	0.441	591.2	81.5
6 h	723.1	0.424	1201.4	170.6
8 h	1433.5	0.413	2411.0	361.3
10 h	2570.2	0.408	4641.7	759.1

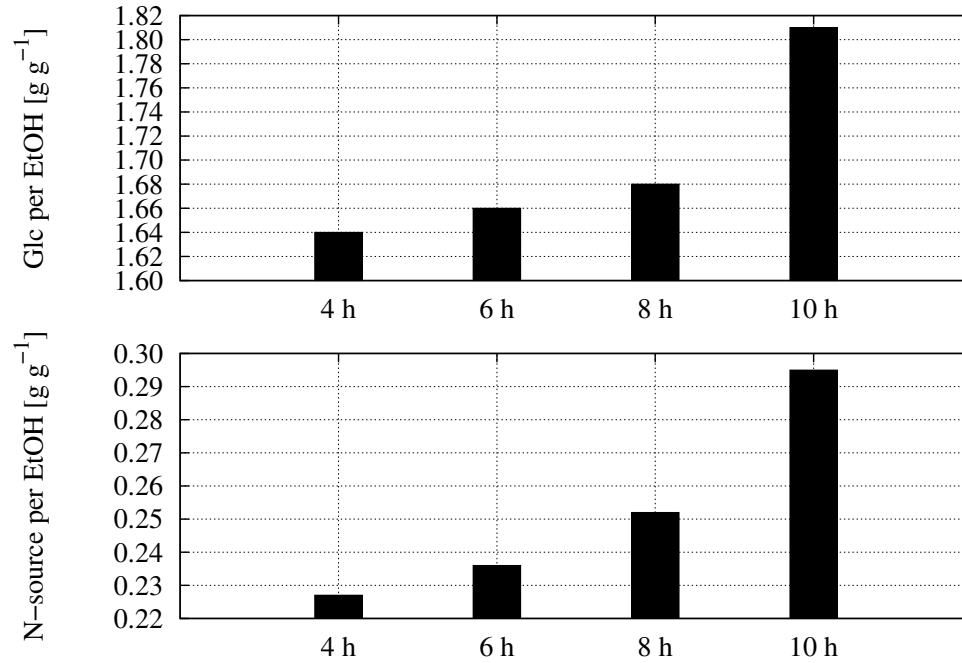


Figure 6.2.: Specific input of glucose (top) and nitrogen source (bottom) per gram ethanol produced. Regarding the substrate usage, the more efficient process is obtained at earlier switching times.

The results show an exponential correlation between the time of switching and the specific consumption values (figures 6.2 to 6.3). Generally speaking, the later the switching time is chosen, the better the ratio of ethanol produced per kilowatt hour of energy inserted gets. At the same time the ratio of ethanol produced per gram of nitrogen source and glucose spent decreases.

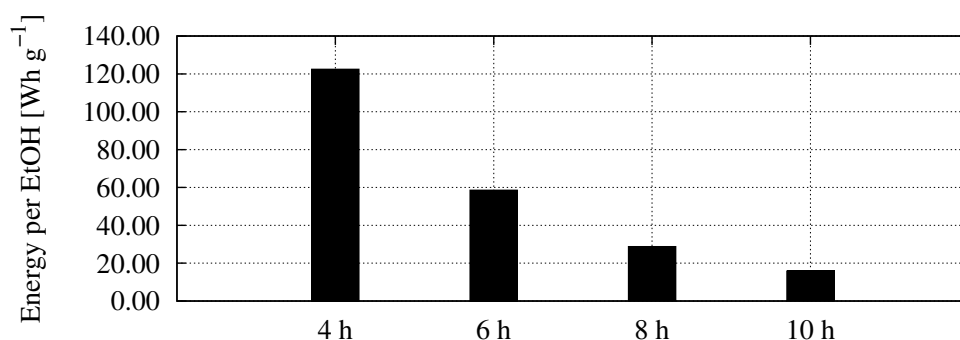


Figure 6.3.: Specific input of energy per gram ethanol produced. Here, the energy efficiency is better at later switching times.

6.2. Cross-flow filtration

Different scenarios were simulated and evaluated concerning the criteria mentioned earlier. The process control strategy was realised with the automatic sequence control shown in chapter 4.3.3 (also figure A.8 in the appendix).

The process aim was to filtrate 10 L cultivation broth with a biomass concentration of $20 \text{ g} \cdot \text{L}^{-1}$ with different combinations of TMP and flow rate. The TMP and the flow rate were controlled with the respective controllers (chapter 4.3.3). Starting volume in the production tank was 10 L. The stopping criterion for the batch experiment was the biomass concentration in the production tank ($100 \text{ g} \cdot \text{L}^{-1}$).

The feed flow rate was controlled at $500 \text{ mL} \cdot \text{min}^{-1}$, $1000 \text{ mL} \cdot \text{min}^{-1}$ and $1500 \text{ mL} \cdot \text{min}^{-1}$. The TMP was controlled at 0.25 bar, 0.5 bar, 0.75 bar, 1.0 bar, 2.0 bar and 3.0 bar. In figure 6.4 the dynamic flux during the whole process is depicted. Following conclusions may be drawn from the results:

- a low trans membrane pressure results in a long process duration,
- with increasing TMP the duration can be reduced,
- higher feed flow rates shorten process duration, due to higher fluxes,
- starting from a certain TMP, a further raise of TMP does not lead to a high gain regarding process time (cake has become very dense),
- the last result shifts with higher flow rates.

In figure 6.5 the corresponding cake height of each simulation run is shown. At low flow rates a cake can develop even with low TMP. When the flow rate is risen, the cake starts developing at higher flow rates. At very high flow rates the force which tears particles back into the retentate flow is stronger than the force performed by the flux, so here a cake starts building only at very high TMP (as described by Rautenbach [1997], see model description on pages 81 - 82).

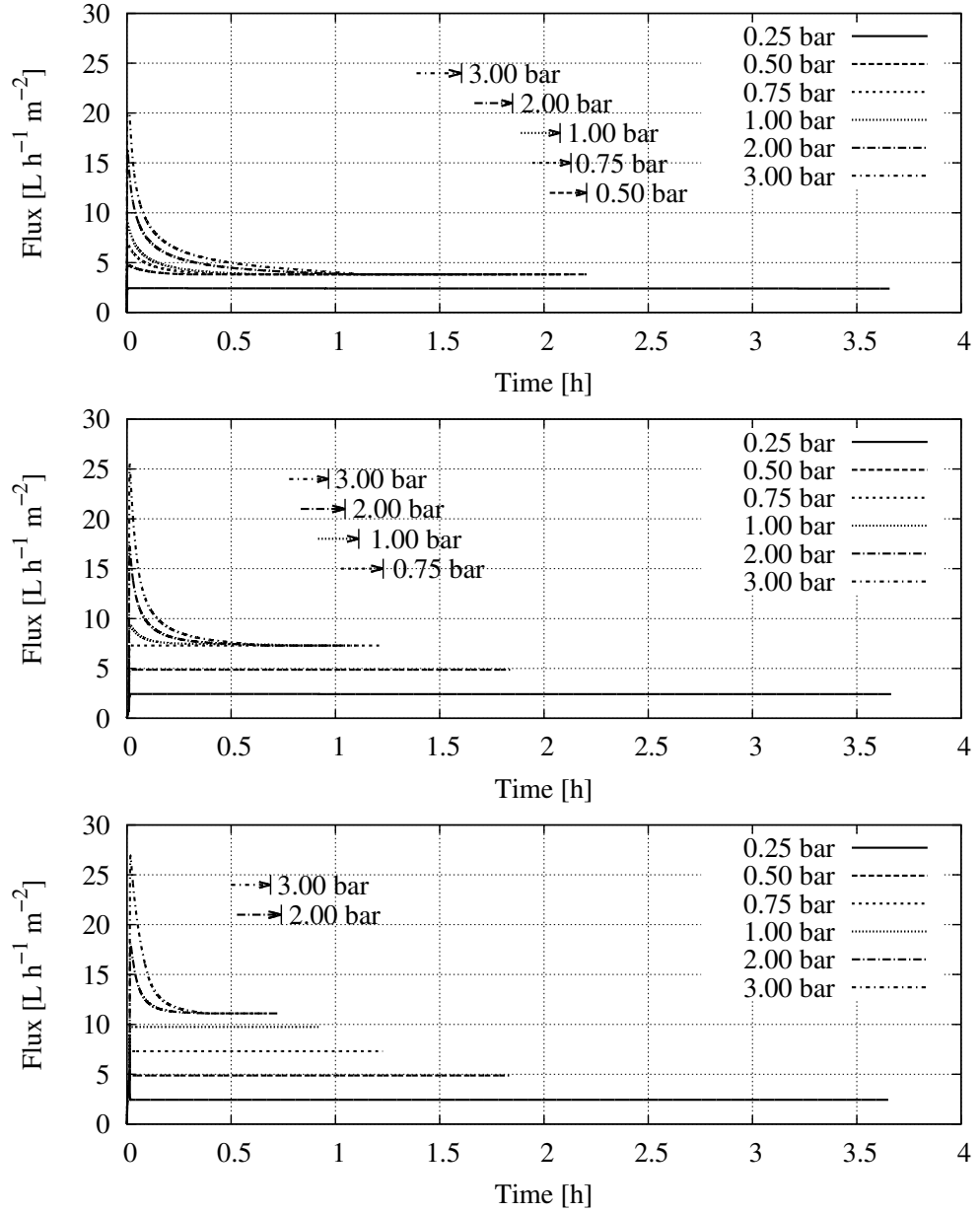


Figure 6.4.: Flux as a function of time for a batch-filtration with different combinations of feed flow rate ($500 \text{ mL} \cdot \text{min}^{-1}$ (top), $1000 \text{ mL} \cdot \text{min}^{-1}$ (middle) and $1500 \text{ mL} \cdot \text{min}^{-1}$ (bottom)) and trans membrane pressures (0.25 - 3.0 bar). The end points of batches with equivalent stationary fluxes are marked.

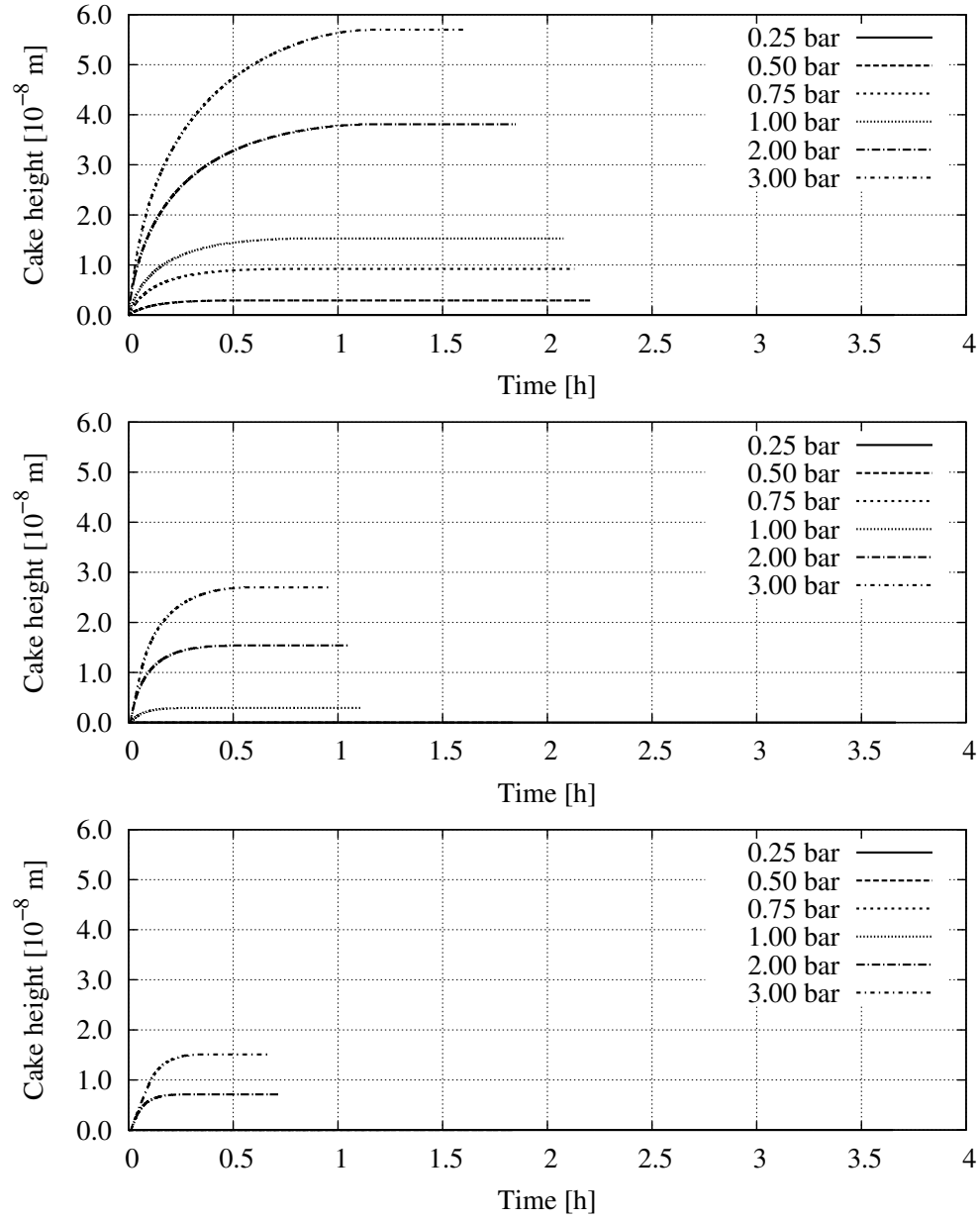


Figure 6.5.: Filter cake height as a function of time for a batch-filtration with different combinations of feed flow rate ($500 \text{ mL} \cdot \text{min}^{-1}$ (top), $1000 \text{ mL} \cdot \text{min}^{-1}$ (middle) and $1500 \text{ mL} \cdot \text{min}^{-1}$ (bottom)) and trans membrane pressures (0.25 - 3.0 bar).

When looking at the energy consumption of the processes, some interesting findings are made (figure 6.6).

- higher feed flow rates cause a higher energy input,
- for every feed flow rate there is a minimum energy input.

At a feed flow rate of $500 \text{ mL} \cdot \text{min}^{-1}$ the minimum energy input is received with TMP of 0.5 bar, 0.75 bar and 1.0 bar. At a feed flow rate of $1000 \text{ mL} \cdot \text{min}^{-1}$ the optimal energy efficiency is reached with a TMP of 1 bar, while a feed flow rate of $1500 \text{ mL} \cdot \text{min}^{-1}$ has its optimal TMP at 2 bar. Depending on the overall production goal (time reduction/ energy reduction) different process control strategies lead to the optimal result.

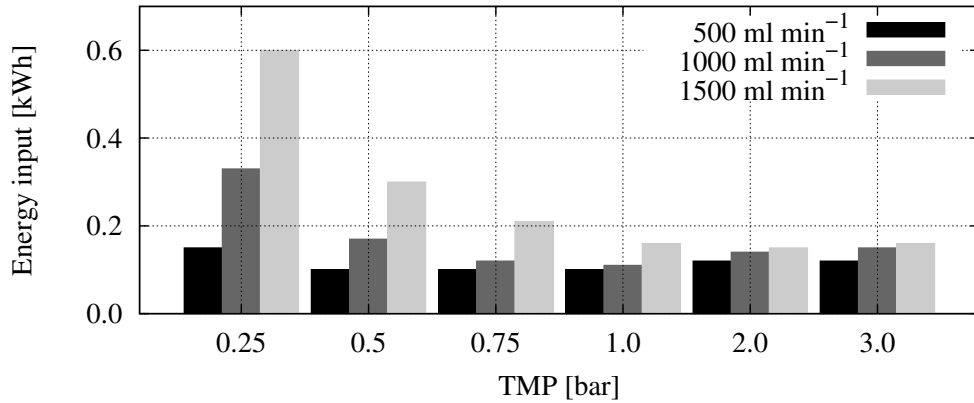


Figure 6.6.: Energy input of the pump at different combinations of TMP and feed flow rate.

6.3. Rectification

In a first experiment McCabe and Thiele's method for determining the number of theoretical stages [Vauck and Müller, 2000] was checked, in order to demonstrate the effectiveness of the implemented model. Figure 6.7 displays the curves for ideal and non-ideal equilibrium, resulting from varied heating power inputs (250 W, 500 W, 750 W, 1000 W, 1250 W, 1500 W) in the reboiler.

By moving the equilibrium curve closer to the 45°-line, the space is decreased. In this decreased space the same number of practical stages as in

ideal equilibrium can be drawn. Practical stages are drawn underneath the non-ideal curve (red steps), while theoretical stages are drawn below the ideal curve (black steps).

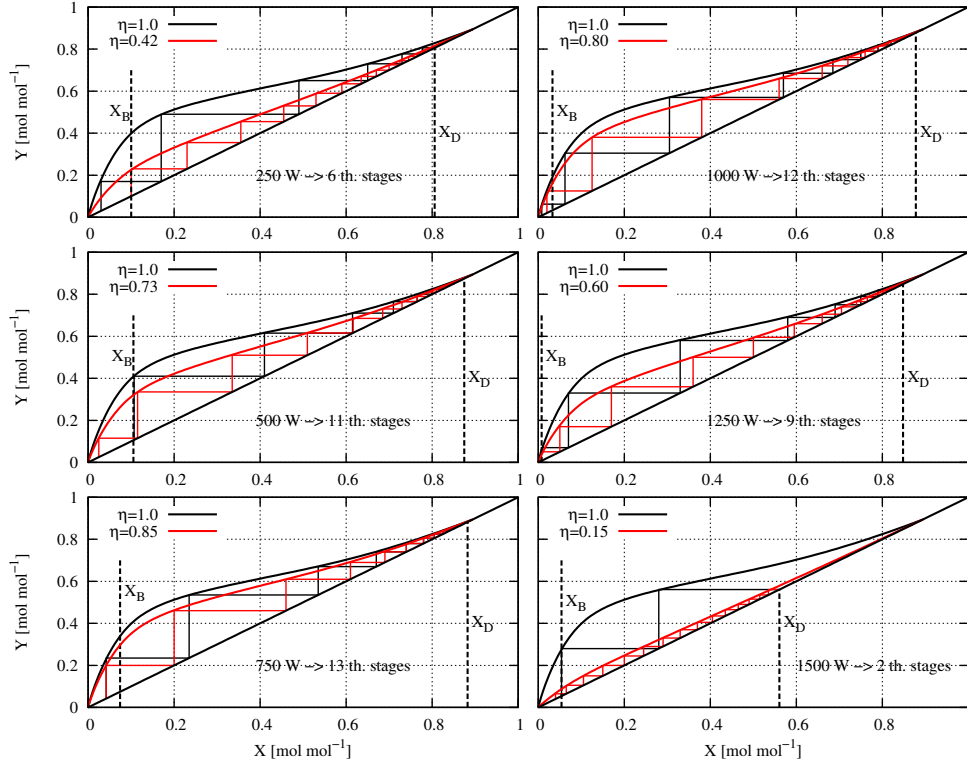


Figure 6.7.: Evaluation of theoretical and practical stages at different heating power input with McCabe and Thiele's method.

Each of the calculated non-ideal curves shows 15 practical stages, while the number of theoretical stages varies, depending on the heating power. The tray efficiency factor in literature is defined as the ratio of number of theoretical and practical stages [Vauck and Müller, 2000]. Comparing efficiencies η' lead to results as shown in table A.3 in the appendix.

$$\eta' = \frac{N_{th}}{N_{pr}} \quad (6.1)$$

The simulator was subsequently used for evaluation of different process control strategies and their effect on the energy demand. For this task

the automatic sequence control (GRAFCET) was used. With the stand-alone training simulator various operational strategies for the batch-rectification were analysed. At first the two main influencing parameters on the process, heating input and reflux ratio, were investigated. For this task an aim was defined to produce 0.5 L of concentrated ethanol from a 10 L mixture with a starting concentration of $260 \text{ g} \cdot \text{L}^{-1}$. In figure 6.8 the energy input required both for heating and cooling is plotted as a function of the reachable product concentration.

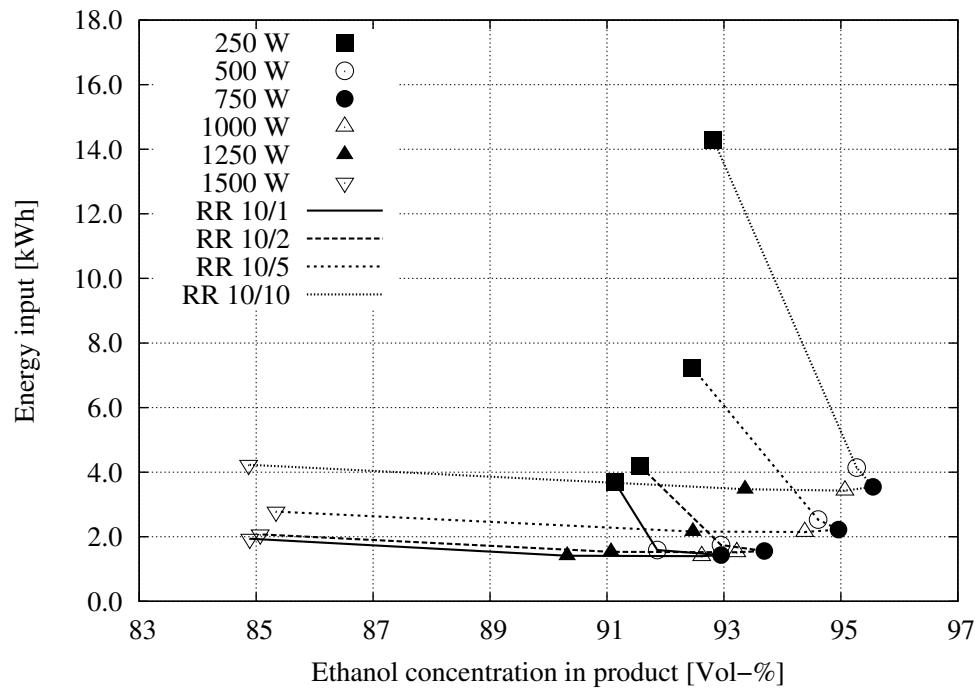


Figure 6.8.: Energy input vs. product concentration for different combinations of reflux ratio (same RR represented by lines) and energy input in the reboiler (same symbols represent identical energy inputs). Aim: production of 0.5 L concentrated ethanol [Kuntzsch et al., 2014].

The curves are connecting points with the same reflux ratio (RR), while the same heating inputs are indicated by the identical symbols. Each reflux ratio has got a maximum product concentration that correlates with a certain energy input. The highest ethanol concentrations are achieved with a heating input of 750 W. Lower heating inputs cause a moderate reduction of the ethanol concentration, whereas higher heating inputs

lead to a considerable decrease of ethanol in the product.

Identical heating ratios lead to a higher ethanol concentration in combination with a higher, constant reflux ratio. Nevertheless, this is accompanied by a higher energy demand. Finally, the investigation shows that a certain ethanol concentration can be received with diverse combinations of heating input and reflux ratio. 93 Vol.-% ethanol may be produced with a combination of reflux ratio 10/1 and heating input 750 W and also with a combination of reflux ratio 10/10 and heating input 750 W. In the first scenario the whole production consumed 1.4 kWh, while the second process control strategy led to a consumption of 14.3 kWh.

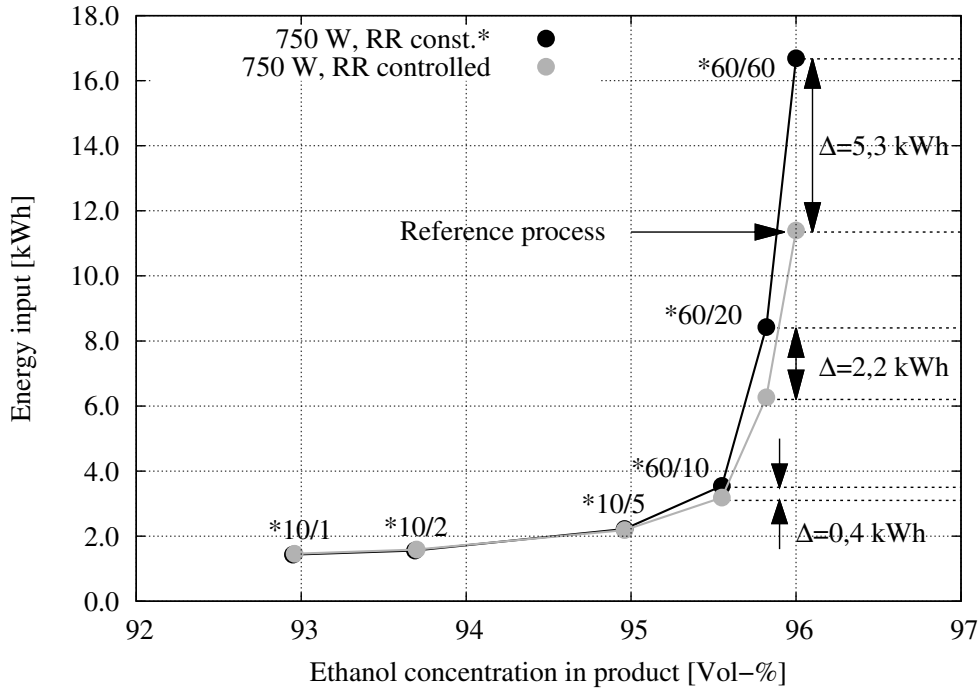


Figure 6.9.: Energy input vs. product concentration. The black line (and symbols) represents a constant reflux ratio, while the gray line (and symbols) represents a controlled reflux ratio. The higher the product concentration gets, the more a controlled reflux ratio reduces the required energy input [Kuntzsch et al., 2014].

In a further simulation experiment the effects of a variable, controlled reflux ratio compared to the constant reflux ratio was carried out. The

control took place via the head temperature (cp. figure 4.45). The product concentrations in the previous experiment were 92.9 Vol.-%, 93.7 Vol.-%, 95.0 Vol.-%, 95.5 Vol.-%, 95.8 Vol.-% and 96.0 Vol.-%. These concentrations represent the maximum concentrations achievable with constant reflux ratios (10/1, 10/5, 10/10, 60/10, 60/20, 60/60). As the set point temperature for the controller, the corresponding boiling temperatures at constant atmospheric pressure were chosen.

Figure 6.9 illustrates the energy input as a function of ethanol concentration in the product. The gray line connects the points of concentrations achieved with a variable reflux ratio (with head temperature control), while the black line connects the ethanol concentrations received with a constant reflux ratio. The energy demand increases with higher ethanol concentrations, both in constant and variable reflux mode. At higher yielded product concentrations the influence of the head temperature control gets considerably visible. With implementation of a head temperature control the energy demand for a 95.5 Vol.-% ethanol may be reduced by 12%. The next higher product concentration (95.8 Vol.-%) leads to a decrease of 26%, while a 96.0 Vol.-% ethanol can be produced with 32% less energy needed.

Table 6.2.: Scenario set-up for the investigation of energy demand [Kuntzsch et al., 2014].

Scenario	Heat input	Heating rate	Start volume	Start heating
reference	750W	$3K \cdot min^{-1}$	10L	after filling
decr. heating input	700W	$3K \cdot min^{-1}$	10L	after filling
incr. starting volume	750W	$3K \cdot min^{-1}$	11L	after filling
decr. heating rate	750W	1K · min ⁻¹	10L	after filling
decr. starting volume	750W	$3K \cdot min^{-1}$	9L	after filling
incr. heating input	800W	$3K \cdot min^{-1}$	10L	after filling
incr. heating rate	750W	5K · min ⁻¹	10L	after filling
earlier heating	750W	$3K \cdot min^{-1}$	10L	while filling

In a concluding experiment the consequences of different process control scenarios compared to a reference process control scenario were investi-

gated. In figure 6.9 the reference process was marked with an arrow.

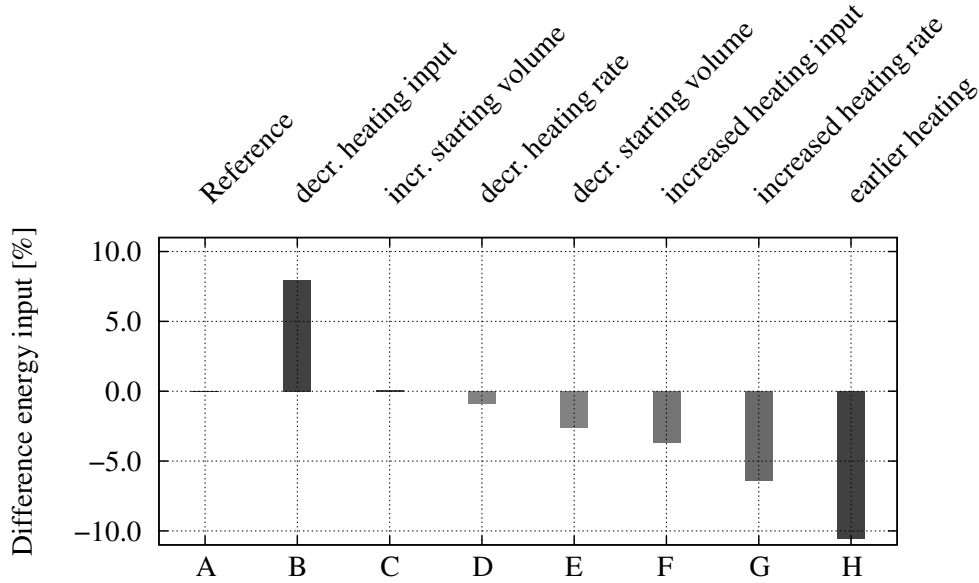


Figure 6.10.: Energy input (heating and cooling) as function of product concentration [Kuntzsch et al., 2014].

The aim of this investigation was to prove, whether the energy demand for producing a 96 Vol.-% ethanol can be further decreased by modifying single operational characteristics of the process control strategy. With the automatic sequence control for a batch-rectification only those boundary conditions were changed, that are depicted in table 6.2. All other possible influences could be excepted with this method. The main task for this analysis was to produce 0.5 L of a 96 Vol.-% ethanol from a 10 L starting mixture containing $260 \text{ g} \cdot \text{L}^{-1}$. The deviation of each scenario from the reference scenario are displayed in figure 6.10.

The reference scenario had an energy demand of 11.35 kWh as heating input and cooling energy. This value was set to 0%. A lower heating input, minus 100 W as compared to the reference scenario, resulted in an approximately 8% higher energy input (scenario B), while a 100 W increase of heating input lead to a saving of 3.7% (scenario F). Raising the starting volume in the reboiler for 10% causes the energy input increasing for 0.05% (scenario C).

On the other hand, a 10% reduction of the starting volume ends up in a 2.6% reduction of energy demand (scenario E). A further change in the

process control strategy regards the heating rate, with which the mixture in the reboiler is heated to boiling temperature. When decreasing the heating rate for $2 \text{ K} \cdot \text{min}^{-1}$, the energy needed is reduced by 0.9% (scenario G) and an uprating for the same amount causes a reduction of energy demand (6.4%, scenario G). 10.6% less energy needs to be spent, when the warming-up is started earlier in the schedule (scenario G).

6.4. Virtual biorefinery

In the following parts the influences of process control strategies on the overall process efficiency are evaluated and demonstrated. It will be shown that changing one parameter (here: the substrate concentrations) in the cultivation process will affect the control strategies of the connected processes, and that this will have an impact on the energy demand of the overall process.

In a first simulation experiment a semi-continuous process was evaluated. Cultivation and cross-flow filtration were carried out continuously, while the rectification was started after cultivation and separation was finished. In the second example a continuous process was investigated, in which all processes were running simultaneously.

6.4.1. Semi-continuous process

Scenario A: high substrate feed concentrations

For the first experiment two scenarios were designed, implemented in a GRAFCET functional plan, and executed with the simulators. Both scenarios differ from each other only in the concentration of glucose and nitrogen source, fed into the bioreactor (A: $500 \text{ g} \cdot \text{L}^{-1}$; B: $250 \text{ g} \cdot \text{L}^{-1}$).

The simulation started with yeast cultivation in bioreactor 2. The starting media was 6 L with a glucose concentration of $3 \text{ g} \cdot \text{L}^{-1}$ and a N-source concentration of $20 \text{ g} \cdot \text{L}^{-1}$. The inoculum was set to 500 mL with a yeast concentration of $15 \text{ g} \cdot \text{L}^{-1}$. During aerobic operation a constant substrate concentration should be provided via the respective substrate tanks (glucose $3 \text{ g} \cdot \text{L}^{-1}$; N-source $5 \text{ g} \cdot \text{L}^{-1}$). Both substrate tanks were equipped with $500 \text{ g} \cdot \text{L}^{-1}$ substrate solutions. Dissolved oxygen (60%), antifoam (high set point 0.01 L), pH (7), temperature (32°C) and level (10 L) controls were activated. Figure 6.11 shows the concentrations and the tank

volumes of the cultivation and cross-flow filtration during the process.

After 12 hours process time the operation was switched from aerobic to anaerobic conditions (set point pO_2 : 0.0). When the set point level had been reached, the level product pump (P-17) pumped surplus cultivation broth into the product tank (B-18). After reaching 2 L of product in the product tank, this volume was transferred to the cross-flow filtration unit (B-19).

After 24 h all controls and supplies were deactivated and all remaining contents were consumed or pumped into the succeeding tanks for further operation.

The automation in the cross-flow simulator was triggered with reaching 2 L product from the cultivation unit (figure A.14 in the Appendix). From buffer tank B-19 media is transferred to the production tank B-20. After reaching 1 L of media in the production tank (see figure 6.11), the feed pump was activated and set to $10 \text{ mL} \cdot \text{min}^{-1}$. The product tank started filling up (see also figure 6.11). The trans membrane pressure control was activated and set to 0.25 bar. Retentate was lead via valve V-8 to buffer tank B11 (figure A.14), where again after reaching 2 L volume the contents were transferred back to the bioreactor.

The bioreactor was continuously fed with a flow rate of $10 \text{ mL} \cdot \text{min}^{-1}$. At this time the loop was closed and the process was running in continuous mode. The particle-free permeate was collected in product tank (B-21) of the cross-flow filtration process. The ethanol concentration in the product tank (B-21), as well as the concentrations of biomass and ethanol in the feed tank are also shown in figure 6.11. The ethanol concentration in B-21 is continuously increasing (red dotted curve).

After approximately 27 h all the concentrations start increasing rapidly. This is due to an increasing feed flow rate in the cross-flow process. The flow rate was increased to $500 \text{ mL} \cdot \text{min}^{-1}$, in order to accelerate the process. As it can be seen from figure 6.11, the outcome of the chosen process control strategy was 14.3 L water-ethanol-mixture with an ethanol concentration of $120.7 \text{ g} \cdot \text{L}^{-1}$. The mixture was transferred to buffer tank B-22 in the rectification.

In the rectification process 1 L of this water-ethanol-mixture was pumped from B-21 into the reboiler B-22. After heating and evaporation an equi-

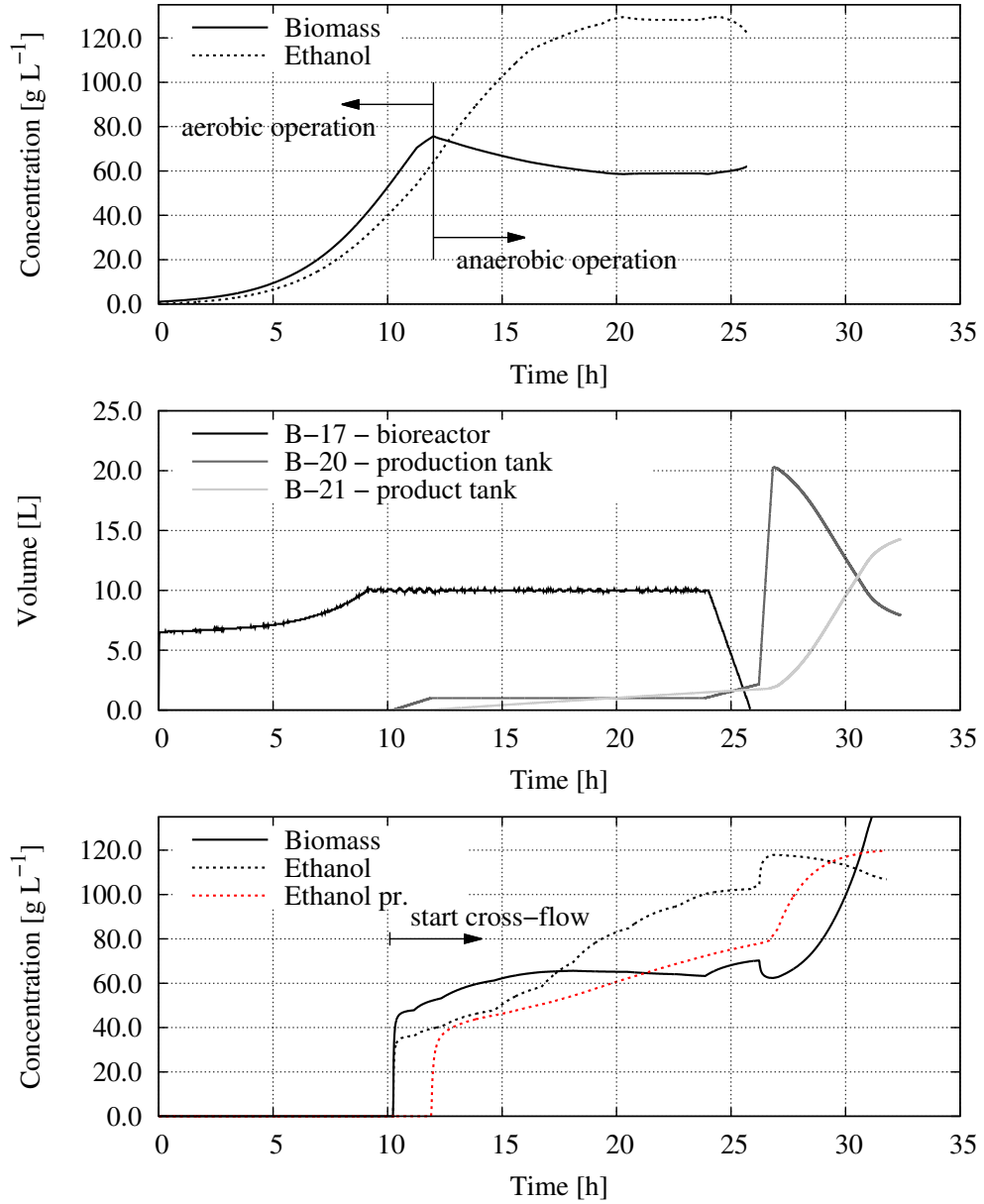


Figure 6.11.: Concentrations of biomass and ethanol in the bioreactor (top), volumes of the bioreactor (B-17), the production tank (B-20) and the product tank (B-21) in the cross-flow filtration (center), and concentrations of biomass and ethanol (bottom) in the production tank (B-20, black) and in the product tank (B-21, red).

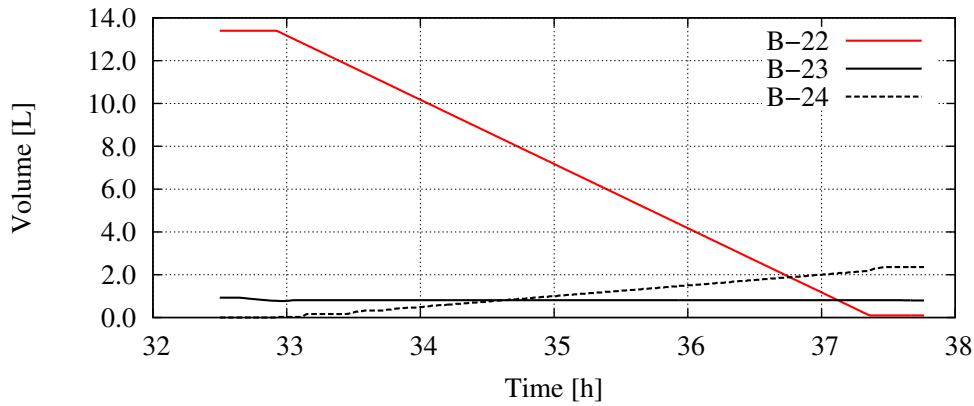


Figure 6.12.: Volumes in buffer tank (B-22), reboiler (B-23) and product tank (B-24) during a continuous rectification process.

librium state was waited for. Then the rest of the mixture was continuously fed ($50 \text{ mL} \cdot \text{min}^{-1}$) via the middle position inlet of the column. Level control in the reboiler was activated. Head temperature control was set to 78.37°C , which represents 91 Vol.-%.

The dynamic evolution of levels in the three tanks (buffer tank B-22, reboiler B23 and product tank B-24) is depicted in figure 6.12. The time line (x-axis) starts with 32.5 h, exactly where the cross-flow process stopped. The buffer tank is continuously emptied while the product tank is continuously filled up with purified ethanol. At the end of the process 2.3 L ethanol with a concentration of 91 Vol.-% have been generated. The complete process has taken 37.7 h.

Scenario B: low substrate feed concentrations

In scenario B the same starting conditions as in scenario A were taken. Only the substrate concentrations in the media tanks were reduced to $250 \text{ g} \cdot \text{L}^{-1}$.

Lower concentrated substrates cause the volumetric flow rate of glucose and N-source feed to increase (due to concentration control). The effect from this modification is represented in figure 6.13. The volumes of the bioreactor (B-17), the production tank (B-20) and the product tank (B-21) are shown. The level in the production tank (which is controlled to 10 L) reaches the set point approximately 1.5 h earlier than in scenario A. The biomass and ethanol concentrations are also reduced, when

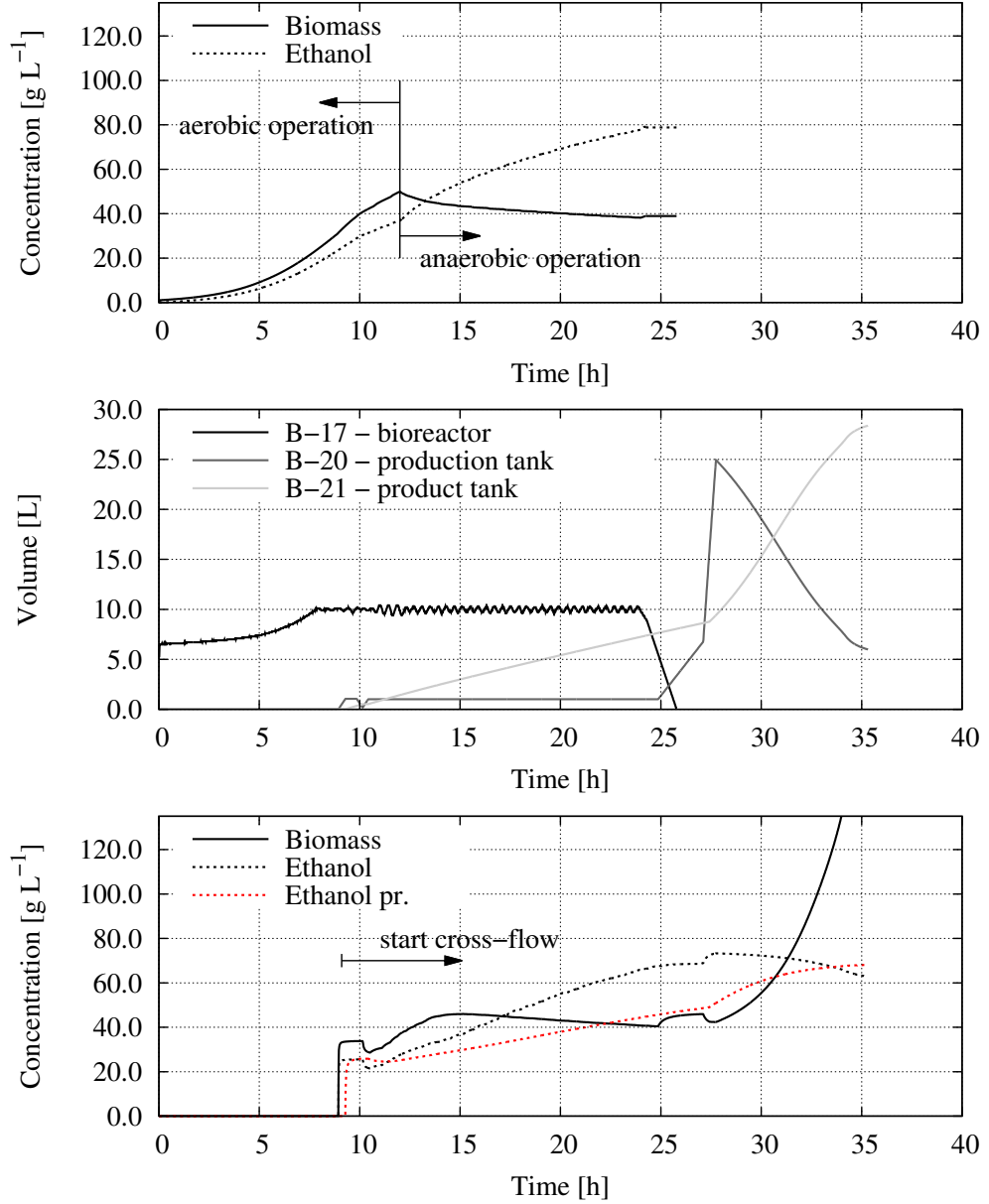


Figure 6.13.: Concentrations of biomass and ethanol in the bioreactor (top), volumes of the bioreactor (B-17), the production tank (B-20) and the product tank (B-21) in the cross-flow filtration (center), and concentrations of biomass and ethanol (bottom) in the production tank (B-20, black) and in the product tank (B-21, red).

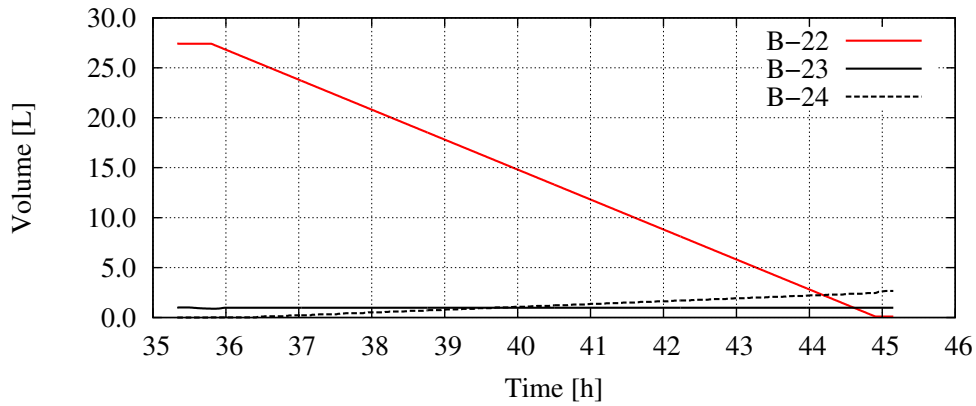


Figure 6.14.: Volumes in buffer tank (B-22), reboiler (B-23) and product tank (B-24) during a continuous rectification process.

compared to scenario A (after 10 h \rightarrow A: ethanol $40 \text{ g} \cdot \text{L}^{-1}$, biomass $50 \text{ g} \cdot \text{L}^{-1}$; B: ethanol $30 \text{ g} \cdot \text{L}^{-1}$, biomass $40 \text{ g} \cdot \text{L}^{-1}$).

According to the high input of liquids the process control strategy was modified, regarding the flow rates. While in the preceding scenario the pump rates were set to $10 \text{ mL} \cdot \text{min}^{-1}$, here $50 \text{ mL} \cdot \text{min}^{-1}$ were chosen. The result of this change is visible when looking at the volumes of the retentate and the product tank (figure A.15). The transfer to the cross-flow process starts earlier, and it happens more often, since the tanks are reaching the control limit of 2 L much earlier. Again the cultivation was terminated after 24 h and the emptying of tanks was awaited.

The cross-flow process is activated approximately 1 h earlier than in scenario A. Due to the higher flow rates, the TMP-set point was changed to 1 bar. In figure 6.13 the effects of these measures may be seen. The product volume increases stronger than in scenario A. A second effect is the decreased ethanol concentration. The figure shows further, that this process control strategy resulted in 28.4 L water/ethanol with an ethanol concentration of $68.1 \text{ g} \cdot \text{L}^{-1}$.

In the rectification process nothing was changed. All parameters of the process control strategy remained the same, except for the starting volume and concentration in the respective buffer tank (B-22). The course of volumes are shown in figure 6.14. The rectification was started after approximately 35.5 h. Due to the higher volume the rectification process took longer. After about 45 h the complete process was finished. At the

end of the process 2.6 L ethanol with a concentration of 91 Vol.-% have been generated.

Comparison of energy and auxiliary materials consumption

In both scenarios the consumption of consumed materials and energy input were evaluated using equations 5.1 to 5.7. Scenario A required more substrates (Glucose + 14%, N-source + 9%), less antifoam agent (-29 %) and more basic solution (+ 16%). Acidic solution and air consumption were the same. Regarding the energy consumption, in all unit operations the energy demand was higher in scenario B (Cultivation: + 8%; Cross-flow filtration: + 52%; Rectification: + 49 %). At the same time 300 mL more purified ethanol were produced (table 6.3).

Table 6.3.: Comparison of consumption and production values in the ethanol production processes. Scenario A (high substrate feed concentration) vs. B (low substrate feed concentration).

	Scenario A	Scenario B
Cultivation		
Glucose	5176 g	4447 g
N-source	1281 g	1166 g
Antifoam agent	0.7 L	0.9 L
Base	3.1 L	2.6 L
Acid	0.0 L	0.0 L
Air	> 6000 L	> 6000 L
Energy	0.409 kWh	0.444 kWh
Cross-flow filtration		
Energy (Pump)	0.371 kWh	0.767 kWh
Rectification		
Energy	7.568 kWh	14.701 kWh
Ethanol	2.3 L (91 Vol.-%)	2.6 L (91 Vol.-%)
Total energy	8.348 kWh	15.912 kWh

Although it seems as if a large amount of base and antifoam agent has been used for controlling the medium, a rather small dilution effect was

caused by this, actually. The main dilution effect can be traced back to the substrate feed. The glucose fed in scenario A (with a concentration of $500 \text{ g} \cdot \text{L}^{-1}$) was dissolved in 10.35 L feed solution (scenario B with $250 \text{ g} \cdot \text{L}^{-1}$: 17.8 L).

6.4.2. Continuous process

For the second simulation experiment bioreactor 2 was run into a stable and continuous state. Compared to the scenarios described earlier, the process was modified, regarding pump flow rates. Since there is a completely continuously running process, the flow rates of pumps in the single simulators were synchronised. This means that the flow rate of the product pumps (P-17, P-18) in the bioreactor (for level control) defines the flow rate for the buffer tank pump (P-19.2) in the cross-flow filtration process.

The retentate flow rate (which results in the cross-flow process from diverse settings as TMP, concentration, feed flow rate), determines the flow rate of the retentate pump (P-11) in the cultivation process. And finally, the product pump (P-21) determines the flow rate of the feed pump (P-22) in the rectification process (figures A.10, A.11 and A.12 in the appendix).

The rectification training simulator (figure A.12) shows online values for the current costs per revenues. In this window all factors influencing the production costs (e. g. heat input, substrate usage, etc.) are merged into one key performance indicator (according to the cost function in equation 5.8). By this means the operator gains a quick and easy overview of effects resulting from modifications in the process control strategy.

From a stable process state a sudden change was executed. The flow rate of the product pump in bioreactor 2 was changed from $100 \text{ mL} \cdot \text{min}^{-1}$ to $500 \text{ mL} \cdot \text{min}^{-1}$. The costs per revenues curve reacted very spontaneously on this change, as shown in figure 6.15. At the beginning the ratio raises as a reaction of the flow rate change. This means the process efficiency gets worse. After a while there is a decline. The decline is to be explained with the averaged time which was used in the denominator of equation 5.8. Comparing the costs per revenues at the beginning and at the end of the example reveals a decline in efficiency by 12%. The reasons for the general curve progression may be found when looking at

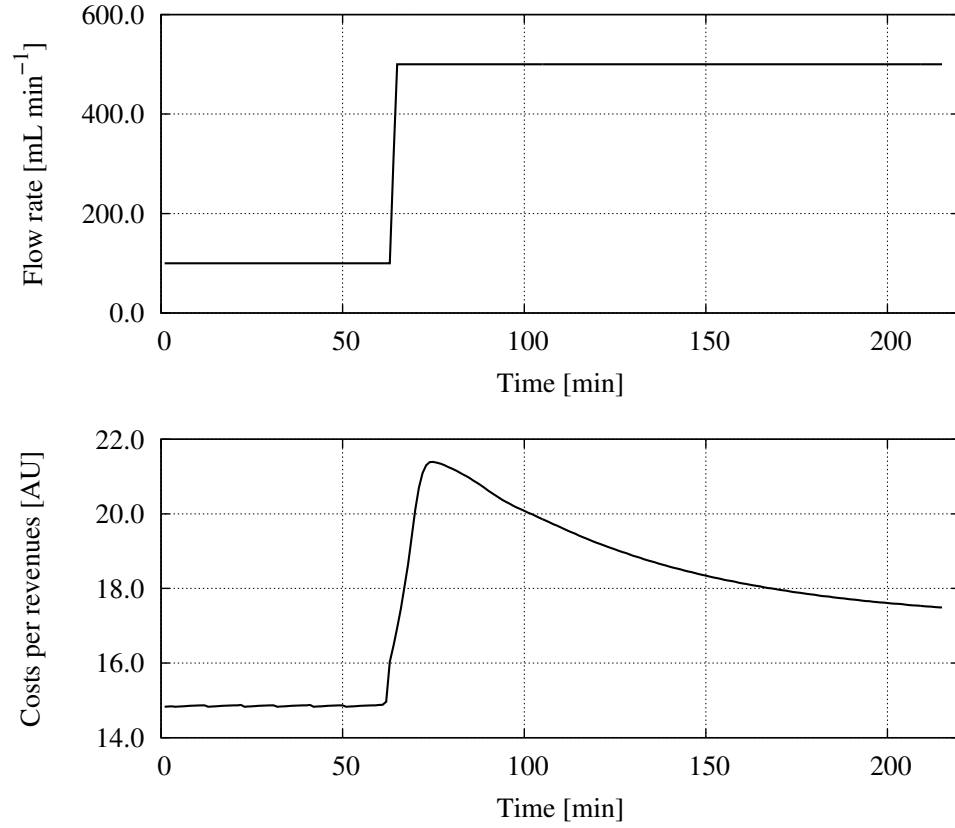


Figure 6.15.: Sudden change of flow rate of the product pump in the cultivation process from $100 \text{ mL} \cdot \text{min}^{-1}$ to $500 \text{ mL} \cdot \text{min}^{-1}$ (top) and the reaction of the cost function (costs per revenues, bottom). An increase of $400 \text{ mL} \cdot \text{min}^{-1}$ causes a quick increase of the costs per revenues, followed by a smooth decline.

certain variables in the single unit operations.

In the bioreactor, the energy input increases at the time of the change as well. This is to be explained with the increasing fluid feed from the cross-flow filtration unit, where the temperature of the medium has cooled down (in the model the feed has a temperature of 20°C). Thus, there is an increased inlet having a lower temperature than the bioreactor contents (32°C). The temperature control of the bioreactor increases the heating fluid temperature, according to the controller parameters and the set point temperature. The energy demand is higher than before

(figure 6.16).

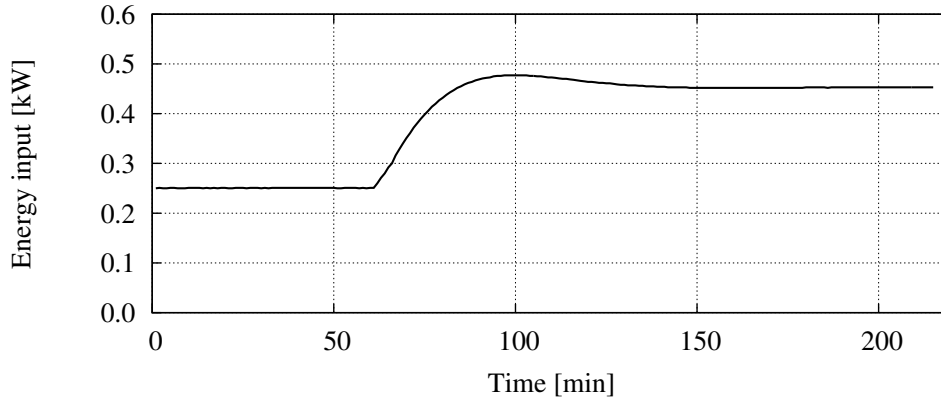


Figure 6.16.: Energy input for keeping the cultivation at set point temperature (top) and bioreactor volume (bottom). The energy demand increases as a reaction of the increased flow rate and decreases slowly afterwards. The bioreactor volume decreases at the time of changed flow rates.

In the cross-flow process a higher flow rate changes the energy demand of the feed pump. The pump needed ca. 0.02 kW at a lower flow rate. At a higher flow rate it needed approximately 0.09 kW (figure 6.17).

The dynamic effect of cake building can also be seen here. A new equilibrium (higher flow rate: particles are dissolved from the cake and go back into the retentate stream \rightarrow less cake resistance \rightarrow higher flux) is reached approximately 40 minutes after the flow rate change.

Furthermore, the permeate flow is determining the feed flow rate for the rectification process. This means that a change from $100 \text{ mL} \cdot \text{min}^{-1}$ to $500 \text{ mL} \cdot \text{min}^{-1}$ in the cultivation affects the rectification process in the way, the column has to separate a larger amount of water-ethanol mixture. This effect gets clear when looking at figure 6.18.

The heat that needs to be conducted increases, due to the changing vapour composition that builds in the column (see equation 4.33). The higher feed input causes the ethanol quality to reduce (figure 6.18 bottom). A worse product quality decreases the revenues for the product.

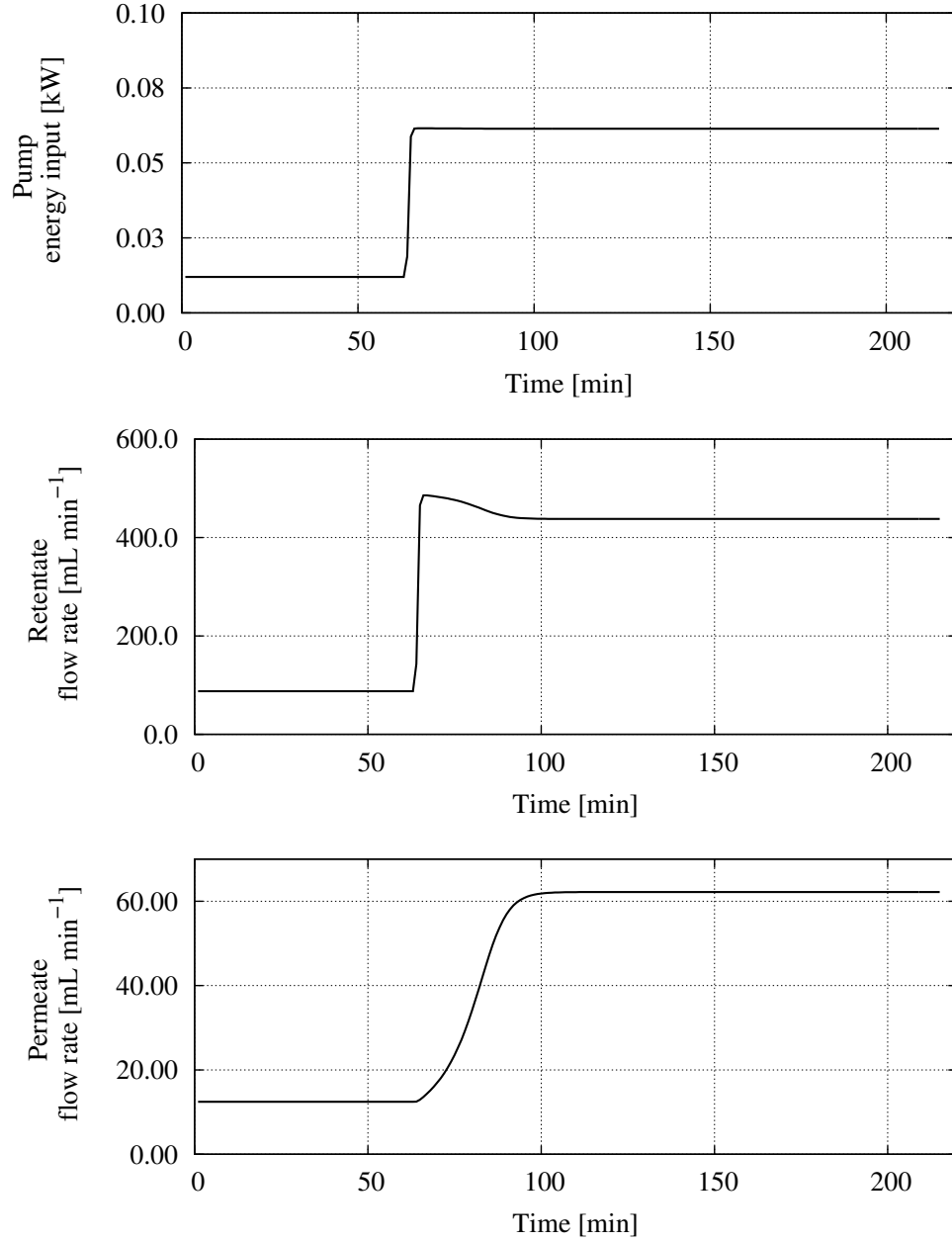


Figure 6.17.: Energy input by the feed pump (top), and retentate (center) and permeate flow rates (bottom) in the cross-flow process. A higher flow rate in the cultivation causes a higher pump energy and higher retentate and permeate flow rates. The discrepancy between extracted and added fluid material in the bioreactor decreases.

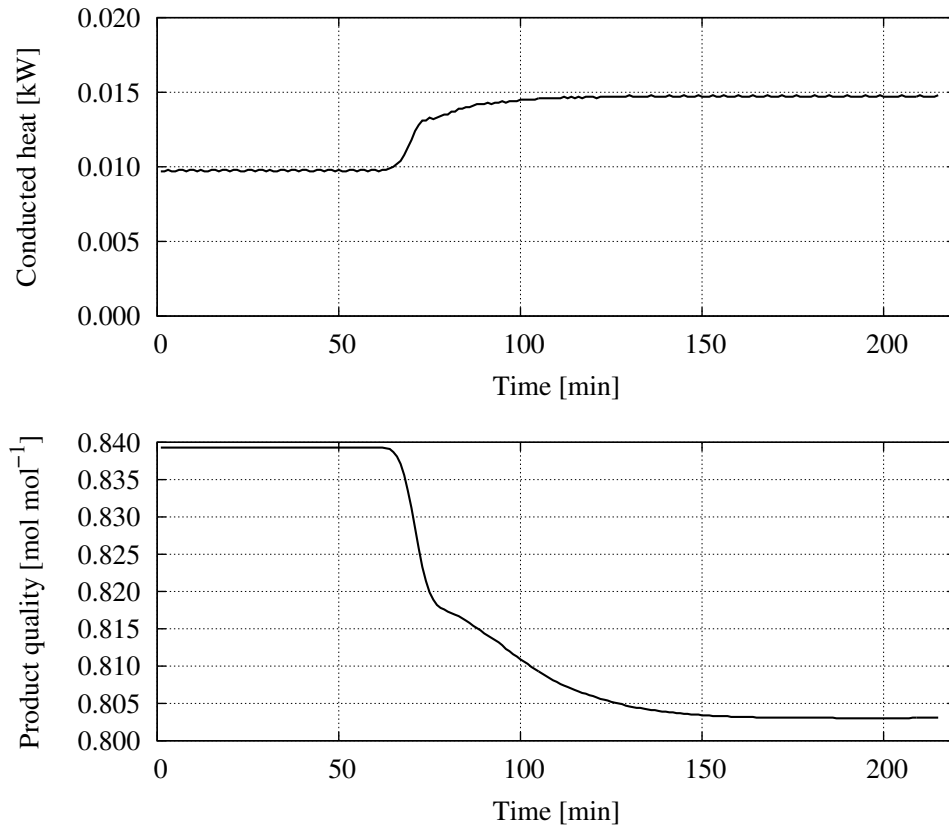


Figure 6.18.: Heat to be conducted (top) and product quality (bottom) in the rectification process. Due to the larger inlet volumetric flow in the column, the heat to be conducted increases, while the product quality decreases. This is due to a shift in the efficiency of the column (changed turbulence).

7. Discussion, conclusions and outlook

7.1. Discussion and conclusions

7.1.1. Method

The present work had the aim to investigate the influence of process control strategies on the energy efficiency of biorefineries. In order to answer this scientific question, a completely new Operator Training Simulator (OTS) for an exemplary bioethanol process was developed. With the general framework for OTS development introduced here (including sub-models for kinetics, units, plants and the automation system), it could be assured that the influence of process operation on the energy demand may be demonstrated in a transparent way. Especially the utilisation of GRAFCET for the design of operational sequences must be pronounced. It is easy and fast to apply, and it assures that scenarios become comparable, since operator failures can be excepted.

The simulator is characterised by its high degree of integration. The process models, the automation and control mechanisms, data monitoring and graphical user interfaces (as required by Klatt [2009] and Bergmann [1999]) are integrated into only two software and simulation tools. No further third-party tools are needed and no additional interfaces have to be determined. This facilitates OTS development considerably. It was possible to develop a biorefinery training simulator within a few years.

Usually, OTS are custom made and only valid for one design process (see chapter 2.4.1). In the present work it was proven that the described method is very well suited for the adaption to quite different processes (cultivation, filtration, rectification). This shows the extraordinary variability of the framework and the software tools. Especially in the environmental or biological technology there are only few OTS [Gerlach et al., 2013; Hass, 2005] in use. This shows the importance of new approaches for a faster and more efficient OTS-development.

In biorefineries, where the efficiency is strongly dependent on the efficiency of the single unit operations [Amigun et al., 2011], optimisation methods are focusing on pre-treatment and process integration in the

design phase. Since it is very difficult to run process control strategy investigations in running biorefineries, the demand for an adequate simulation tool is definitely given. No such investigations are reported in literature up to now.

7.1.2. Simulation results

With the cultivation simulator experiments were carried out that showed the influence of the switching time from aerobic to anaerobic conditions on the resources consumed and the energy demand of the process. For this investigation an automatic sequence control was developed and a control mechanism for the desired concentration of substrates within the bioreactor was installed. In this way reproducible results could be achieved.

In the cross-flow filtration experiments a similar effect of process variables on the energy demand could be demonstrated. The two main influencing parameters trans membrane pressure and flow rate in various combinations led to quite different energy demands. For three different flow rates and six different TMPs the energy demand was evaluated. It was shown that for every chosen flow rate a minimum energy demand can be found with a certain TMP. This is due to energy drain of the feed pump model, as described in section 6.2. In VERDER Deutschland GmbH [2013] the correlation between systematic pressure, flow rate (delivery volume) and the power input of a comparable pump are given and the results are similar.

The rectification process was modeled with a new approach taking the tray efficiency into consideration. With the idea, moving the equilibrium curve closer to the 45°-line (depending on the vapour flow rate), the tray efficiency could be modeled quite sufficiently [Vauck and Müller, 2000]. This aspect is very important for the efficiency analysis of the overall production process. The rectification, as a very energy intensive process, is responsible for a large amount of the overall energy consumption. Thus, it is very important to achieve a good compliance between model and literature values at this point. With the simulation studies carried out, a further aspect could be demonstrated: the influence of controllers on the energy efficiency. The utilisation of a controller resulted in a 30% more efficient process, when compared to manual process control.

Other, very interesting findings, were made with the combined training simulator, i. e. the virtual biorefinery. It could be shown that in a semi-continuous bioethanol process the demand for consumption materials, substrates and energy are strongly connected to the process control strategy. In the example (chapter 6.4.1) the concentrations of substrates in the feed tanks of the cultivation process had a very strong impact on the energy demand. When the concentrations were increased by 50%, the energy input approximately doubled (+52%). This aims at the statements by Walker [2011] and Semencenko et al. [2013], who determined the ethanol yield variations of different feedstock. When sugar and starch contents vary over time, process control modification might be a key measure for energy efficiency optimisation.

In continuous operation the effects of a pump flow rate in one unit operation has got on the other unit operations. The efficiency of the overall process is closely linked to the overall process control strategy. When increasing the pump flow rate from $100 \text{ mL} \cdot \text{min}^{-1}$ to $500 \text{ mL} \cdot \text{min}^{-1}$, the costs per revenues increased from 15 to 17 AU. These effects are difficult to achieve with static simulation methods, as Bieker and Erdmann [1990] state, since the complexity of the process is quite high and the effects that occurred during the experiments were of dynamic nature (influence of controller parameters, tank volumes, consistency of flow rates throughout the process).

Nonetheless, in all simulation experiments it was shown that plant operators have considerable influence on the sustainability of processes. Thus, it is very important to train the operators with suitable tools, as e. g. training simulators. With their graphical user interfaces (GUI) a proper training is possible, as Gerlach et al. [2013] has demonstrated. In biorefineries Operator Training Simulators may contribute to an improved efficiency and sustainability.

7.2. Outlook

In future work there are several aspects that should be pursued, for advancing the findings: in this work the human influence was consciously left out by replacing the operator by an automatic sequence control. On the one hand this helps receiving reproducible results that can be compared in scenarios. On the other hand the human influence (misuse of valves, pumps etc.) seems to be a very interesting question to put re-

search effort in. A question could be how big the difference between automatically running processes and manually operated processes is, always with respect to energy and resource efficiency.

Furthermore, the influence of operator training on the efficiency could be evaluated. Is it possible to reduce the differences of automatic and manual operation only by training? Is there any difference at all? Can operators perform better than automation systems? How much training needs to be carried out to achieve considerable improvements? Also, for the answering of those kinds of questions the basis was built with the present work.

8. Abstract

In biorefineries biogenic resources are processed and converted into different valuable products and renewable energy carriers. It is expected that biorefineries will considerably contribute to an environmentally sustainable future. However, a prerequisite for this goal is their resource conserving and energy efficient operation. This leads to great demands on plant operators and automation systems, since complex process dynamics have to be considered. Process dynamics are supposed to have an important influence on resource- and energy efficiency.

While currently the main research is dealing with the technical optimisation of substrate utilization and the pretreatment methods, the enhancement of the resource spectrum, the improvement of bio-transformation or process intensification, research is almost completely missing, which systematically investigates the influence of process control strategies and automation on the energy efficiency of biorefineries. A reason for this may be that suitable experiments are difficult to carry out, especially in running processes. At this place training simulators can help. Unfortunately, the development costs for such custom-built training simulators are still quite high and there are rarely methods or strategies that facilitate developing adequate process simulators.

In this thesis the influence of process control and automation strategies on the sustainable operation of bioethanol producing biorefineries is investigated. For this task a new methodical and systematical approach for the efficient development of full-scope dynamic simulators had to be designed and adopted.

Exemplarily the dynamic behaviour of a bioethanol plant, producing bioethanol from glucose, was tested. The process consists of 2 bioreactors for the cultivation of *S. cerevisiae* followed by a cross-flow filtration unit for cell recirculation (perfusion), and a rectification unit, operated at atmospheric pressure.

In order to dynamically map the bioethanol plant, including controller behaviour and automation, Operator Training Simulators (OTS) are

suited. The OTS presented here is based on mechanistic and dynamic process models for the unit operations yeast cultivation, cross-flow filtration and rectification. The dissimilarity of the simulated unit operations proves that the framework for OTS development is clearly structured and easy to adapt to different processes.

All process models, describing the aforementioned unit operations, have a consistent structure. They consist of a kinetics sub-model, in which the kinetics of a reaction, conversion or equilibrium mechanisms are described. Around this sub-model the unit sub-model is collocated. Here the mass- and energy-balances are formulated. The unit sub-model basically describes a volumetric space, i. e. the bioreactor or a theoretical stage in the rectification column. The surrounding plant sub-model completes the respective plant with all components, like valves, pumps, tanks. Finally, the plant is embedded into the automation sub-model. This sub-model describes all control loops and the automatic sequence control, that was used for the design of process control strategies.

After the verbal description of the unit operation's functions, the sub-models were formulated. The kinetics and unit sub-models were implemented in eStIM, a FORTRAN-based programming environment. eStIM offers algorithms for the numeric solving of systems composed of ordinary differential equations (ODE). The evaluated sub-models were then translated into dynamic link libraries (DLL) and implemented into WinErs, a process control and simulation system, where the sub-models were assembled and control loops and graphical user interfaces were designed. GRAFCET, a description language for process sequences, was used to create process control strategies. In this way three stand-alone training simulators (that may be combined to form a biorefinery) were developed that were validated either experimentally or with the help of literature data.

The present work has shown that a biorefinery training simulator can be developed within a few years, including the development of two completely new dynamic process models for unit operations (cross-flow filtration and rectification) and several aggregates (pumps, valves, tanks, heat exchangers). The new process simulators could easily be connected with an existing training simulator for yeast cultivation. With all single unit operations, as well as with the virtual biorefinery, process control strategies could be designed, tested and evaluated.

The stand-alone simulators and the virtual biorefinery were used to run batch-, semi-continuous and continuous simulation experiments. In the fermentation process it was shown, that the time of switching from aerobic to anaerobic operation has a strong effect on the energy demand. By enhancing the switching time from 4 h to 10 h, the specific energy input per ethanol output could be decreased from $120 \text{ kWh}^{-1} \cdot \text{kg}$ to below $20 \text{ kWh}^{-1} \cdot \text{kg}$.

In the cross-flow process it was demonstrated that different combinations of feed flow rate and trans membrane pressure show minimum energy demands. The biggest difference (-0.5 kWh) occurred between a flow rate of $1500 \text{ mL} \cdot \text{min}^{-1}$ with a trans membrane pressure of 0.25 bar and a flow rate of $500 \text{ mL} \cdot \text{min}^{-1}$ with a trans membrane pressure of 0.75 bar.

In the rectification process it could be pointed out that head temperature control for the reflux valve leads to less energy input as compared to a constant reflux ratio, especially for high (96 Vol.-%) product concentrations (-5.3 kWh).

With the virtual biorefinery the influence of substrate concentrations fed to the fermenter on the overall energy demand of the bioethanol production was shown. Reducing the concentrations by 50% leads to an almost doubled energy demand. In continuous operation a further example for the evaluation of energy demand is given. This example shows the direct impact of changes in one unit operation (pump flow rate) with respect to the other unit operations in terms of a key performance indicator, here the costs per revenues, which increased by 12%.

A. Appendix

A.1. Model parameters

A.1.1. Cross-flow filtration

Table A.1.: Model parameters of the cross-flow filtration process

Name	Description	Value
λ	friction factor	0.99 –
ρ	density	1000.0 $kg \cdot m^{-3}$
A	viscosity parameter	1.0 –
B	viscosity parameter	1.0 –
C	viscosity parameter	100.0 –
D	viscosity parameter	0.5 –
RM	membrane resistance	100.0 m^1
A	filter area	1.0 m^2
h	height of feed channel	0.002 m
r_C	specific resistance	$1.0 \cdot 10^{10} m^{-2}$

A.1.2. Rectification

Table A.2.: Model parameters of the cross-flow filtration process

Name	Description	Value
T_0	reference temperature	20.0°C
$c_{p,M}$	spec heat capacity (material)	500.0 $J \cdot kg^{-1} \cdot K^{-1}$
M_M	mass column element	1.0 kg
$\Delta H_{V,E}$	heat of evaporation (ethanol)	40.66 $kJ \cdot mol^{-1}$
$\Delta H_{V,W}$	heat of evaporation (water)	38.74 $kJ \cdot mol^{-1}$
M_W	molar weight (water)	18.0 $g \cdot mol^{-1}$
M_E	molar weight (ethanol)	46.07 $g \cdot mol^{-1}$

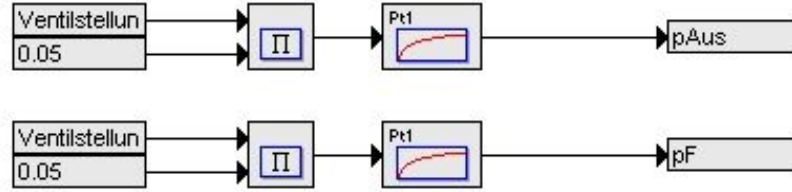
Continued on next page

Table A.2 – continued from previous page

Name	Description	Value
ρ_W	density (water)	$1000.0 \text{ g} \cdot \text{L}^{-1}$
ρ_E	density (ethanol)	$790.0 \text{ g} \cdot \text{L}^{-1}$
k	heat transfer coefficient	$2.0 \text{ W} \cdot \text{m}^{-2} \cdot \text{K}^{-1}$
A	exchange area	0.1 m^2
α	heat transmission coefficient	$100.0 \text{ W} \cdot \text{m}^{-2} \cdot \text{K}^{-1}$
r_1	inner column radius	0.05 m
r_2	stage run-off radius	0.001 m
t_N	time constant for evaporation	100.0 s
K_P	gain for evaporation	0.02 –
$c_{M,W}$	molar heat capacity (water)	$75.3 \text{ J} \cdot \text{mol}^{-1} \cdot \text{K}^{-1}$
$c_{M,E}$	molar heat capacity (ethanol)	$110.0 \text{ J} \cdot \text{mol}^{-1} \cdot \text{K}^{-1}$

A.2. Cross-flow filtration block structures

Calculation of pressure from valve opening degree fo retentate and permeate side



Calculation of pressure drop and pressure on feed side

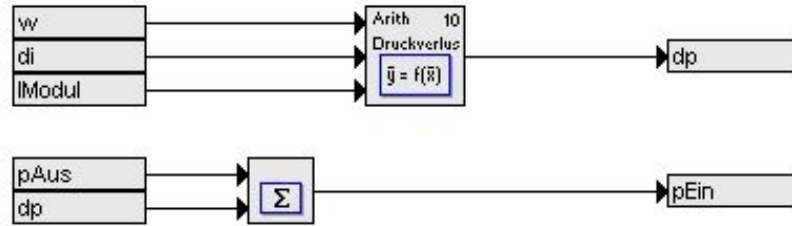


Figure A.1.: Pressure calculations.

Calculation of flow velocity, inner diameter and viscosity

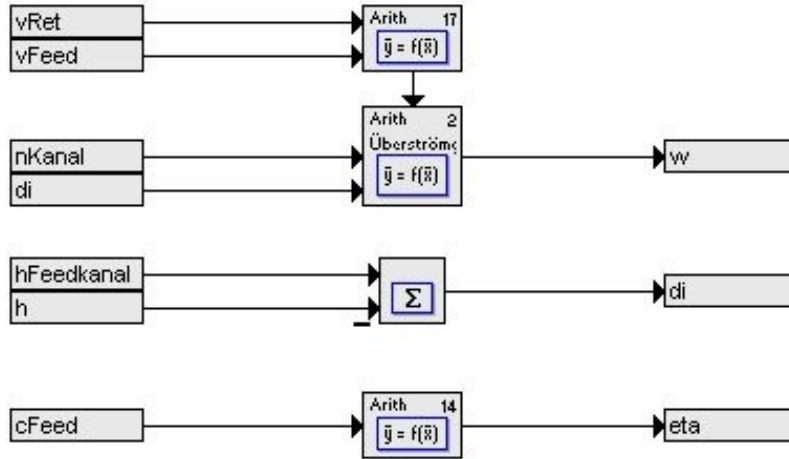


Figure A.2.: Flow velocity, inner diameter and viscosity.

Calculation of TMP and flux

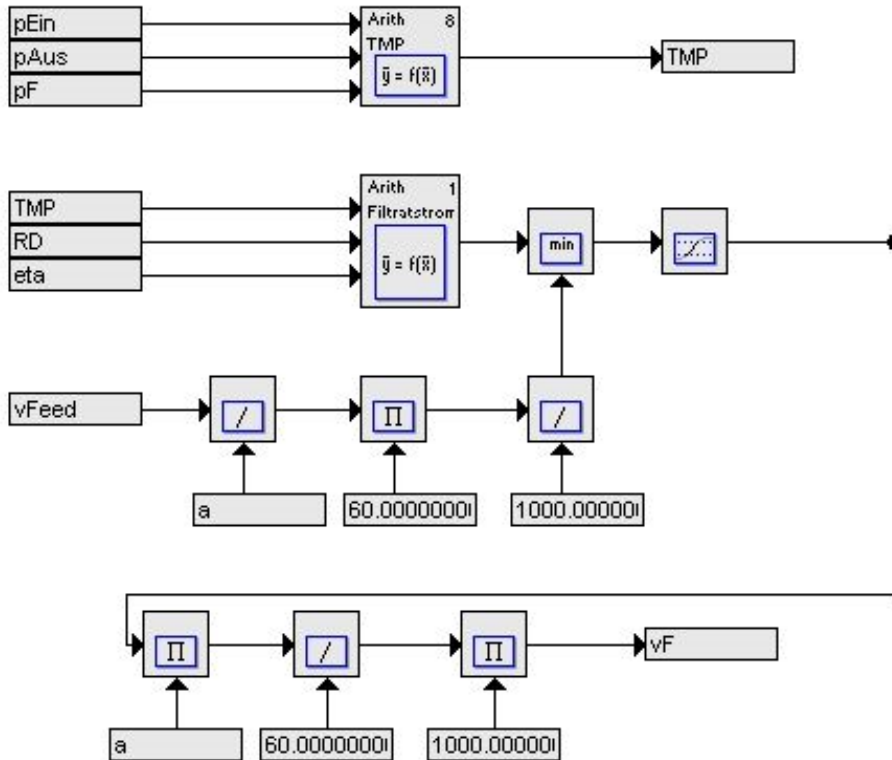


Figure A.3.: TMP and flux calculation in Block structures.

Calculation of cake resistance, cake height and particle mass flow to cake

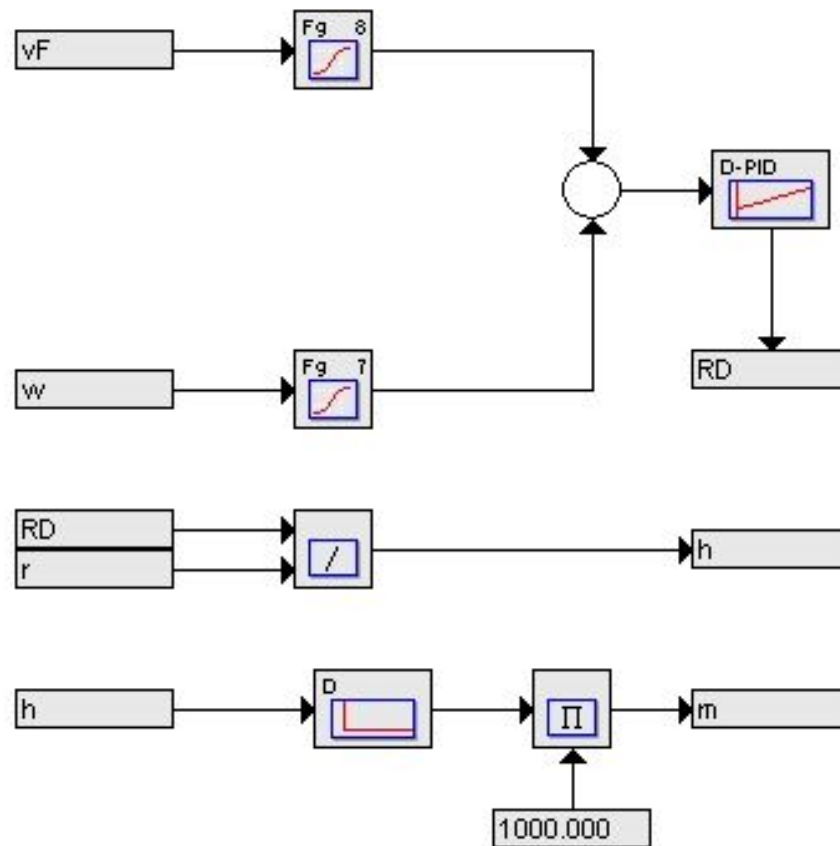


Figure A.4.: Cake resistance, cake height and particle mass flow.

Calculation of volumes and concentrations in the tanks

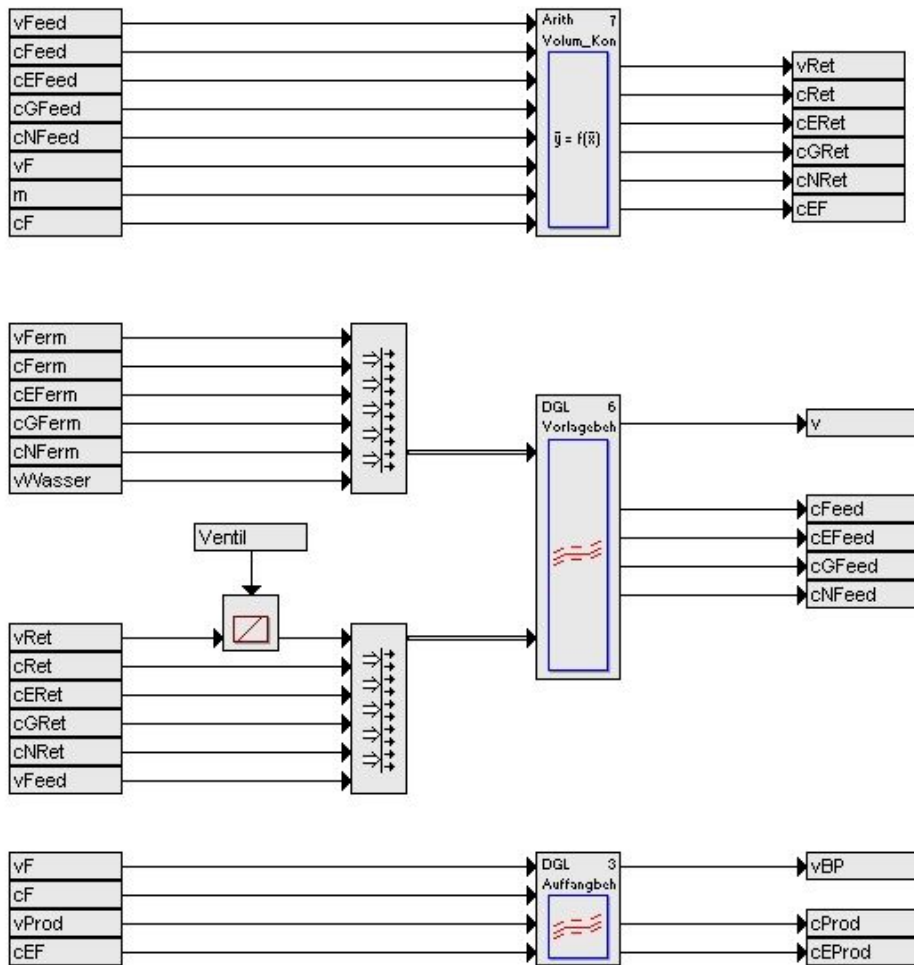


Figure A.5.: Volumes and concentrations in the tanks.

A.3. Rectification source code

```

1
2 subroutine MD0000(t, y, ypkt)
3 !
4 ! Modell einer Destillations-Kolonne
5 ! Author: Stefan Kuntzsch
6 !
7 include 'ModelModules.inc'
8 !
9 implicit none
10 !
11 real(REALTYPE) :: t
12 real(REALTYPE), dimension(*) :: y
13 real(REALTYPE), dimension(*) :: ypkt
14 !
15 !
16 integer :: iResponse
17 integer :: j
18 integer, parameter :: N=15
19 !
20 !DGLs
21 real(REALTYPE), dimension(N) :: xH2O, dH2O
22 real(REALTYPE), dimension(N) :: xEtO, dEtO
23 real(REALTYPE), dimension(N) :: yH2O
24 real(REALTYPE), dimension(N) :: yEt
25 real(REALTYPE), dimension(N) :: yEtO
26 real(REALTYPE), dimension(N) :: nRla
27 real(REALTYPE), dimension(N) :: nVap
28 real(REALTYPE), dimension(N) :: T_Bo, dT_B
29 real(REALTYPE), dimension(N) :: T_Ge, dT_G
30
31 real(REALTYPE) :: MBo
32 real(REALTYPE) :: cpBo
33
34 real(REALTYPE), dimension(N) :: nH2O
35 real(REALTYPE), dimension(N) :: nEtO
36
37 real(REALTYPE), dimension(N) :: yi__, dedt
38
39 real(REALTYPE), dimension(N) :: e
40 real(REALTYPE), dimension(N) :: ypi
41 real(REALTYPE), dimension(N) :: Phas
42 real(REALTYPE), dimension(N) :: Ener
43
44
45 real(REALTYPE) :: QVtot
46 real(REALTYPE), dimension(N) :: QTrans
47 real(REALTYPE) :: Q0
48 real(REALTYPE), dimension(N) :: QFeed
49 real(REALTYPE), dimension(N) :: QVer
50 real(REALTYPE), dimension(N) :: QRla
51 real(REALTYPE), dimension(N) :: QVap
52 real(REALTYPE) :: cpWl
53 real(REALTYPE) :: cpEl
54 real(REALTYPE), dimension(N) :: nFed
55 real(REALTYPE) :: xFeed
56 real(REALTYPE) :: TFeed
57
58 real(REALTYPE) :: hVpW
59 real(REALTYPE) :: hVpE
60 real(REALTYPE) :: k
61 real(REALTYPE) :: A
62 real(REALTYPE), dimension(N) :: kV
63 real(REALTYPE) :: kL
64 real(REALTYPE) :: AV
65 real(REALTYPE) :: Tref
66 real(REALTYPE) :: TRl0
67 real(REALTYPE), dimension(N) :: TSie
68 real(REALTYPE) :: ti
69 real(REALTYPE) :: kp
70 real(REALTYPE) :: TUm
71
72 real(REALTYPE) :: L0
73 real(REALTYPE) :: x0
74 real(REALTYPE) :: V0
75 real(REALTYPE) :: y0
76
77 ! Torricelli-Variablen
78 real(REALTYPE), dimension(N) :: w !Ausflussgeschwindigkeit
79 real(REALTYPE) :: r !Radius der Bodenöffnung
80 real(REALTYPE) :: r1 !Radius eines Bodens
81 real(REALTYPE), dimension(N) :: h !Füllhöhe auf Boden

```

A.3. RECTIFICATION SOURCE CODE

```
82
83 !Für den Bodenwirkungsgrad
84 real (REALTYPE) :: alpha !Bodenwirkungsgrad
85 real (REALTYPE) :: fS !Strömungsgeschwindigkeitsbeiwert
86
87
88 character (len=6) :: NameBuffer
89 external :: StringPlusNumber
90
91 ! -----
92 ! do the initialization part here (eventually use a subroutine instead ...)
93 if (INIT) then
94     GLTYP = 'DGL'
95     MDKENN = 'kolonne3'
96
97
98     SIGANZ = 5*N
99 do j=1, N
100     call StringPlusNumber(NameBuffer, 'T_Bo', j)
101     signam(j) = NameBuffer
102     call StringPlusNumber(NameBuffer, 'nH2O', j)
103     signam(j+N) = NameBuffer
104     call StringPlusNumber(NameBuffer, 'nEtO', j)
105     signam(j+2*N) = NameBuffer
106     call StringPlusNumber(NameBuffer, 'yi__', j)
107     signam(j+3*N) = NameBuffer
108     call StringPlusNumber(NameBuffer, 'T_Ge', j)
109     signam(j+4*N) = NameBuffer
110 enddo
111
112
113     PARANZ = 8
114     parnam(1) = 'cpWl'
115     parnam(2) = 'cpEl'
116     parnam(3) = 'TUm'
117     parnam(4) = 'Tref'
118     parnam(5) = 'MBo'
119     parnam(6) = 'cpBo'
120     parnam(7) = 'k'
121     parnam(8) = 'A'
122
123
124     ZGANZ = 5*N+2
125 do j=1, N
126     call StringPlusNumber(NameBuffer, 'xEtO', j)
127     zgnam(j) = NameBuffer
128     call StringPlusNumber(NameBuffer, 'yEtO', j)
129     zgnam(j+N) = NameBuffer
130     call StringPlusNumber(NameBuffer, 'nVap', j)
131     zgnam(j+2*N) = NameBuffer
132     call StringPlusNumber(NameBuffer, 'nRla', j)
133     zgnam(j+3*N) = NameBuffer
134     call StringPlusNumber(NameBuffer, 'kv', j)
135     zgnam(j+4*N) = NameBuffer
136 enddo
137     zgnam(5*N+1) = 'QVtot'
138     zgnam(5*N+2) = 'h'
139
140
141     FEEDANZ = N+12
142 do j=1, N
143     call StringPlusNumber(NameBuffer, 'nFed', j)
144     Feednam(j) = NameBuffer
145 enddo
146     FEEDNAM(N+1) = 'V0'
147     FEEDNAM(N+2) = 'y0'
148     FEEDNAM(N+3) = 'TRl0'
149     FEEDNAM(N+4) = 'L0'
150     FEEDNAM(N+5) = 'x0'
151     FEEDNAM(N+6) = 'AV'
152     FEEDNAM(N+7) = 'xFeed'
153     FEEDNAM(N+8) = 'TFeed'
154     FEEDNAM(N+9) = 'r'
155     FEEDNAM(N+10) = 'kL'
156     FEEDNAM(N+11) = 'alpha'
157     FEEDNAM(N+12) = 'fS'
158
159
160     iResponse = ReadFeedFile( 1 )
161     iResponse = ReadFeedFile( 2 )
162     iResponse = ReadFeedFile( 3 )
163     iResponse = ReadFeedFile( 4 )
164     iResponse = ReadFeedFile( 5 )
165     iResponse = ReadFeedFile( 6 )
```

DISSERTATION - STEFAN KUNTZSCH
164

A.3. RECTIFICATION SOURCE CODE

```

250 hVpE = 37400.0
251 r1 = 0.05
252
253
254 j=1 !erster Boden der Kolonne
255
256 if (xEtO(j).le.0.2608) then
257   TSie(j) = -38606.0*(xEtO(j)**(5)) + 31125.0*(xEtO(j)**(4)) &
258             -10545.0*(xEtO(j)**(3)) + 2054.1*(xEtO(j)**(2)) &
259             -259.68*xEtO(j) + 99.925
260 else
261   TSie(j) = 1.213*(xEtO(j)**(3))+11.412*(xEtO(j)**(2)) &
262             -18.377*xEtO(j)+86.314
263 endif
264
265 !Unterhalb des Siedepunktes des Leichtersiedenden:
266 if (T_Ge(j).lt.TSie(j)) then
267
268   xEtO(j) = nEtO(j)/(nEtO(j)+nH2O(j))
269   xH2O(j) = 1.0-xEtO(j)
270
271   if (xEtO(j).le.0.2608) then
272     yEt_(j) = -8919.6*(xEtO(j)**6) + 9405.1*(xEtO(j)**5) &
273               -4055.1*(xEtO(j)**4) + 935.68*(xEtO(j)**3) &
274               -127.96*(xEtO(j)**2) + 11.053*xEtO(j) + 0.00007
275     yEtO(j) = yEt_(j)-((1-alpha)*(yEt_(j)-xEtO(j)))
276   else
277     yEt_(j) = 0.6395*(xEtO(j)**3) - 0.7129*(xEtO(j)**2) &
278               +0.6513*xEtO(j) + 0.4249
279     yEtO(j) = yEt_(j)-((1-alpha)*(yEt_(j)-xEtO(j)))
280   endif
281   yH2O(j) = 1.0-yEtO(j)
282
283
284 !Berechnung der Wärmeströme
285 kV(j) = kL
286 QFeed(j) = nFed(j)*(1.0-xFeed)*cpWl*TFeed+nFed(j)*xFeed*cpEl*TFeed
287 QVer(j) = kV(j)*AV*(T_Bo(j)-TUm)
288 QRla(j) = (nRla(j)*xH2O(j)*cpWl*T_Ge(j))+(nRla(j)*xEtO(j)*cpEl*T_Ge(j))
289 QVap(j) = (nVap(j)*yH2O(j)*hVpW)+(nVap(j)*yEtO(j)*hVpE)
290 Q0 = (V0*(1.0-y0)*hVpW)+(V0*y0*hVpE)
291 QTrans(j) = k*A*(T_Ge(j)-T_Bo(j))
292
293 if (nH2O(j).ge.0.0) then
294   dH2O(j) = (nFed(j)*(1.0-xFeed)+V0*(1.0-y0))+(nRla(j+1)*xH2O(j+1)) &
295             -(nRla(j)*xH2O(j)) - (nVap(j)*yH2O(j))
296 else
297   dH2O(j) = (nFed(j) * (1.0-xFeed) + V0*(1.0-y0)) &
298             +(nRla(j+1)*xH2O(j+1))
299 endif
300 if (nEtO(j).ge.0.0) then
301   dEtO(j) = (nFed(j) * xFeed + V0*y0) + (nRla(j+1)*xEtO(j+1)) &
302             -(nRla(j)*xEtO(j)) - (nVap(j)*yEtO(j))
303 else
304   dEtO(j) = (nFed(j) * xFeed + V0*y0) + (nRla(j+1)*xEtO(j+1))
305 endif
306
307 dT_B(j) = (QTrans(j)-QVer(j))/(MBo*cpBo)
308 dT_G(j) = (QFeed(j)+Q0-QTrans(j)+QRla(j+1)-QRla(j)-QVap(j)) &
309           /((nH2O(j)*cpWl)+(nEtO(j)*cpEl))
310
311 if (xEtO(j).le.0.2608) then
312   TSie(j) = -38606.0*(xEtO(j)**(5)) + 31125.0*(xEtO(j)**(4)) &
313             -10545.0*(xEtO(j)**(3)) + 2054.1*(xEtO(j)**(2)) &
314             -259.68*xEtO(j) + 99.925
315 else
316   TSie(j) = 1.213*(xEtO(j)**(3))+11.412*(xEtO(j)**(2)) &
317             -18.377*xEtO(j)+86.314
318 endif
319
320 !Rücklauf unter Berücksichtigung potentiellen Flutens:
321 h(j) = ((nH2O(j)*18./1000000.)+(nEtO(j)*46.07/790000.)) &
322       /(pi*(r1**2))
323 w(j) = fS*sqrt(2.*9.81*abs(h(j)))
324 if (h(j).gt.0.0001) then
325   nRla(j) = (w(j)*(pi*(r**2)) *1000.*1000./18.*xH2O(j)) &
326             +(w(j)*(pi*(r**2)) *1000.*790./46.07*xEtO(j))
327 else
328   nRla(j) = 0.0
329 endif
330
331 !Regelung der Verdampfungsraten und dadurch der Temperatur
332 ti = 100.0
333 kp = 0.02

```

```

334
335     e(j)          = T_Ge(j)-TSie(j)
336     dedt(j)       = e(j)
337
338     if (ypi(j).gt.0.00) then
339         ypi(j)     = kp*(dedt(j)+yi__(j)*(1.0/ti))
340         nVap(j)    = ypi(j)
341     else
342         nVap(j)    = 0.0
343         dedt(j)    = 0.0
344     endif
345
346     Phas(j)       = 1.0
347     Ener(j)       = QFeed(j)+Q0-QVer(j)+QRla(j+1)-QRla(j)-QVap(j)
348
349
350                                     !Siedepunkt des Ethanols erreicht!
351     !!!!!!!!!!!!!!!!!!!!!!!!!!!!!!!!!!!!!!!!!!!!!!!!!!!!!!!!!!!!!!!!!!!!!!!!!!!!!
352     !!!!!!!!!!!!!!!!!!!!!!!!!!!!!!!!!!!!!!!!!!!!!!!!!!!!!!!!!!!!!!!!!!!!!!!!!!!!!
353     !!!!!!!!!!!!!!!!!!!!!!!!!!!!!!!!!!!!!!!!!!!!!!!!!!!!!!!!!!!!!!!!!!!!!!!!!!!!!
354
355     elseif(T_Ge(j).ge.TSie(j)) then
356
357     !Bestimmung der Siedetemperatur
358     if (xEtO(j).le.0.2608) then
359         TSie(j)     = -38606.0*(xEtO(j)**(5)) + 31125.0*(xEtO(j)**(4)) &
360                     -10545.0*(xEtO(j)**(3)) + 2054.1*(xEtO(j)**(2)) &
361                     -259.68*xEtO(j) + 99.925
362     else
363         TSie(j)     = 1.213*(xEtO(j)**(3))+11.412*(xEtO(j)**(2)) &
364                     -18.377*xEtO(j)+86.314
365     endif
366
367     !Regelung der Verdampfungsraten und dadurch der Temperatur
368     ti           = 100.0
369     kp           = 0.02
370
371     e(j)          = T_Ge(j)-TSie(j)
372     dedt(j)       = e(j)
373
374     ypi(j)        = kp*(dedt(j)+yi__(j)*(1.0/ti))
375     if (ypi(j).ge.0.00) then
376         nVap(j)    = ypi(j)
377     else
378         nVap(j)    = 0.0
379     endif
380
381     !Berechnung der Wärmeströme
382     kV(j)         = kL / (0.05 + exp(-0.1/(nVap(j)+0.01))) * 100.
383     QFeed(j)      = nFed(j)*(1.0-xFeed)*cpWl*TFeed+nFed(j)*xFeed*cpEl*TFeed
384     QVer(j)       = kV(j)*AV*(T_Bo(j)-TUm)
385     QRla(j)       = (nRla(j)*xH2O(j)*cpWl*T_Ge(j))+(nRla(j)*xEtO(j)*cpEl*T_Ge(j))
386     QVap(j)       = (nVap(j)*yH2O(j)*hVpW)+(nVap(j)*yEtO(j)*hVpE)
387     Q0            = (V0*(1.0-y0)*hVpW)+(V0*y0*hVpE)
388     QTrans(j)     = k*A*(T_Ge(j)-T_Bo(j))
389
390     !Dampfzusammensetzung
391     xEtO(j)       = nEtO(j)/(nEtO(j)+nH2O(j))
392     xH2O(j)       = 1.0-xEtO(j)
393
394     if (xEtO(j).le.0.2608) then
395         yEt_(j)    = -8919.6*(xEtO(j)**6) + 9405.1*(xEtO(j)**5) &
396                     -4055.1*(xEtO(j)**4) + 935.68*(xEtO(j)**3) &
397                     -127.96*(xEtO(j)**2) + 11.053*xEtO(j) + 0.00007
398         yEtO(j)    = yEt_(j)-((1-alpha)*(yEt_(j)-xEtO(j)))
399     else
400         yEt_(j)    = 0.6395*(xEtO(j)**3) - 0.7129*(xEtO(j)**2) &
401                     +0.6513*xEtO(j) + 0.4249
402         yEtO(j)    = yEt_(j)-((1-alpha)*(yEt_(j)-xEtO(j)))
403     endif
404     yH2O(j)       = 1.0-yEtO(j)
405
406     !Berechnung der Veränderungen
407     if (nH2O(j).ge.0.0) then
408         dH2O(j)    = (nFed(j) * (1.0-xFeed) + V0*(1.0-y0)) &
409                     +(nRla(j+1)*xH2O(j+1)) - (nRla(j)*xH2O(j)) &
410                     -(nVap(j)*yH2O(j))
411     else
412         dH2O(j)    = (nFed(j) * (1.0-xFeed) + V0*(1.0-y0)) &
413                     +(nRla(j+1)*xH2O(j+1))
414     endif
415     if (nEtO(j).ge.0.0) then
416         dEtO(j)    = (nFed(j) * xFeed + V0*y0) + (nRla(j+1)*xEtO(j+1)) &
417                     -(nRla(j)*xEtO(j)) - (nVap(j)*yEtO(j))

```

A.3. RECTIFICATION SOURCE CODE

```

418     else
419         dEtO(j)      = (nFed(j) * xFeed + V0*y0)      + (nRla(j+1)*xEtO(j+1))
420     endif
421
422     dT_B(j)        = (QTrans(j)-QVer(j))/(MBo*cpBo)
423     dT_G(j)        = (QFeed(j)+Q0-QTrans(j)+QRla(j+1)-QRla(j)-QVap(j)) &
424                     /((nH2O(j)*cpWl)+(nEtO(j)*cpEl))
425
426     !Rücklauf unter Berücksichtigung potentiellen Flutens:0
427     h(j)           = ((nH2O(j)*18./1000000.)+(nEtO(j)*46.07/790000.)) &
428                     /(pi*(r1**2))
429     w(j)           = fS*sqrt(2.*9.81*abs(h(j)))
430     if(h(j).gt.0.0001) then
431         nRla(j)     = (w(j)*(pi*(r**2)) *1000.*1000./18.*xH2O(j)) &
432                     +(w(j)*(pi*(r**2)) *1000.*790./46.07*xEtO(j))
433     else
434         nRla(j)     = 0.0
435     endif
436
437     Phas(j)        = 2.0
438     Ener(j)        = QFeed(j)+Q0-QVer(j)+QRla(j+1)-QRla(j)-QVap(j)
439
440     endif
441
442
443
444     do j=2, N-1 !mittlere Böden der Kolonne
445
446         if(xEtO(j).le.0.2608) then
447             TSie(j)  = -38606.0*(xEtO(j)**(5)) + 31125.0*(xEtO(j)**(4)) &
448                     -10545.0*(xEtO(j)**(3)) + 2054.1*(xEtO(j)**(2)) &
449                     -259.68*xEtO(j) + 99.925
450         else
451             TSie(j)  = 1.213*(xEtO(j)**(3))+11.412*(xEtO(j)**(2)) &
452                     -18.377*xEtO(j)+86.314
453         endif
454
455         !Unterhalb des Siedepunktes des Leichtersiedenden:
456         if(T_Ge(j).lt.TSie(j)) then
457
458             xEtO(j)   = nEtO(j)/(nEtO(j)+nH2O(j))
459             xH2O(j)   = 1.0-xEtO(j)
460
461             if(xEtO(j).le.0.2608) then
462                 yEt_(j) = -8919.6*(xEtO(j)**6) + 9405.1*(xEtO(j)**5) &
463                         -4055.1*(xEtO(j)**4) + 935.68*(xEtO(j)**3) &
464                         -127.96*(xEtO(j)**2) + 11.053*xEtO(j) + 0.00007
465             else
466                 yEt_(j) = yEt_(j)-((1-alpha)*(yEt_(j)-xEtO(j)))
467             yEt_(j)     = 0.6395*(xEtO(j)**3) - 0.7129*(xEtO(j)**2) &
468                         +0.6513*xEtO(j) + 0.4249
469             yEt_(j)     = yEt_(j)-((1-alpha)*(yEt_(j)-xEtO(j)))
470         endif
471         yH2O(j)        = 1.0-yEtO(j)
472
473         !Berechnung der Wärmeströme
474         kV(j)          = kL
475         QFeed(j)       = nFed(j)*(1.0-xFeed)*cpWl*TFeed+nFed(j)*xFeed*cpEl*TFeed
476         QVer(j)        = kV(j)*AV*(T_Bo(j)-TUm)
477         QRla(j)        = (nRla(j)*xH2O(j)*cpWl*T_Ge(j)+(nRla(j)*xEtO(j)*cpEl*T_Ge(j))
478         QVap(j)        = (nVap(j)*yH2O(j)*hVpW)+(nVap(j)*yEtO(j)*hVpE)
479         QTrans(j)      = k*A*(T_Ge(j)-T_Bo(j))
480
481         if(nH2O(j).ge.0.0) then
482             dH2O(j)     = (nFed(j) * (1.0-xFeed) + nVap(j-1)*yH2O(j-1)) &
483                     +(nRla(j+1)*xH2O(j+1)) - (nRla(j)*xH2O(j)) &
484                     -(nVap(j)*yH2O(j))
485         else
486             dH2O(j)     = (nFed(j) * (1.0-xFeed) + nVap(j-1)*yH2O(j-1)) &
487                     +(nRla(j+1)*xH2O(j+1))
488         endif
489         if(nEtO(j).ge.0.0) then
490             dEtO(j)     = (nFed(j) * xFeed + nVap(j-1)*yEtO(j-1)) &
491                     +(nRla(j+1)*xEtO(j+1)) - (nRla(j)*xEtO(j)) &
492                     -(nVap(j)*yEtO(j))
493         else
494             dEtO(j)     = (nFed(j) * xFeed + nVap(j-1)*yEtO(j-1)) &
495                     +(nRla(j+1)*xEtO(j+1))
496         endif
497
498         dT_B(j)        = (QTrans(j)-QVer(j))/(MBo*cpBo)
499         dT_G(j)        = (QFeed(j)+QVap(j-1)-QTrans(j)+QRla(j+1)-QRla(j)-QVap(j)) &
500                     /((nH2O(j)*cpWl)+(nEtO(j)*cpEl))
501

```

```

502   if(xEtO(j).le.0.2608)then
503     TSie(j) = -38606.0*(xEtO(j)**(5)) + 31125.0*(xEtO(j)**(4)) &
504             -10545.0*(xEtO(j)**(3)) + 2054.1*(xEtO(j)**(2)) &
505             -259.68*xEtO(j) + 99.925
506   else
507     TSie(j) = 1.213*(xEtO(j)**(3))+11.412*(xEtO(j)**(2)) &
508             -18.377*xEtO(j)+86.314
509   endif
510
511 !Rücklauf unter Berücksichtigung potentiellen Flutens:
512   h(j) = ((nH2O(j)*18./1000000.)+(nEtO(j)*46.07/790000.))/(pi*(r1**2))
513   w(j) = fS*sqrt(2.*9.81*abs(h(j)))
514   if(h(j).gt.0.0001)then
515     nRla(j) = (w(j)*(pi*(r**2)) *1000.*1000./18.*xH2O(j)) &
516             +(w(j)*(pi*(r**2)) *1000.*790./46.07*xEtO(j))
517   else
518     nRla(j) = 0.0
519   endif
520
521 !Regelung der Verdampfungsraten und dadurch der Temperatur
522   ti = 100.0
523   kp = 0.02
524
525   e(j) = T_Ge(j)-TSie(j)
526   dedt(j) = e(j)
527
528   if(ypi(j).gt.0.00)then
529     ypi(j) = kp*(dedt(j)+yi__(j)*(1.0/ti))
530     nVap(j) = ypi(j)
531   else
532     nVap(j) = 0.0
533     dedt(j) = 0.0
534   endif
535
536   Phas(j) = 1.0
537   Ener(j) = QFeed(j)+QVap(j-1)-QVer(j)+QRla(j+1)-QRla(j)-QVap(j)
538
539
540
541   !Siedepunkt des Ethanol erreicht!
542   !!!!!!!!!!!!!!!!!!!!!!!!!!!!!!!!!!!!!!!!!!!!!!!!!!!!!!!!!!!!!!!!!!!!!!!!!!!!!
543   !!!!!!!!!!!!!!!!!!!!!!!!!!!!!!!!!!!!!!!!!!!!!!!!!!!!!!!!!!!!!!!!!!!!!!!!!!!!!
544
545   elseif(T_Ge(j).ge.TSie(j))then
546
547   !Bestimmung der Siedetemperatur
548   if(xEtO(j).le.0.2608)then
549     TSie(j) = -38606.0*(xEtO(j)**(5)) + 31125.0*(xEtO(j)**(4)) &
550             -10545.0*(xEtO(j)**(3)) + 2054.1*(xEtO(j)**(2)) &
551             -259.68*xEtO(j) + 99.925
552   else
553     TSie(j) = 1.213*(xEtO(j)**(3))+11.412*(xEtO(j)**(2)) &
554             -18.377*xEtO(j)+86.314
555   endif
556
557 !Regelung der Verdampfungsraten und dadurch der Temperatur
558   ti = 100.0
559   kp = 0.02
560
561   e(j) = T_Ge(j)-TSie(j)
562   dedt(j) = e(j)
563
564   ypi(j) = kp*(dedt(j)+yi__(j)*(1.0/ti))
565   if(ypi(j).ge.0.00)then
566     nVap(j) = ypi(j)
567   else
568     nVap(j) = 0.0
569   endif
570
571 !Berechnung der Wärmeströme
572   kV(j) = kL
573   QFeed(j) = nFed(j)*(1.0-xFeed)*cpWl*TFeed+nFed(j)*xFeed*cpEl*TFeed
574   QVer(j) = kV(j)*AV*(T_Bo(j)-TUm)
575   QRla(j) = (nRla(j)*xH2O(j)*cpWl*T_Ge(j))+(nRla(j)*xEtO(j)*cpEl*T_Ge(j))
576   QVap(j) = (nVap(j)*yH2O(j)*hVpW)+(nVap(j)*yEtO(j)*hVpE)
577   QTrans(j) = kA*(T_Ge(j)-T_Bo(j))
578
579 !Dampfzusammensetzung
580   xEtO(j) = nEtO(j)/(nEtO(j)+nH2O(j))
581   xH2O(j) = 1.0-xEtO(j)
582
583   if(xEtO(j).le.0.2608)then
584     yEt_(j) = -8919.6*(xEtO(j)**6) + 9405.1*(xEtO(j)**5) &
585             -4055.1*(xEtO(j)**4) + 935.68*(xEtO(j)**3) &

```

A.3. RECTIFICATION SOURCE CODE

```

586      -127.96*(xEtO(j)**2) + 11.053*xEtO(j) + 0.00007
587      yEtO(j) = yEt_(j)-((1-alpha)*(yEt_(j)-xEtO(j)))
588      else
589      yEt_(j) = 0.6395*(xEtO(j)**3) - 0.7129*(xEtO(j)**2) &
590      +0.6513*xEtO(j) + 0.4249
591      yEtO(j) = yEt_(j)-((1-alpha)*(yEt_(j)-xEtO(j)))
592      endif
593      yH2O(j) = 1.0-yEtO(j)
594
595      !Berechnung der Veränderungen
596      if(nH2O(j).ge.0.0) then
597      dH2O(j) = (nFed(j) * (1.0-xFeed) + nVap(j-1)*yH2O(j-1)) &
598      +(nRla(j+1)*xH2O(j+1)) - (nRla(j)*xH2O(j)) &
599      -(nVap(j)*yH2O(j))
600      else
601      dH2O(j) = (nFed(j) * (1.0-xFeed) + nVap(j-1)*yH2O(j-1)) &
602      +(nRla(j+1)*xH2O(j+1))
603      endif
604      if(nEtO(j).ge.0.0) then
605      dEtO(j) = (nFed(j) * xFeed + nVap(j-1)*yEtO(j-1)) &
606      +(nRla(j+1)*xEtO(j+1)) - (nRla(j)*xEtO(j)) &
607      -(nVap(j)*yEtO(j))
608      else
609      dEtO(j) = (nFed(j) * xFeed + nVap(j-1)*yEtO(j-1)) &
610      +(nRla(j+1)*xEtO(j+1))
611      endif
612      dT_B(j) = (QTrans(j)-QVer(j))/(MBo*cpBo)
613      dT_G(j) = (QFeed(j)+QVap(j-1)-QTrans(j)+QRla(j+1)-QRla(j)-QVap(j)) &
614      /((nH2O(j)*cpWl)+(nEtO(j)*cpEl))
615
616      !Rücklauf unter Berücksichtigung potentiellen Flutens:
617      h(j) = ((nH2O(j)*18./1000000.)+(nEtO(j)*46.07/790000.))/(pi*(r1**2))
618      w(j) = fS*sqrt(2.*9.81*abs(h(j)))
619      if(h(j).gt.0.0001) then
620      nRla(j) = (w(j)*(pi*(r**2)) *1000.*1000./18.*xH2O(j)) &
621      +(w(j)*(pi*(r**2)) *1000.*790./46.07*xEtO(j))
622      else
623      nRla(j) = 0.0
624      endif
625
626      Phas(j) = 2.0
627      Ener(j) = QFeed(j)+QVap(j-1)-QVer(j)+QRla(j+1)-QRla(j)-QVap(j)
628
629      endif
630      enddo
631
632      j=N      !letzter Boden der Kolonne
633
634      if(xEtO(j).le.0.2608) then
635      TSie(j) = -38606.0*(xEtO(j)**(5)) + 31125.0*(xEtO(j)**(4)) &
636      -10545.0*(xEtO(j)**(3)) + 2054.1*(xEtO(j)**(2)) &
637      -259.68*xEtO(j) + 99.925
638      else
639      TSie(j) = 1.213*(xEtO(j)**(3))+11.412*(xEtO(j)**(2)) &
640      -18.377*xEtO(j)+86.314
641      endif
642
643      !Unterhalb des Siedepunktes des Leichtersiedenden:
644      if(T_Ge(j).lt.TSie(j)) then
645      xEtO(j) = nEtO(j)/(nEtO(j)+nH2O(j))
646      xH2O(j) = 1.0-xEtO(j)
647
648      if(xEtO(j).le.0.2608) then
649      yEt_(j) = -8919.6*(xEtO(j)**6) + 9405.1*(xEtO(j)**5) &
650      -4055.1*(xEtO(j)**4) + 935.68*(xEtO(j)**3) &
651      -127.96*(xEtO(j)**2) + 11.053*xEtO(j) + 0.00007
652      yEtO(j) = yEt_(j)-((1-alpha)*(yEt_(j)-xEtO(j)))
653      else
654      yEt_(j) = 0.6395*(xEtO(j)**3) - 0.7129*(xEtO(j)**2) &
655      +0.6513*xEtO(j) + 0.4249
656      yEtO(j) = yEt_(j)-((1-alpha)*(yEt_(j)-xEtO(j)))
657      endif
658      yH2O(j) = 1.0-yEtO(j)
659
660      !Berechnung der Wärmeströme
661      kV(j) = kL
662      QFeed(j) = nFed(j)*(1.0-xFeed)*cpWl*TFeed+nFed(j)*xFeed*cpEl*TFeed
663      QVer(j) = kV(j)*AV*(T_Bo(j)-TUm)
664      QRla(j) = (nRla(j)*xH2O(j)*cpWl*T_Ge(j)+(nRla(j)*xEtO(j)*cpEl*T_Ge(j))
665      QVap(j) = (nVap(j)*yH2O(j)*hVpW)+(nVap(j)*yEtO(j)*hVpE)
666      Q0 = (L0*(1.0-x0)*cpWl*(TR10-Tref))+(L0*x0*cpEl*(TR10-Tref))
667      QTrans(j) = k*A*(T_Ge(j)-T_Bo(j))

```



```

670
671   if (nH2O(j).ge.0.0) then
672     dH2O(j) = (nFed(j) * (1.0-xFeed) + nVap(j-1)*yH2O(j-1)) &
673               + L0*(1.0-x0) - (nRla(j)*xH2O(j)) - (nVap(j)*yH2O(j))
674   else
675     dH2O(j) = (nFed(j) * (1.0-xFeed) + nVap(j-1)*yH2O(j-1)) + L0*(1.0-x0)
676   endif
677   if (nEtO(j).ge.0.0) then
678     dEtO(j) = (nFed(j) * xFeed + nVap(j-1)*yEtO(j-1)) + L0*x0 &
679               - (nRla(j)*xEtO(j)) - (nVap(j)*yEtO(j))
680   else
681     dEtO(j) = (nFed(j) * xFeed + nVap(j-1)*yEtO(j-1)) + L0*x0
682   endif
683
684   dT_B(j) = (QTrans(j)-QVer(j))/(MBo*cpBo)
685   dT_G(j) = (QFeed(j)+QVap(j-1)-QTrans(j)+Q0-QRla(j)-QVap(j)) &
686             / ((nH2O(j)*cpW1)+(nEtO(j)*cpE1))
687
688   if (xEtO(j).le.0.2608) then
689     TSie(j) = -38606.0*(xEtO(j)**(5)) + 31125.0*(xEtO(j)**(4)) &
690              -10545.0*(xEtO(j)**(3)) + 2054.1*(xEtO(j)**(2)) &
691              -259.68*xEtO(j) + 99.925
692   else
693     TSie(j) = 1.213*(xEtO(j)**(3))+11.412*(xEtO(j)**(2)) &
694              -18.377*xEtO(j)+86.314
695   endif
696
697   !Rücklauf unter Berücksichtigung potentiellen Flutens:
698   h(j) = ((nH2O(j)*18./1000000.)+(nEtO(j)*46.07/790000.))/(pi*(r1**2))
699   w(j) = fS*sqrt(2.*9.81*abs(h(j)))
700   if (h(j).gt.0.0001) then
701     nRla(j) = (w(j)*(pi*(r**2)) *1000.*1000./18.*xH2O(j)) &
702               +(w(j)*(pi*(r**2)) *1000.*790./46.07*xEtO(j))
703   else
704     nRla(j) = 0.0
705   endif
706
707   !Regelung der Verdampfungsraten und dadurch der Temperatur
708   ti = 100.0
709   kp = 0.02
710
711   e(j) = T_Ge(j)-TSie(j)
712   dedt(j) = e(j)
713
714   if (ypi(j).gt.0.00) then
715     ypi(j) = kp*(dedt(j)+yi__(j)*(1.0/ti))
716     nVap(j) = ypi(j)
717   else
718     nVap(j) = 0.0
719     dedt(j) = 0.0
720   endif
721
722   Phas(j) = 1.0
723   Ener(j) = QFeed(j)+QVap(j-1)-QVer(j)+Q0-QRla(j)-QVap(j)
724
725
726   !Siedepunkt des Ethanol's erreicht!
727   !!!!!!!!!!!!!!!!!!!!!!!!!!!!!!!!!!!!!!!!!!!!!!!!!!!!!!!!!!!!!!!!!!!!!!!!!!!!!
728   !!!!!!!!!!!!!!!!!!!!!!!!!!!!!!!!!!!!!!!!!!!!!!!!!!!!!!!!!!!!!!!!!!!!!!!!!!!!!
729   !!!!!!!!!!!!!!!!!!!!!!!!!!!!!!!!!!!!!!!!!!!!!!!!!!!!!!!!!!!!!!!!!!!!!!!!!!!!!
730   !!!!!!!!!!!!!!!!!!!!!!!!!!!!!!!!!!!!!!!!!!!!!!!!!!!!!!!!!!!!!!!!!!!!!!!!!!!!!
731
732   elseif (T_Ge(j).ge. TSie(j)) then
733
734   !Bestimmung der Siedetemperatur
735   if (xEtO(j).le.0.2608) then
736     TSie(j) = -38606.0*(xEtO(j)**(5)) + 31125.0*(xEtO(j)**(4)) &
737              -10545.0*(xEtO(j)**(3)) + 2054.1*(xEtO(j)**(2)) &
738              -259.68*xEtO(j) + 99.925
739   else
740     TSie(j) = 1.213*(xEtO(j)**(3))+11.412*(xEtO(j)**(2)) &
741              -18.377*xEtO(j)+86.314
742   endif
743
744   !Regelung der Verdampfungsraten und dadurch der Temperatur
745   ti = 100.0
746   kp = 0.02
747
748   e(j) = T_Ge(j)-TSie(j)
749   dedt(j) = e(j)
750
751   ypi(j) = kp*(dedt(j)+yi__(j)*(1.0/ti))
752   if (ypi(j).ge.0.00) then
753     nVap(j) = ypi(j)

```

A.3. RECTIFICATION SOURCE CODE

```

754     else
755         nVap(j)      = 0.0
756     endif
757
758
759 !Berechnung der Wärmeströme
760 kV(j)      = kL
761 QFeed(j)   = nFed(j)*(1.0-xFeed)*cpWl*TFeed+nFed(j)*xFeed*cpEl*TFeed
762 QVer(j)    = kV(j)*AV*(T_Bo(j)-TUm)
763 QRla(j)    = (nRla(j)*xH2O(j)*cpWl*T_Ge(j))+(nRla(j)*xEtO(j)*cpEl*T_Ge(j))
764 QVap(j)    = (nVap(j)*yH2O(j)*hVpW)+(nVap(j)*yEtO(j)*hVpE)
765 Q0         = (L0*(1.0-x0)*cpWl*(TRl0-Tref))+(L0*x0*cpEl*(TRl0-Tref))
766 QTrans(j)  = k*A*(T_Ge(j)-T_Bo(j))
767
768 !Dampfzusammensetzung
769 xEtO(j)    = nEtO(j)/(nEtO(j)+nH2O(j))
770 xH2O(j)    = 1.0-xEtO(j)
771
772 if (xEtO(j).le.0.2608) then
773     yEt_(j) = -8919.6*(xEtO(j)**6) + 9405.1*(xEtO(j)**5) &
774             -4055.1*(xEtO(j)**4) + 935.68*(xEtO(j)**3) &
775             -127.96*(xEtO(j)**2) + 11.053*xEtO(j) + 0.00007
776     yEtO(j) = yEt_(j)-((1-alpha)*(yEt_(j)-xEtO(j)))
777 else
778     yEt_(j) = 0.6395*(xEtO(j)**3) - 0.7129*(xEtO(j)**2) &
779             +0.6513*xEtO(j) + 0.4249
780     yEtO(j) = yEt_(j)-((1-alpha)*(yEt_(j)-xEtO(j)))
781 endif
782 yH2O(j)    = 1.0-yEtO(j)
783
784 !Berechnung der Veränderungen
785 if (nH2O(j).ge.0.0) then
786     dH2O(j)  = (nFed(j) * (1.0-xFeed) + nVap(j-1)*yH2O(j-1)) &
787             +L0*(1.0-x0) - (nRla(j)*xH2O(j)) - (nVap(j)*yH2O(j))
788 else
789     dH2O(j)  = (nFed(j) * (1.0-xFeed) + nVap(j-1)*yH2O(j-1)) + L0*(1.0-x0)
790 endif
791 if (nEtO(j).ge.0.0) then
792     dEtO(j)  = (nFed(j) * xFeed + nVap(j-1)*yEtO(j-1)) + L0*x0 &
793             -(nRla(j)*xEtO(j)) - (nVap(j)*yEtO(j))
794 else
795     dEtO(j)  = (nFed(j) * xFeed + nVap(j-1)*yEtO(j-1)) + L0*x0
796 endif
797
798 dT_B(j)     = (QTrans(j)-QVer(j))/(MBo*cpBo)
799 dT_G(j)     = (QFeed(j)+QVap(j-1)-QTrans(j)+Q0-QRla(j)-QVap(j)) &
800             /((nH2O(j)*cpWl)+(nEtO(j)*cpEl))
801
802 !Rücklauf unter Berücksichtigung potentiellen Flutens:
803 h(j)        = ((nH2O(j)*18./1000000.)+(nEtO(j)*46.07/790000.))/(pi*(r1**2))
804 w(j)        = fS*sqrt(2.*9.81*abs(h(j)))
805 if (h(j).gt.0.0001) then
806     nRla(j)  = (w(j)*(pi*(r**2)) *1000.*1000./18.*xH2O(j))+(w(j) &
807             *(pi*(r**2)) *1000.*790./46.07*xEtO(j))
808 else
809     nRla(j)  = 0.0
810 endif
811
812 Phas(j)     = 2.0
813 Ener(j)     = QFeed(j)+QVap(j-1)-QVer(j)+Q0-QRla(j)-QVap(j)
814
815 endif
816
817
818 QVTot       = QVer(1)+QVer(2)+QVer(3)+QVer(4)+QVer(5)+QVer(6)+QVer(7) &
819             +QVer(8)+QVer(9)+QVer(10)+QVer(11)+QVer(12)+QVer(13) &
820             +QVer(14)+QVer(15)
821
822                                     !Ende!
823 !!!!!!!!!!!!!!!!!!!!!!!!!!!!!!!!!!!!!!!!!!!!!!!!!!!!!!!!!!!!!!!!!!!!!!!!!!!!!
824 !!!!!!!!!!!!!!!!!!!!!!!!!!!!!!!!!!!!!!!!!!!!!!!!!!!!!!!!!!!!!!!!!!!!!!!!!!!!!
825
826
827 !Zuordnungen
828 do j=1, N
829     ypkt(j)      = dT_B(j)
830     ypkt(j+N)    = dH2O(j)
831     ypkt(j+2*N)  = dEtO(j)
832     ypkt(j+3*N)  = dedt(j)
833     ypkt(j+4*N)  = dT_G(j)
834 enddo
835
836
837 !Zwischengrößen

```

```

838     do j=1, N
839         zgvec(j) = xEtO(j)
840         zgvec(j+N) = yEtO(j)
841         zgvec(j+2*N) = nVap(j)
842         zgvec(j+3*N) = nRla(j)
843         zgvec(j+4*N) = kv(j)
844     enddo
845     zgvec(5*N+1) = QVtot
846     zgvec(5*N+2) = h(1)
847
848 endif
849
850
851 end subroutine
852
853 subroutine StringPlusNumber( string , firstname , number)
854     implicit none
855     character(len=6) :: string
856     character(len=4) :: firstname
857     integer :: number
858
859     character(len=2) :: buffer
860
861     if (number .lt. 10) then
862         write(buffer,1000), number
863     else if (number .lt. 100) then
864         write(buffer,2000), number
865     endif
866
867     string(1:4) = firstname(1:4)
868     string(5:6) = buffer(1:2)
869
870
871 ! format with one and two integers respectively
872 1000 format("0", i1)
873 2000 format(" ", i2)
874
875 end subroutine

```

A.4. Technical description of the BioProcess Trainer

Switching on the BioProcess Trainer

Press the *Power*-button at the upper right screen border. After activation, a red surface will appear on the button. In addition numerical values appear in the main graphical user interface (GUI) and some switch buttons are activated.

Starting a cultivation

Press the button *Start new process* on the right screen border. A control panel appears offering the choice of simulation mode (accelerated). For the execution of a simulation in real time press the button with number 1 in that control panel. The window will close automatically after a short time. Select one of the numbers 5 , 10 or 15 to simulate the process with increased speed. Generally a 5-time process speed is recommended. In the upper right screen area, the process time will start with the specified process speed. Furthermore , the current time and date are specified.

Setting/ Preparation of the inoculum

Press the button *Prepare inoculum*. A control panel *Inoculum preparation* appears. The control panel provides the input masks *Biomass concentration in inoculum* and *Volume of the inoculum* for inserting a nu-

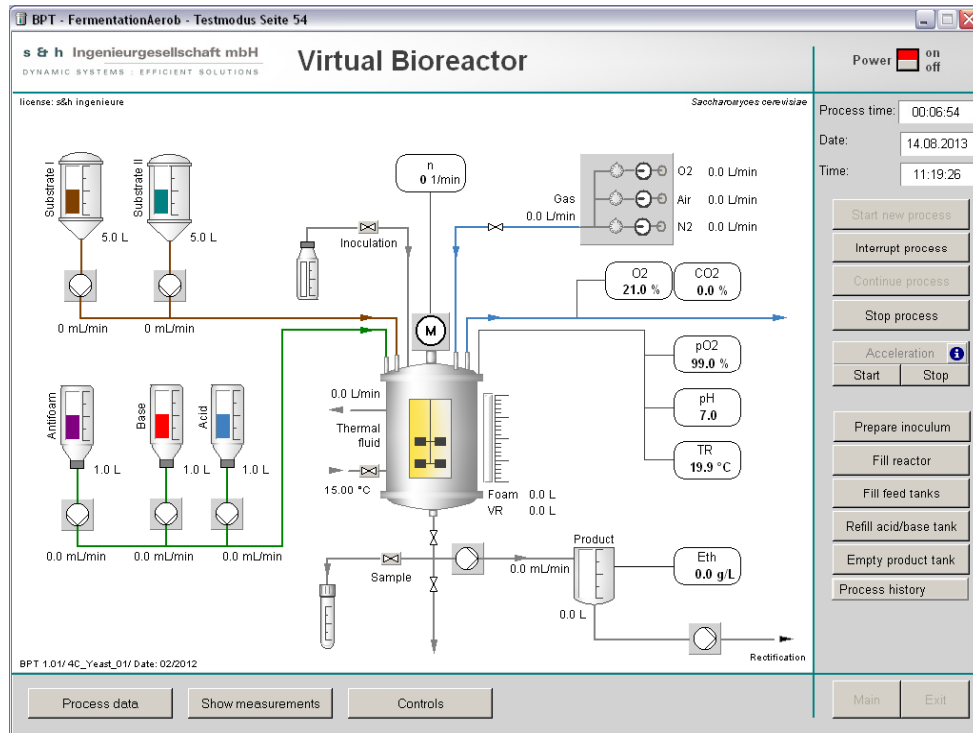


Figure A.6.: Main graphical user interface of the Virtual Bioreactor.

merical value. Click in the input field and enter the desired biomass concentration in the inoculum , e. g. $50.0 \text{ g} \cdot \text{L}^{-1}$, and the volume of the inoculum, e. g. 200 mL. Confirm the input with *Return*. Close the window *Inoculum preparation* by clicking *Exit*.

Filling the bioreactor with medium

Press the button *Fill reactor* in the right part of the process picture border. A control panel will appear. The control panel includes the input fields *Substrates concentrations* and *Volume* for the input of numerical values. To change the values indicated there, proceed as follows: Click in the input field *Substrates concentration* and enter the desired substrate concentration in the medium, e.g. $12.0 \text{ g} \cdot \text{L}^{-1}$. Confirm the entry with *Return*. Click in the input field *volume* and enter the desired medium volume (e.g. 4.8 L). Confirm the input with *Return*. Press the operating knob to start the filling procedure. The bioreactor will fill with medium of the desired specification. After the filling procedure is completed, the window *Medium preparation* closes automatically.

Filling the feed tanks

Press the button *Fill feed tanks*. The control panel *Prepare feed tanks* appears. The control panel contains the input fields *Substrate tank I and II* and *Substrates concentration I and II* as well as *Anti-foam tank*, *Acid tank* and *Base tank*. To change the values indicated, proceed as follows: Click in an input field of *Substrate tank I and II* and enter the desired substrate volume, e. g. 30.0 L. Confirm the input with *Return*.

Click in the input field for *Substrate concentration I and II* and enter the desired substrate concentration in the inlet, e. g. $100.0 \text{ g} \cdot \text{L}^{-1}$ and end the input with *Return*. Click in the input field of *Antifoam tank* and enter the desired anti-foam volume, e. g. 2.0 L. Confirm with *Return*.

Click in the input field of *Acid tank*. Enter the desired acid volume, e. g. 1.0 L and confirm the input with *Return*. Click in the input field *Base tank*. Enter the desired basic solution volume, e. g. the value 1.0 L and end the input with *Return*.

Press the push button *Fill tanks* to start the filling process of the feed tanks. The containers are filled. After the filling procedure the window *Prepare Feed tanks* closes automatically (Substrate I “Glucose; Substrate II “Nitrogen source).

Switching on the stirrer

Above the bioreactor you will find a symbolized motor. Press on that *Motor symbol*. An additional GUI *Motor speed* appears with a control element for *Motor speed*. Click in the input field of the control element *Motor speed*. Enter the desired motor speed, e. g. $150.0 \text{ l} \cdot \text{min}^{-1}$ and confirm the input with *Return*. Close the window *Motor speed* by pressing *Exit*. Above the motor symbol on top of the bioreactor the entered value appears. The symbolized motor in the bioreactor starts to rotate.

Switching on temperature control

Left down of the bioreactor in the inlet pipe to the heating control jacket there is a *Valve* symbol. Click this symbol and an additional GUI appears (*Heating jacket control panel*). In this GUI the control elements *Flow rate* and *Temperature* are located. Click in the input field of the control element *Flow rate* and enter the desired flow rate, e.g. $5.0 \text{ L} \cdot \text{min}^{-1}$. Confirm the input with *Return*. Click in the input field for *Temperature* and enter the desired temperature, e. g. $35.0 \text{ }^{\circ}\text{C}$. Confirm the input with *Return*. Close the window *Heating Jacket control panel* by pressing

Exit.

Sampling

Press the button *Sample*, located at bottom left of the cultivation tank. The biomass, substrate I and II and ethanol concentration at the time of sampling is stored with the simulator. These values are represented in the additional GUI *Process data*.

Inoculation

Click the valve with the description *Inoculate*, located on the left side above the bioreactor. After clicking the valve, 200 mL of prepared inoculum is delivered into the bioreactor. The current inoculation procedure is indicated by a colored inlet conduit. After inoculation a sample should be taken.

Aeration

Right above the cultivation tank are three inlets for gases with valve-symbols. Press the valve *Gas* and an additional GUI named *Gas mixing station* pops up with the control elements *Flow rate O₂*, *Flow rate air* and *Flow rate N₂*. Click in the input field of the control element *Flow rate air*. Enter the desired aeration rate, e. g. $2.5 \text{ L} \cdot \text{min}^{-1}$ and confirm the input with *Return*. Close the window *Gas mixing station* with *Exit*.

Observation of the current process run

For the observation of the process run, there are different diagrams and auxiliary process features available. The additional GUI named *Process data* shows important current process data in the form of bar graphs as well as the values of biomass, substrates (glucose, nitrogen source) and ethanol concentrations at the time of the last sampling in numerical presentation.

The diagrammatic pictures of the current process run are found in the lower border of the process picture. After pressing the button *Show measurements* the process picture appears. It can be chosen between *Gas data* and *pO₂ plot*, *Stirrer speed* and *Gas flow rates*, *Feeding profiles* and *Temperature* and *Volume*. The associated diagrams will pop up. Several diagrams can be opened simultaneously.

Representation of a process run (history)

By clicking *Process history* a pull-down menu showing the recorded process runs will open. Here different categories (e. g. different temper-

atures, flow rates) can be chosen. The recordings will subsequently be presented in a graphical form.

Operating a cultivation

The cultivation process is operated by push buttons in the process picture (valves, pumps, etc.). After pressing the highlighted push buttons, different auxiliary GUIs are opened. During a cultivation the following parameters can be varied:

- supply of substrate,
- supply of anti-foam agent,
- supply of acid and base,
- discharge of product,
- motor speed,
- aeration rate,
- heating jacket: temperature, flow rate, and
- sampling

The variation of supplies is achieved by clicking the pump symbols. The auxiliary GUI *Pump station* appears.

Controlled operation

The Virtual Bioreactor has some automatic controllers that simplify process control. After pressing *Controls* on the lower process picture border, an auxiliary GUI opens. Altogether five automatic controllers are offered:

- pO_2 -control,
- anti-foam control,
- temperature control,
- pH regulation, and
- level-control

After inserting the set point values, the controllers must be switched on by clicking the buttons *On* for each controller. By switching on of the automatic controllers, the corresponding pumps and valves, as well as the stirrer motor, are set to *remote* operation. Manual adjustment of the controller is not possible in this mode.

Termination of a cultivation

By pressing *Stop process* on the right side of the process picture the cultivation is terminated. After pressing the button, there will be no more meaningful data in the current process pictures to regulate. A choice to select historical data of the recently terminated cultivation is still represented via *Process history*. The recorded data can be exported to a text file which may be further processed in supplementary software (e.g. Excel).

Termination of the program

The reactor is switched off by pressing the *Power*-button. The program is terminated by pressing the button *Exit VBR*. This button is locked, as long as the reactor is turned on. The program cannot be terminated when the reactor is running.

A.5. GRAFCET-plans

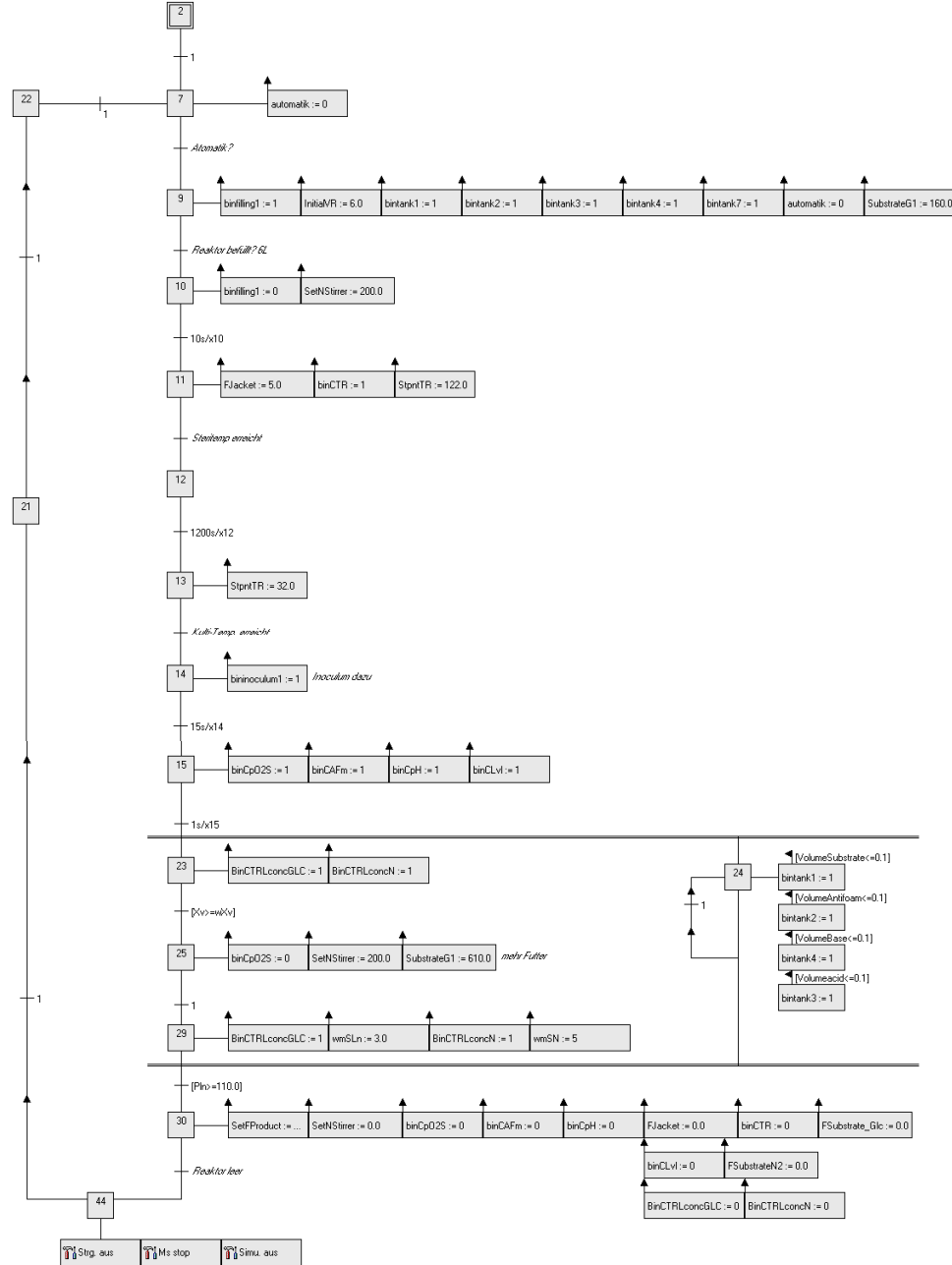


Figure A.7.: GRAFCET plan of a batch-fermentation, including sterilisation, aerobic biomass growth and anaerobic ethanol production.

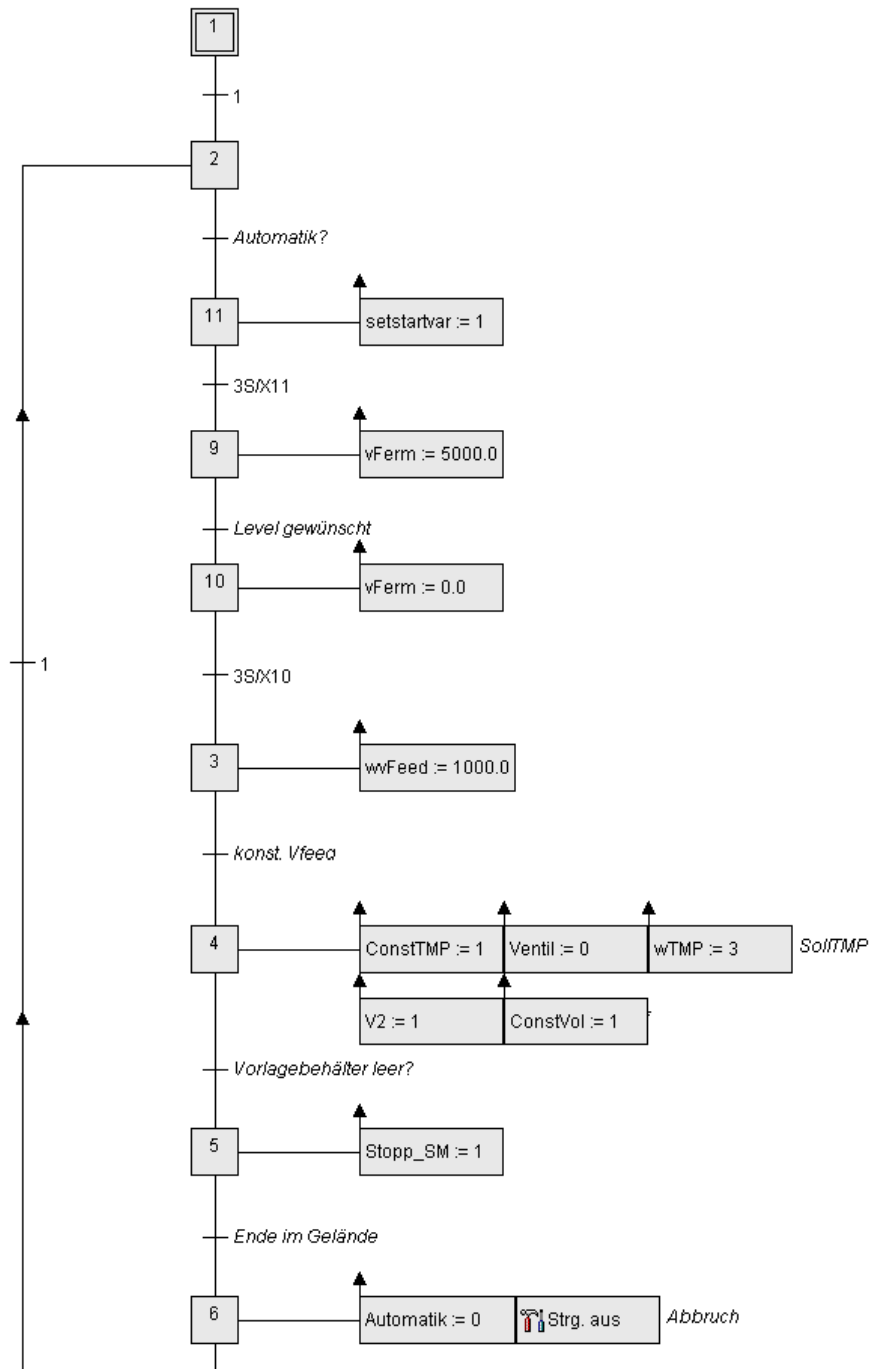


Figure A.8.: Automatic sequence control implemented as GRAFCET-plan in WinErs. The parameters feed flow rate, set point TMP, starting concentrations and volume and set point pressure drop may be changed for testing process control strategies.

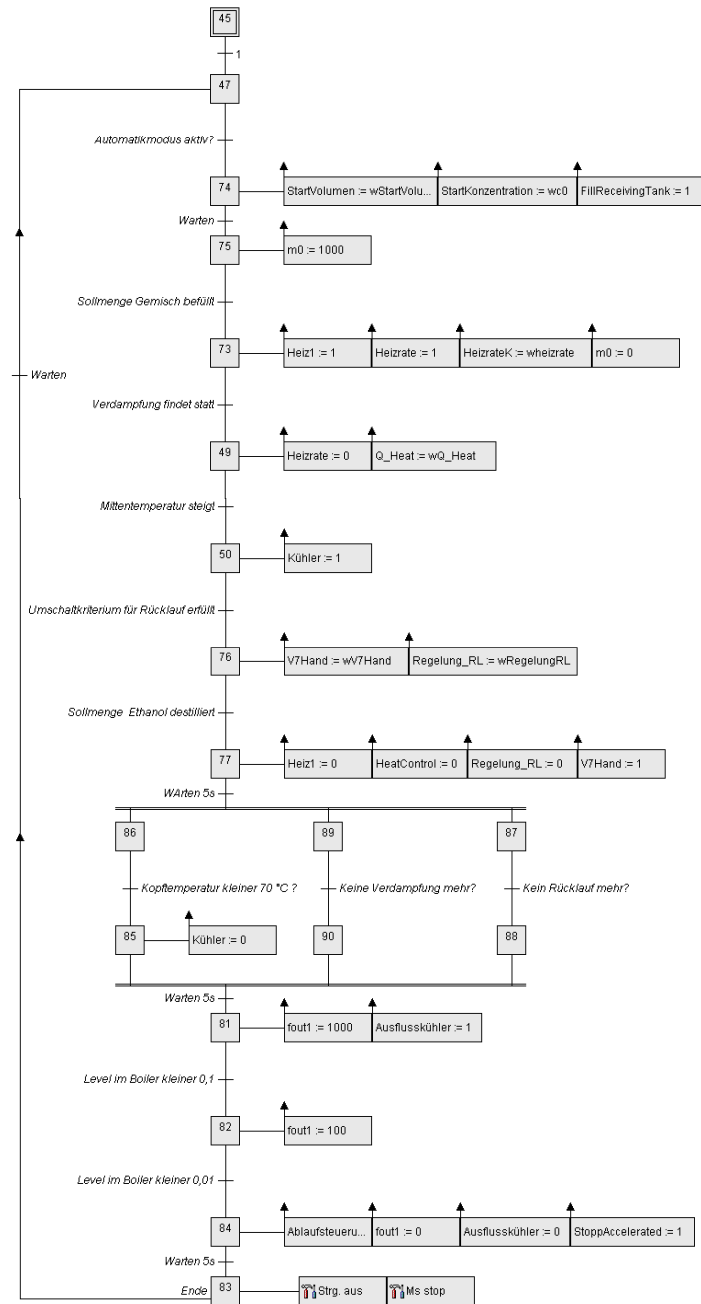


Figure A.9.: GRAFCET plan for a batch-rectification process. By varying parameters in the transitions and actions of this plan (constant/ variable reflux ratio, reflux interval, reflux ratio, desired product quality and quantity in the reboiler, and heating rate and heating power input), the process control strategy can be changed.

A.6. Virtual Biorefinery - connected in a continuous process

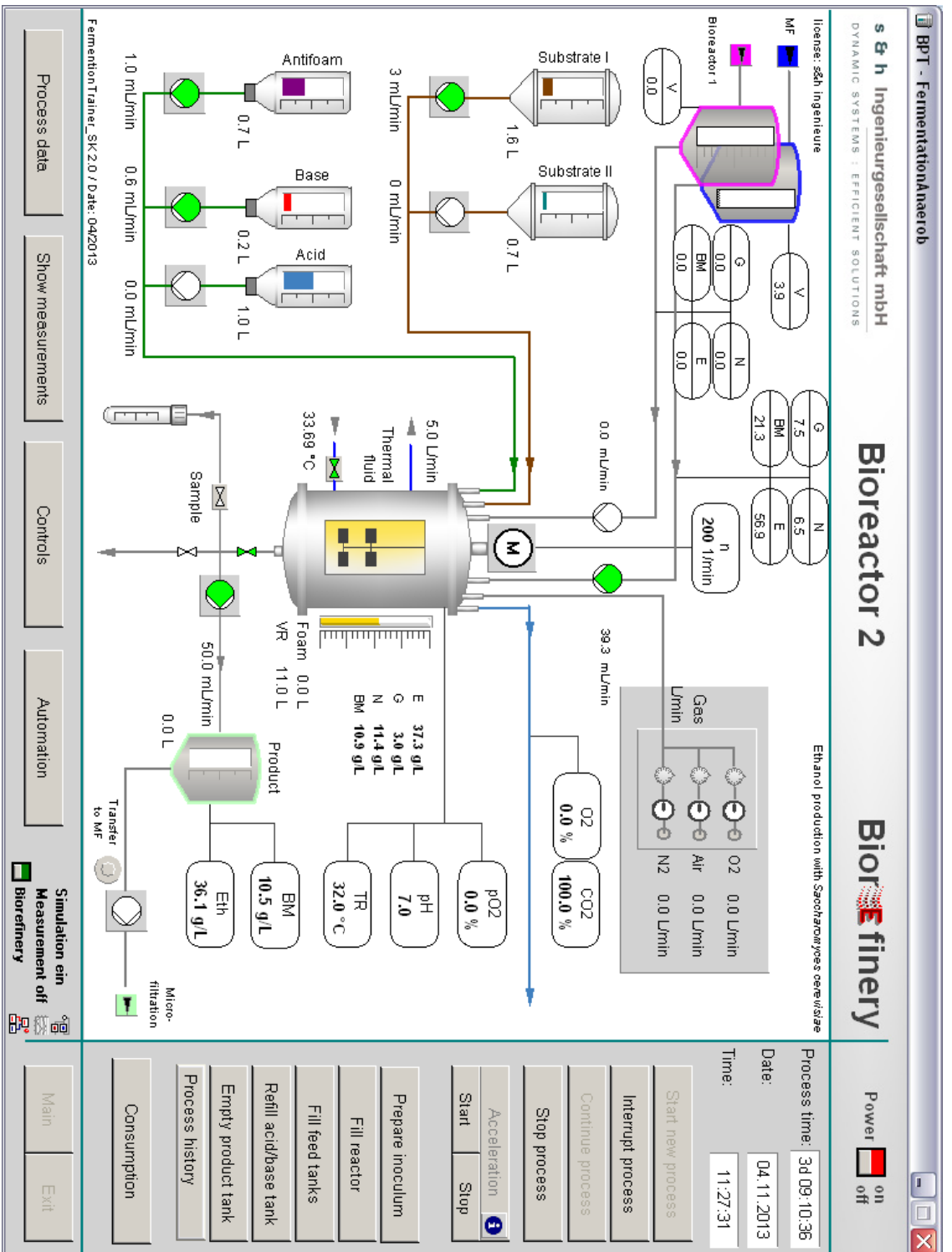


Figure A.10.: Bioreactor 1 in biorefinery mode. A continuous recirculation of fermentation broth is realised by the respective pumps that have identical flow rates.

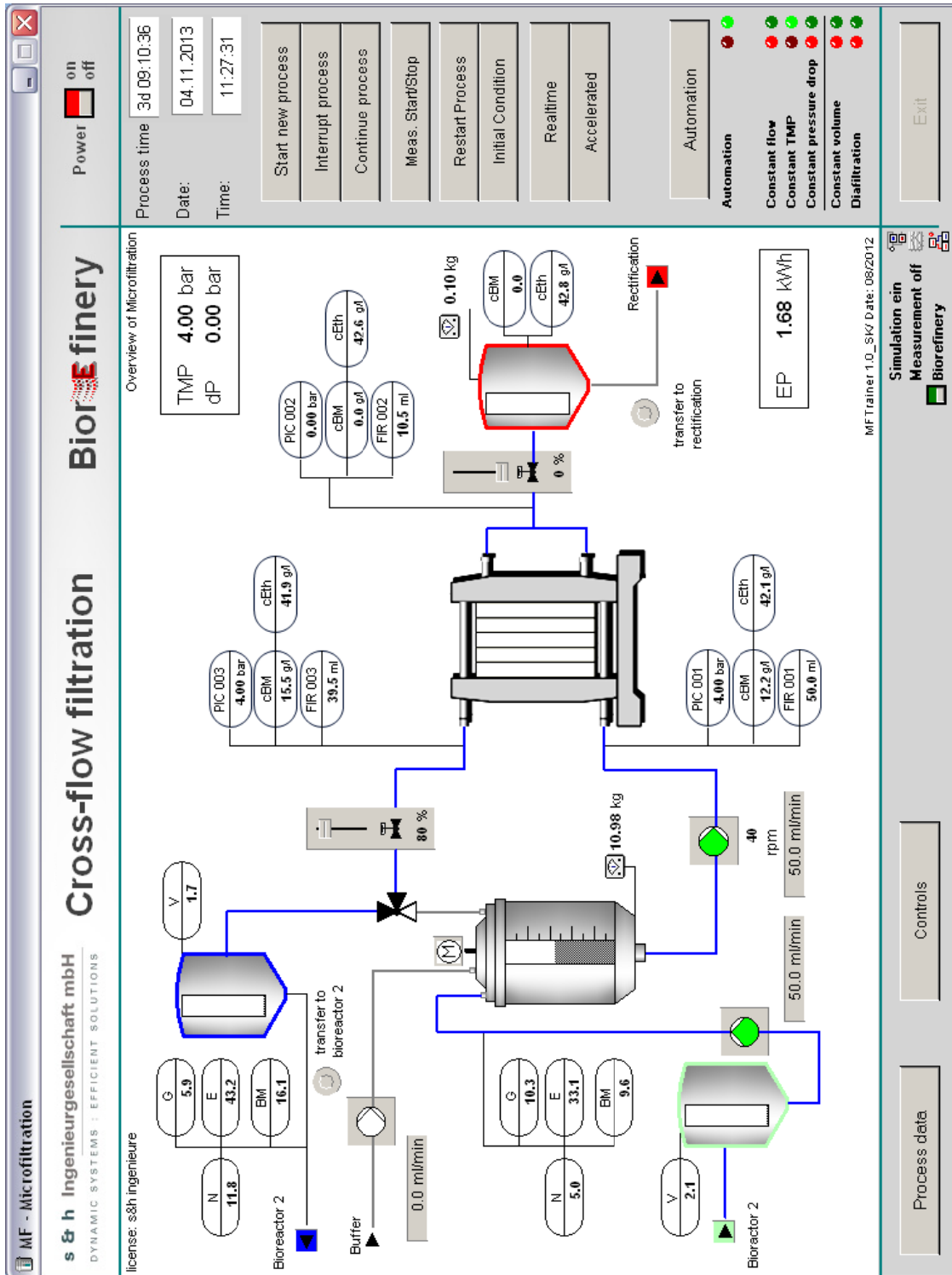


Figure A.11.: Cross-flow filtration in biorefinery mode. A continuous recirculation of fermentation broth is realised by the respective pumps that have identical flow rates.

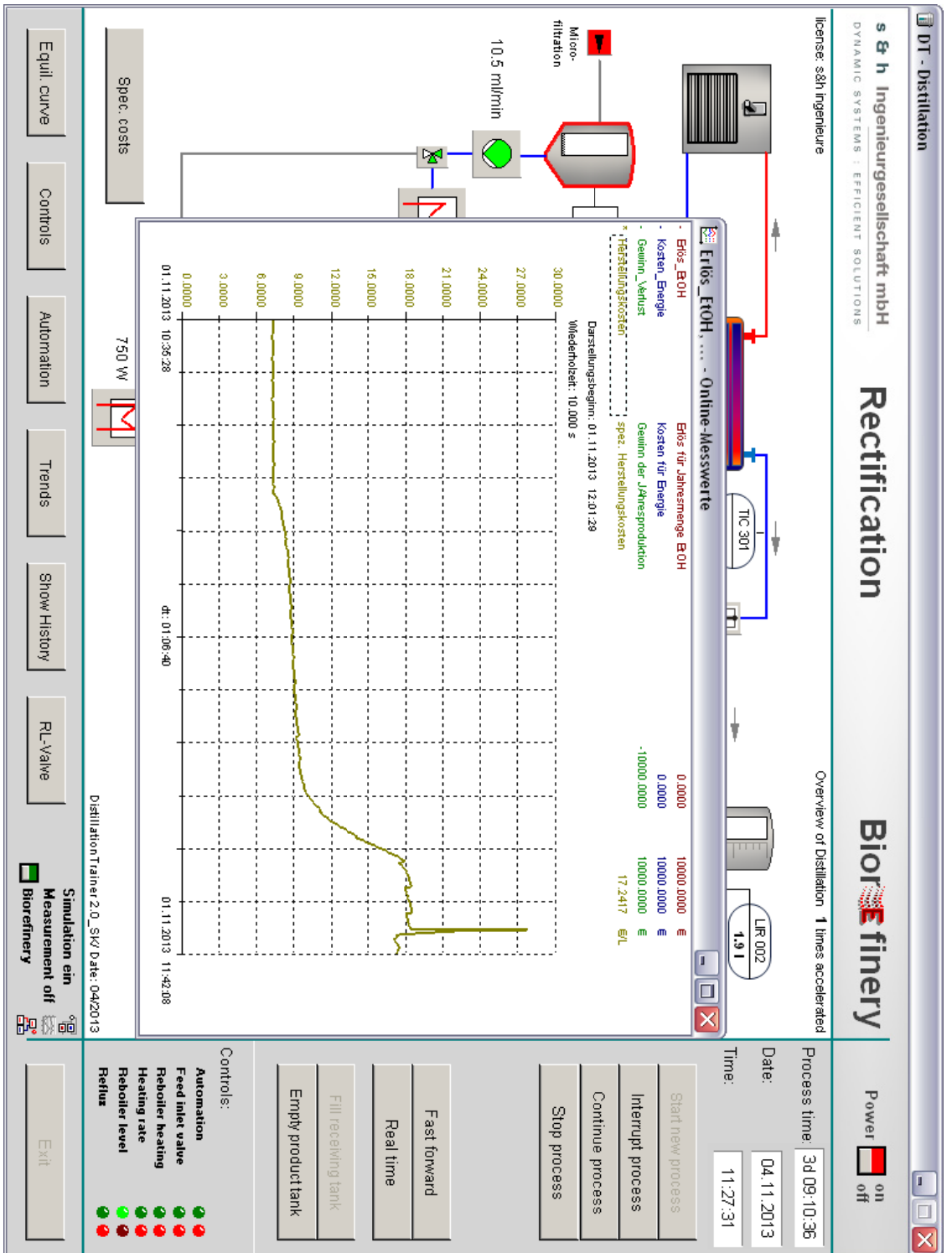


Figure A.12.: Rectification in biorefinery mode. The continuous feed into the rectification column is determined by the permeate flow rate in the cross-flow simulator. The auxiliary window shows the online trend of the cost function, which represents the actual specific production costs. Consequences of process control strategy modifications in any of the sub-units are visualized here.

A.7. Comparing efficiencies

Table A.3.: Comparison of tray efficiency factors model η' and literature η' [Vauck and Müller, 2000].

Heating power	η' model	η' literature
250 W	0.42	0.40
500 W	0.73	0.73
750 W	0.85	0.86
1000 W	0.80	0.80
1250 W	0.60	0.60
1500 W	0.15	0.13

A.8. P&ID flow chart of the biorefinery

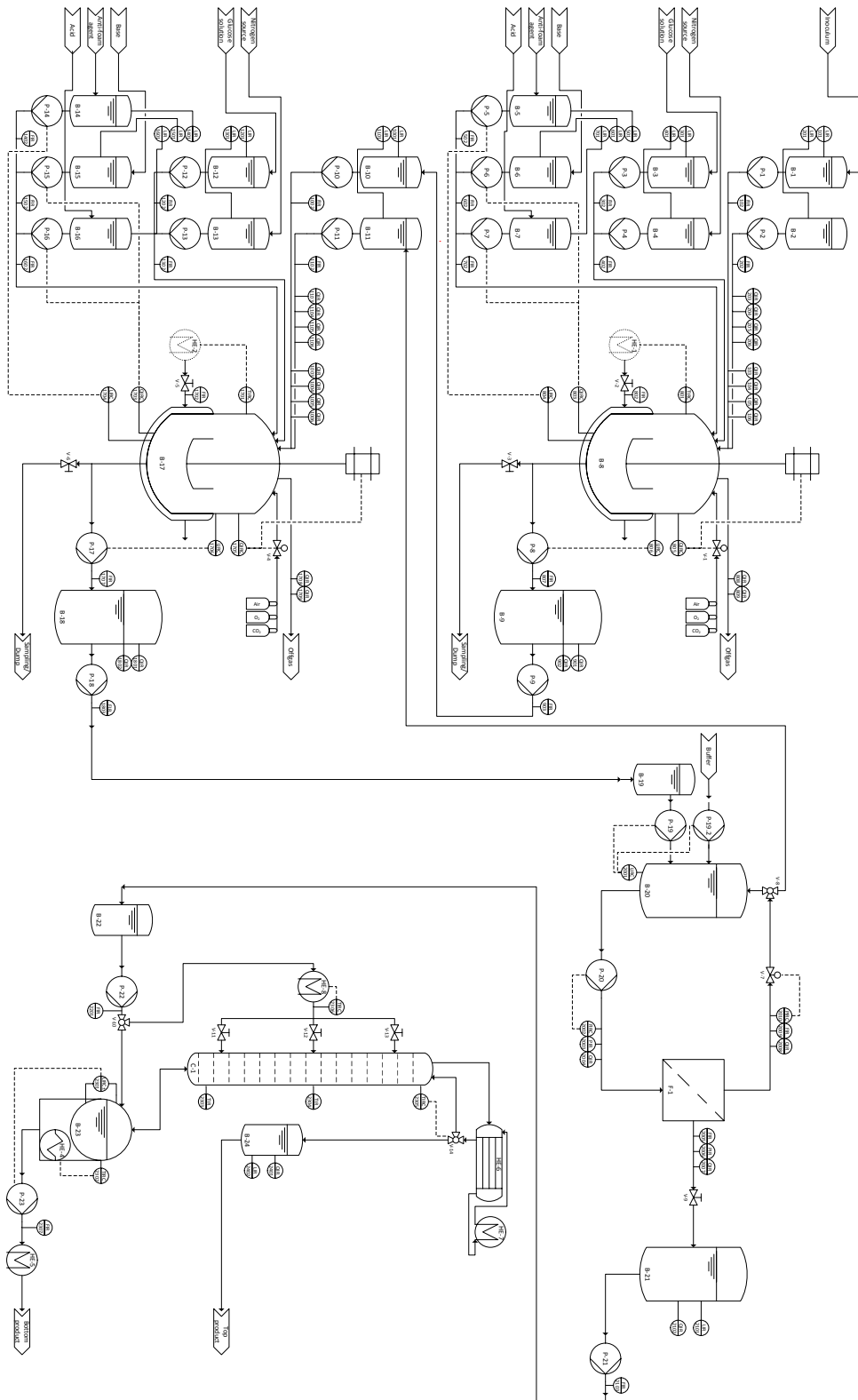


Figure A.13.: P&ID diagram of the bioethanol process.

A.9. Biorefinery process - tank volumes

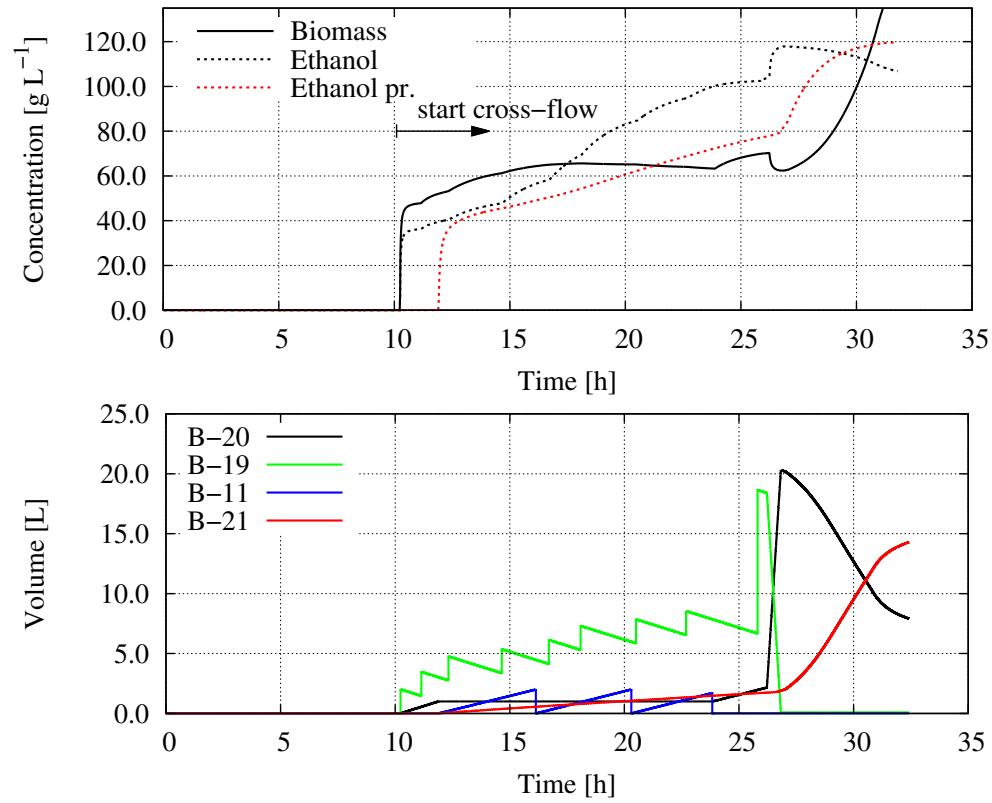


Figure A.14.: Concentrations of biomass and ethanol (top) in the feed tank B-20 (black) and in the product tank B-21 (red) and volumes of all tanks in the cross-flow filtration process (bottom). When the buffering tank (B-11) reaches 2 L volume, its contents are transferred to the respective tank in the cultivation. Further explanation see text.

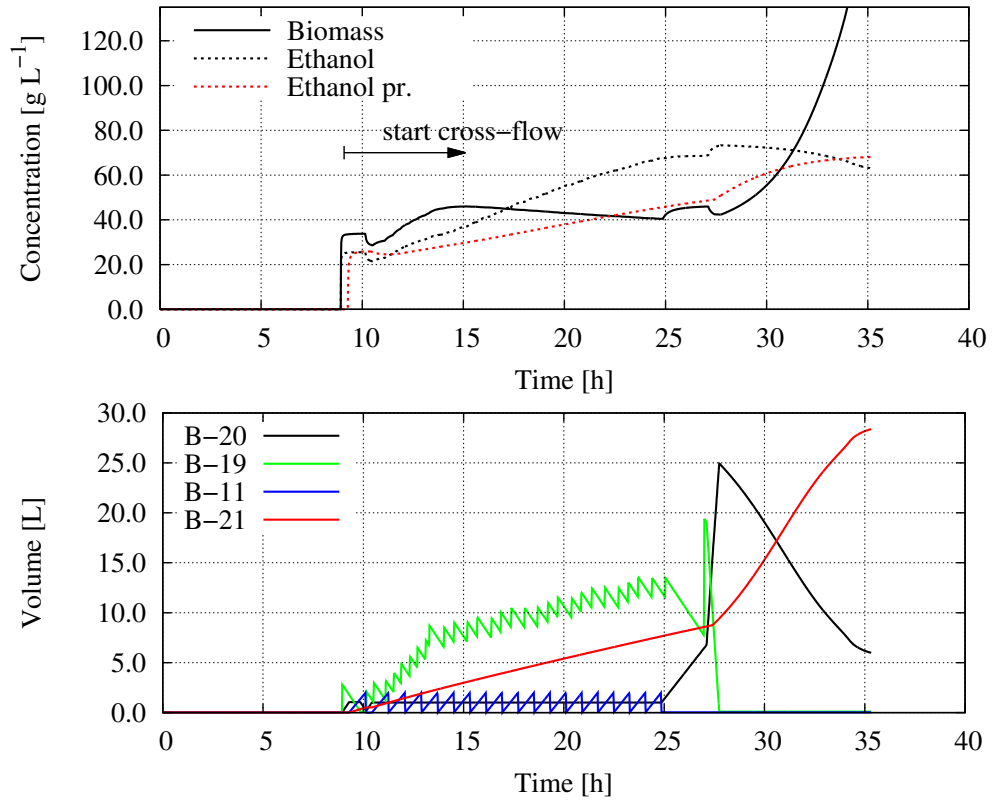


Figure A.15.: Concentrations of biomass and ethanol (top) in the feed tank B-20 (black) and in the product tank B-21 (red) and volumes of all tanks (bottom) in the cross-flow filtration process. When buffer tank B-11 reaches 2 L of volume, its contents are transferred to the respective tank in the cultivation. Further explanation see text.

Bibliography

- Alriols, M. G., García, A., Hajji, N., Chouaibi, F., and Labidi, J. (2010). Lignocellulosic biorefinery processes energy integration. *CHISA / ECCE7 Compilation of Full Texts*, J5.4, 0807.
- Amigun, B., Musango, J. K., and Stafford, W. (2011). Biofuels and sustainability in africa. *Renewable and Sustainable Energy Reviews*, 15(2):1360 – 1372.
- B. Braun Biotech International (2000). *Betriebshandbuch biostat c*.
- Balat, M., Balat, H., and Öz, C. (2008). Progress in bioethanol processing. *Progress in Energy and Combustion Science*, 34(5):551 – 573.
- Balaton, M., Nagy, L., and Szeifert, F. (2013). Operator training simulator process model implementation of a batch processing unit in a packaged simulation software. *Computers & Chemical Engineering*, 48(0):335 – 344.
- Bayrakci, A. G. and Kocar, G. (2014). Second-generation bioethanol production from water hyacinth and duckweed in izmir: A case study. *Renewable and Sustainable Energy Reviews*, 30(0):306 – 316.
- Beauchet, R., Berberi, V., Corcos, P.-O., Guimont-Montpetit, G., Dion, Y., Eudes, F., and Lavoie, J.-M. (2013). Fermentation of {C6} carbohydrates from triticale straw hemicellulosic fraction as pretreatment for xylose purification. *Industrial Crops and Products*, 51(0):463 – 469.
- Bergmann, J. (1999). *Lehr- und Übungsbuch Automatisierungs- und Prozeßleittechnik : eine Einführung für Ingenieure und Betriebswirtschaftler*. Fachbuchverl. Leipzig im Hanser Verl., München [u.a.].
- Bieber, T. and Erdmann, H.-H. (1990). Short-Cut-Methoden bei Prozeß-Simulatoren und Experten-Systemen. *Chemie Ingenieur Technik*, 62(5):397–400.
- Birk, J. und Holl, P. (1995). Schulungssimulator zur Reglereinstellung. *Chemie Ingenieur Technik*, 67(2):190–192.

- Blanco, L. and Isenhouer, M. (2010). Powering america: The impact of ethanol production in the corn belt states. *Energy Economics*, 32(6):1228 – 1234.
- Blesgen, A. (2009). *Entwicklung und Einsatz eines interaktiven Biogas-Echtzeit-Simulators*. PhD thesis, Hochschule Bremen.
- Blesgen, A. and Hass, V. C. (2010). Strategies for the development of operator training simulators for engineering education and training. In *Proceedings of the 19th International Congress on Chemical and Process Engineering*, Prague, Czech Republic.
- Bohl, W. (2002). *Technische Strömungslehre*. Vogel Fachbuchverl.
- Braunschweig, B. and Gani, R. (2002). *Software Architectures and Tools for Computer Aided Process Engineering: Computer-Aided Chemical Engineering*, volume 11. Access Online via Elsevier.
- Brookman, H. (2010). Bioraffinerie.
<http://de.wikipedia.org/wiki/Bioraffinerie>.
- Brueggemann Alcohol Wittenberg (2012). Market prices for ethanol. personal interview.
- Bumbac, G., Ciornei, C., Turcu, A., and Muntean, O. (2008). New solution for thermal coupling between a crude distillation unit and a fluid catalytic cracking unit. *Revue Roumaine de Chimie*, 53(8):635–641.
- Butcher, J. C. (1987). *The numerical analysis of ordinary differential equations*. Wiley-VCH Verlag GmbH & Co. KGaA.
- Cherubini, F. (2010). The biorefinery concept: Using biomass instead of oil for producing energy and chemicals. *Energy Conversion and Management*, 51/7:1412–1421.
- Claus, M. J. and Berglund, K. A. (2009). Defining still parameters using chemcad batch distillation model for modeling fruit spirits distillations. *Journal of Food Process Engineering*, 32(6):881–892.
- Corriou, J. P. (2004). *Process Control - Theory and Applications*. Springer Verlag.

- Díaz, M., Garrido, D., Romero, S., Rubio, B., Soler, E., and Troya, J. M. (2006). Experiences with component-oriented technologies in nuclear power plant simulators. *Software: Practice and Experience*, 36(13):1489–1512.
- DDBST GmbH (2013). Dortmund databank.
- de Souza Ferreira Filho, J. B. and Horridge, M. (2014). Ethanol expansion and indirect land use change in brazil. *Land Use Policy*, 36(0):595 – 604.
- Delucchi, M. A. (2010). Impacts of biofuels on climate change, water use, and land use. *Annals of the New York Academy of Sciences*, 1195(1):28–45.
- Deutsches Institut für Normung DIN (2002). GRAFCET - Specification language for sequential function charts (IEC 60848:2002); German version EN 60848:2002.
- Doran, P. M. (2012). *Bioprocess Engineering Principles*. Academic Press Oxford.
- Duessel, R., Stichlmair, J., and Groebel, M. (2006; 2008). *Rektifikation*, chapter 8, pages 689–798. Fluidverfahrenstechnik. Wiley-VCH Verlag GmbH & Co. KGaA.
- Ebenezer, S. A. (2005). Removal of carbon dioxide from natural gas for lng production. <http://www.ipt.ntnu.no/jsg/studenter/prosjekt/Salako2005.pdf>, accessed 08.11.2013.
- Epple, B., Leithner, R., Linzer, W., and Walter, H. (2009). *Simulation von Kraftwerken und wärmetechnischen Anlagen*. Springer Wien-NewYork.
- European Parliament and the EU (2009). RICHTLINIE 2009/28/EG DES EUROPÄISCHEN PARLAMENTS UND DES RATES zur Förderung der Nutzung von Energie aus erneuerbaren Quellen und zur Änderung und anschließenden Aufhebung der Richtlinien 2001/77/EG und 2003/30/EG.
- Evans, G. (2008). Liquid transport biofuels technology status report. *Liquid Transport Biofuels - Technology Status Report*.
- Festo Didactic GmbH & Co. KG, Troisdorf (2008). *GRAFCET*, volume 1. Bildungsverlag EINS GmbH.

- Feyo de Azevedo, S., Oliveira, F., and Capelo Cardoso, A. (1994). Teacon - a simulator for computer-aided teaching of process control. *Computer Applications in Engineering Education*, 1(4):307/319.
- Gear, C. W. (1971). *Numerical Initial-Value Problems in Ordinary Differential Equations*. Prentice-Hall.
- Gerlach, I., Hass, V. C., Brüning, S., and Mandenius, C.-F. (2013). Virtual bioreactor cultivation for operator training and simulation: application to ethanol and protein production. *J Chem Technol Biotechnol*, page n/a.
- Gernaey, K. V., Glassey, J., Skogestad, S., Krämer, S., Weiß, A., Engell, S., Pistikopoulos, E. N., and Cameron, D. B. (2000). *Process Systems Engineering, 5. Process Dynamics, Control, Monitoring, and Identification*, chapter 5, pages 1–60. Wiley-VCH Verlag GmbH & Co. KGaA.
- Ghaee, A., Sotudeh-Gharebagh, R., and Mostoufi, N. (2008). Dynamic optimization of the benzene extractive distillation unit. *Brazilian Journal of Chemical Engineering*, 25 (4):765 – 776.
- Gonzalez-Garcia, S., Moreira, M. T., Feijoo, G., and Murphy, R. J. (2012). Comparative life cycle assessment of ethanol production from fast-growing wood crops (black locust, eucalyptus and poplar). *Biomass and Bioenergy*, 39(0):378 – 388.
- Götz, M., Köppel, W., Reimert, R., and Graf, F. (2012). Optimierungspotenzial von Wäschen zur Biogasaufbereitung Teil 2. Chemische Wäschen. *Chemie Ingenieur Technik*, 84(1-2):81–87.
- Hass, V. C. (2005). Verbesserung der verfahrenstechnischen Ausbildung durch einen "Virtuellen Bioreaktor". *Chemie Ing. Technik*, 77(1 – 2):161 – 167.
- Hass, V. C. and Pörtner, R. (2011). *Praxis der Bioprozesstechnik mit virtuellem Praktikum*. Spektrum Verlag.
- Hausberg, B. (2010). Bioraffinerie - Von der Nischenlösung zum Markttreiber.
- Herbst, M. (2012). Verbesserung der Ökobilanz der Bio-Ethanolfermentation durch Optimierung der Prozessführung. Master's thesis, Hochschule Bremen.

- Hoffmann, U. und Kotter, M. (2002). Simulation eines geregelten Rührkessels mit LabVIEW. *Praxiswissen Elektronik- Industrie*, 3:65–71.
- Holl, P., Göttman, O., and Perne, R. (1995). Management von Trainingssimulatorprojekten. Technical report, NAMUR-Arbeitsblatt NA 60.
- Jayanthi, T., Seetha, H., Narayanan, K., Jasmine, N., Nawlakha, R., Sankar, B., Chakraborty, J., SatyaMurty, S., and Swaminathan, P. (2011). Simulation and integrated testing of process models of {PFBR} operator training simulator. *Energy Procedia*, 7(0):653 – 659.
- Jovic, F., Grasovec, M., Dejanovic, I., and Kosar, V. (2013). Dynamic simulation of high-pressure tubular reactor for low-density polyethylene production. *Journal of Elastomers & Plastics*, n/a:1 – 10.
- Kaltschmitt, H. (2007). Leitfaden Bioenergie. *Fachagentur Nachhaltende Rohstoffe*.
- Kamm, B. (2010). Statusbericht Bioraffinerie - Wann kommt die integrierte Bioraffinerie?
- Kamm, B. and Kamm, M. (2004). Biorefinery - systems. *Chem. Biochem. Eng.*, 18 (1):1–6.
- Kühn, K. (2012). Bioprocess trainer (ethanolproduction with s. cerevisiae) - quick guide.
- Kiyan, M., Bingöl, E., Melikoglu, M., and Albostan, A. (2013). Modelling and simulation of a hybrid solar heating system for greenhouse applications using matlab/simulink. *Energy Conversion and Management*, 72(0):147 – 155.
- Klatt, K.-U. (2009). Trainingssimulation - Erfahrungen und Perspektiven aus Sicht der chemisch-pharmazeutischen Industrie. *atp - Automatisierungstechnische Praxis*, 1-2.2009:66–71.
- Klemola, T. K. and Ilme, J. K. (1997). Effect of two-pass trays on distillation efficiencies. *Chemical Engineering & Technology*, 20(7):478–484.
- Kneebone, R. (2003). Simulation in surgical training: educational issues and practical implications. *Medical Education*, 37(3):267–277.

- Kroll, A. (2003). Trainingssimulation für die Prozessindustrie: Status, Trends, Ausblick- Teil 1+2. *Automatisierungstechnische Praxis atp*, 45(2)/ 45(3):50–57/ 55–60.
- Kuhnen, F. (2008). Modellierungssystem eStIM. Kurzeinführung. Unpublished.
- Kuhnen, F. and Meiwes, C. (2008). ph-modell. Modellbeschreibung. Unpublished.
- Kuntzsch, S., Hass, V. C., and Winterhalter, M. (2014). Einsatz eines neuen Trainingssimulators zur Untersuchung des Energiebedarfs der batch-Rektifikation bei unterschiedlichen Fahrweisen. *Chemie Ingenieur Technik*, accepted for publication:n/a.
- Lam, H. L., Klemes, J. J., Kravanja, Z., and Varbanov, P. S. (2011). Software tools overview: process integration, modelling and optimisation for energy saving and pollution reduction. *Asia-Pacific Journal of Chemical Engineering*, 6(5):696–712.
- Lee, Y.-H. and Liu, B.-S. (2003). Inflight workload assessment: Comparison of subjective and physiological measurements. *Aviation, Space, and Environmental Medicine*, 74:1078–1084(7).
- Li, F., Zeng, L., Velazquez-Vargas, L. G., Yoscovits, Z., and Fan, L.-S. (2010). Syngas chemical looping gasification process: Bench-scale studies and reactor simulations. *AIChE Journal*, 56(8):2186–2199.
- Liefeldt, A., Löhl, T., Pegel, S., Fritsch, C., Engell, S., and Schmid, C. (2002). DYNAMIT & Learn2Control - Neue Wege in der regelungstechnischen Ausbildung. *Chemie Ingenieur Technik*, 74(5):648.
- Liu, S. (2010). The biorefinery: Sustainably renewable route to commodity chemicals, energy, and materials. *Biotechnology Advances*, 28:41 – 42.
- Madhavan, S. (1984). Ammonia process simulator. *Plant/Operations Progress*, 3(1):14–17.
- Marichal, R. L. and González, E. J. (2012). Ullsimgraf: An educational tool with syntax control for grafcet notation. *Computer Applications in Engineering Education*.

- Martinez, D., Acevedo, P., and Kafarov, V. (2010). Life cycle assessment for joint production of biodiesel and bioethanol from african palm. *Chemical Engineering Transactions*, 21:1314 – 1319.
- Mathworks (2013). Matlab/ simulink. <http://www.mathworks.de/products/matlab/>, accessed 08.11.2013.
- Mohr, A. and Raman, S. (2013). Lessons from first generation biofuels and implications for the sustainability appraisal of second generation biofuels. *Energy Policy*, 63(0):114 – 122.
- Molaverdi, M., Karimi, K., Khanahmadi, M., and Goshadrour, A. (2013). Enhanced sweet sorghum stalk to ethanol by fungus *mucor indicus* using solid state fermentation followed by simultaneous saccharification and fermentation. *Industrial Crops and Products*, 49(0):580 – 585.
- Murai, K., Okazaki, T., and Hayashi, Y. (2011). A few comments on visual systems of a ship handling simulator for sea pilot training: Training for entering a port. *Electronics and Communications in Japan*, 94(9):10–17.
- Nguyen, M. T. (2004). *Deckschichtbildung in Kapillarmembranen bei der Querstrom-Mikrofiltration und ihre Beeinflussung durch polymere Flockungsmittels*. PhD thesis, Technische Universität Dresden.
- Ochoa, S., Wozny, G., and Repke, J.-U. (2010). Plantwide optimizing control of a continuous bioethanol production process. *Journal of Process Control*, 20(9):983 – 998.
- Ogden-Swift, A. (2013). Advances in abnormal situation management.
- Pahl, I., Melzner, D., and Reif, O. W. (2006). *Membranen - Grundlagen, Verfahren und industrielle Anwendungen*, chapter 7 - Membranen für biotechnologische Verfahren, pages 189–215. Wiley-VCH Verlag GmbH & Co. KG.
- Park, J., Jung, W., Ha, J., and Shin, Y. (2004). Analysis of operators’ performance under emergencies using a training simulator of the nuclear power plant. *Reliability Engineering & System Safety*, 83(2):179 – 186.
- Park, M., Kim, H. Y., Koo, B. W., Yeo, H., and Choi, I. G. (2010). Organosolv pretreatment with various catalysts for enhancing enzymatic hydrolysis of pitch pine (*pinus rigida*). *Bioresource Technology*, 101/18:7057–7064.

- Petzold, L. R. (1982). 10. international mathematics and computers simulation congress on systems simulation and scientific computation.
- Pilavtepe, M., Celiktaş, M. S., Sargin, S., and Yesil-Celiktaş, O. (2013). Transformation of *Posidonia oceanica* residues to bioethanol. *Industrial Crops and Products*, 51(0):348 – 354.
- Quesada-Medina, J., Lopez-Cremades, F. J., and Olivares-Carrillo, P. (2010). Organosolv extraction of lignin from hydrolyzed almond shells and application of the @d-value theory. *Bioresource Technology*, 101/21:8252–8260.
- Rautenbach, R. (1997). *Membranverfahren - Grundlagen der Modul- und Anlagenauslegung*. Springer-Verlag Berlin Heidelberg.
- Reinig, G., Winter, P., Linge, V., and Nögler, K. (2004). Trainingssimulatoren: Engineering und Einsatz. *Chemie Ingenieur Technik*, 69(12):1759–1764.
- Sartorius Stedim Biotech GmbH (2012). Operating Manual | Betriebsanleitung SARTOFLOW® Study Crossflow Filtration System | Crossflow Filtrationsanlage.
- Schaich, D. and Friedrich, M. (2003). Operator-Training Simulation (OTS) in der chemischen Industrie - Erfahrungen und Perspektiven. *Automatisierungstechnische Praxis atp*, 45(2).
- Schmidt, E. F. (1967). Wärmeübergang und Druckverlust in Rohrschlangen. *Chemie Ing. Technik*, 13:781–832.
- Schoop, K.-M. (2008). Technische Beschreibung des Prozessautomatisierungssystems WinErs. www.schoop.de – 02.12.2008.
- Semencenko, V. V., Mojovic, L. V., Ć Vukovic, A. P., Radosavljevic, M. M., Terzic, D. R., and Milacinovic Cereme, M. S. (2013). Suitability of some selected maize hybrids from serbia for the production of bioethanol and dried distillers’ grains with solubles. *Journal of the Science of Food and Agriculture*, 93(4):811–818.
- Shaikh, L., Pandit, A., and Ranade, V. (2013). Crystallisation of ferrous sulphate heptahydrate: Experiments and modelling. *The Canadian Journal of Chemical Engineering*, 91(1):47–53.
- Sieker, T. (2010). Grassilage als Rohstoff für die chemische Industrie. *Chemie Ingenieur Technik*, 82, No. 8:1153–1159.

- Soccol, C. R., de Souza Vandenberghe, L. P., Medeiros, A. B. P., Karp, S. G., Buckeridge, M., Ramos, L. P., Pitarelo, A. P., Ferreira-Leitao, V., Gottschalk, L. M. F., Ferrara, M. A., da Silva Bon, E. P., de Moraes, L. M. P., de Amorim Araújo, J., and Torres, F. A. G. (2010). Bioethanol from lignocelluloses: Status and perspectives in brazil. *Bioresource Technology*, 101(13):4820 – 4825.
- Thompson, W. and Meyer, S. (2013). Second generation biofuels and food crops: Co-products or competitors? *Global Food Security*, 2(2):89 – 96.
- Toledano, A., Egües, I., Andrés, M., Llano-Ponte, R., and Labidi, J. (2010). Lignocellulosic biorefinery approach: a challenge for a new world. *CHISA / ECCE7 Compilation of Full Texts*, P7.120, 1195.
- Ulber, R. (2010). Statusbericht Bioraffinerie - Wann kommt die integrierte Bioraffinerie?
- Unkelbach, G., Pindel, E., and Schweppe, R. (2009). Lignin/Tannin-Abtrennung aus Lignocellulosen. *Chemie Ingenieur Technik*, 81(11):1767–1771.
- Vane, L. M. and Alvarez, F. R. (2013). Hybrid vapor stripping - vapor permeation process for recovery and dehydration of 1-butanol and acetone/butanol/ethanol from dilute aqueous solutions. part 1. process simulations. *Journal of Chemical Technology & Biotechnology*, 88(8):1436–1447.
- Vauck, W. R. A. and Müller, H. A. (2000). *Grundoperationen chemischer Verfahrenstechnik*, volume 11. Dt. Verl. für Grundstoffindustrie, Stuttgart.
- Velez, G., Matey, L., Amundarain, A., Suescun, A., Marin, J. A., and de Dios, C. (2013). Modeling of shotcrete application for use in a real-time training simulator. *Computer-Aided Civil and Infrastructure Engineering*, 28(6):465–480.
- VERDER Deutschland GmbH (2013). *Verderflex DURA Industrieschlauchpumpe*. Rheinische Straße 43, D-42781 Haan.
- Walker, G. M. (2011). 125th anniversary review: Fuel alcohol: Current production and future challenges. *Journal of the Institute of Brewing*, 117(1):3–22.

- Wang, L., Littlewood, J., and Murphy, R. J. (2013a). Environmental sustainability of bioethanol production from wheat straw in the {UK}. *Renewable and Sustainable Energy Reviews*, 28(0):715 – 725.
- Wang, L., Sharifzadeh, M., Templer, R., and Murphy, R. J. (2013b). Bioethanol production from various waste papers: Economic feasibility and sensitivity analysis. *Applied Energy*, 111(0):1172 – 1182.
- Weinberg, J. and Kaltschmitt, M. (2013). Greenhouse gas emissions from first generation ethanol derived from wheat and sugar beet in germany - analysis and comparison of advanced by-product utilization pathways. *Applied Energy*, 102(0):131 – 139.
- Witte, V. C. (1996). *Mathematische Modellierung und adaptive Prozeßsteuerung der Kultivierung von Cyathus striatus*. Number 144(17) in Fortschr.-Ber. VDI Reihe. VDI Verlag, Düsseldorf.
- Yang, S., Yang, L., and He, C. (2001). Improve safety of industrial processes using dynamic operator training simulators. *Process Safety and Environmental Protection*, 79(6):329 – 338.
- Yoon, M. H., Lee, Y. W., Lee, C. H., and Seo, Y. B. (2012). Simultaneous production of bio-ethanol and bleached pulp from red algae. *Bioresource Technology*, 126(0):198 – 201.
- Young, B., Mahoney, D., and Syrczek, W. (2001). Real-time computer simulation workshops for the process control educations of undergraduate chemical engineers. *Computer Applications in Engineering Education*, 9(1):57–62.
- Zhiyun, Z., Baoyu, C., Xinjun, G., and Chenguang, C. (2003). The development of a novel type chemical process operator-training simulator. In Chen, B. and Westerberg, A. W., editors, *Process Systems Engineering 2003, 8th International Symposium on Process Systems Engineering*, volume 15 of *Computer Aided Chemical Engineering*, pages 1447 – 1452. Elsevier.

Publications

Kuntzsch, S.; Kuhnen, F.; Blesgen, A.; Hass, V. C.: Entwicklung eines modularisierten Trainingssimulators für Biomassekraftwerke, *Chemie Ingenieur Technik*, 82(9), 1351, (2010). DOI: 10.1002/cite.201050159

Kuntzsch, S.; Kuhnen, F.; Blesgen, A.; Hass, V. C.: Development of a Modular Training Simulator for Biomass Power Plants, presentation at the *19th International Congress of Chemical and Process Engineering CHISA 2010 and the 7th European Congress of Chemical Engineering ECCE-7*, 28. August - 1. September (2010), Prague, Czech Republic.

Hass, V. C.; Kuntzsch, S.; Gerlach, I.; Kühn, K. and Winterhalter M.: Towards the development of a training simulator for biorefineries. *Chem Eng Trans* 29:247–252 (2012). DOI: 10.3303/CET1229042

Kuntzsch, S.; Westhues, D.; Schoop, K.-M.; Hass, V. C.: WinErs als Entwicklungswerkzeug für Trainingssimulatoren, presentation at *IDA 2013 - Integrierte Digitale Anlagenplanung und -führung*, 21. - 22. March (2013), DECHEMA-Haus, Frankfurt am Main.

Kuntzsch, S.; Winterhalter, M.; Kuhnen, F.; Schoop, K.-M.; Hass, V. C.: Optimizing the Process Control Strategy of a Batch- Bioethanol-Rectification-Process using a Novel Training Simulator with GRAFCET-Automation, poster presentation at the *2nd European Congress of Applied Biotechnology World Forum*, 21. - 25. April (2013), The Hague, The Netherlands.

Kuntzsch, S.; Hass, V. C.: Entwicklung und Anwendung einer Virtuellen Bioraffinerie, poster presentation at *ProcessNet - Sustainable Production, Energy and Resources (SuPER)*, 5. - 6. November (2013).

Kuntzsch, S.; Hass, V. C.: Einsatz eines neuen Trainingssimulators zur Untersuchung des Energiebedarfs der batch-Rektifikation bei unterschiedlichen Fahrweisen. *Chemie Ingenieur Technik*, n/a, accepted for publication, (2014).

